

**Spectroscopic Studies of Chemical Reactions  
Using Carbon Dioxide Lasers.**

by

**Ghalib Adrees Atiya**

**A Thesis submitted for the degree of Doctor of  
Philosophy at the University of Leicester**

**August 1990**

UMI Number: U038754

All rights reserved

INFORMATION TO ALL USERS

The quality of this reproduction is dependent upon the quality of the copy submitted.

In the unlikely event that the author did not send a complete manuscript and there are missing pages, these will be noted. Also, if material had to be removed, a note will indicate the deletion.



UMI U038754

Published by ProQuest LLC 2015. Copyright in the Dissertation held by the Author.  
Microform Edition © ProQuest LLC.

All rights reserved. This work is protected against  
unauthorized copying under Title 17, United States Code.



ProQuest LLC  
789 East Eisenhower Parkway  
P.O. Box 1346  
Ann Arbor, MI 48106-1346



7500678029

STATEMENT

The work presented in this thesis has been carried out by the author in the Department of Chemistry at the University of Leicester between October 1986 and August 1990 unless stated otherwise.

This work has not been presented and is not currently being presented for any other degree.

Signed: *G. A. Atija* ..... Date: *14/9/1990* .....

**DEDICATION:**

To my parents, brothers, sisters, wife and daughters.

## Spectroscopic Studies of Chemical Reactions Using Carbon Dioxide Lasers.

by Ghalib Adrees Atiya.

### Abstract

The laser powered homogeneous pyrolysis (LPHP) technique was used to promote chemical reactions. The temperature and the geometry of the temperature produced in the reaction cell by a continuous wave IR CO<sub>2</sub> laser were photographed and measured using chemiluminescence, spectroscopic (IR diode laser source spectrometer) and chemical standard techniques. The distribution of the temperature over the volume of the cell was found to be inhomogeneous, and the diffusion effects on the reaction rate were negligible.

The mechanism of the decomposition of CH<sub>3</sub>I, d<sub>3</sub>-CH<sub>3</sub>I and their mixture was investigated using the LPHP technique. The rate of the decomposition of d<sub>3</sub>-CH<sub>3</sub>I was faster than that of CH<sub>3</sub>I. No significant amount of mixed isotopes of the products were observed during the irradiation of the mixture.

The reactions of (CH<sub>3</sub>)<sub>4</sub>Sn (TMT) and (CH<sub>3</sub>)<sub>3</sub>SnSn(CH<sub>3</sub>)<sub>3</sub> (HMDT) showed they decomposed, and the major products were CH<sub>4</sub> and metallic layer deposited on the walls of the reaction cell. A significant amount of CH<sub>3</sub>D was observed during the reaction of TMT in presence of D<sub>2</sub> at a relatively high laser power.

The reaction of (CH<sub>3</sub>)<sub>3</sub>Al (TMAL) was investigated using LPHP technique and the mechanism of its reaction was presented. A monomeric TMAL form was detected during the reaction using FTIR spectrometer scanning of the reaction zone perpendicularly with the incident CO<sub>2</sub> laser beam. A (CH<sub>3</sub>)<sub>2</sub>Al (DMAL) radical was found as a result of the decomposition of TMAL. The DMAL radical was trapped and isolated as stable compounds: (CH<sub>3</sub>)<sub>2</sub>AlF (DMAF) in dimeric and tetrameric forms, and (CH<sub>3</sub>)<sub>2</sub>AlCl (DMAC) in dimeric form, using SF<sub>6</sub> and CCl<sub>4</sub>, CHCl<sub>3</sub> and CDCl<sub>3</sub> as radical scavengers, respectively. The presence of H<sub>2</sub> and D<sub>2</sub>, which are widely used as carrier gases in the metal organic chemical vapour deposition (MOCVD) technique, did not have major effect on the mechanism of the reaction, but were shown to have isotopic effects on the thermal conductivity of the reaction cell, slowing down the reaction.

A new photoacoustic spectroscopic technique, based on the change of the resonance frequency of the reaction cell (r.f.), was introduced to follow and examine the chemical reactions, revealing the change of the cell composition. The results obtained by this technique were fairly comparable with those obtained by IR spectroscopic methods.

## ACKNOWLEDGEMENTS

I would like to thank Dr. D. K. Russell for supervising this work. His advice, patience and continuous encouragement during the course of this study is very much appreciated.

I also thank my colleagues Dave Pape and Andy Grady for their comments, useful discussion, and help.

Further, I would like to express my gratitude to Dr. K. W. Morcom, Dr. G. Griffith, K. Wilkinson, R. Batchen, L. Colley, P. Acton, M. Al-Mukhtar, S. Akona and others for their assistance and help. I also thank Ann Crane for drawing the figures in this thesis.

Moreover, I am extremely grateful to my wife Rabab and my two daughters Fatima and Burak for their love, patience and encouragement.

Last but not least, I acknowledge with appreciation the Ministry of Higher Education in Iraq for the scholarship.

## TABLE OF CONTENTS

|   |       |
|---|-------|
| ABSTRACT. . . . .   | iv    |
| ACKNOWLEDGEMENTS. . . . .   | v     |
| LIST OF FIGURES . . . . .   | xii   |
| LIST OF TABLES. . . . .   | xviii |
| <u>CHAPTER 1- GENERAL INTRODUCTION</u> . . . . .  | 1     |
| <u>CHAPTER 2- THEORETICAL BACKGROUND</u> . . . . .                                      | 4     |
| 2.1    Introduction. . . . .  | 4     |
| 2.2    The Laser Powered Homogeneous<br>Pyrolysis (LPHP) technique. . . . .             | 4     |
| 2.3    Measurement of the rate of the<br>reaction. . . . .                              | 14    |
| 2.4    The advantages and disadvantages of<br>the photosensitization technique. . . . . | 17    |
| 2.5    The photoacoustic technique . . . . .  | 18    |
| 2.6    Composition measurements using<br>photoacoustic technique . . . . .              | 19    |
| 2.7    The advantages and disadvantages of<br>the photoacoustic technique . . . . .     | 20    |
| 2.8    References. . . . .  | 22    |
| <u>CHAPTER 3- EQUIPMENT AND EXPERIMENTAL DETAILS</u> . . . . .                          | 27    |
| 3.1    Introduction. . . . .  | 27    |
| 3.2    The CO <sub>2</sub> laser . . . . .  | 27    |
| 3.3    Description of the CO <sub>2</sub> laser. . . . .                                | 29    |
| 3.4    Alignment of CO <sub>2</sub> laser. . . . .                                      | 31    |
| 3.5    IR spectrometers. . . . .  | 33    |
| 3.5.1  IR diode laser spectrometer . . . . .  | 35    |
| 3.6    Reaction cells. . . . .  | 35    |
| 3.6.1  Short length reaction cell. . . . .  | 36    |
| 3.6.2  The trapping cell . . . . .  | 36    |

|       |  |    |
|-------|--|----|
| 3.6.3 | The side windows cell . . . . .  | 36 |
| 3.6.4 | The temperature distribution<br>measurement cell. . . . .                        | 40 |
| 3.7   | Photoacoustic cell. . . . .  | 40 |
| 3.7.1 | The long photoacoustic cell . . . . .  | 40 |
| 3.7.2 | The short photoacoustic cell. . . . .  | 42 |
| 3.7.3 | Adjustable volume cell. . . . .  | 42 |
| 3.8   | The experimental arrangements . . . . .  | 46 |
| 3.8.1 | Arrangements for IR CO <sub>2</sub> laser<br>induced chemical reactions. . . . . | 46 |
| 3.8.2 | Arrangements for spectroscopic<br>experiments during the irradiation             | 46 |
| 3.8.3 | Arrangements for the temperature<br>distribution measurements . . . . .          | 48 |
| 3.8.4 | Arrangements for photoacoustic<br>experiments . . . . .                          | 48 |
| 3.8.5 | Arrangements for the freezing point<br>experiments . . . . .                     | 51 |
| 3.9   | Electrical equipment. . . . .  | 51 |
| 3.9.1 | The microphone. . . . .  | 51 |
| 3.9.2 | AC amplifier. . . . .  | 52 |
| 3.9.3 | Light chopper . . . . .  | 52 |
| 3.9.4 | CO <sub>2</sub> laser modulator . . . . .  | 52 |
| 3.9.5 | The power meter . . . . .  | 54 |
| 3.10  | Vacuum line . . . . .  | 54 |
| 3.11  | Chemicals . . . . .  | 55 |
| 3.12  | References. . . . .  | 56 |

**CHAPTER 4- TEMPERATURE DISTRIBUTION** . . . . . 57

|       |   |    |
|-------|---|----|
| 4.1   | Introduction. . . . .   | 57 |
| 4.2   | Review. . . . .   | 58 |
| 4.3   | Temperature model . . . . .   | 61 |
| 4.4   | Experiments . . . . .   | 66 |
| 4.4.1 | Diffusion effects . . . . .   | 67 |
| 4.4.2 | Photographing the reaction zone . . . . .                               | 67 |
| 4.4.3 | Temperature measurements using<br>a chemical standard . . . . .         | 67 |
| 4.4.4 | Temperature measurements using the<br>spectroscopic technique . . . . . | 70 |

|       |   |    |
|-------|---|----|
| 4.5   | Results . . . . .   | 72 |
| 4.5.1 | Diffusion effects . . . . .                               | 72 |
| 4.5.2 | Chemiluminescence measurements. . . . .                   | 72 |
| 4.5.3 | Results of the chemical standard<br>measurements. . . . . | 74 |
| 4.5.4 | Results of the spectroscopic<br>measurements. . . . .     | 74 |
| 4.6   | Discussion. . . . .                                       | 77 |
| 4.7   | Conclusion. . . . .                                       | 81 |
| 4.8   | References. . . . .                                       | 82 |

CHAPTER 5- LASER POWERED HOMOGENEOUS PYROLYSIS

|       |  |     |
|-------|--|-----|
|       | <u>OF METHYL IODIDE</u> . . . . .  | 84  |
| 5.1   | Introduction. . . . .  | 84  |
| 5.2   | Review. . . . .  | 84  |
| 5.3   | Experimental. . . . .  | 93  |
| 5.3.1 | Irradiation of Methyl Iodide ( $\text{CH}_3\text{I}$ ) in<br>the absence of photosensitizer. . . . .                                     | 93  |
| 5.3.2 | Reaction of Methyl Iodide ( $\text{CH}_3\text{I}$ ). . . . .   | 93  |
| 5.3.3 | Reaction of $\text{d}_3$ -Methyl Iodide ( $\text{CD}_3\text{I}$ ) . . . . .  | 95  |
| 5.3.4 | Reaction of mixtures of Methyl<br>Iodide ( $\text{CH}_3\text{I}$ ) and $\text{d}_3$ -Methyl<br>Iodide ( $\text{CD}_3\text{I}$ ). . . . . | 95  |
| 5.4   | Results . . . . .  | 95  |
| 5.4.1 | Irradiation of $\text{CH}_3\text{I}$ alone . . . . .   | 95  |
| 5.4.2 | The reaction of $\text{CH}_3\text{I}$ in the<br>presence of $\text{SF}_6$ . . . . .  | 96  |
| 5.4.3 | The reaction of $\text{CD}_3\text{I}$ in the<br>presence of $\text{SF}_6$ . . . . .  | 96  |
| 5.4.4 | The reaction of the mixture of<br>$\text{CH}_3\text{I}$ and $\text{CD}_3\text{I}$ . . . . .  | 96  |
| 5.5   | Discussion. . . . .  | 104 |
| 5.6   | Conclusion. . . . .  | 110 |
| 5.7   | References. . . . .  | 111 |

CHAPTER 6- PYROLYSIS OF TETRAMETHYLTIN, TMT

|     |   |     |
|-----|---|-----|
|     | <u>AND HEXAMETHYLDITIN, HMDT.</u> . . . . . | 114 |
| 6.1 | Introduction. . . . .                       | 114 |

|       |   |     |
|-------|---|-----|
| 6.2   | Review. . . . .   | 114 |
| 6.3   | Experimental. . . . .   | 118 |
| 6.3.1 | Pyrolysis of TMT. . . . .   | 119 |
| 6.3.2 | The pyrolysis of TMT in presence of O <sub>2</sub> . . . . .              | 119 |
| 6.3.3 | The pyrolysis of TMT in presence of<br>Deuterium D <sub>2</sub> . . . . . | 119 |
| 6.3.4 | The pyrolysis of HMDT . . . . .   | 119 |
| 6.4   | Kinetic measurements. . . . .   | 122 |
| 6.4.1 | The kinetic measurements of TMT . . . . .                                 | 122 |
| 6.4.2 | The kinetic measurements of HMDT. . . . .                                 | 122 |
| 6.5   | Results . . . . .   | 127 |
| 6.5.1 | The decomposition of TMT. . . . .   | 127 |
| 6.5.2 | The decomposition of TMT in presence<br>of O <sub>2</sub> . . . . .       | 127 |
| 6.5.3 | The decomposition of TMT in presence<br>of D <sub>2</sub> . . . . .       | 130 |
| 6.5.4 | The decomposition of HMDT . . . . .                                       | 130 |
| 6.6   | Discussion. . . . .   | 132 |
| 6.7   | Conclusion. . . . .   | 133 |
| 6.9   | References. . . . .   | 134 |

CHAPTER 7- THE DECOMPOSITION OF TRIMETHYLALUMINIUM. . 135

|       |   |     |
|-------|---|-----|
| 7.1   | Introduction. . . . .   | 135 |
| 7.2   | Review. . . . .   | 135 |
| 7.3   | Preparation of the sample . . . . .   | 139 |
| 7.4   | Pyrolysis of Trimethylaluminium, TMAL. . . . .  | 139 |
| 7.4.1 | TMAL During the Pyrolysis . . . . .   | 139 |
| 7.4.2 | Pyrolysis of TMAL . . . . .   | 140 |
| 7.4.3 | Pyrolysis of TMAL in presence of<br>hydrogen, H <sub>2</sub> . . . . .                    | 144 |
| 7.4.4 | Pyrolysis of TMAL in presence of D <sub>2</sub> . . . . .                                 | 144 |
| 7.4.5 | Pyrolysis of TMAL in presence of<br>Tetrachloromethane, CCl <sub>4</sub> . . . . .        | 147 |
| 7.4.6 | The Reaction of TMAL in Presence<br>of Chloroform, CHCl <sub>3</sub> . . . . .            | 152 |
| 7.4.7 | The reaction of TMAL in presence of<br>deuterated chloroform, CDCl <sub>3</sub> . . . . . | 152 |
| 7.5   | Trapping intermediates as stable<br>compounds . . . . .                                   | 159 |

|       |  |     |
|-------|--|-----|
| 7.5.1 | Products of the reaction of TMAL<br>with SF <sub>6</sub> . . . . .   | 159 |
| 7.5.2 | Characterization of the products<br>from TMAL pyrolysis in the<br>presence of CCl <sub>4</sub> . . . . .                     | 171 |
| 7.5.3 | Characterization of the products<br>from TMAL pyrolysis in the<br>presence of chloroform, CHCl <sub>3</sub> . . . . .        | 175 |
| 7.5.4 | Characterization of products from<br>TMAL pyrolysis in the presence<br>of deuterated chloroform, CDCl <sub>3</sub> . . . . . | 175 |
| 7.6   | Kinetic Measurements of TMAL Pyrolysis.  | 175 |
| 7.7   | Results and Discussion . . . . .   | 177 |
| 7.7.1 | The decomposition of TMAL in the<br>presence of SF <sub>6</sub> . . . . .  | 181 |
| 7.7.2 | The pyrolysis of TMAL in presence<br>of H <sub>2</sub> . . . . .   | 183 |
| 7.7.3 | The Pyrolysis of TMAL in presence<br>of D <sub>2</sub> . . . . .   | 185 |
| 7.7.4 | The pyrolysis of TMAL in presence<br>of CCl <sub>4</sub> . . . . .   | 186 |
| 7.7.5 | The pyrolysis of TMAL in presence<br>of CHCl <sub>3</sub> . . . . .  | 187 |
| 7.7.6 | The pyrolysis of TMAL in presence<br>of CDCl <sub>3</sub> . . . . .  | 187 |
| 7.8   | Conclusion. . . . .  | 188 |
| 7.9   | References. . . . .  | 189 |

CHAPTER 8- THE PHOTOACOUSTIC MEASUREMENTS . . . . . 192

|       |   |     |
|-------|---|-----|
| 8.1   | Introduction. . . . .                           | 192 |
| 8.2   | Review. . . . .                                 | 192 |
| 8.3   | Experimental. . . . .                           | 195 |
| 8.3.1 | Long Pyrex Photoacoustic Cell . . . . .         | 195 |
| 8.3.2 | Adjustable Length Cell. . . . .                 | 206 |
| 8.3.3 | The Short Length Photoacoustic Cell . . . . .   | 208 |
| 8.4   | Results . . . . .                               | 217 |
| 8.4.1 | Results of Using Long Glass Cell. . . . .       | 217 |
| 8.4.2 | Results of the Adjustable Length Cell . . . . . | 218 |
| 8.4.3 | Results of the IR-Photoacoustic Cell. . . . .   | 218 |

|   |                     |     |
|---|---------------------|-----|
| 8.5                                     | Discussion. . . . . | 219 |
| 8.6                                     | Conclusion. . . . . | 223 |
| 8.7                                     | References. . . . . | 224 |
| <u>CHAPTER 9- CONCLUSIONS . . . . .</u> |                     | 226 |

## LIST OF FIGURES

| <u>Figure</u> |   | <u>Page</u> |
|---------------|---|-------------|
| 2.1           | Partial energy distribution pathways for various energy levels of SF <sub>6</sub> . . . . .   | 9           |
| 2.2           | FTIR spectrum of 2 torr (CH <sub>3</sub> ) <sub>4</sub> Sn and 10 torr SF <sub>6</sub> . . . . .  | 15          |
| 3.1           | Block diagram of energy level for the CO <sub>2</sub> laser. . . . .  | 28          |
| 3.2           | Schematic diagram showing the CO <sub>2</sub> laser, gas handling, water cooling, and the discharge tube . . . . .                        | 30          |
| 3.3           | Schematic diagram showing the alignment of the CO <sub>2</sub> laser . . . . .  | 32          |
| 3.4           | Schematic diagram of a conventional IR spectrometer . . . . .   | 34          |
| 3.5           | Schematic diagram of the interferometer of an FTIR spectrometer. . . . .  | 34          |
| 3.6           | Schematic diagram of the pyrolysis cell. . . . .  | 37          |
| 3.7           | Schematic diagram of the pyrolysis cell with the cold trap . . . . .  | 38          |
| 3.8           | Schematic diagram showing the side window cell used to monitor the reaction during CO <sub>2</sub> laser irradiation of the cell. . . . . | 39          |
| 3.9           | Schematic diagram of the temperature measurement cell showing the side windows positioned at the entrance window. . . . .                 | 41          |

|      |  |    |
|------|--|----|
| 3.10 | Schematic diagram of a low resonance frequency photoacoustic cell . . . . .  | 42 |
| 3.11 | Schematic diagram of a high resonance frequency photoacoustic cell . . . . .   | 44 |
| 3.12 | Schematic diagram for the adjustable volume photoacoustic cell. . . . .  | 45 |
| 3.13 | Schematic diagram illustrating the experimental settings to induce the reaction .  | 47 |
| 3.14 | Experimental settings to study the reaction of TMAL while CO <sub>2</sub> laser is shone through the reaction cell. . . . .  | 47 |
| 3.15 | Schematic diagram of the temperature distribution measurements. . . . .  | 49 |
| 3.16 | Schematic diagram of the Photoacoustic experiments. . . . .  | 50 |
| 3.17 | Freezing point apparatus . . . . .   | 52 |
| 4.1  | Normalized plots of amount of the decomposed CH <sub>3</sub> CHO vs time for the reaction of a mixture of 10 torr CH <sub>3</sub> CHO and 10 torr SF <sub>6</sub> irradiated with 12.5 Watts CO <sub>2</sub> laser power. . . . .  | 68 |
| 4.2  | Photograph of emission of iodine vapour in presence of 10 torr SF <sub>6</sub> excited with 30 Watts CO <sub>2</sub> laser power. . . . .  | 70 |
| 4.3  | Normalized plots of the ln (intensity) of CH <sub>3</sub> COOCH <sub>2</sub> CH <sub>3</sub> at 1224 cm <sup>-1</sup> vs time for mixture of 10 torr CH <sub>3</sub> COOCH <sub>2</sub> CH <sub>3</sub> and 10 torr SF <sub>6</sub> at various CO <sub>2</sub> laser powers. . . . . | 71 |
| 4.4  | Plot of the measured temperature in K vs laser power in Watts . . . . .  | 76 |

|     |  |     |
|-----|--|-----|
| 4.5 | Plot of $\ln\{(\ln(I_{in}/I_{out}))/J(J+1)\}$ vs $J(J+1)$ of the lines R18, 20, 22, 24, 25, 27, and 29 of CO spectrum . . . . .  | 78  |
| 4.6 | FTIR spectra of 10 torr CO mixed with 10 torr SF <sub>6</sub> before during irradiation with 10 Watts of laser power . . . . .   | 79  |
| 5.1 | Typical IR spectra for 5 torr of CH <sub>3</sub> I and 10 torr of SF <sub>6</sub> using a conventional spectrometer before and after 21 minutes irradiation with 7.5 Watts of laser power. . .   | 94  |
| 5.2 | The IR vibrational spectra of SF <sub>6</sub> , CH <sub>3</sub> I and CD <sub>3</sub> I . . . . .  | 97  |
| 5.3 | IR spectra of 7 torr of CH <sub>3</sub> I, 7 torr of CD <sub>3</sub> I and 10 torr of SF <sub>6</sub> . . . . .  | 98  |
| 5.4 | IR spectra of 5 torr of CH <sub>3</sub> I and 10 torr of SF <sub>6</sub> before and after irradiation with 8.0 watts of laser power for 10 minutes. . . .  | 100 |
| 5.5 | IR spectra of 5 torr of CD <sub>3</sub> I and 10 torr of SF <sub>6</sub> before and after irradiation with 10.0 Watts of laser power for 10 minutes . . .  | 103 |
| 5.6 | IR spectra of a mixture of 5 torr of CD <sub>3</sub> I, 5 torr of CH <sub>3</sub> I and 10 torr of SF <sub>6</sub> before and after irradiation with 8.75 Watts laser power. . . . .   | 105 |
| 5.7 | Normalized plots of the appearance of CH <sub>4</sub> and CD <sub>4</sub> measured from their peak intensities from the reaction of a mixture of 5 torr of CH <sub>3</sub> I, CD <sub>3</sub> I and 10 torr of SF <sub>6</sub> irradiated with 8.75 watts of laser power . . . . . | 107 |
| 5.8 | First order plot for the reaction of 5 torr of CH <sub>3</sub> I and 10 torr of SF <sub>6</sub> ; and 5 torr   |     |

|     |  |     |
|-----|--|-----|
|     | of $\text{CD}_3\text{I}$ and 10 torr of $\text{SF}_6$ at laser power<br>of 8.75 Watts. . . . .   | 108 |
| 5.9 | IR radiation absorption in $\text{CH}_3\text{I}$ , $\text{CD}_3\text{I}$ and<br>$\text{SF}_6$ as a function of the excitation line<br>of the 001-100 transition of $\text{CO}_2$ laser . . . . | 110 |
| 6.1 | IR spectra of 2 Torr of TMT and 10 Torr of<br>$\text{SF}_6$ irradiated with a laser power of 8.25<br>Watts: a) before, b) after 25 Sec. and<br>c) after 60 Sec. of irradiation. . . . .        | 120 |
| 6.2 | $\ln$ (intensity) of TMT vs time at various<br>laser powers . . . . .  | 123 |
| 6.3 | Relative rate of the reaction of TMT vs<br>laser power in Watts . . . . .  | 125 |
| 6.4 | $\ln$ (intensity) of HMDT vs time at various<br>laser powers . . . . .   | 126 |
| 6.5 | Relative rates of the reaction of HMDT vs<br>laser power in Watts . . . . .  | 128 |
| 6.6 | The IR spectra of 2 torr TMT, 3.5 torr $\text{O}_2$<br>and 10 torr $\text{SF}_6$ before and after irradiation<br>with a laser power of 6.25 Watts . . . . .                                    | 129 |
| 6.7 | IR spectra of 2 torr of TMT, 10 torr of $\text{D}_2$<br>and 10 torr $\text{SF}_6$ before and after irradiation<br>with a laser power of 7.50 Watts . . . . .                                   | 131 |
| 7.1 | 3 torr TMAL + 5 torr $\text{SF}_6$ irradiated with<br>12.5 W laser power: a) before, b) during and<br>c) after irradiation . . . . .   | 141 |
| 7.2 | 2 torr TMAL + 10 torr $\text{SF}_6$ irradiated with<br>7.5 W laser power: a) before, b) after 2<br>minutes and c) after 5 minutes irradiation . .  | 145 |

|       |   |     |
|-------|---|-----|
| 7.3   | Plots of the intensity of bands of TMAL and products in a mixture of 2 torr TMAL + 10 torr SF <sub>6</sub> irradiated with 7.5 W laser power . . .  | 146 |
| 7.4   | Plots of ln (intensity) of the peak at 777 cm <sup>-1</sup> vs time: a) 1 torr of TMAL + 10 torr SF <sub>6</sub> + 5 torr H <sub>2</sub> irradiated with 7.5 W laser power, and b) 1 torr TMAL + 10 torr SF <sub>6</sub> + 5 torr D <sub>2</sub> irradiated with 7.5 W laser power. . . | 148 |
| 7.5   | IR spectra of 2 torr of CCl <sub>4</sub> + 10 torr SF <sub>6</sub> before and after 10 minutes irradiation with 7.5 W laser power. . . . .  | 150 |
| 7.6   | IR spectra of 2 torr CCl <sub>4</sub> + 3 torr TMAL + 10 torr SF <sub>6</sub> before and after 10 minutes irradiation with 3.75 Watts laser power. . . .  | 151 |
| 7.7   | IR spectra of 2 torr CHCl <sub>3</sub> + 10 torr SF <sub>6</sub> before after 10 minutes irradiation with 5.0 W laser power. . . . .  | 153 |
| 7.8   | IR spectra of mixture of 2 torr CHCl <sub>3</sub> + 3 torr TMAL + 10 torr SF <sub>6</sub> before and after irradiation with 2.5 W laser power . . . . .   | 156 |
| 7.9   | IR spectra of mixture of 3 torr CDCl <sub>3</sub> + 10 torr SF <sub>6</sub> before and after 10 minutes irradiation with 5.0 W laser power . . . . .  | 158 |
| 7.10  | IR spectra for 3 torr TMAL + 2 torr CDCl <sub>3</sub> + 10 torr SF <sub>6</sub> before and after 10 minutes irradiation with 3.75 W laser power. . . . .  | 160 |
| 7.11  | <sup>1</sup> H, <sup>19</sup> F and <sup>13</sup> C NMR spectra of DMAF with CF <sub>3</sub> CH <sub>2</sub> OH as a reference compound. . . . .  | 162 |
| 7.12a | IR spectra of DMAF: a) IR (liquid), b) IR (gas), and c) IR (gas) of TMAL . . . . .  | 167 |

|       |  |     |
|-------|--|-----|
| 7.12b | Liquid phase Raman spectra of DMAF . . . . .   | 168 |
| 7.13  | IR and Raman spectra of DMACl: a) gas phase<br>IR and b) liquid phase Raman spectrum. . . . .  | 173 |
| 7.14  | <sup>1</sup> H NMR spectrum for DMACl dissolved in<br>CDCl <sub>3</sub> with a trace amount of CHCl <sub>3</sub> as lock<br>reference. . . . .   | 176 |
| 7.15  | Plots of ln(intensity) of the bridging peak<br>at 777cm <sup>-1</sup> vs time for various laser powers:<br>a) 5.0, b) 6.25, c) 8.75 and d) 12.50 Watts. . . . .                          | 178 |
| 7.16  | Plot of the 1st order rate constant k vs<br>laser power. . . . .   | 180 |
| 7.17  | Estimated temperature profiles in the<br>reaction cell: a) SF <sub>6</sub> only, b) with D <sub>2</sub><br>and c) with H <sub>2</sub> . . . . .  | 184 |
| 8.1   | Plot of amplitude of the photoacoustic<br>signal vs laser power. . . . .   | 196 |
| 8.2   | Resonance frequency spectrum for the 27 cm<br>long photoacoustic cell. . . . .   | 198 |
| 8.3   | Calibration curve for the photoacoustic cell . . . . .   | 199 |
| 8.4   | Plot of the laser power vs r.f; 10 torr of<br>SF <sub>6</sub> was used and cell length was 25 cm . . . . .   | 202 |
| 8.5   | Plot of the change in the r.f. of the<br>photoacoustic cell vs time for different<br>compounds. . . . .  | 204 |
| 8.6   | IR spectra of a mixture of 10 torr of CH <sub>3</sub> CHO<br>and 10 torr of SF <sub>6</sub> irradiated with 10 Watts<br>of laser power: a) before and b) after<br>the reaction . . . . . | 205 |

|      |  |     |
|------|--|-----|
| 8.7  | Plot of the r.f. of the cell vs cell length. . . . .   | 207 |
| 8.8  | Resonance frequency spectrum for the short<br>length IR-Photoacoustic cell . . . . .   | 212 |
| 8.9  | Calibration curve for the IR-photoacoustic<br>cell . . . . .   | 213 |
| 8.10 | Plots of normalized results of the reaction<br>of $\text{CH}_3\text{CHO}$ vs time using mixture of 10 torr<br>of $\text{CH}_3\text{CHO}$ and 10 torr of $\text{SF}_6$ irradiated<br>with 10 Watts of laser power . . . . . | 215 |
| 8.11 | Plot of normalized results of the intensity<br>of the peak $1123\text{ cm}^{-1}$ of ethyl acetate and<br>the change in the difference of the r.f. of<br>the cell vs time . . . . .   | 216 |
| 8.12 | IR spectra of the decomposition of a mixture<br>of 10 torr of $\text{CH}_3\text{COOCH}_2\text{CH}_3$ and 10 torr of<br>$\text{SF}_6$ before and after 15 minutes irradiation<br>with 5.3 Watts of laser power. . . . .     | 220 |
| 8.13 | IR spectra of a mixture of 10 torr of<br>$\text{CH}_3\text{COOH}$ and 10 torr of $\text{SF}_6$ irradiated with<br>about 5.0 Watts: a) before and b) during<br>the irradiation. . . . .                                     | 221 |

## LIST OF TABLES

| <u>Table</u> | <u>Page</u>   |
|--------------|---|
| 2.1          | List of SF <sub>6</sub> vibrations and their assignments . . . . . 10   |
| 2.2          | Lifetimes for energy transfer processes of<br>some SF <sub>6</sub> mixtures. . . . . 12   |
| 4.1          | The amount of CH <sub>3</sub> CHO decomposed during<br>irradiation with 12.5 Watts CO <sub>2</sub> laser power<br>for a total exposure of 60 seconds and<br>variable interval exposures. . . . . 73 |
| 4.2          | The average temperature calculated from<br>the reaction of ethylacetate CH <sub>3</sub> CH <sub>2</sub> COOCH <sub>3</sub><br>using known arrhenius parameters . . . . . 76                         |
| 5.1          | The bond dissociation energy of C-I in<br>CH <sub>3</sub> I and the technique utilized in its<br>determination. . . . . 85  |
| 5.2          | IR vibrations of CH <sub>3</sub> I and CD <sub>3</sub> I and<br>their assignments. . . . . 99   |
| 5.3          | Wavenumbers of the characteristic product<br>bands from the decomposition of CH <sub>3</sub> I . . . . . 101  |
| 5.4          | Wavenumbers of the characteristic product<br>bands from the decomposition of CD <sub>3</sub> I . . . . . 102  |
| 6.1          | The IR bands of TMT and their assignments. . . . . 121  |
| 6.2          | Relative rates (signal intensity sec <sup>-1</sup> ) of<br>the reaction of TMT and HMDT at various<br>laser powers . . . . . 124  |
| 6.3          | List of new bands after irradiating a mixture<br>of TMT + SF <sub>6</sub> + D <sub>2</sub> with laser power . . . . . 130   |

|       |  |     |
|-------|--|-----|
| 7.1.a | IR absorption spectrum of TMAL. . . . .  | 142 |
| 7.1.b | Raman absorption spectrum of TMAL. . . . .   | 143 |
| 7.2   | CCl <sub>4</sub> peaks before reaction and the new peaks appearing after 10 minutes irradiation with 7.5 Watts of laser power. . . . .   | 149 |
| 7.3   | IR bands of CHCl <sub>3</sub> before and after 10 minutes irradiation with 5.0 Watts of laser power. . . . .   | 154 |
| 7.4   | IR bands of the new identified compounds and their assignments, appearing after irradiation of a mixture of 3 torr of TMAL, 2 torr of CHCl <sub>3</sub> and 10 torr of SF <sub>6</sub> . . . . . | 155 |
| 7.5   | IR bands of 3 torr CDCl <sub>3</sub> and 10 torr SF <sub>6</sub> before and after 10 minutes irradiation with 5.0 Watts of laser power. . . . .  | 157 |
| 7.6   | <sup>1</sup> H, <sup>19</sup> F and <sup>13</sup> C NMR chemical shift (ppm) for TMAL and DMAF, each in CDCl <sub>3</sub> and CHCl <sub>3</sub> solution . . . . .                               | 165 |
| 7.7   | The integrated area of <sup>1</sup> H and <sup>19</sup> F and ratios for DMAF and CF <sub>3</sub> CH <sub>2</sub> OH. . . . .  | 166 |
| 7.8   | Liquid and gas phase IR bands (cm <sup>-1</sup> ) for DMAF and their assignments with those of reference 20. . . . .   | 169 |
| 7.9   | Elemental analysis of DMAF . . . . .   | 172 |
| 7.10  | IR and Raman bands of DMACl (cm <sup>-1</sup> ) compared with those of reference 24 . . . . .  | 174 |
| 7.11  | First order rate constants of the decomposition of 2 torr of TMA and 10 torr of SF <sub>6</sub> and the laser power . . . . .  | 179 |

|     |   |     |
|-----|---|-----|
| 8.1 | Effect of the pressure of the photosensitizer<br>on the r.f. of the cell. . . . .   | 200 |
| 8.2 | Effects of pressure, laser power, and cell<br>length on the rate of pyrolysis of CH <sub>3</sub> CHO. . .   | 209 |
| 8.3 | Measurements of IR absorbance of CH <sub>3</sub> CHO at<br>1124 cm <sup>-1</sup> , and resonance frequency of the<br>cell, as a function of time. . . . . | 210 |

## CHAPTER 1

### GENERAL INTRODUCTION

The discovery of the laser phenomenon in the sixties has led to great developments in many fields of science. Among the laser's most important applications in chemistry are the promotion of chemical reactions, high temperature production, high resolution spectroscopy, and many others. Among the applications of lasers in promoting chemical reactions are several different types: photolytic reactions (usually with visible or UV lasers), very fast pulsed studies, selective reactions (usually related to isotope separation), multiphoton infrared dissociation, and photosensitised infrared laser reactions. This last category, usually carried out in the gas phase and called Laser Powered Homogeneous Pyrolysis (LPHP), is the subject of this thesis.

The most significant factors in using a laser to induce thermal chemical reactions are:

- 1) Energy can be delivered directly to the target molecule, rather via hot walls as in a heated cell.
- 2) Monitoring of the reaction in progress is generally rather easier, using infrared spectroscopy or other techniques.
- 3) Only small amounts of sample and simple equipment are needed.
- 4) Very sensitive and complex compounds can be studied.

The main objectives of this study were to use a continuous wave IR CO<sub>2</sub> laser to induce chemical reactions, and to use and develop spectroscopic and other methods to follow and examine the kinetics and the mechanism of laser induced reactions. The latter methods include IR, Raman, NMR, solid state IR diode laser, photoacoustic spectroscopy and cryscopic measurements. The results of this study are presented in the following eight chapters.

#### Chapter 2.

In this chapter, the relevant theoretical background

for the Laser Powered Homogeneous Pyrolysis (LPHP) technique and a brief review of the applications of lasers are outlined. It also discusses the photosensitization effects, the measurements of the rate constants of the reactions and the applicability of the photoacoustic technique to reactive systems.

### Chapter 3.

Here, the nature and the specifications of some important equipment used in this study are described. The experimental settings, the chemical reagents and the description of each cell used in the experiments in this chapter are also included.

### Chapter 4.

This chapter covers: the study of temperature distribution in the reaction cell which is induced by the IR CO<sub>2</sub> laser; a review of previous studies; a model for temperature distribution produced by the LPHP technique; methods such as chemiluminescence, chemical standards and spectroscopy to measure the temperature and its geometry in the reaction cell; and the study of diffusion effects on the reaction.

### Chapter 5.

In this chapter, the mechanism of the reaction of CH<sub>3</sub>I and CD<sub>3</sub>I and their mixtures using the LPHP technique was investigated. Experiments with these compounds were conducted in order to gain some practical experience for subsequent usage of the technique.

### Chapter 6.

Here, the reactions of (CH<sub>3</sub>)<sub>4</sub>Sn and (CH<sub>3</sub>)<sub>3</sub>SnSn(CH<sub>3</sub>)<sub>3</sub>, which can be used in many optical and electronic applications, induced by the LPHP technique were examined. An attempt was made to understand the mechanism of the reactions of the above mentioned compounds using isotope labelling of the products.

### Chapter 7.

In this chapter, the decomposition of trimethyl aluminium (TMAL), which has useful applications in optics and electronics, using the LPHP technique was examined by Fourier Transform Infrared (FTIR) spectroscopy.

An attempt was made to follow the reaction by FTIR during laser pyrolysis, by monitoring perpendicularly to the laser beam. In addition, radical traps such as  $\text{CCl}_4$ ,  $\text{CHCl}_3$ , and  $\text{CDCl}_3$  were added to the system in order to identify short-lived intermediates in the reaction.

The effects of carrier gases such as  $\text{H}_2$  and  $\text{D}_2$  on the reaction of TMAL were tested too. The findings of this chapter are described in a paper published by Atiya et al. (J. Organomet. Chem. 378 (1989) 307).

### Chapter 8.

This chapter describes the utilization of the photoacoustic spectroscopy method to study chemical reactions. This method is known to be a powerful tool to examine energy pathways and to obtain thermochemical data using the phase shift or the amplitude of the photoacoustic signal.

This chapter introduces a new photoacoustic technique to follow and examine chemical reactions based on the change in the resonance frequency (r.f.) of the cell. Different photoacoustic cells were designed to study this phenomenon. The affect of volume of the cell, the composition of the cell, the laser power, the amount of the photosensitizer and the modulation of the laser radiation on the r.f. of the cell were investigated. The new frequency dependent photoacoustic technique was used on reactive and unreactive systems, and its results were found to be comparable with the IR results using the FTIR spectrometer. This work has been patented ( British Patent Application No. 8904808.6).

### Chapter 9.

This chapter contains a summary of the conclusions.

## CHAPTER 2

### THEORETICAL BACKGROUND

#### 2.1 INTRODUCTION

In this chapter the relevant theoretical background to the following chapters is outlined. Firstly, the technique of Laser Powered Homogeneous Pyrolysis (LPHP), the mechanism of the photosensitization technique, and the measurement of Arrhenius parameters, are described.

Secondly, the photoacoustic technique, including the basis and the mechanism of technique, the derivation of the relevant equations, and the measurement of the rates of reactions are discussed.

Finally the advantages and disadvantages of the above mentioned techniques are presented.

#### 2.2 THE LASER POWERED HOMOGENEOUS PYROLYSIS (LPHP) TECHNIQUE

The infrared CO<sub>2</sub> laser has been widely used as a source of energy to induce chemical reactions,<sup>1-3</sup> and has useful applications in industry and other fields. The most important properties of this laser are: 1) it can be tuned to several wave numbers between 9 and 11  $\mu\text{m}$  ( $\sim 900\text{-}1100\text{ cm}^{-1}$ ) with narrow bandwidth ( $\sim 0.03\text{ cm}^{-1}$ ) for both pulsed and continuous wave operation and 2) it can produce very high power. These increase the opportunity for using many reactants, e.g. CCl<sub>3</sub>H, CCl<sub>3</sub>D, SF<sub>6</sub>, S<sub>2</sub>F<sub>10</sub>, SiF<sub>4</sub>, BCl<sub>3</sub>, and NH<sub>3</sub>,<sup>4,5</sup> whose strongest absorptions lie in the same region as the CO<sub>2</sub> laser. These compounds have a significant vapour pressure and strong IR absorption and therefore interact with the CO<sub>2</sub> laser radiation

at their characteristic absorption wavelength. The energy deposited in a specific vibrational mode is very rapidly distributed among other vibrational modes<sup>6,7</sup> in a time scale depending on the characteristics of the compound. The excited molecules normally lose their energy in numbers of different mechanisms<sup>8-10</sup>: emission, and vibrational and translational transfer of energy to other nonexcited molecules.

The efficiency of the vibrational energy transfer processes has been found to depend on the nature and energies of the vibrational states and the transition moments of the species involved. It has been generally accepted that near resonant processes (so called because the energy defect or energy converted to translation or rotation is small) are caused by long range attractive forces while short range repulsive interactions are believed to cause the energy transfer processes with large energy defects.<sup>11-13</sup>

At reasonably high pressures (~10-100 torr) collisional relaxation occurs much faster than any chemical reaction, as well as the intramolecular relaxation. Under these conditions the CO<sub>2</sub> laser excitation is not very different from thermal heating. Thus laser methods can be used for studying thermal chemical reactions. In such studies the reaction may be induced by direct or sensitized excitation.

One of the compounds, which is widely used as a very strong absorber of the CO<sub>2</sub> laser radiation, is SF<sub>6</sub> (the photosensitizer). The behaviour of the latter with CO<sub>2</sub> laser radiation has been widely studied.<sup>14-20</sup>

The interaction of this molecule (SF<sub>6</sub>) and the laser radiation has been the object of many studies. Many effects,

including saturation, infrared-infrared double resonance, self induced transparency and induced fluorescence, have been observed. The results yielded from collisionless multiphoton dissociation of SF<sub>6</sub> under intense CO<sub>2</sub> laser radiation have led to even greater interest in this molecule. SF<sub>6</sub> has 15 vibrational degrees of freedom, which result in six fundamental vibrational modes. Of these, it is the  $\nu_3$  S-F stretching vibration near 948 cm<sup>-1</sup> which absorbs the CO<sub>2</sub> laser radiation; the remaining fundamental vibrational modes of SF<sub>6</sub> lie below  $\nu_3$  in energy.<sup>21,22</sup> The processes of V-V and V-T,R energy transfer in the lower vibrational states of SF<sub>6</sub> have been well investigated by infrared fluorescence, double resonance and ultrasonic absorption studies.<sup>6,10,14,23-26</sup> On the other hand, the analysis of the fluorescence at wavelengths between 10  $\mu$ m and 16  $\mu$ m following absorption of a short CO<sub>2</sub> laser radiation pulse has shown that the  $\nu_3$  mode pumped by the laser equilibrates directly with the ground state via V-T,R relaxation at a much slower rate. An interesting result of V-T,R relaxation in SF<sub>6</sub> is that the values measured from fluorescence and double resonance are reasonably comparable, but both are about 3.5 times faster than that yielded from the ultrasonic measurements. This is because the high excitation in the laser experiments leads to a nonlinear coupling between the lowest vibrational state and the states probed in the fluorescence and double resonance studies. The bulk thermal measurements<sup>27</sup> (shock-wave and ultrasonic densitometric measurements) are sensitive to the total vibrational energy, which at modest temperature consists mostly of contributions from the lowest frequency modes.

Measurements using laser induced fluorescence have shown the total fundamental fluorescence intensity emitted from the  $\nu_4$  mode at  $614\text{ cm}^{-1}$  is directly proportional to the energy in the mode as a consequence of the interaction of the  $\text{CO}_2$  laser radiation. Thus it is not surprising that the spectroscopic results differ from those obtained by the bulk thermal methods.<sup>27,28</sup>

The nature and behaviour of molecules in highly excited states cannot necessarily be predicted by their behaviour in lower excited states. Recently published papers<sup>29-31</sup> indicate that collisionless processes become important in redistribution of vibrational energy when  $\text{SF}_6$  is highly excited, even though the vibrational relaxation in  $\text{SF}_6$  excited with a lower power of  $\text{CO}_2$  laser is dominated by collision processes.<sup>6,10,23,32</sup> For polyatomic molecules, very little information is available on reactions of vibrationally excited molecules.

Numerous experimental and theoretical studies demonstrate collisionless and isotopically selective multiphoton excitation and dissociation in  $\text{SF}_6$ . Recently, significant progress has been made in characterising a mechanism for these types of processes. But the essential aspects of the molecular structure that makes this event possible have not been fully identified.<sup>1,33,34</sup>

Most of the experimental and theoretical studies on multiphoton absorptions of IR radiation have concentrated on the nature of the initial vibrational excitation states, that is the route by which a molecule absorbs the first two to five photons before reaching its vibrational quasicontinuum (in the

quasicontinuum region the density of states of the  $\text{SF}_6$  is sufficiently high such that the absorption spectrum becomes effectively continuous)<sup>35</sup>. In fact, that is very important for the isotopic selectivity of multiphoton dissociation in molecules, as the isotopic shift is small. The problem here is that the anharmonicity of the vibrations (which displace to longer wavelength for higher  $(n\nu_3 \rightarrow (n+1)\nu_3$  transitions) subsequently becomes out of resonance with the incident laser frequency. Many studies have failed to give an answer to such phenomena.<sup>34,36,37</sup> Theoretical consideration of the  $\nu_3$  mode of  $\text{SF}_6$  shows for  $n \geq 2$  the degenerate  $n\nu_3$  levels will be split by anharmonic coupling, which are calculated to cause a nearly resonant pathway for  $\text{CO}_2$  laser photons up to  $n = 5$ ,<sup>38,39</sup> even though that is not consistent with recent observations on the overtone absorption spectra of  $\nu_3$  mode.<sup>40,41</sup>

These types of processes (multiphoton absorption and dissociation reactions) seem to be restricted to molecules which have strong absorption. Hence, the selectively excited molecules may react at an accelerated rate, as a result of multiphoton absorption.<sup>42</sup> In cases where the molecule is transparent to the incident laser, direct excitation cannot be possible for laser induced reaction, but the reaction can be promoted using a sensitizer, which strongly absorbs the incident laser radiation.

The  $\nu_3$  is the mode of  $\text{SF}_6$  IR region spectrum which interacts with  $\text{CO}_2$  laser radiation ( $948 \text{ cm}^{-1}$ ),<sup>43,44</sup> see Figure 2.1 and Table 2.1. This photosensitizer has a very strong absorption coefficient ( $\alpha = 0.5 \text{ torr}^{-1} \text{ cm}^{-1}$ ) at  $948 \text{ cm}^{-1}$  for the P20  $\text{CO}_2$  laser line. At the P20 line the maximum

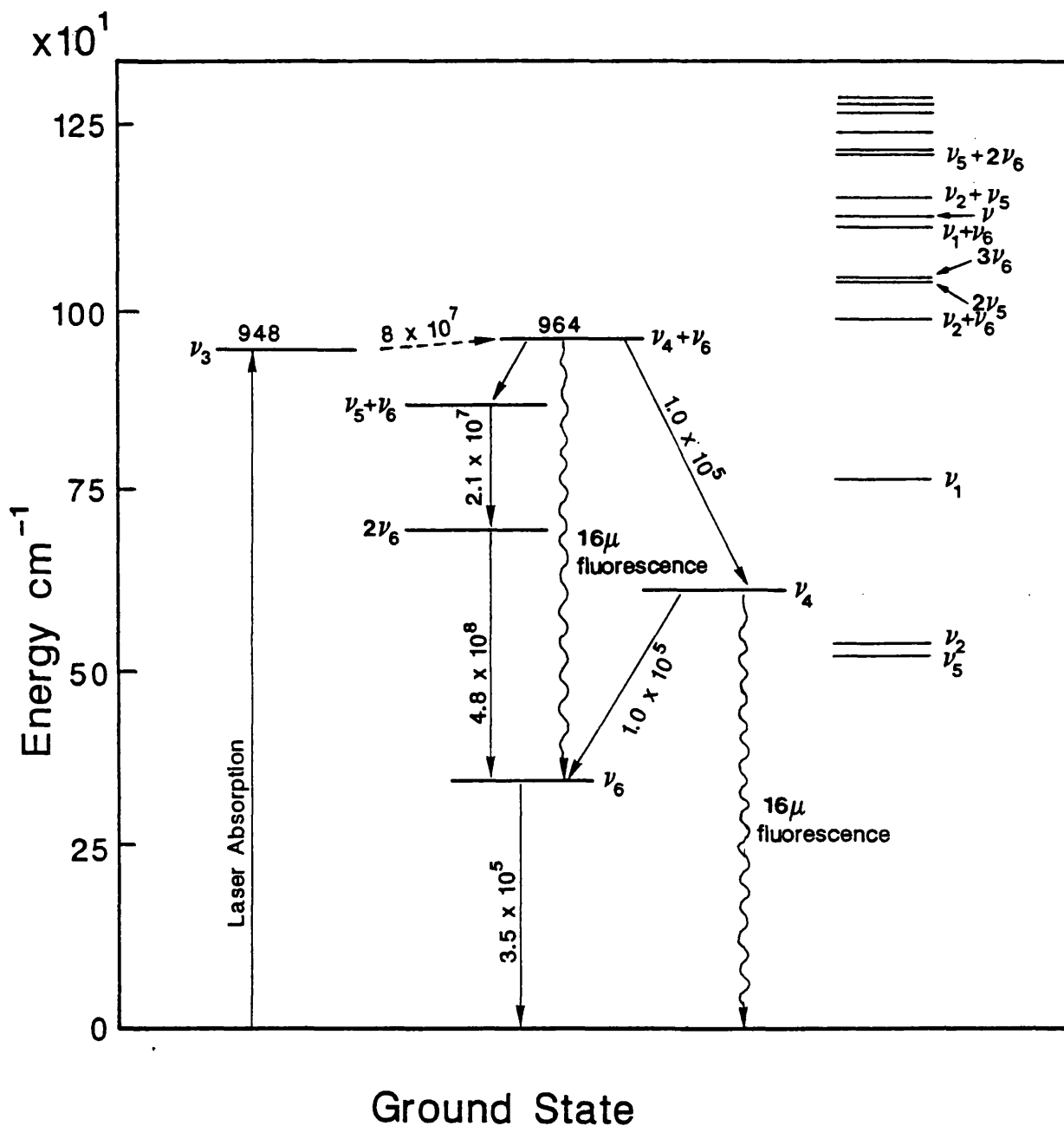


Figure 2.1:

Partial energy distribution pathways among various energy levels of  $\text{SF}_6$ ; the wavy arrows represents the radiation emission, and straight arrows are the energy pathways.

Table 2.1:

List of SF<sub>6</sub> vibrations and their assignments.

---

| frequency (cm <sup>-1</sup> ) | mode assignment |
|-------------------------------|-----------------|
| 350                           | $\nu_6$         |
| 522                           | $\nu_5$         |
| 540                           | $\nu_2$         |
| 614                           | $\nu_4$         |
| 700                           | $2\nu_6$        |
| 770                           | $\nu_1$         |
| 872                           | $\nu_5+\nu_6$   |
| 948                           | $\nu_3$         |
| 964                           | $\nu_4+\nu_6$   |
| 990                           | $\nu_2+\nu_6$   |
| 1044                          | $2\nu_5$        |
| 1050                          | $3\nu_6$        |
| 1120                          | $\nu_1+\nu_6$   |
| 1136                          | $\nu_4+\nu_5$   |
| 1162                          | $\nu_2+\nu_5$   |
| 1222                          | $\nu_5+2\nu_6$  |
| 1228                          | $2\nu_4$        |
| 1254                          | $\nu_2+\nu_4$   |
| 1280                          | $2\nu_2$        |
| 1292                          | $\nu_1+\nu_5$   |
| 1298                          | $\nu_3+\nu_6$   |

---

power of the  $\text{CO}_2$  laser can be obtained.  $\text{SF}_6$  also has a very fast vibrational relaxation time of  $\mu\text{secs}$ ,<sup>15,16</sup> (see Table 2.2).  $\text{SF}_6$  also is chemically stable. Therefore, this compound acts as a vehicle for absorption of CW  $\text{CO}_2$  laser radiation in circumstances where the reactants are transparent, generating a controlled inhomogeneous temperature bath from 500 to 1500 K.<sup>45</sup> For high pressure systems (above 10 torr), excitation using pulse or continuous wave irradiation can lead to a very close to a thermal system. So, it is valuable to study such systems, to investigate the induced chemical reactions and any special behaviour under such system conditions.<sup>46</sup>

Several workers have attempted to study the temperature distribution profile produced in the reaction cell using various methods. Special assumptions were used in these studies; for example, the induced laser beam intensity was assumed to be uniform, the absorption coefficient of the photosensitizer was assumed not to vary with temperature, the variation of the density of the gas absorber was ignored, or heat convection effects were neglected<sup>4,47-54</sup>. Obviously, the calculations based on the above assumptions do not give the correct results for the temperature distribution profile in the reaction cell. An attempt to measure the temperature distribution in such systems is described in Chapter 4.

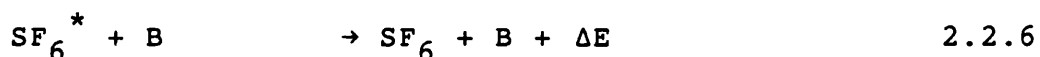
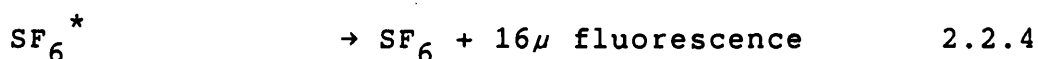
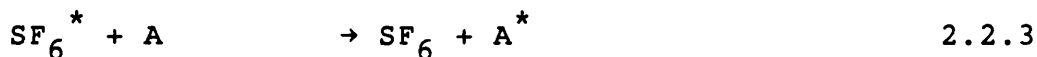
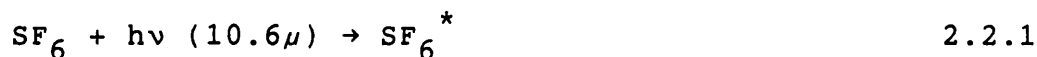
Since  $\text{SF}_6$  has a very strong absorption of the  $\text{CO}_2$  laser radiation, it can be pumped by the laser to upper energy levels. The excited molecule can transfer its energy by Vibrational-Vibrational (V-V), Vibrational-Rotational (V-R) and Vibrational-Translational (V-T) transfer of energy. This energy can be transferred to another molecule within  $\mu\text{secs}$  as

Table 2.2:

Lifetimes for Energy Transfer Processes of Some SF<sub>6</sub> Mixtures.

| Process  | ( $\mu$ Sec torr) | Reference |
|--|-------------------|-----------|
| V-V transfer SF <sub>6</sub> + He                                | 1.9               | 6         |
| V-V transfer SF <sub>6</sub> + Ar                                | 3.6               | 6         |
| V-V transfer SF <sub>6</sub> + Kr                                | 4.0               | 6         |
| V-V transfer SF <sub>6</sub> + Xe                                | 3.3               | 6         |
| V-V transfer SF <sub>6</sub> + SF <sub>6</sub>                   | 1.1               | 6         |
| V-V transfer SF <sub>6</sub> + SF <sub>6</sub>                   | 1.51              | 10        |
| V-V transfer SF <sub>6</sub> + SF <sub>6</sub>                   | 0.75              | 10        |
| V-T transfer SF <sub>6</sub> + He                                | 41.00             | 11        |
| V-T transfer SF <sub>6</sub> + Ne                                | 194.00            | 11        |
| V-T transfer SF <sub>6</sub> + Kr                                | 3040.00           | 11        |
| V-T transfer SF <sub>6</sub> + (CH <sub>3</sub> ) <sub>2</sub> O | 5.3               | 11        |
| V-T transfer SF <sub>6</sub> + CH <sub>3</sub> Br                | 14.0              | 11        |
| V-T transfer SF <sub>6</sub> + CHF <sub>2</sub> Cl               | 19.0              | 11        |
| V-T transfer SF <sub>6</sub> + H <sub>2</sub>                    | 9.3               | 11        |
| V-T transfer SF <sub>6</sub> + N <sub>2</sub>                    | 103.0             | 11        |
| V-T transfer SF <sub>6</sub> + Cl <sub>2</sub>                   | 80.00             | 11        |
| V-T transfer SF <sub>6</sub> + CH <sub>4</sub>                   | 20.00             | 11        |
| V-T transfer SF <sub>6</sub> + SF <sub>6</sub>                   | 122.00            | 60        |

shown in the scheme below:



where  $\text{SF}_6^*$  is the excited molecule of  $\text{SF}_6$ , A is the reactant,  $\text{A}^*$  is the excited molecule of the reactant, B is the product of the induced reaction and  $\Delta E$  is the energy released from the reaction and the deactivation process with  $\text{SF}_6$  and B.

The molecule undergoes decomposition if the transferred energy to the reactant is high. Here, a very high temperature bath is created and the reaction occurs in the incident laser beam zone under homogeneous conditions.

The reaction 2.2.1 is the first step in the above outlined scheme in which the  $\nu_3$  mode of  $\text{SF}_6$  is pumped to an excited energy level to give the energetic species  $\text{SF}_6^*$ .<sup>20</sup> The excited molecule of  $\text{SF}_6$  can lose its energy through different pathways as in the steps 2.2.2, 2.2.3, 2.2.4 and 2.2.6. In the last, products (B) which appear during the reaction in the cell contribute to the deactivation process of the  $\text{SF}_6^*$ . If B

is a very light molecule, eg,  $H_2$ , this can lead to an increased rate of energy transfer throughout the cell. Consequently, the conductivity of the cell contents is increased, lowering the maximum temperature achieved and slowing down the reaction dramatically.

### 2.3 MEASUREMENT OF THE RATE OF THE REACTION

The measurement of the rate of the reaction of the experiments in the following chapters are based on applying IR spectroscopy to measure the concentration of the reactants and the products.

If the starting material has an absorption which is very weak (compared to 100% absorption, Figure 2.2), the Beer-Lambert law can be applied as follows:

$$dI/dl \propto l C \quad 2.3.1$$

$$\log I = \epsilon l C \quad 2.3.2$$

where  $I$  is the intensity of the IR radiation,  $l$  is the cell length, and  $\epsilon$  is the absorption coefficient of the sample. Since

$$I = I'/I'_a \quad 2.3.3$$

where  $I'$  is the intensity of the absorbed radiation and  $I'_a$  is the nonabsorbed radiation, then

$$\log I'/I'_a = \epsilon l C \quad 2.3.4$$

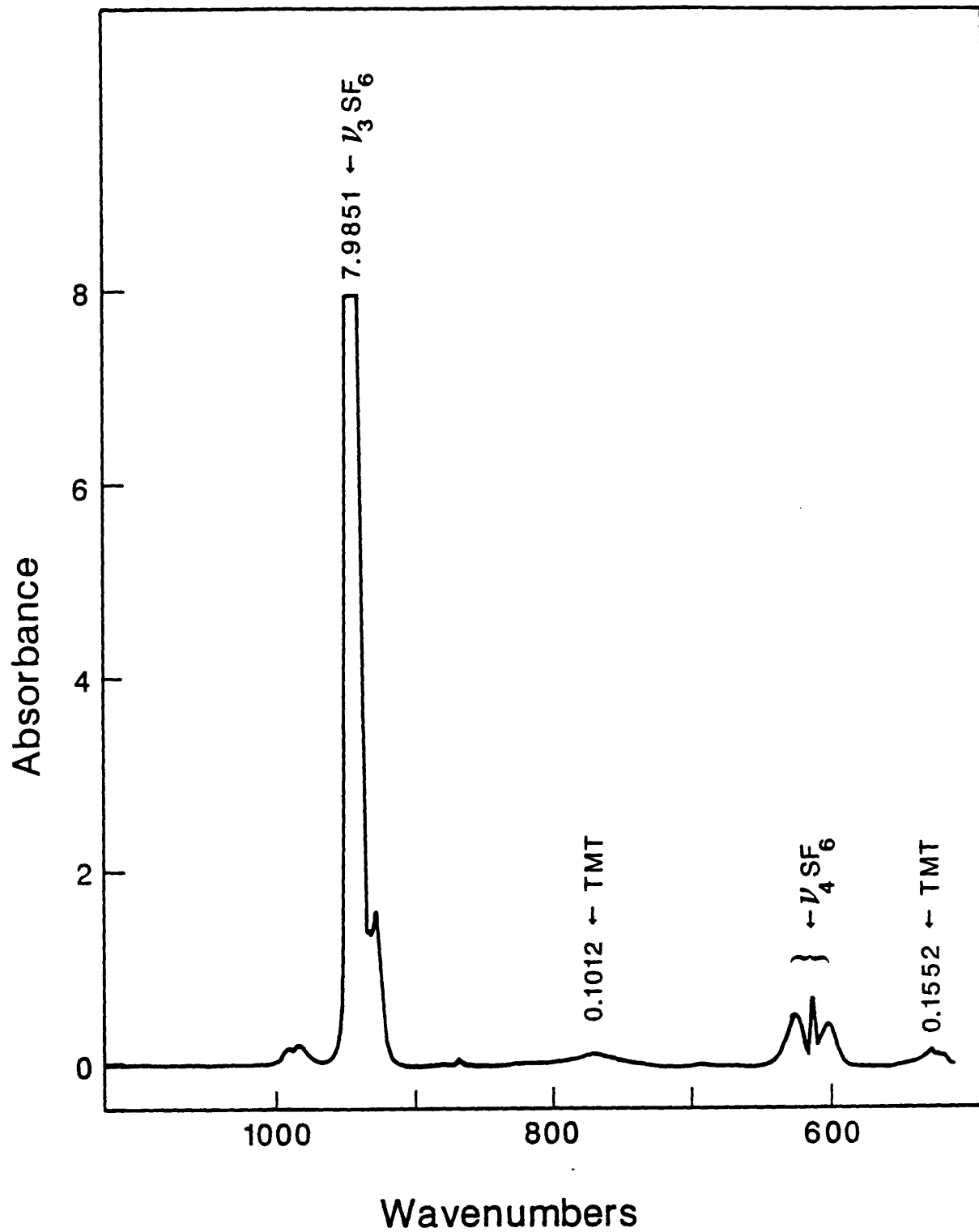


Figure 2.2:

FTIR spectrum of 2 torr  $(\text{CH}_3)_4\text{Sn}$  and 10 torr  $\text{SF}_6$ ; the spectrum reveals the strongest bands for both compounds and their relative intensities.

where  $I' = I - I'_a$ .

Equation 2.3.4 then can be written as follows:

$$\log \left( \frac{I - I'_a}{I'} \right) = \epsilon l C \quad 2.3.5$$

If  $I'_a$  is very weak, then  $I' = I$ , and Equation 2.3.5 can be written as follows:

$$\log (1 - I'_a/I') = - \epsilon C l \quad 2.3.6$$

but  $\ln (1 - X) = -X$  if  $X \ll 1$  then Equation 2.3.6 becomes:

$$I'_a/I' \approx 2.303 \epsilon C l \quad 2.3.7$$

where  $I'_a \approx C$  which is true only when  $I'_a \ll I$ , and the intensity of the IR spectra of the reactants or the products is proportional to the concentration. In the experiments described here, pressures are sufficiently low that this approximation is quite good.

Since the concentrations are monitored in the absence of laser radiation, it is essentially the average concentration in the cell that is measured. Russell<sup>55</sup> has shown that in the  $\text{SF}_6$  photosensitized system, diffusion is sufficiently fast that the rate of change of this average concentration is governed by the rate constant of the reaction averaged over the temperature distribution of the cell. Thus, for a first order reaction, for example

$$\ln(c_{av}) = - k_{av} t \quad 2.3.8$$

where  $k_{av} = (1/V) \int k(r) dr$  2.3.9

V being the volume of the cell. Since k depends on the position in the cell because of the temperature variation, measurement of kinetic parameters (eg, activation energies) requires a knowledge of this temperature distribution.

## 2.4 THE ADVANTAGES AND DISADVANTAGES OF THE PHOTSENSITIZATION TECHNIQUE

The major advantages and disadvantages of utilisation of the photosensitization technique for inducing chemical reactions are as follows:

1. the use of small amounts of sample, which is very important for kinetic measurements, especially of expensive materials,
2. very simple equipment can be used for this type of investigation,
3. the temperature path of the reaction can be well controlled, and a high temperature is produced in a time scale of  $\mu$ secs, and
4. the contribution of the surface of the reaction vessel to the reaction is negligible, since the reaction occurs in the center of the vessel.

The disadvantages of this technique are: (1) the heat capacity and conductivity of the reaction cell may change during the reaction because of the presence of new compounds, altering the conditions, and (2) the temperature bath produced by the CO<sub>2</sub> laser varies throughout the reaction cell. The first

problem can be avoided, firstly by using a small amount of the sample, and also by using the initial rate for the kinetic measurements. The variation of the temperature over the cell of the reaction can be measured as discussed in Chapter 4.

## 2.5 THE PHOTOACOUSTIC TECHNIQUE

In 1880 Alexander Graham Bell observed that acoustic waves (sound) can be produced by exposing an absorbing gas in a constant volume container to an intense modulated IR radiation. He explained that part of the radiation is absorbed by the gas, raising the temperature and hence the pressure in the constant volume enclosure. A periodic modulation of the incident intensity thus produces an alternating pressure component which becomes audible for proper choices of the experimental parameters. Bell also mentioned the possibility of using the effect to investigate the absorption spectra of gases; he proposed a spectrophone, an instrument constructed for this purpose.<sup>44,56</sup> This process was interpreted in detail after the molecular theory was invented.<sup>57</sup> When molecules absorb radiation the energy absorbed appears as quanta of vibrational energy (excited to upper energy levels). The excited molecules may lose the energy taken up; (i) by spontaneous emission of radiation, (ii) induced emission or (iii) by transfer of energy to kinetic translational energy. This last process occurs in collisions, when the vibrational energy is transferred to translational energy<sup>15</sup>; an increase in the kinetic energy means the gas will heat and reach a new temperature. If the gas is irradiated by a cw CO<sub>2</sub> laser, which is interrupted periodically (chopped mechanically or modulated), it will heat and cool,

subsequently a periodic change of pressure will be observed in a constant volume system. Since the pressure periodically changes, acoustic waves are generated which can be detected by means of a microphone.

## 2.6 COMPOSITION MEASUREMENTS USING PHOTOACOUSTIC TECHNIQUE

In most previous applications of photoacoustic technique, either the amplitude and the phase difference of the photoacoustic phenomena were employed for various purposes.

Launey et. al.<sup>58</sup> found the dependence of resonance frequency (r.f.) on the thermodynamic and transport properties of the buffer gas, and molecular weight of the buffer gas.

The resonance frequency r.f. of a cylindrical cell containing a binary gas mixture is given by<sup>59</sup>:

$$f_{mnp} = v_s/2 [(\alpha_{mn}/r)^2 + (p/l)^2]^{1/2} \quad 2.6.1$$

Where  $f_{mnp}$  is the frequency at which the acoustical modes occur. The subscripts values refer to the radial, azimuthal, and longitudinal modes respectively;  $r$  is the radius,  $l$  is the length of the cell,  $\alpha_{mn}$  is the  $m$ th zero of the derivative of the Bessel function  $dJ_n(\pi\alpha)/d\alpha$ , and  $v_s$  is the sound velocity in a mixture of ideal gases which is given as below:

$$v_s = (\gamma RT/M)^{1/2} \quad 2.6.2$$

Here,  $R$  is the ideal gas constant,  $\gamma$  is the effective specific heat ratio, and  $M$  is the average molecular weight for the mixture. The specific heat ( $\gamma$ ) and the average molecular weight

of the mixture (M) can be calculated as below:

$$\gamma = (\chi C_p^b + (1-\chi)C_p^a) / (\chi C_v^b + (1-\chi)C_v^a) \quad 2.6.3$$

$$M = \chi M^b + (1-\chi)M^a \quad 2.6.4$$

Here,  $C_p^b$ ,  $C_v^b$ ,  $C_p^a$  and  $C_v^a$  are the heat capacity of the reactant and the absorbing gas respectively,  $M^b$ , and  $M^a$  are their molecular weights, and  $\chi$  is the mole fraction of the reaction gas in the cell.

From Equation 2.6.1, it can be seen that the acoustic resonance frequency is determined by the combined properties of reactant and the photosensitizer, as well as the products. If the temperature and the pressure of the cell are assumed to be constant, then from the equations (2.6.1) and (2.6.2) we can get:

$$f = C 1/\sqrt{\gamma/M} \quad 2.6.5$$

where C in this case represents a combination of constants, obtained from the graph of the Equation 2.6.5. From this equation (2.6.5), if the reaction is assumed to be producing known products, then the concentration could be calculated. In Chapter 8, measurements using this novel technique are described.

## 2.7 THE ADVANTAGES AND DISADVANTAGES OF THE PHOTOACOUSTIC TECHNIQUE

The advantages of this technique are:

1. The measurement of r.f. is not affected by turbulence phenomena.
2. Can be used for measuring the heat capacity of gaseous systems.
3. Can be used to follow reactions which give known products.

The disadvantage of this technique is that the r.f. is affected when the temperature and the heat capacity of the system are changed.

## 2.8 REFERENCES

1. P.A. Schulz, A. S. Sudbø, D. J. Krajnovich, H. S. Kwok, Y. R. Shen and Y. T. Lee.  
Ann. Rev. Phys. Chem. 30 (1979) 379.
2. R. N. Zitter, D. F. Koster, A. Cantoni, and J. Pleil.  
Springer ser. Chem. Phys. 6 (1979) 277.
3. J. Tardieu De Maleissye, F. Lempereur, C. Marsal and R. I. Ben-Aim.  
Chem. Phys. Lett. 42 (1976) 46.
4. C. Steel, V. Starov, R. Leo, P. John and R. G. Harrison.  
Chem. Phys. Lett. 62 (1979) 121.
5. J. D. Campbell, G. Hancock, J. B. Halpern and K. H. Welge.  
Chem. Phys. Lett. 44 (1976) 404.
6. J. Thomas Knudtson and George W. Flynn.  
J. Chem. Phys. 58 (1973) 1467.
7. V. N. Bagratashvili, Yu. G. Vainer, V. S. Dolzhikov, S. F. Kol'yakov, V. S. Letokhov, A. A. Makarov, L. P. Malyavkin, E. A. Ryabov, E. G. Sil'kis and V. D. Titov.  
Sov. Phys. JETP 53 (1981) 512.
8. R. D. Dates Jr., G. W. Flynn, J. T. Knudtson and A. M. Ronn.  
J. Chem. Phys. 53 (1970) 3621.
9. H. J. Bauer, F. D. Shields, and H. E. Bass.  
J. Chem. Phys. 57 (1972) 4624.
10. R. D. Bates Jr., J. T. Knudtson, G. W. Flynn and A. M. Ronn.  
Chem. Phys. Lett. 8 (1971) 103.

11. J. I. Steinfeld, I. Burak, D. G. Sutton, and A. V. Nowak.  
J. Chem. Phys. 52 (1970) 5421.
12. Tadashi Aoki and Mikio Katayama.  
Jap. J. Appli. Phys. 10 (1971) 1303.
13. Kenneth M. Beck and Robert J. Gordon.  
J. Chem. Phys. 87 (1987) 5681.
14. M. Dilonardo, M. Capitelli and C. D. Cantrell.  
Chem. Phys. 101 (1986) 337.
15. J. Stone, M. F. Goodman and D. A. Dows.  
Chem. Phys. Lett. 44 (1976) 411.
16. J. G. Black, Eli Yablonovitch, N. Bloembergen and S.  
Mukamel.  
Phys. Rev. Lett. 38 (1977) 1131.
17. W. Fuss and J. Hartmann.  
J. Chem. Phys. 70 (1979) 5468.
18. R. N. Schwartz, Z. I. Slawsky and K. F. Herzfeld.  
J. Chem. Phys. 20 (1952) 1591.
19. R. D. Sharma and C. A. Brau.  
Phys. Rev. Lett. 19 (1967) 1273.
20. R. D. Sharma and C. A. Brau.  
J. Chem. Phys. 50 (1969) 924.
21. S. Abramowitz and I. W. Levin.  
J. Chem. Phys. 44 (1966) 3353.
22. V. V. Bertsev, T. D. Kdomiitseva, and N. M. Tsyganenko.  
Spectrosc. 37 (1974) 263.
23. R. D. Bates, Jr, J. T. Knudtson, G. W. Flynn and A. M.  
Ronn.  
J. Chem. Phys. 57 (1971) 4174.
24. I. Burak, A. V. Nowak, J. I. Steinfeld and D. G. Sutton.

- J. Chem. Phys. 51 (1969) 2275.
25. J. D. Lambert, D. G. Smith and J. L. Stretton.  
Proc. R. Soc. A, 282 (1964) 280.
26. K. Holmes and M. A. Stott.  
J. Phys. DI (1968) 1331.
27. W. D. Breshears.  
Chem. Phys. Lett. 20 (1973) 429.
28. W. D. Breshears and L. S. Blair.  
J. Chem. Phys. 58 (1973) 2056.
29. D. S. Frankel, Jr. and T. J. Manuccia.  
Chem. Phys. Lett. 54 (1978) 451.
30. T. F. Deutsch and S. R. J. Brueck.  
Chem. Phys. Lett. 54 (1978) 258.
31. T. F. Deutsch and S. R. J. Brueck.  
J. Chem. Phys. 70 (1979) 2063.
32. D. S. Frankel, Jr.  
J. Chem. Phys. 65 (1976) 1696.
33. C. D. Contrell and K. Fox.  
Optics. Lett. 2 (1978) 151.
34. N. Blomberger.  
Opt. Commun. 15 (1975) 416.
35. D. M. Larsen and N. Blomberger.  
Opt. Commun. 17 (1976) 254.
36. N. Blomberger, C. D. Cantrell and D. M. Larsen.  
"Tunable Lasers and Applications", A. Mooradian, T. Tager  
and P. Stokseth, ed. Springer-Verlag, Berlin, 1976.
37. R. V. Ambartzumian, Yu. A. Gorokhov, V. S. Letokhov, G. N.  
Markarov and A. A. Poretzkii.  
JETP Lett. 23 (1976) 266.

38. C. D. Cantrell and H. W. Galbraith.  
Opt. Commun. 18 (1976) 513.
39. C. C. Jensen, W. B. Parson, B. J. Krohn and J. Overend.  
Opt. Commun. 20 (1977) 275.
40. H. Kildal.  
J. Chem. Phys. 67 (1977) 1287.
41. J. R. Ackerhalt, H. Flickerm, H. W. Galbraith, J. King and  
W. B. Preson.  
J. Chem. Phys. 69 (1978) 1461.
42. G. Koren and U. P. Oppenheim.  
Chem. Phys. Lett. 67 (1979) 289.
43. Armstrong J.J.  
Desser. Abstra. Int. 33-B (1972) 191.
44. M. H. Ali.  
Desser. Abstra. Int. 46-B (1986) 4279.
45. W. M. Shaub and Bauer.  
Int. J. Chem. Kinetics VII (1975) 509.
46. P. Kubat and J. Pola.  
Collection Czechoslovak Chem. Commun. 49 (1984) 1354.
47. R. N. Zitter, D. F. Koster, and A. Ringwelski.  
Chem. Phys. 57 (1981) 11.
48. H. Dai, E. Specht and R. Berman.  
J. Chem. Phys 77 (1982) 4494.
49. R. N. Zitter, D. F. Koster, A. Cantoni and J. Pleil.  
Chem. Phys. 46 (1980) 107.
50. R. N. Zitter, D. F. Koster, A. Cantoni and A. Ringwelski.  
High Temp. Sci. 12 (1980) 209.
51. D. F. McMillen, K. E. Lewis, G. P. Smith and D. M. Golden.  
J. Phys. Chem. 86 (1982) 709.

52. S. Ruschin and S. H. Bauer.  
J. Phys. Chem. 88 (1984) 5042.
53. J. P. Holland and R. N. Rosenfeld.  
Chem. Phys. Lett. 145 (1988) 481.
54. J. Zhu and E. Yeung.  
J. Phys. Chem. 92 (1988) 2184.
55. D. K. Russell.  
Unpublished work.
56. Pao Yoh-Han (Optoacoustic Spectroscopy and  
Detection) Academic Press New York 1977.
57. T. L. Cottrell and J. C. McCoubrey.  
(Molecular Energy Transfer in Gases) Butterworths London,  
1961.
58. L. J. Thomas III, M. J. Kelly, and N. M. Amer.  
Appl. Phys. Lett. 32 (1978) 738.
59. P. M. Morse and K. U. Ingard.  
(Theoretical acoustics) McGraw-Hill, New York, 1968).
60. G. L. Connor.  
J. Acoust. Soc. Am. 26 (1954) 361.

CHAPTER 3  
EQUIPMENT AND EXPERIMENTAL DETAILS

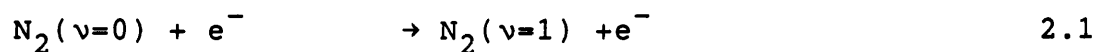
### 3.1 INTRODUCTION

In this chapter the electrical equipment and their specifications utilized in the experimental work are described. A simple description of the cw CO<sub>2</sub> laser action, CO<sub>2</sub> laser realignment, conventional and Fourier Transform IR spectrometers and solid state IR diode laser is also given.

### 3.2 THE CO<sub>2</sub> LASER

The CO<sub>2</sub> laser can be produced by exciting CO<sub>2</sub> molecules to an excited vibrational state (001), Figure 3.1; the molecules then radiatively decay to the levels (100) or (020) emitting IR radiation at wavelengths 10.6 and 9.6 μm, respectively.<sup>1</sup>

This process is only achieved when the CO<sub>2</sub> molecules in the energy level (001) outnumber the CO<sub>2</sub> molecules in the lower state (100) or (020) (population inversion). The population inversion can be achieved by passing an electric discharge through the CO<sub>2</sub> and is found to be more effective if N<sub>2</sub> is mixed with CO<sub>2</sub>. The molecules of N<sub>2</sub> excited by the electric discharge to its energy level v=1 (equation 2.1) transfer their energy:



by resonance collisions to CO<sub>2</sub> (001) level efficiently (Equation 2.2) because the energy level of N<sub>2</sub> v=1 lies very close to the energy level of CO<sub>2</sub> (001) (the transition wavelengths are 4.31 μm for N<sub>2</sub> and 4.29 μm for CO<sub>2</sub>). The excited molecules of CO<sub>2</sub>

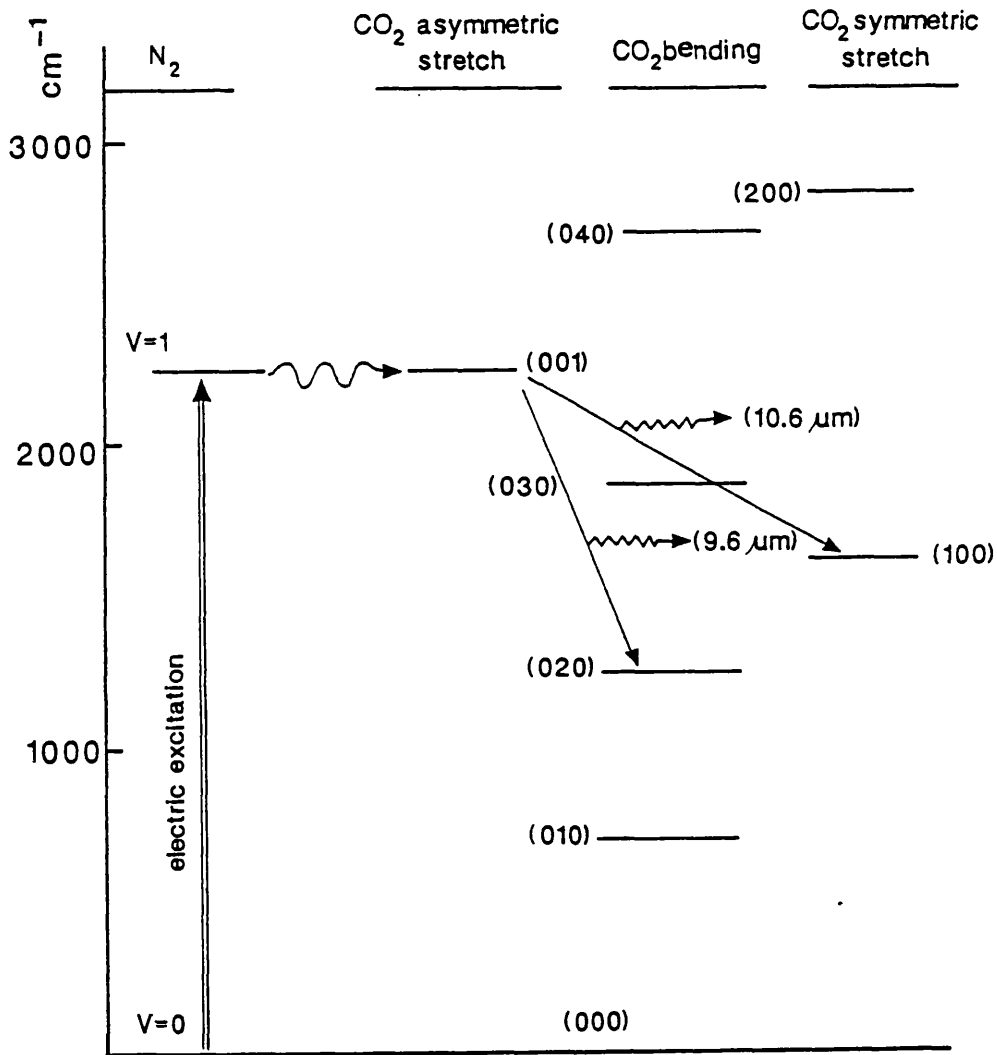
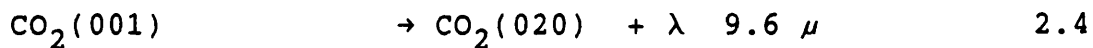
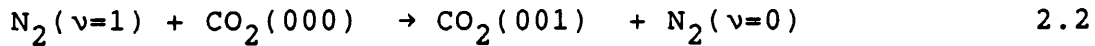


Figure 3.1:

Block diagram of energy levels for the  $\text{CO}_2$  laser. The levels of the three  $\text{CO}_2$  vibrational modes are shown and those for  $\text{N}_2$ . The wavy line shows collisional transfer of energy from  $\text{N}_2(v=1)$  to  $\text{CO}_2(001)$  levels.

then decay as in Equations 3 and 4.



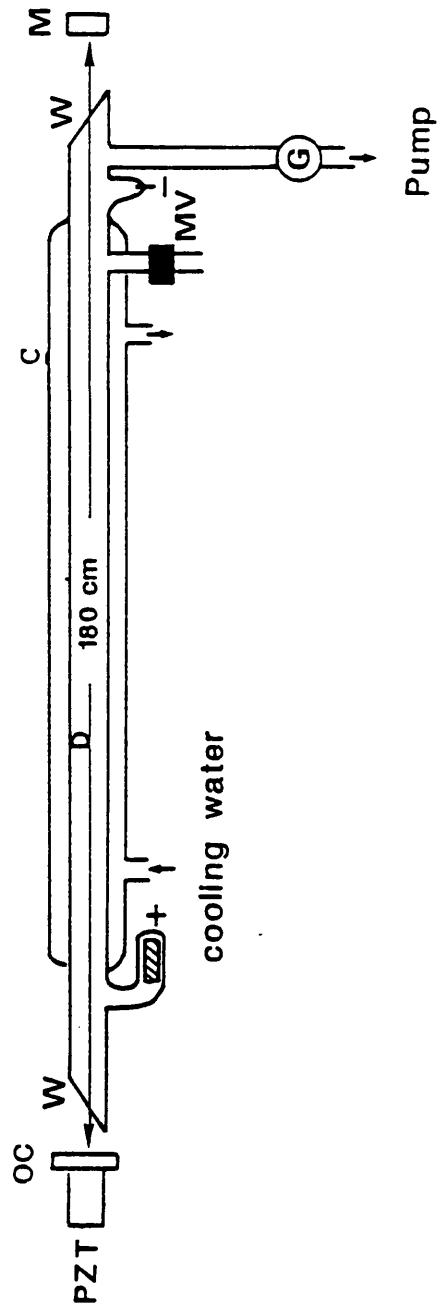
If this action happens between two parallel mirrors spaced at an integral of the wavelength of the emitted radiation we can get a coherent intense wave of the radiation passing through a semitransparent output mirror, that is, a laser (acronym Light Amplification by Stimulated Emission of Radiation).

### 3.3 DESCRIPTION OF THE CO<sub>2</sub> LASER

The Edinburgh Instruments PL4 CO<sub>2</sub> laser consists of a 130 cm long discharge glass tube (D), (Figure 3.2) sealed with anti reflection coated ZnSe windows (W), which are fully transmitting for IR radiation in the region of 10  $\mu$ . A cavity of length 180 cm with a back mirror (M) and output coupling mirror (OC) is mounted on a piezo-electric (PZT) stack enables cavity tuning and stabilization to be achieved.

A mixture of 9% CO<sub>2</sub>, 13.5% N<sub>2</sub>, and 77.5% He passes through the discharge tube and is pumped out continuously. The electric discharge is produced by a (PS4R) power supply producing current up to 30mA and potential difference up to 30 KV. The continuous flow gas mixture serves to cool the laser gas and remove the impurities and vibrational excited gas, and also discharge products such as CO which may affect the efficiency of the

**Figure 3.2:**  
Schematic diagram showing the CO<sub>2</sub> laser, gas handling, water cooling and the discharge tube.



laser.<sup>2</sup> Further cooling is provided by thermal conduction through the discharge tube walls using a water jacket (C) surrounding the discharge tube.

The pressure inside the discharge tube was controlled by a meter valve (MV) and measured by a gauge (G) which is connected to the outlet of the discharge tube to a rotary pump (Edwards ESM2).

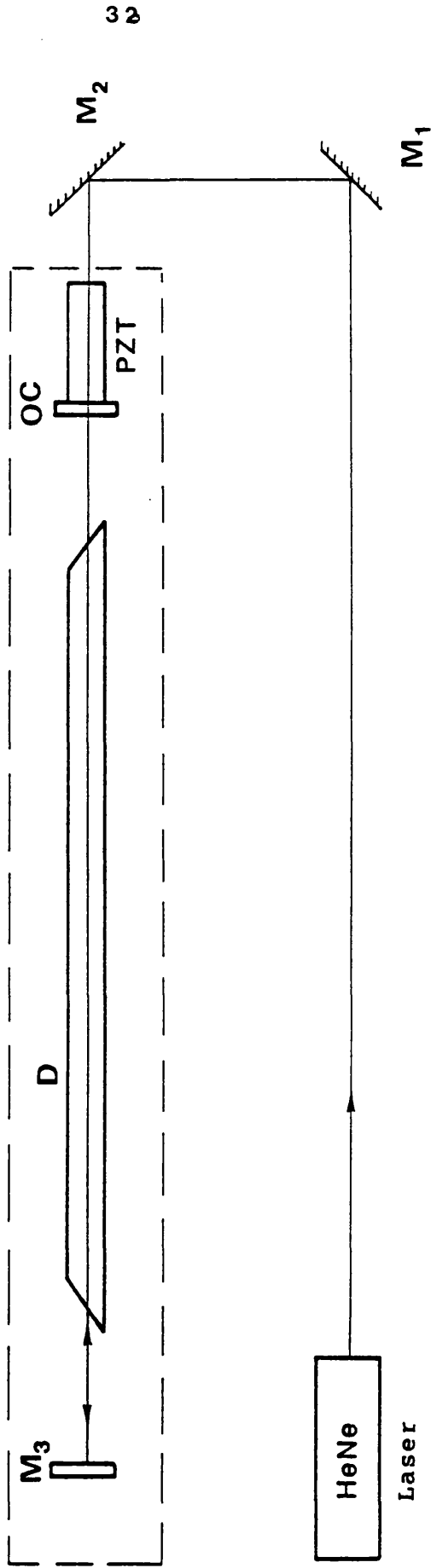
The laser power could be varied continuously from 0.5 to 50 Watts at a wavelength of radiation of 10.59 micron (the P<sub>20</sub> line) by controlling the laser gas and the current supply. The beam diameter is 7.5 mm with beam divergence less than 2 milliradians and mode more than 90% TEM<sub>00n</sub>.

#### 3.4 ALIGNMENT OF CO<sub>2</sub> LASER

After a long period of use of the CO<sub>2</sub> laser, efficiency was found to decrease and the mode of the beam to change. The reason for this is that vibrations in the laboratory caused by pumps or other equipment are found to cause movement of the mirrors, and affect their alignment.

Realignment was carried out using a He-Ne laser. The He-Ne laser beam was adjusted using mirrors m1 and m2 (Figure 3.3) to pass through the output coupler mirror (OC) to the back mirror m3 passing through the center of the discharge tube (D). Then the m3, and (OC) mirrors were adjusted until the He-Ne laser beam reflected back to the He-Ne laser output. Final adjustment was carried out using a power meter and switching on the CO<sub>2</sub> laser to maximize the output power by fine adjustment to the OC and m3 mirrors.

**Figure 3.3:**  
Schematic diagram showing the alignment of CO<sub>2</sub> laser.



### 3.5 IR SPECTROMETERS

Another most important part of our equipment is the IR spectrophotometers, which were used to measure and detect the combination of the reaction mixtures before and after the reaction. Two types of IR spectrometers were used in this study, the Dispersive Conventional IR Spectrometer (DCIRS) which was used initially, and the Fourier Transform IR Spectrometer (FTIRS) which was used later. The DCIRS is based on passing the IR radiation through the sample and a reference beam through the reference; these are then directed toward the monochromator (Figure 3.4), which is usually a prism or grating, and then to the detector. The FTIRS is based on the interference of the IR beam using an interferometer (Figure 3.5). The IR beam is passed through a beam splitter, reflecting 50% of the beam toward a fixed mirror and the other half to a movable mirror. The reflected beam from the fixed mirror is passed through the beam splitter toward the detector, and the reflected beam from the movable mirror is also reflected toward the detector by the beam splitter and combined with the reflected beam from the fixed mirror (the beam splitter reflects and transmits 50% of the reflected beam from the fixed and movable mirrors toward the source respectively). If the two mirrors are the same distance from the beam splitter, then the light beam will exit from the interferometer unchanged but the intensity is reduced to 50%. However if the path length of the movable mirror has changed by one-fourth of the wavelength of monochromatic light, the light will interfere destructively and no light will exit from the

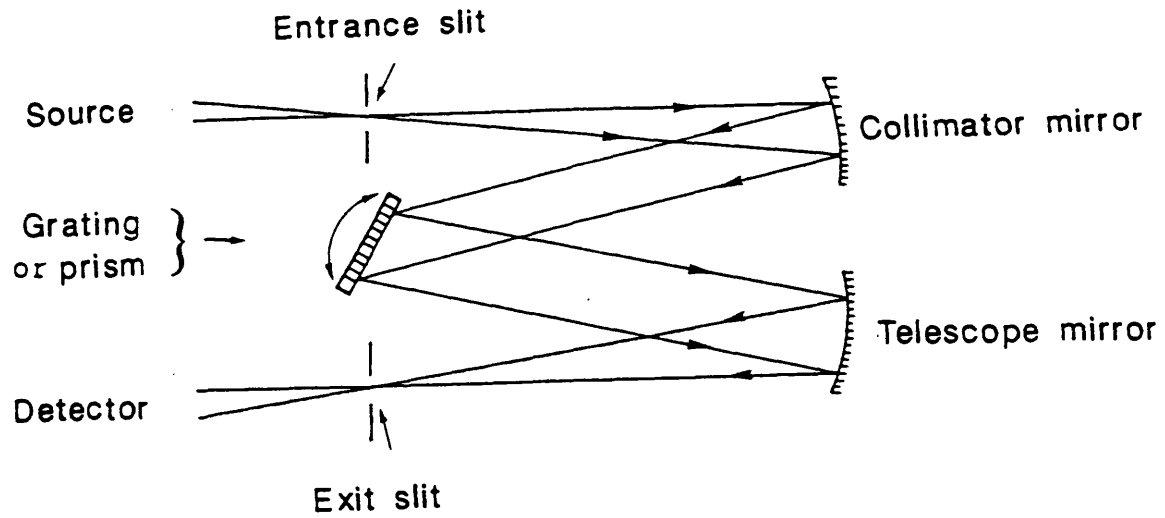


**Figure 3.4:**

Schematic diagram of a conventional IR Spectrometer.

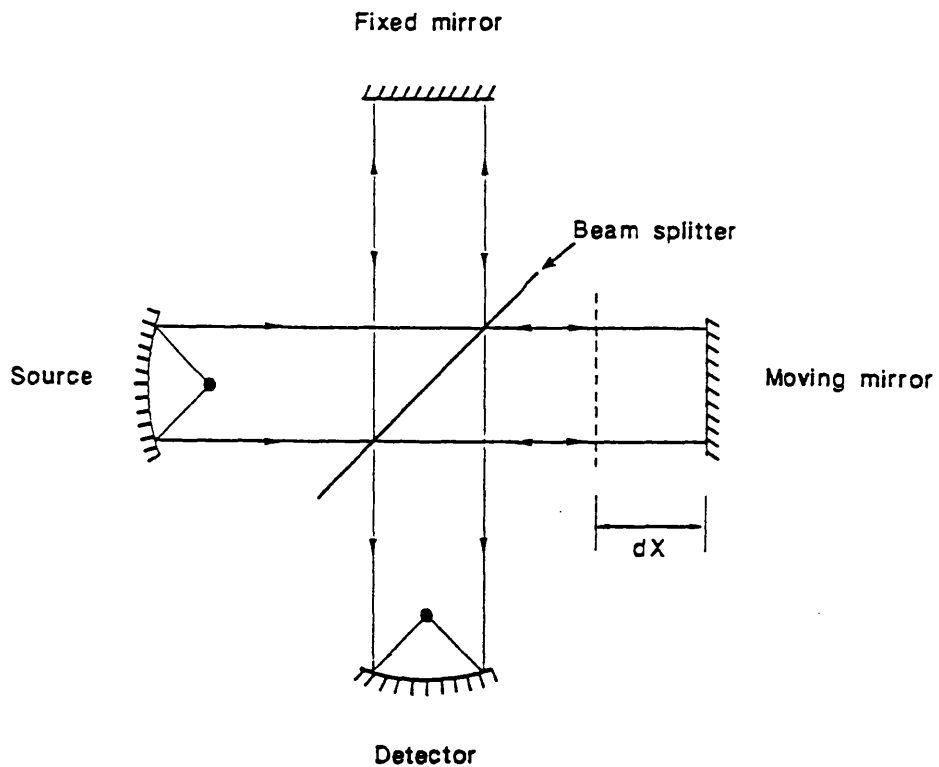


**Figure 3.5:**

Schematic diagram of the interferometer of an FTIR Spectrometer.

interferometer. Thus, the movement of the movable mirror causes a constructive and destructive light wave to exit from the interferometer as output; only when the mirrors are an equal distance from the beam splitter will the light interfere constructively; at other distances they will interfere destructively, and a complex signal arises from displacement of mirror (called the interferogram). The most important advantages of the FTIRS are:

- a. In DCIRS we examine each spectral wavelength sequentially whereas FTIRS observes all frequencies simultaneously; thus the signal can be accumulated and averaged to eliminate the noise.
- b. The movement of the mirrors, slits and other optics in the DCIRS may cause inaccurate measurements, whereas there are slits and fewer movable parts in the FTIRS in comparison with the DCIRS.
- c. Spectrum accumulation is very much faster for the FTIRS than for the DCIRS.

### 3.5.1 IR diode LASER spectrometer

A Spectra Physics IR Diode Laser spectrometer (SP5000) was used in the temperature distribution measurements. This is a very sensitive and very high resolution spectrometer, in which a solid-state semi-conductor diode laser (PdSnSe) operates at very low temperature (10 to 30 K). Laser tuning is achieved by controlling the temperature and the diode current.

### 3.6 REACTION CELLS

### 3.6.1 Short length reaction cell

A 3 cm outside diameter (OD) 8 cm long pyrex glass cell was used for pyrolysis reactions. The cell was designed to fit the Perkin-Elmer 681 IR Spectrometer and FTIR spectrometer (FTS 40). The cell was fitted with two anti-reflection coated ZnSe windows Figure 3.6; two rubber O-rings are mounted on two stainless steel gaskets, which were used to retain the rubber O-rings between the window and the edges of the cell, and to prevent them folding inside the cell during the evacuation. Two rubber caps were used to hold the windows in position on the sides of the cell. The two ends caps were secured by using two brass rings, held together by two brass screws. The cell was fitted with a 1/4" J. Young valve, which was used to connect the cell to the vacuum line.

### 3.6.2 The trapping cell

This cell was used to trap the products of the reactions. The design of the cell is the same as the above cell, but 1 cm longer. The cell was fitted with a second Young valve opposite the main inlet; a cold trap, usually a NMR sample tube, could be attached to this, see Figure 3.7.

### 3.6.3 The side windows cell

This cell was designed to fit in the FTIRS, allowing the IR beam to pass through the side windows to monitor the products while the reaction was initiated by CO<sub>2</sub> laser through the main entrance window.

This cell was 10 cm long (Figure 3.8) and 3.9 cm OD, with about 1.5 cm side windows fitted with two ZnSe windows; these

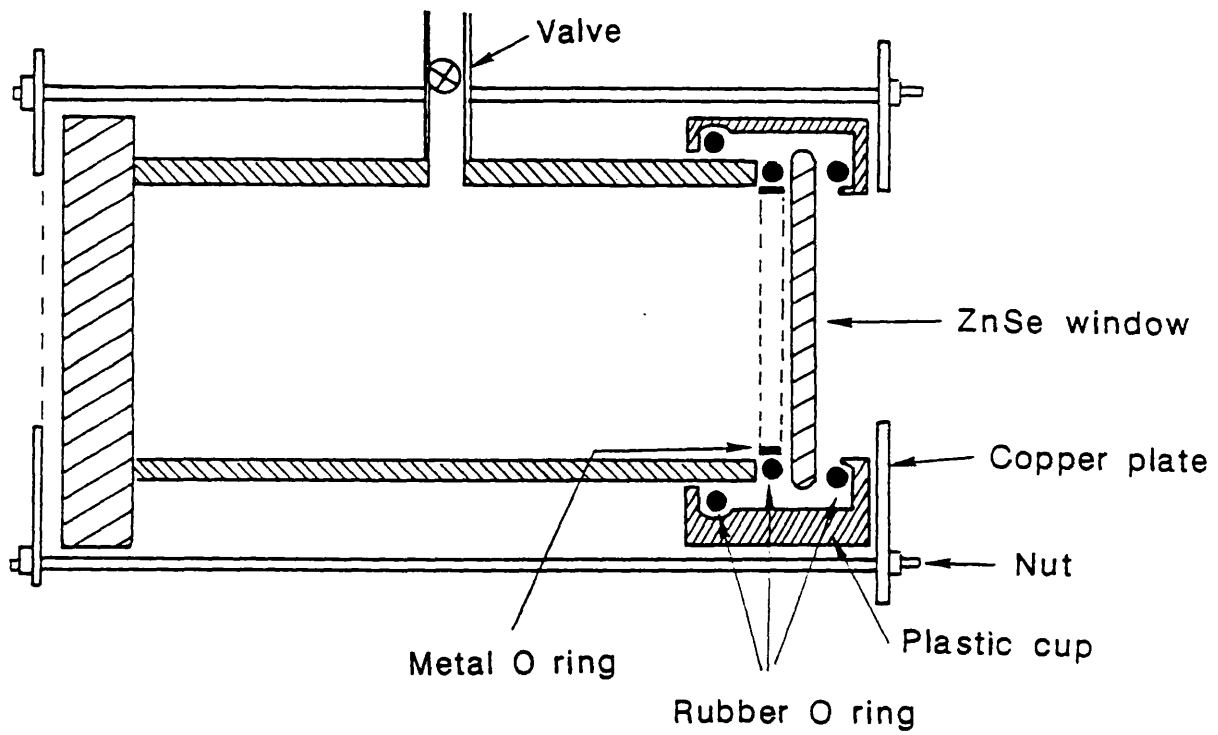


Figure 3.6:  
Schematic diagram of the pyrolysis cell.

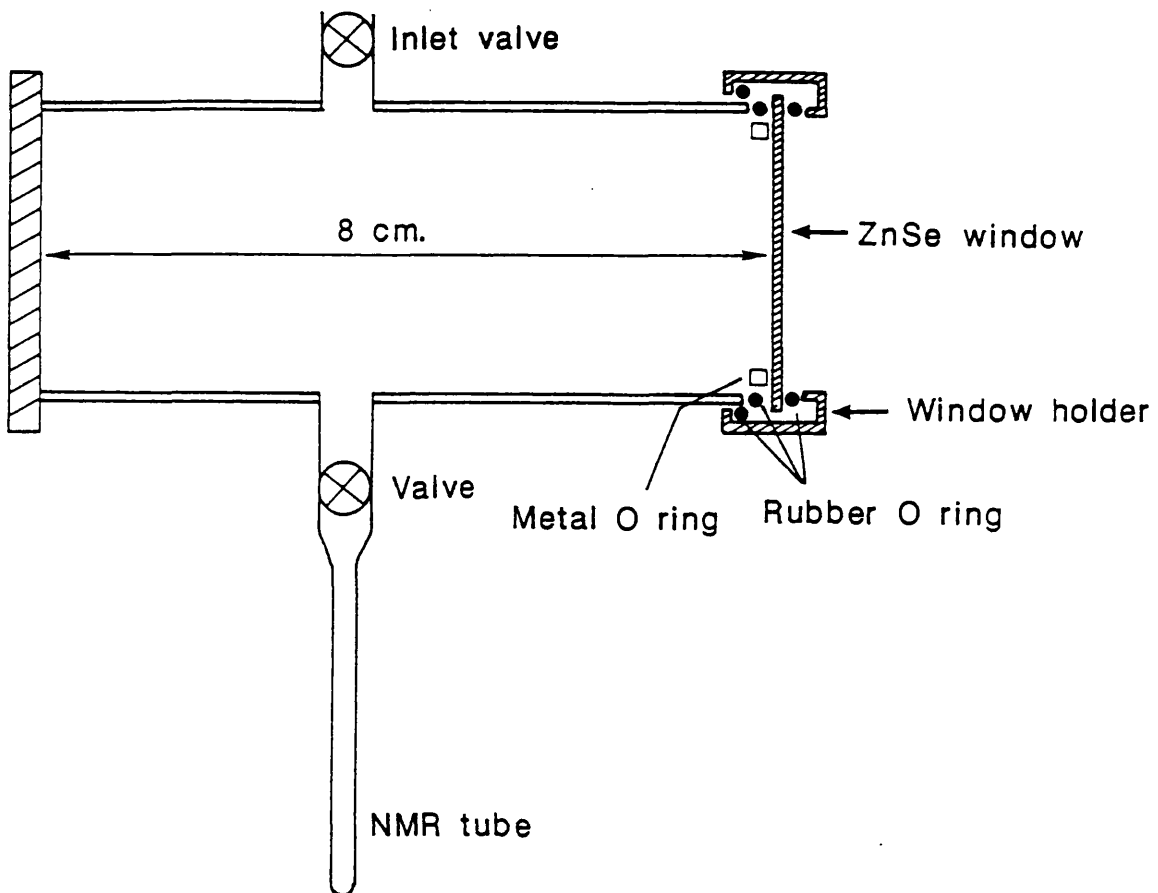


Figure 3.7:

Schematic diagram of the pyrolysis cell with the cold trap.

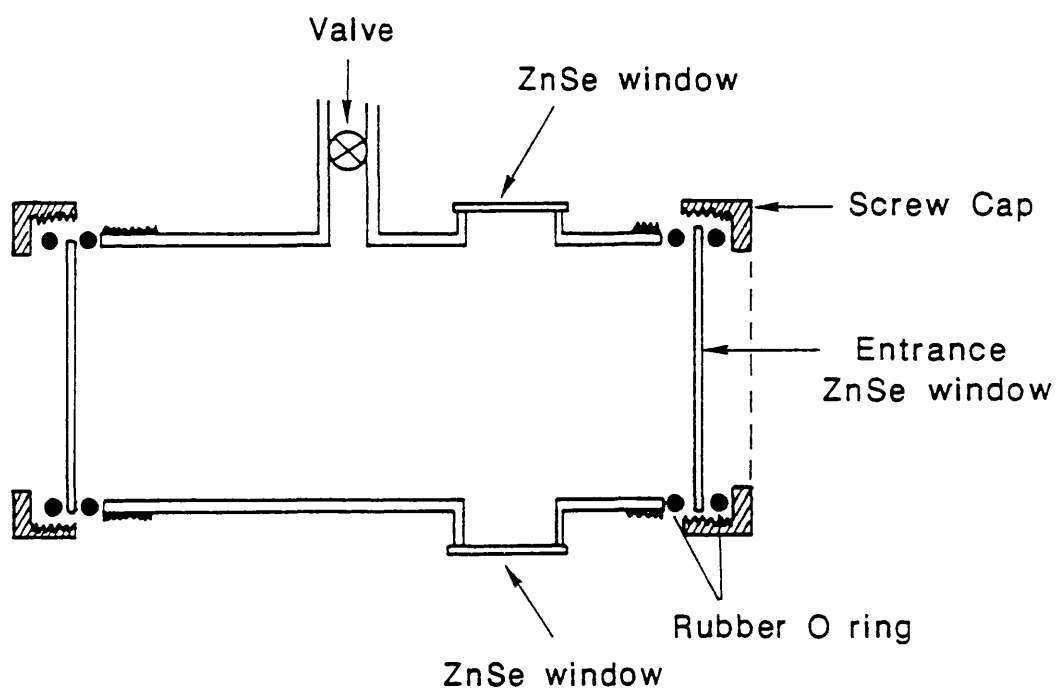


Figure 3.8:

Schematic diagram showing the side window cell which was used to monitor the reaction during  $\text{CO}_2$  laser irradiation of the cell.

were glued with silicon rubber. The ends of the cell were fitted with 3.9 cm OD ZnSe windows, with rubber O-rings between the glass and the windows. The windows were secured by two caps to the threaded ends of the cell.

#### 3.6.4 The temperature distribution measurement cell

This cell was used to measure the temperature distribution in the reaction cell. It is made of brass, with two side parallel slots fitted with two  $\text{CaF}_2$  windows, and a single ZnSe end window. The  $\text{CO}_2$  laser radiation is admitted through the ZnSe window, as in the pyrolysis cell. The side windows allow passage of the beam from the IR diode laser spectrometer. In this way, the IR spectrum of the cell contents can be measured in a direction perpendicular to the axis, at positions ranging from the front window to 3 cm down the cell (see Figure 3.9). All windows were glued to the cell by epoxy resin, and the back of the cell was blocked by a thin disk of brass glued to the cell body. The cell was connected to the main vacuum line with a brass vacuum valve. The cell was mounted on a mechanical stage equipped with vernier screws, allowing the cell to be moved back and forwards, or up and down.

### 3.7 PHOTOACOUSTIC CELL

Three types of photoacoustic cell were used to study the reactions as described below.

#### 3.7.1 The long photoacoustic cell

This was a 30 cm long and 3.9 cm OD pyrex glass cylinder, sealed at one end and equipped at the other end with a ZnSe

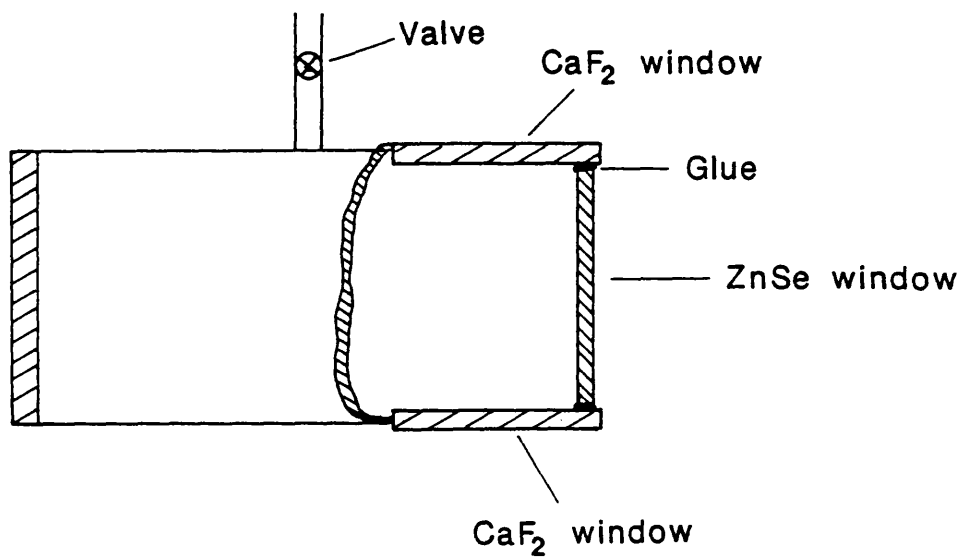


Figure 3.9:

Schematic diagram of the temperature measurement cell, showing the side windows positioned at the entrance window.

window (Figure 3.10) to admit the CO<sub>2</sub> laser radiation. An electret microphone was glued into the side of the cell in a 1 cm hole 1.5 cm from the entrance end. A 1/4" Young valve was attached midway between the ends of the cell for connection to vacuum line. A 30 cm cell was chosen to make the resonance frequency of the cell fall in the frequency range from 300 to 900 Hz, allowing the use a mechanical chopper (frequency limit 1000 Hz).

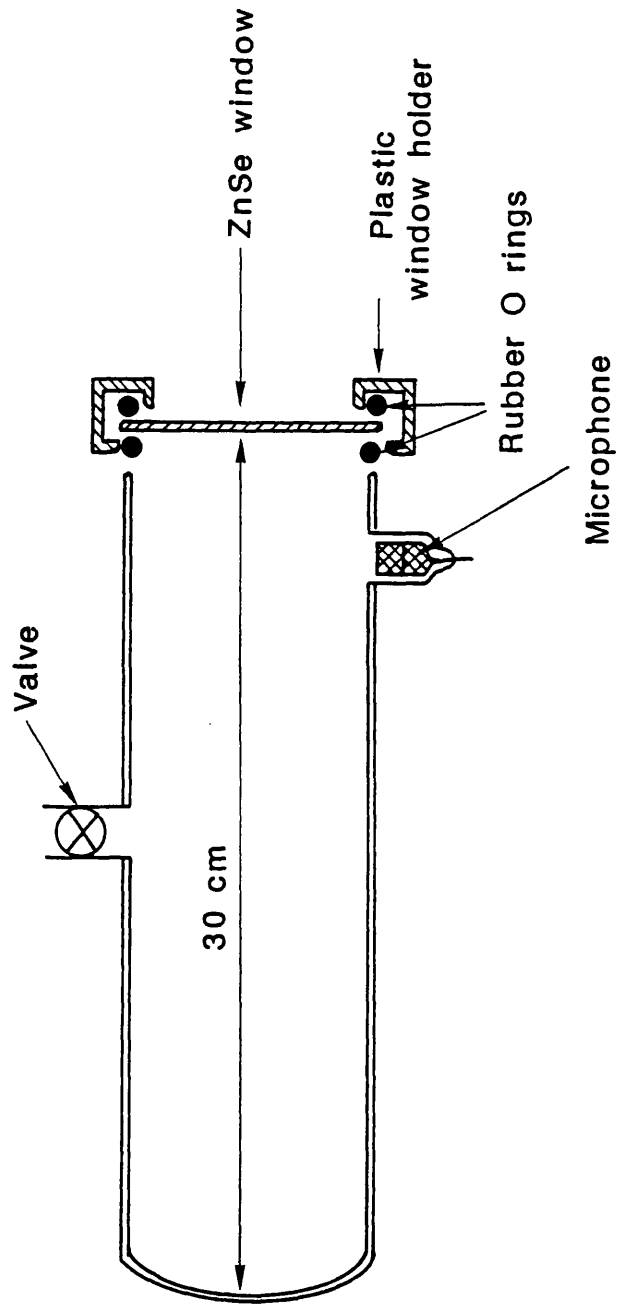
### 3.7.2 The short photoacoustic cell

This cell was a 7 cm long and 3.9 cm OD pyrex glass cylinder, the two ends being equipped with AR-coated ZnSe windows. The windows were secured to the ends of the cell as described in Section 5.1. The electret microphone was glued with epoxy resin midway between the ends (Figure 3.11). This cell had a high resonance frequency (above 2000 Hz) for use in the laser-modulated experiments (see below).

### 3.7.3 Adjustable volume cell

This cell was designed to study the effect of the volume on the rate of reaction. The cell was made of stainless steel tubing; the entrance end was fitted with a AR-coated ZnSe window secured to the cell by a brass screw cap (Figure 3.12). Its diameter was 3.0 cm, and its maximum length 30 cm. The other end was fitted with a movable piston equipped with a rubber O-ring for good sealing to the internal wall, to allow adjustment of the cell length and volume. The microphone was placed 3 cm from the entrance window, and the cell was equipped with a valve to connect it to the vacuum line.

**Figure 3.10:**  
Schematic diagram of low resonance frequency photoacoustic cell.



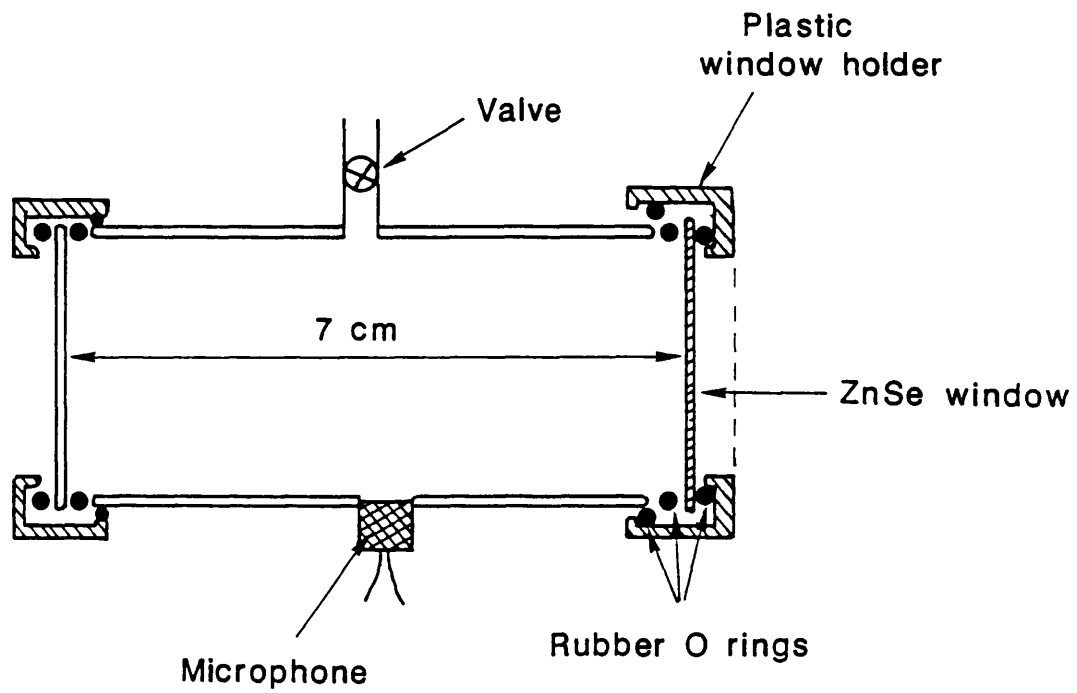
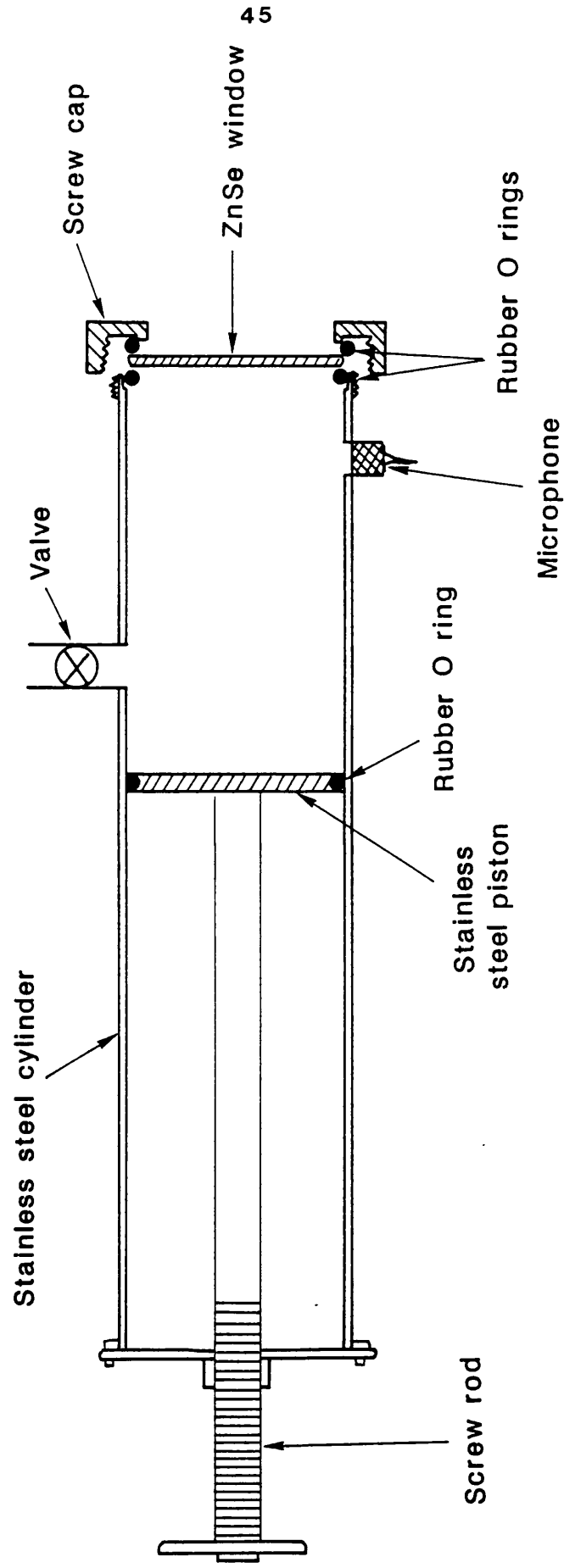


**Figure 3.11:**  
Schematic diagram of the high resonance frequency photoacoustic cell.

Figure 3.12:

Schematic diagram for the adjustable volume photoacoustic cell.



### 3.8 THE EXPERIMENTAL ARRANGEMENTS.

#### 3.8.1 Arrangements for IR CO<sub>2</sub> laser induced chemical reactions.

The arrangements for the IR CO<sub>2</sub> laser induced chemical reactions for all the experiments, which are described in this thesis, are shown in Figure 3.13. After introducing the appropriate pressure of reactants and the photosensitiser (SF<sub>6</sub>) into the reaction cell using the vacuum line, the laser power was chosen and set, and checked using the power meter. The cell was then placed about 8 cm away from the output window of the CO<sub>2</sub> laser and aligned to allow the beam to pass through the centre of the cell. The power meter was used to monitor whether any radiation passed through the cell. The laser frequency could be partially tuned manually to keep it in resonance with the  $\nu_3$  band of SF<sub>6</sub> until all radiation was absorbed.

#### 3.8.2 Arrangements for Spectroscopic experiments during the irradiation

The aim of this experiment was to inspect the contents of the reaction cell during irradiation with the CO<sub>2</sub> laser. The arrangement for this experiment is as in Figure 3.14. After preparing the sample in the side window cell (Figure 3.8) the CO<sub>2</sub> laser radiation beam was aligned perpendicularly to the IR radiation of the FTIR spectrometer. The cell was then placed in the FTIR spectrometer and a slab of ceramic was placed behind the rear window of the cell to prevent any damage being caused by the CO<sub>2</sub> laser radiation passing through the cell.

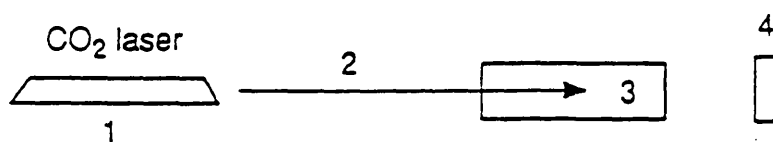


**Figure 3.13:**

Schematic diagram illustrating the experimental settings to induce the reaction:

1 is CO<sub>2</sub> laser; 2 CO<sub>2</sub> is laser beam; 3 is the reaction cell; and 4 is power meter.

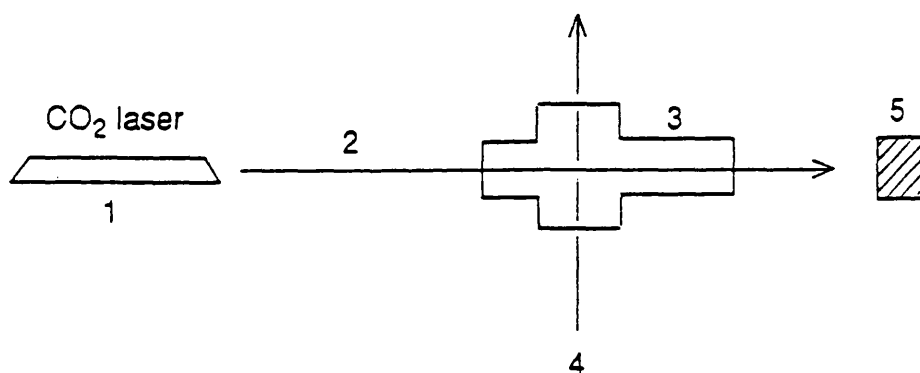


**Figure 3.14:**

Experimental setting to study the reaction of TMAL while CO<sub>2</sub> laser is shone through the reaction cell:

1 is CO<sub>2</sub> laser; 2 is incident laser beam; 3 is side window cell; 4 is the FTIR probe beam; and 5 is a ceramic slab for CO<sub>2</sub> laser beam dump.

### 3.8.3 Arrangements for the temperature distribution measurements

The experimental settings to carry out these measurements are shown in Figure 3.15. After preparing the sample in the side window cell (Figure 3.9), the cell was mounted on a mobile x-y stage with an accuracy of 0.01 cm. The CO<sub>2</sub> laser was aligned to enter the cell through the centre of the entrance window. The CO<sub>2</sub> laser beam was carefully adjusted to be horizontal and perpendicular to the probe IR diode laser beam. The probe beam was brought out of the optical box of the spectrometer and reflected back through the side windows of the cell back into the optical box by adjustable mirrors. Two cells filled with about 30 torr of SF<sub>6</sub> were placed inside the optical box to prevent any damage that can be caused by the CO<sub>2</sub> laser radiation to the detector and the diode laser sources. A compressed air flow was used to keep the cell at room temperature.

### 3.8.4 Arrangements for Photoacoustic Experiments

The photoacoustic experiments were carried out using three types of cell (Figures 3.10,11,12) and two types of laser beam modulation either chopping the laser beam or electric modulation to the laser radiation (Section 9.4). The experimental settings were as in Figure 3.16.

After preparing the sample in the cell, the cell was placed about 8 cm from the output of the CO<sub>2</sub> laser. The photoacoustic signal from the microphone was amplified, displayed on the oscilloscope and measured. The frequency was measured by a frequency meter. For the experiments in which the short length cell was used, electric modulation of the laser PZT was used to provide high frequency modulation which is required for the

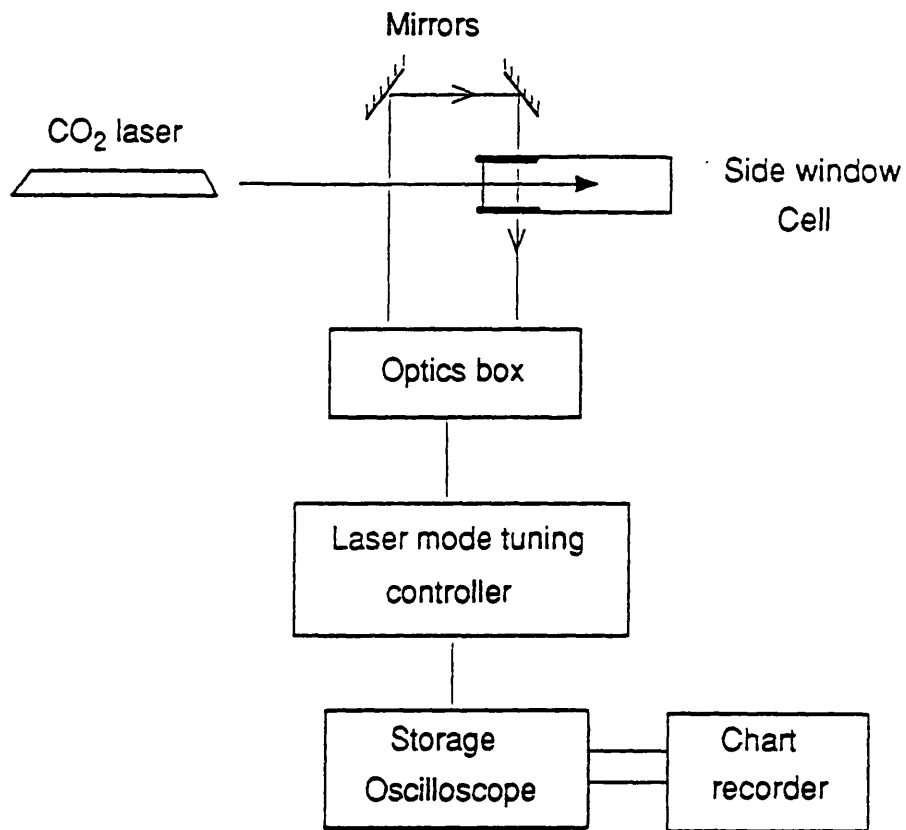


**Figure 3.15:**

Schematic diagram of the temperature distribution measurements (the side window cell is mounted on a vernier mechanical stage).

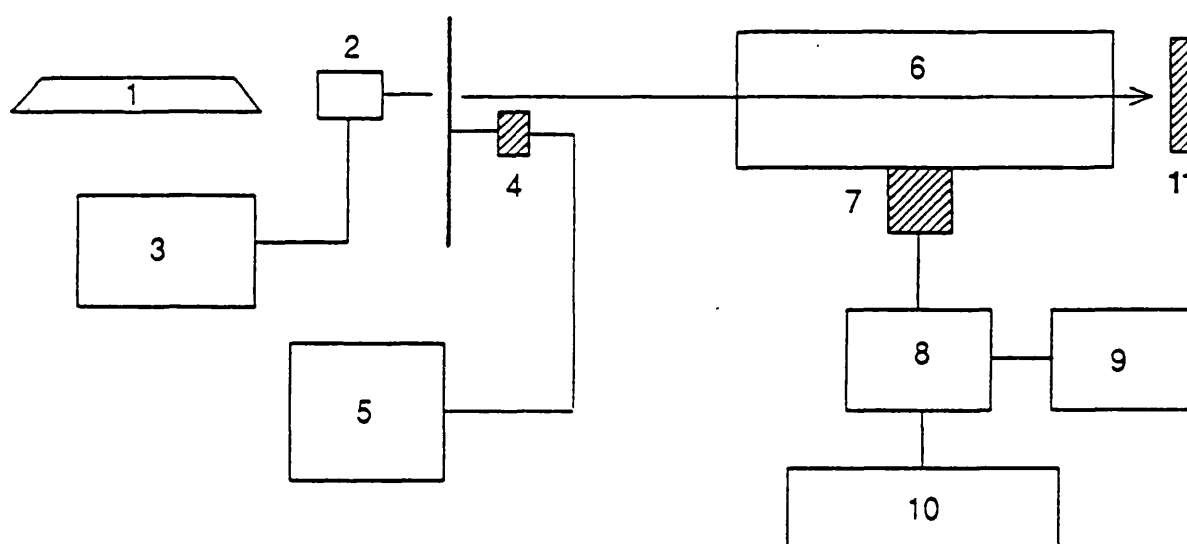


**Figure 3.16:**

Schematic diagram of the Photoacoustic experiments:

1 is CO<sub>2</sub> laser; 2 is PZT stack; 3 is modulator; 4 is Chopper; 5 is chopper frequency controller; 6 is photoacoustic cell; 7 is microphone and preamplifier; 8 is AC amplifier with Voltmeter; 9 is frequency meter; 10 is Oscilloscope; and 11 is power meter.

Note: either the laser modulator or the chopper was used in a given experiment.

short cell. A mechanical chopper was used for the longer and the adjustable length cell, which provides up to 1 kHz modulation sufficient for this type of cell.

### 3.8.5 Arrangements for the freezing point experiments.

This apparatus is shown in Figure 3.17 as previously described by Cooney<sup>3</sup>. The sample cell has three outlets which hold a suba-seal as in Figure 3.17, a platinum resistance thermometer in a stainless steel probe with accuracy of  $\pm 25$  mK (Automatic Systems Laboratories, Model F25) which reached almost to the bottom of the cell and a stirrer. The thermometer was connected to a digital voltmeter (Racal-Dana) linked to a Commodore Pet computer (Model 3032), a plotter (J.J. Instruments), and a printer (Commodore, Model 4022). This enabled a temperature against time plot to be obtained during a cooling run.

The sample was injected by a syringe fitted with an 8" needle through the suba-seal. The cell was then placed in a glass tube and a small silvered dewar placed around this as in Figure 3.17; this insured that the liquid nitrogen did not come into direct contact with the cell, and a slow uniform rate of cooling could be achieved using a larger liquid nitrogen dewar. The contents of the cell were stirred vertically by a stirrer wound around the thermometer probe and driven by a rotating motor.

## 3.9 ELECTRICAL EQUIPMENT

### 3.9.1 The microphone

The most important part of the photoacoustic cell is the

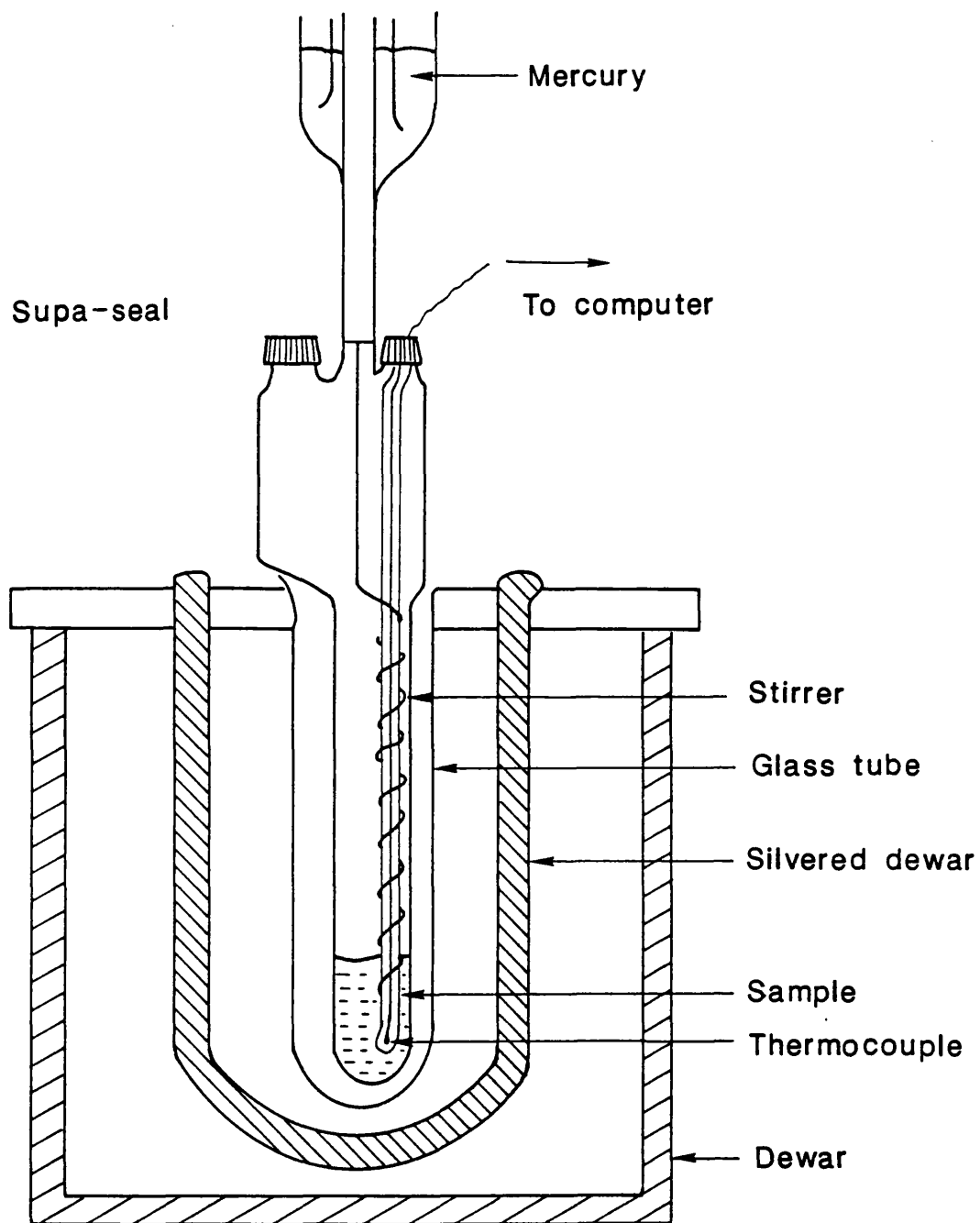


**Figure 3.17:**  
Freezing point apparatus.

microphone; this is a Tie Back Electret Condenser microphone with frequency response from 50 to 15000 Hz, and 800 Ohms impedance. This type of microphone is very sensitive, because the vibrating diaphragm is very thin (4 microns). The signal was preamplified with a built-in preamplifier.

### 3.9.2 AC amplifier

A Brookdeal precision AC amplifier 9452 model 11 with output voltmeter was used to amplify the acoustic signal from the microphone, and to display it on the Solartron oscilloscope.

### 3.9.3 Light chopper

A Brookdeal light chopper 9479 (maximum frequency is 1000 Hz) was used to chop the CO<sub>2</sub> laser beam for the lower frequency experiments.

### 3.9.4 CO<sub>2</sub> laser modulator

A LF Signal Generator type SG 66 was used to modulate the power of the CO<sub>2</sub> laser radiation by modulating the PZT electric output coupler. When a potential is applied across this, it causes a small change in its length (a few microns); as a consequence, the cavity length of the CO<sub>2</sub> laser is changed. This in turn produces a change in the wavelength emitted by the laser, causing it to move out of resonance with the SF<sub>6</sub> absorption. When the potential becomes zero in the PZT, the CO<sub>2</sub> laser radiation returns to its original wavelength. The resulting variation in the absorption by SF<sub>6</sub> of the laser radiation causes a variation in the amount of heat deposited during full or partial absorption. This variation in the

temperature was found to be enough to generate acoustic waves in the reaction cell, strong enough to detect by a sensitive microphone. It was found that a signal of amplitude 10 V. was strong enough to drive the PZT to generate the acoustic waves; this modulation affects the average output laser power by less than 4%. The maximum amplitude of the signal generator is 30 V. and its frequency range is from 50 Hz to 50 KHz.

### 3.9.5 The power meter

The power meter is a Coherent Power meter Model 201 calibrated to give a signal of 0.40 mV/Watt of power absorbed. The rise time of this meter is about one second; this means that it measures the average power in modulated experiments.

### 3.10 VACUUM LINE

A specially designed vacuum line was required for all the experiments which are described in this thesis, because of the air and moisture sensitive nature of the samples, the small scale of quantities used, and for sample preparation, degassing and purification.

The vacuum line was a 1/2" pyrex glass tube fitted with six outlet greaseless J. Young taps; these permitted connection to the reaction cells, reactant vessels, photosensitiser gas cylinder and the other required gas cylinders.

It was also equipped with a liquid N<sub>2</sub> trap, a two stage rotary pump and a U-shaped silicone fluid manometer with an accuracy of 0.2 torr. The best vacuum achieved with liquid N<sub>2</sub> in the trap was  $5.0 \times 10^{-2}$  torr.

The line was always conditioned by introducing a quantity of

the material to be studied to react with remaining water and oxygen on the surface of the glass, and then pumped out.

### 3.11 CHEMICALS

|  |                                   |
|--|-----------------------------------|
| TMA  | Aldrich Chemical Co.              |
| TMT  | "                                 |
| HMDT   | Courtesy of Dr. R. D. W. Kemmitt. |
| CH <sub>3</sub> I                                  | BDH Laboratory reagents           |
| CD <sub>3</sub> I                                  | Aldrich Chemical Co.              |
| H <sub>2</sub>                                     | British Oxygen Special gases      |
| D <sub>2</sub>                                     | " " " "                           |
| SF <sub>6</sub>                                    | " " " "                           |
| CCl <sub>4</sub>                                   | BDH Laboratory reagents           |
| CDCl <sub>3</sub>                                  | BDH Laboratory reagents           |
| CHCl <sub>3</sub>                                  | BDH Laboratory reagents           |
| CH <sub>3</sub> CH <sub>2</sub> COOCH <sub>3</sub> | BDH Laboratory reagents           |
| CH <sub>3</sub> CHO                                | BDH Laboratory reagents           |
| CH <sub>3</sub> COOH                               | BDH Laboratory reagents           |
| CO   | British Oxygen.                   |
| O <sub>2</sub>                                     | British Oxygen.                   |

All gases were used without further purification. All liquids were subjected to a few freeze-pump-thaw cycles to remove volatile impurities.

### 3.11 REFERENCE

1. J. P. Bromberg  
Physical Chemistry, London, 2nd Ed. 1984.
2. CO<sub>2</sub> laser specifications.
3. A. M. Cooney.  
Thermodynamic properties of binary liquid mixtures  
containing fluoroalcohols. Ph.D. University of  
Leicester 1988.

## CHAPTER 4

### TEMPERATURE DISTRIBUTION

#### 4.1 INTRODUCTION

The use of CO<sub>2</sub> lasers for inducing chemical reactions has become an active field of research. The previous chapter describes one application, in which the excitation of gaseous reactions by an IR laser with SF<sub>6</sub> as photosensitizer was used. As described in Chapter 2 the photosensitization technique generates an inhomogeneous temperature profile in the reaction zone. To obtain reliable information about the rate parameters, the spatial and temporal distribution of the temperature in the reaction cell must be known.

In this chapter the temperature distribution which is produced by using CO<sub>2</sub> laser and SF<sub>6</sub> as a photosensitizer is investigated. Quantitative and qualitative measurements were carried out to investigate the temperature produced by SF<sub>6</sub> absorption of the incident CO<sub>2</sub> laser radiation. Three different methods were used to examine the temperature distribution in the reaction cell. The first was visual determination of the reaction area by photographing the emission of iodine atoms produced in a chemiluminescent reaction, the second was using a standard reaction as a 'chemical thermometer', and the third was a spectroscopic technique using a stable internal indicator such carbon monoxide (CO) and a very sensitive and high resolution IR diode laser spectrometer. A simple model is suggested for our measurements and previous work has also been reviewed.

#### 4.2 REVIEW

Reactions induced by using continuous wave CO<sub>2</sub> laser irradiation with a photosensitizer are considered to be basically thermal reactions. The most common photosensitizers used are SF<sub>6</sub>, SiF<sub>4</sub>, NH<sub>3</sub><sup>1,2</sup>. Some reactants have strong absorption in the CO<sub>2</sub> laser region<sup>3</sup> such as chlorofluorocarbons, (CCl<sub>2</sub>F<sub>2</sub> and CClF<sub>2</sub>CClF<sub>2</sub>) and can be excited directly leading to thermal decomposition or ionisation.<sup>4,5</sup>

The most common photosensitizer and widely used in applications is sulphur hexafluoride (SF<sub>6</sub>). The most important characteristics of this photosensitizer are:

- i) very strong absorption coefficient for CO<sub>2</sub> laser radiation,
- ii) very short vibrational and translational relaxation times,
- iii) thermal and chemical stability towards the reactants,
- iv) its ability to stay in resonance with the CO<sub>2</sub> laser radiation, even when excited to very high levels<sup>6,7</sup>; this arises from the very high density of energy levels in high vibrational states, and
- v) its low thermal conductivity, permitting the generation of large temperature gradients.

The temperature profiles produced using this technique have been measured and calculated by several groups using various methods, including chemical thermometers,<sup>1,6,8,9</sup> interferometry<sup>3,10</sup>, direct measurement using thermocouples<sup>11</sup>, fluorescence<sup>12</sup>, and spectroscopy<sup>13-15</sup>.

Shaub and Bauer and other workers<sup>1,6,8,9</sup> were the first to measure the temperature produced by a CO<sub>2</sub> laser with SF<sub>6</sub>

photosensitization by measuring the rate of decomposition of compounds of very well known Arrhenius equation parameters (eg, cyclopropane which undergoes a well characterized unimolecular isomerization to propene). They used the expression:

$$k_{av} = A \exp\{-E/RT_{av}\} \quad 4.2.1$$

(where  $k_{av}$  is the rate constant averaged over the entire cell) to estimate the average cell temperature  $T_{av}$ .

They had also tried to calculate the temperature profile by means of the conduction equation. Their measurements were of limited value, because the average temperature,  $T_{av}$ , actually depends on the activation energy  $E$ . Their calculations are also questionable, because they neglected important factors such as convection and the variation of absorption coefficient and conductivity of  $SF_6$  with temperature.

Zitter and coworkers<sup>16-18</sup> had also studied the temperature produced by  $CO_2$  lasers using chemical thermometers. They also studied the temperature produced by  $CO_2$  laser through  $SF_6$  absorption at different pressures<sup>3,10</sup>; interferometric techniques were employed in their later measurements. They found the temperature depends on the input laser power and  $SF_6$  pressure. A straight forward application of the formula below:

$$F = (L/\lambda) (n_0 - 1) (1 - 300/T) \quad 4.2.2$$

was used to obtain the average temperature. Here  $F$  is the fringe number (ie the number of fringes between the room temperature and heated light paths),  $L$  is the cell length,  $\lambda$  is

the vacuum wavelength of the He-Ne laser (which was used in their interferometric measurements),  $n_0$  is the refractive index at 300K, and  $T$  is the temperature. This technique can only measure the temperature average along the He-Ne laser light path in the cell.

MacMillen et al<sup>12</sup> in 1981 studied the temperature produced by pulsed CO<sub>2</sub> laser using a strongly IR fluorescent molecule, such as CO. It was assumed that the single shot fluorescence signal strength,  $S$  (suitably filtered) is proportional to  $e^{-h\nu/kT}$  as below:

$$S \propto e^{-h\nu/kT}$$

4.2.3

where  $h$  is Planck's constant,  $\nu$  is the emitted radiation frequency,  $k$  is Boltzmann's constant, and  $T$  is the temperature.

Kubat and Pola<sup>11</sup> investigated the temperature distribution in such systems using a direct thermocouple measurement technique. They found that the maximum temperature is produced at the entrance window, and that the addition of highly conducting He lowers the temperature in the centre of the incident laser beam. The problem with this technique is the unknown perturbing influence of the thermocouples themselves.

Spectroscopic techniques have also been used to study the energy deposited in the nascent products,<sup>13-15</sup> using a time resolved tunable diode laser. In this case, the products which are produced with excess energy give very important information about the potential energy surfaces upon which fragmentation occurs. The method can also be applied in probing translational energy released in many chemical and physical processes, such

as photolysis and pyrolysis.

Selamoglu et al<sup>19</sup> have also measured the temperature produced using a CO<sub>2</sub> laser with hexafluorobenzene (C<sub>6</sub>F<sub>6</sub>) as both a photosensitizer and a temperature probe. Spectroscopic techniques were also employed in their measurements, whereby the change in absorbance in the UV absorption spectrum of C<sub>6</sub>F<sub>6</sub>, which is strongly temperature dependent, was monitored.

The most recent and reliable calculations have been carried out by Zhu and Yeung<sup>20</sup>. In their work, they took into account the explicit temperature dependence of heat capacities, thermal conductivities, molar absorptivities, and gas densities. Their calculations were checked using transmittance of the CO<sub>2</sub> laser beam, and also by using pyrolysis of C<sub>2</sub>H<sub>5</sub>Cl as a chemical thermometer; both results were in reasonable agreement with values predicted from their calculated temperature distributions.

This brief review has described some of the techniques employed to investigate and measure the temperature produced by a CO<sub>2</sub> laser. Most of these techniques (with the exception of the thermocouple measurements) have measured only average temperatures, whereas the entire distribution is needed. In our measurements of chemiluminescence, chemical thermometers and high resolution IR spectroscopy have been employed. A model has also been proposed to predict the temperature distribution over the reaction cell.

#### 4.3 TEMPERATURE MODEL

It is well known that the CO<sub>2</sub> laser radiation is very strongly absorbed by SF<sub>6</sub>, causing an inhomogeneous temperature

distribution bath within the cell, described by  $T(x,r)$ ;  $x$  the distance along the cell, and  $r$  the distance from the cell axis. This of course leads to a change in the density distribution of the mixture in the cell

$\rho(x,r)$  and the absorption coefficient  $\epsilon(x,r)$  for the photosensitizer. A model describing the temperature profile produced by continuous irradiation is much simpler than that caused by pulsed irradiation. In the latter, the gas dynamics involved in the expansion of the heated column into the rest of the cell must be considered.

Since the energy in the incident laser beam is not uniformly distributed, and it is attenuated as it travels along the cell, the temperature produced is not uniformly distributed both axially and radially.

The measurement of the temperature produced using such techniques is very important. Use of a high resolution tunable diode laser has enabled us to measure the temperature using an IR spectroscopic technique in very narrow segments of the cell, by looking at the spectrum of the photosensitizer or any other suitable internal indicator. The following derivation of the theoretical expression for the intensities of the vibration-rotation lines of a diatomic molecule (eg, CO) is based on unpublished work by Dr D. K. Russell.

The following assumptions simplify our model:

- i) the temperature and other distributions are cylindrically symmetrical; thus we can neglect any convection effects,
- ii) the probe diode laser beam is narrow compared with

characteristic distances for significant temperature variation, which means that we can ignore the x-variation of temperature for perpendicular viewing, and

- iii) the vibrational, rotational and translational degrees of freedom of the gas mixture are in equilibrium. This means that we may use the gas bulk temperature (T) for all the three temperatures.

From the Beer-Lambert law,

$$dI = I \epsilon \rho dr \quad 4.3.1$$

where I is the intensity of the probe laser radiation,  $\epsilon$  is the absorption coefficient of the internal indicator gas and  $\rho$  is the gas density.

The absorption of the probe beam as it traverses the cell may therefore be calculated as:

$$\ln(I_{in}/I_{out}) = \int_{r=-a}^{r=+a} \epsilon \rho dr \quad 4.3.2$$

where a is the radius of the cell.

In the Equation 4.3.2 we examine the temperature dependence of  $\epsilon$  and  $\rho$ . From the ideal gas law, we have:

$$\rho = P/RT \quad 4.3.3$$

When the thermal equilibrium is established through the cell,

the pressure  $P$  is constant. It may be determined by direct measurement under conditions of laser illumination, or by appealing to the conservation of mass within the cell as below:

The total amount  $N$  in the cell is given by

$$\int \rho \, d\tau = N \quad 4.3.4$$

where  $d\tau$  is the volume element in the cell, and the integral runs over the volume of the cell.

From the ideal gas law above, we see that:

$$P \int d\tau / T = NR \quad 4.3.5$$

for a fixed amount in a fixed volume cell. Thus, we can obtain

$$\rho(x,r) = N / \{ T(x,r) \int d\tau / T(x,r) \} \quad 4.3.6$$

$\rho = N/V$  could be obtained for a uniform temperature distribution, and this can be used with the measurements in the absence of  $\text{CO}_2$  laser irradiation to obtain the constants appearing in this relation.

The absorption coefficient for a transition  $|n'',J''\rangle \rightarrow |n',J'\rangle$  depends on the difference of the fraction of molecules,  $f(n,J)$  in these two states, and the matrix elements for electric dipole transitions between such states. The fraction of molecules in the state  $|n,J\rangle$  is given by:

$$f(n,J) = g(n,J) \exp\{-E(n,J)/kT\} / \{Q_v(T) \cdot Q_r(T)\} \quad 4.3.7$$

where  $E(n,J)$  is the energy and  $g(n,J)$  is the degeneracy of the state  $|n,J\rangle$ , and the  $Q$ 's are the partition functions for vibration and rotation. Using the simple harmonic oscillator expression for energy, we get for  $Q_v$  the expression:

$$Q_v(T) = 1 + \exp\{-h\nu/kT\} + \exp\{-2h\nu/kT\} + \dots$$

$$= 1 / [1 - \exp\{-h\nu/kT\}] \quad 4.3.8$$

For the rotational partition function, using the high-temperature approximation we obtain:

$$Q_r(T) = \sum_{J=0}^{\infty} (2J+1) \exp\{-BJ(J+1)/kT\}$$

$$\approx kT/B \quad 4.3.9$$

Finally, we place  $E(n,J) = nh\nu + BJ(J+1)$ , to give:

$$f(n,J) = g(n,J) B/kT [1 - \exp\{-h\nu/kT\}]$$

$$\exp\{-nh\nu/kT - BJ(J+1)/kT\} \quad 4.3.10$$

If we consider, in particular, the R-branch fundamental transition  $|n,J\rangle \rightarrow |n+1,J+1\rangle$ , the intensity will be proportional to the difference in fractional population  $f(n,J) - f(n+1,J+1)$ , ie to

$$B/kT [1 - \exp\{-h\nu/kT\}] \exp\{-nh\nu/kT\} \exp\{-BJ(J+1)/kT\}$$

$$x [1 - \exp\{-h\nu/kT\} \exp\{-2B(J+1)/kT\}] \quad 4.3.11$$

where the degeneracy factors are absorbed into the matrix elements; the matrix element for this transition yields a contribution of

$$|\langle n, J | U | n+1, J+1 \rangle|^2 \propto (n+1)(J+1) \quad 4.3.12$$

with an analogous expression for a P-branch transition. This enables us to express the absorption in Equation 3.3 as an integral function of temperature, for which the complete expression is:

$$\begin{aligned} \ln\{I_{in}/I_{out}\} = C \int_{r=-a}^{r=+a} dr (n+1)(J+1) [1 - \exp\{-h\nu/kT\}] \\ \times \exp\{-nh\nu/kT\} \exp\{-BJ(J+1)/kT\} \\ \times [1 - \exp\{-h\nu/kT\} \exp\{-2B(J+1)/kT\}] / T^2 \\ / \int dt / T \quad 4.3.13 \end{aligned}$$

The integration of (Equation 4.3.13) to yield an explicit expression requires the functional dependence of T on r. This is discussed below.

#### 4.4 EXPERIMENTS

Experiments were carried out to examine diffusion effects, and to make quantitative and qualitative measurements of the temperature distribution produced by CO<sub>2</sub> laser beam in the reaction cell. This section is divided into three subsections

according to the method used. The experimental arrangements and equipment were described in Chapter 3.

#### 4.4.1 Diffusion effects

The goal of this experiment is a quantitative test of the effects of the diffusion on reaction in the cell. The experiment was carried out using the 7 cm long glass cell filled with 10 torr of  $\text{CH}_3\text{CHO}$  and 10 torr of  $\text{SF}_6$ . In each case, the mixture was exposed to 12.5 Watts  $\text{CO}_2$  laser for a total exposure of 60 seconds. The experiment was repeated five times using an interval of exposure of 5, 10, 20, 30, and 60 seconds. The decay of the reactant was followed by the FTIR spectrometer. The percentages of the  $\text{CH}_3\text{CHO}$  decomposed in each case are plotted in Figure 4.1.

#### 4.4.2 Photographing the reaction zone

This experiment was carried out by introducing small crystals of elemental iodine,  $\text{I}_2$ , into the cell as a light emitter during the photosensitization, and 10 torr of  $\text{SF}_6$ . The cell was left for a few minutes and warmed up gently using a hair dryer to increase the  $\text{I}_2$  vapour pressure. The cell then was exposed to about 12 Watts of laser power. A weak yellow emission was observed along the incident laser beam. The emission was photographed using a 35 mm camera see Figure 4.2.

#### 4.4.3 Temperature measurements using a chemical standard

The aim of this experiment was to measure the temperature produced using the laser technique. Ethyl acetate was used as a chemical standard, since its kinetic parameters are very well

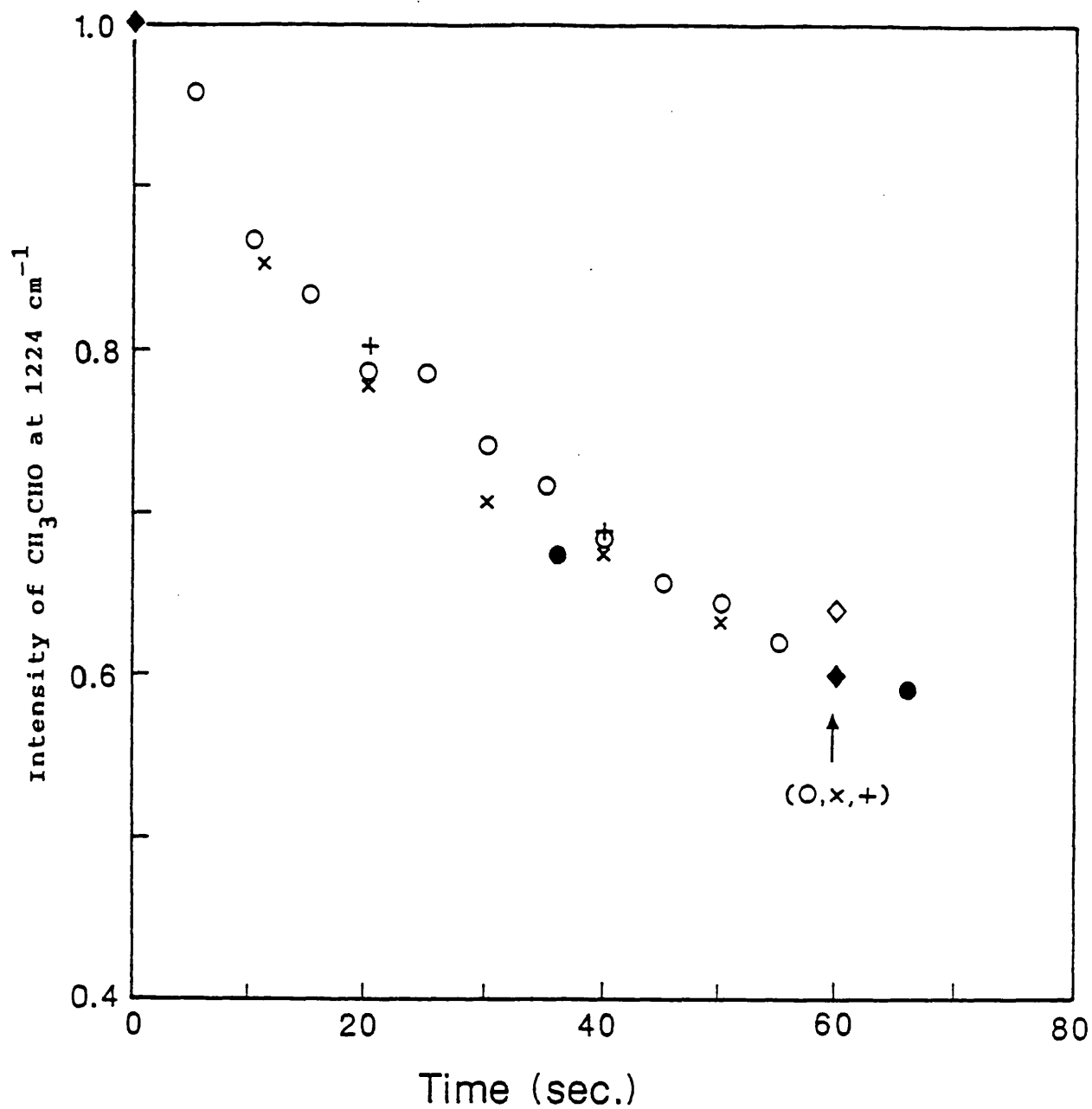


Figure 4.1:

Plots of normalized amount of the decomposed CH<sub>3</sub>CHO vs time for the reaction of mixture of 10 torr CH<sub>3</sub>CHO and 10 torr SF<sub>6</sub> irradiated with 12.5 Watts CO<sub>2</sub> laser power. Total exposure each time was 60 seconds. o, x, +, •, and ◊ represent the interval time of exposure of 5, 10, 20, 30, and 60 seconds respectively.

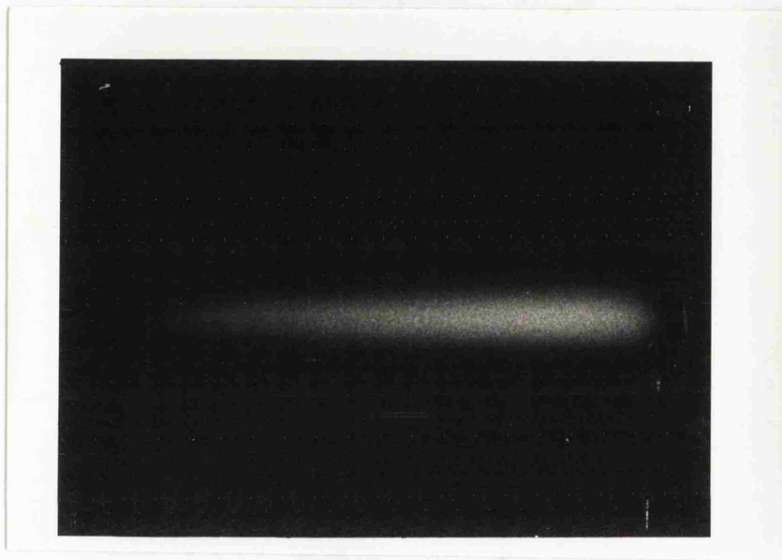


Figure 4.2:

Photograph of emission of iodine vapour in presence of 10 torr  $\text{SF}_6$  excited with 30 Watts of  $\text{CO}_2$  laser power; the reaction cell diameter was 3 cm (OD), and it was 7 cm long. The front window of the cell is approximately 0.5 cm to the right of the visible emission.

known. The experiment was carried out by introducing 10 torr of ethyl acetate and 10 torr of SF<sub>6</sub> into the reaction cell. The mixture then irradiated with the CO<sub>2</sub> laser. The same procedure was repeated varying the laser power. The reaction was followed using the FTIR spectrometer. The decay of the peak at 1246 cm<sup>-1</sup> was followed. The initial rate was taken at all powers; see Figure 4.3.

#### 4.4.4 Temperature measurements using the spectroscopic technique

The aim of this experiment was to measure the temperature profile along the incident laser beam accurately. The experimental settings are shown in Chapter 3 (Figure 4). The sample was prepared by introducing about 0.5 torr of carbon monoxide CO and 10 torr of SF<sub>6</sub> into the reaction cell. The cell was then mounted onto a mobile x-y stage (with an accuracy of 0.1 mm). The probe IR diode laser beam traverses the cell through side windows, allowing the probe beam to cross the path of the incident CO<sub>2</sub> laser beam at right angles. Measurements were made from the entrance window up to 3 cm along the beam towards the back of the cell. The measurements were carried out by following several lines of the CO vibration-rotation spectrum. The intensities of these lines were recorded before and during the irradiation with the CO<sub>2</sub> laser. The intensity of each line was measured for two positions along the cell with 0.0 and 1.8 cm interval from the entrance window (the probe beam width was 0.3 cm). The laser power was also varied up to 15 Watts with about 2.5 Watts interval.

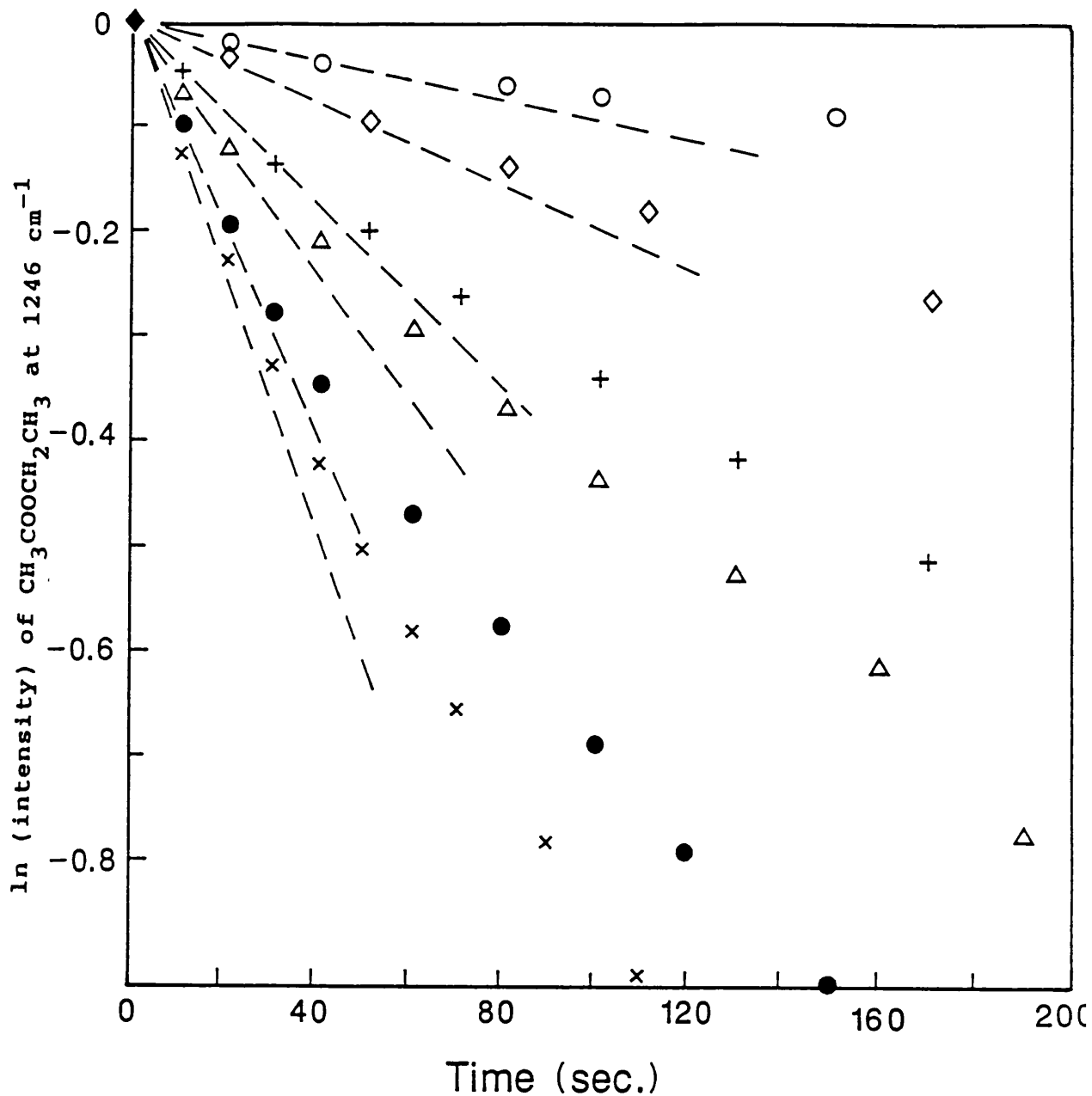


Figure 4.3:

Normalized plots of the  $\ln$  (intensity) of  $\text{CH}_3\text{COOCH}_2\text{CH}_3$  at  $1224\text{ cm}^{-1}$  vs time for mixture of 10 torr of  $\text{CH}_3\text{COOCH}_2\text{CH}_3$  and 10 torr  $\text{SF}_6$  at various  $\text{CO}_2$  laser powers; the dashed lines represent the initial rate for about 40% decomposition. o, ◇, +, Δ, ● and x represent the reactions carried out using laser powers of 5.00, 6.25, 7.50, 8.75, 10.00 and 11.25 Watts respectively.

## 4.5 RESULTS

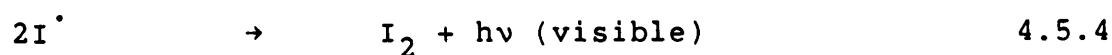
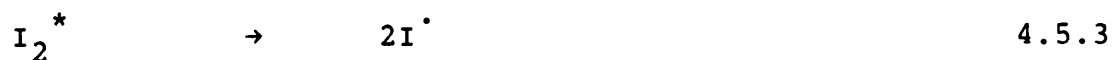
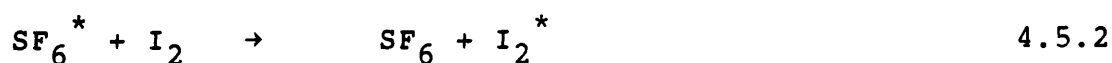
The results obtained from the above experiments are described below:

### 4.5.1 Diffusion effects

The experiment described in Section 4.4.1 shows that the extent of decomposition of  $\text{CH}_3\text{CHO}$  over 60 seconds is independent of the period of exposure, with the slight exception of that for continuous exposure; see Table 4.1. One can deduce that diffusion into the hot reaction zone is fast, and is not therefore the rate-limiting step in our experiments.

### 4.5.2 Chemiluminescence measurements

The photograph of the emission of the excited iodine (Figure 4.2) shows the most intense area is about 0.5 cm away from the entrance window, and on the axis of the cell. Also, the photograph shows that the emission forms a conical shape from about half way along the cell. The mechanism of the emission is as below:



From the scheme above, the iodine-iodine bond is

**Table 4.1:**

The amount of  $\text{CH}_3\text{CHO}$  decomposed during irradiation with 12.5 Watts  $\text{CO}_2$  laser power for a total exposure 60 seconds, and variable interval exposures.

---

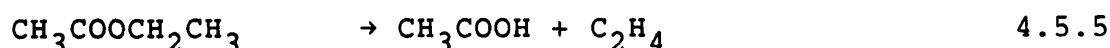
| Total time exposure<br>(Sec.) | Interval time<br>(Sec.) | % decomposed of<br>( $\text{CH}_3\text{CHO}$ ) |
|-------------------------------|-------------------------|--|
| 60                            | 60                      | 64.0   |
| 60                            | 30                      | 59.0   |
| 60                            | 20                      | 60.0   |
| 60                            | 10                      | 59.9   |
| 60                            | 5                       | 59.9   |

---

dissociated by hot  $\text{SF}_6^*$ ; the I atoms then recombine, emitting visible radiation. The radiation which is emitted during the first few seconds is brighter than at later times.

#### 4.5.3 Results of the chemical standard measurements

The results of the reaction of the ethyl acetate are plotted in Figures 4.3 and 4.4. The reaction is approximately first order. It decomposes as in the reaction below:



The rate of the reaction was measured at various laser powers, and the mean temperature T estimated using the Arrhenius relation:

$$k = A e^{-E/RT} \quad 4.5.6$$

where k is the rate constant, A the frequency factor, E is the activation energy, and R is the universal gas constant. Values of  $10^{12.59} \text{ Sec}^{-1}$  and  $201 \text{ kJ mol}^{-1}$  for A and the activation energy E of ethyl acetate respectively were used<sup>9</sup>. The temperatures yielded using these measurements are listed in Table 4.2.

#### 4.5.4 Results of the spectroscopic measurements

Results from the spectroscopic measurement are shown in Table 4.2 and Figure 4.4. These show that the temperature at the front window is a little lower than that about 1.5 cm away

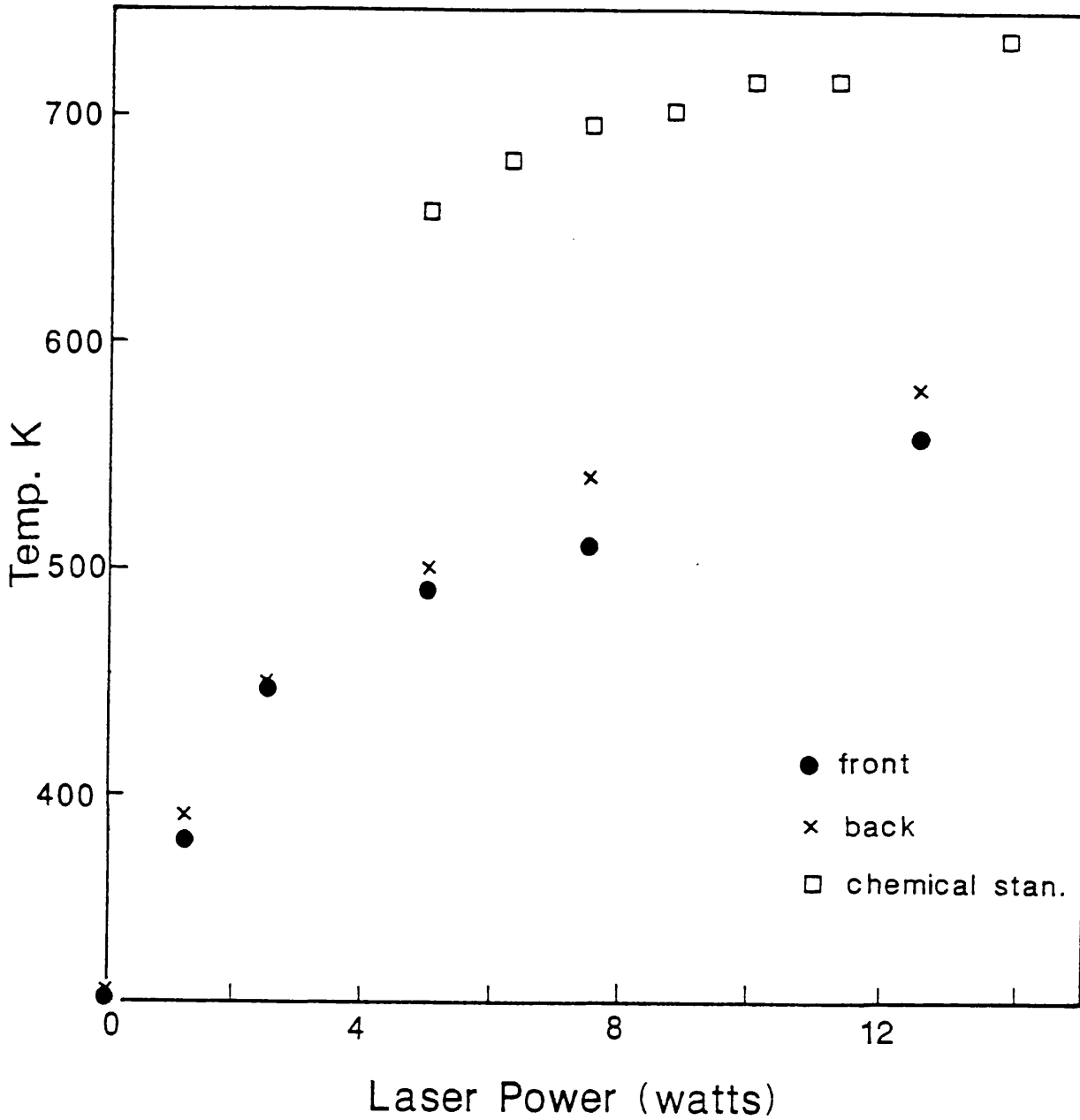


Figure 4.4:

Plot of the temperature (K) vs laser power (Watts); ● and x represent the measured temperature, carried out using the IR spectroscopic technique, at 0.0 and 1.8 cm from the front window respectively; and □ represents the measured temperature using a chemical standard; (the probe beam width is 0.3 cm).

**Table 4.2:**

Average temperature calculated from the reaction of ethylacetate  $\text{CH}_3\text{CH}_2\text{COOCH}_3$  using known Arrhenius parameters (ref 9), and that measured using the spectroscopy method: (a) at the front window and (b) at 1.8 cm from the front window.

| Laser power<br>(watts) | Temperature measured<br>by chemical standered<br>(K) | Temperature measured<br>by spectroscopy<br>(K) |     |
|------------------------|--|--|-----|
|                        |  | (a)  | (b) |
| 0.00                   | 310  | 310  | 310 |
| 1.25                   | -  | 380  | 390 |
| 2.50                   | -  | 450  | 450 |
| 5.00                   | 657  | 490  | 500 |
| 6.25                   | 679  | -  | -   |
| 7.50                   | 695  | 510  | 540 |
| 8.75                   | 701  | -  | -   |
| 10.00                  | 715  | 520  | 570 |
| 11.25                  | 716  | -  | -   |
| 12.50                  | -  | 560  | 580 |
| 13.75                  | 734  | -  | -   |

from the front window. These temperatures result from calculations using the expression (4.3.13); they are derived from the slopes of best fit plots (see Figure 4.5).

#### 4.6 DISCUSSION

The experiments described in Section 4.5 give two important results: first, the diffusion to the reaction zone is very fast compared with reaction rates; second, the hottest part of the reaction cell is about 1.8 cm from the entrance window, and it is slightly cooler at about 0.0 cm from the entrance window. This is clearly confirmed by the photograph of the reaction zone, assuming that the brightest area is the hottest.

Measurements of the average temperature produced in the cell using a chemical standard show that the mean temperature increased with laser power up to a certain level (see Figure 4.4), indicating that the photosensitizer is "bleached" at this power, and no further energy can be absorbed on increasing the power.

There are several important points to be made here:

- a) The plot according to Relation 4.3.13 is not expected to give a straight line, because the effective temperature over all rotational levels is not the same. Our measurements were carried out over a limited range of rotational lines of the reference gas (CO) (R18, 20, 22, 24, 25, 27 and 29) because the higher J levels are less populated at room temperature. Consequently, the measurements cannot be carried out because the intensity of the lines becomes too weak and unmeasurable at this sort of pressure (0.5 torr of CO); see Figure 4.6, which

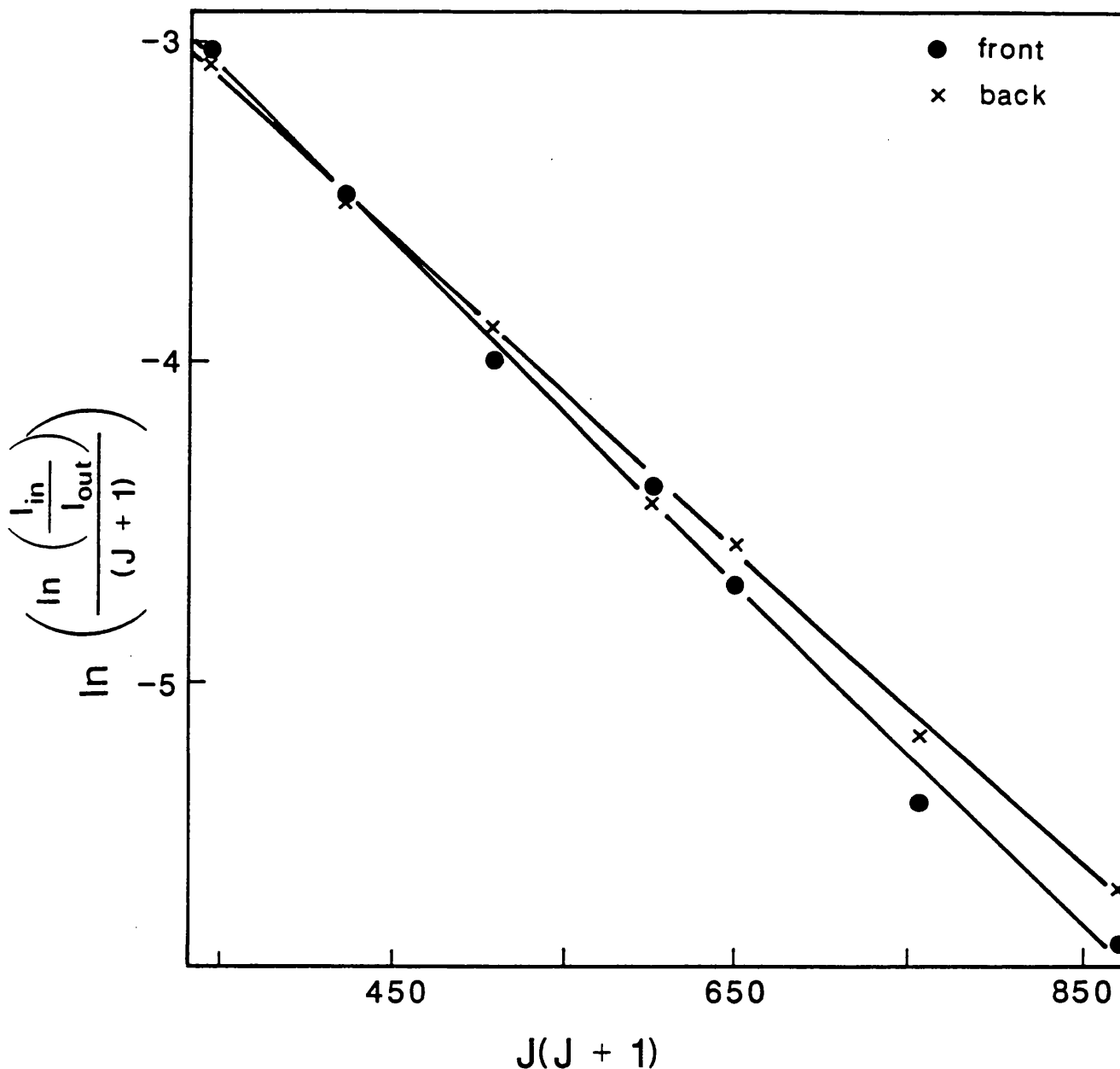


Figure 4.5:

Plot of  $\ln\left\{\frac{\ln(I_{in}/I_{out})}{J+1}\right\}$  vs  $J(J+1)$  of the lines R18, 20, 22, 24, 25, 27, and 29 of CO spectrum; the mixture was about 0.5 torr CO and 10 torr  $SF_6$  irradiated with 10 Watts  $CO_2$  laser power; o and x represent the measurements carried out at 0.0 and 1.8 cm from the front window respectively; (the probe beam width is 0.3 cm).

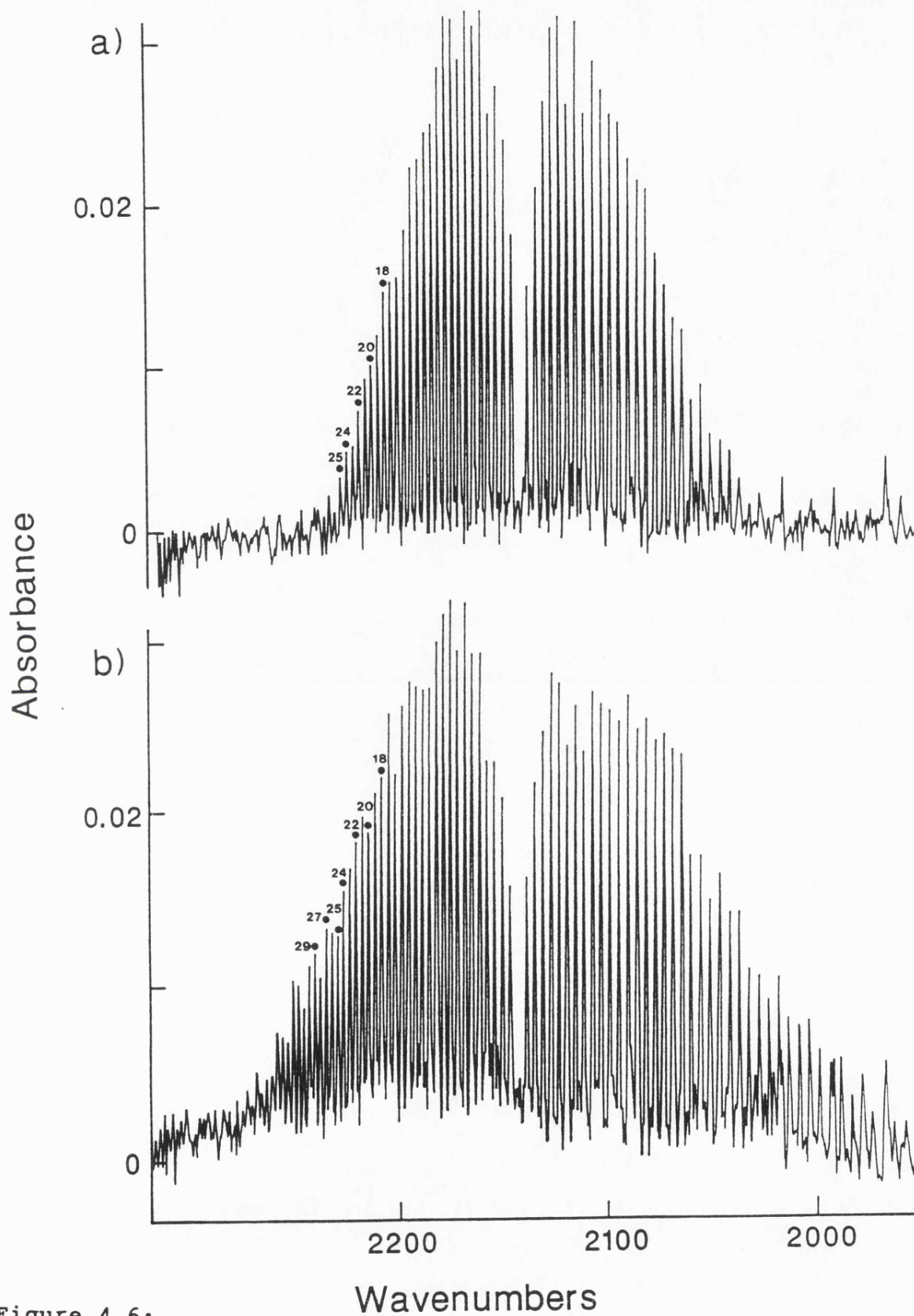


Figure 4.6:

FTIR spectra of 10 torr CO mixed with 10 torr  $\text{SF}_6$ ; (a) before and (b) during irradiation with 10 Watts of laser power; the identified lines were used to carry out the temperature measurements.

shows pre and post FTIR spectra of CO, and note how the weak lines become more intense on laser radiation.

- b) Measurements using the spectroscopic methods show that the temperature at about 0.0 cm from the front window is lower than that at about 1.8 cm. The point here is that the temperature is lowered by conduction of heat to the front window, as well as the side wall. A slightly different temperature distribution is expected in the brass cell because of contributions from the beam reflected from the back brass disk, particularly at higher laser powers.
- c) Measurements using these two methods (chemical standard and spectroscopy) confirm that the temperature is not uniform over the cell. There is a difference in the measurement of temperature between the two methods, but the same pattern of increase in mean temperature with laser power is observed using both methods. This difference in the temperature is due the relation 4.3.14, which is the average temperature across the cell determined using rotational energies of lines in the range 5-20 kJ mol<sup>-1</sup>, whereas the average temperature over the cell measured using the chemical standard was determined by the activation energy of CH<sub>3</sub>COOCH<sub>2</sub>CH<sub>3</sub> (E= 201 kJ mol<sup>-1</sup>). The above results are plotted Figure 4.4.

#### 4.7 CONCLUSION

The experiments described above show that the temperature produced by CO<sub>2</sub> laser radiation is not uniform throughout the reaction cell. The hottest part is near, but not at the entrance window. The temperature increased with the laser power to a certain level, and then only slowly increased with power.

4.8 REFERENCES

1. C. Steel, V. Starov, R. Leo, P. John  
and R. G. Harrison.  
Chem. Phys. Lett. 62 (1979) 121.
2. J. D. Campbell, G. Hancock, J. B. Halpern and K. H. Welge.  
Chem. Phys. Lett. 44 (1976) 404.
3. R. N. Zitter, D. F. Koster, A. Cantoni and A. Ringwelski.  
Chem. Phys. 57 (1981) 11.
4. F. F. Crim, G. H. Kwei and J. L. Kinsey.  
Chem. Phys. Lett. 49 (1977) 526.
5. J. G. Black, E. Yablonovitch, N. Bloembergen and S.  
Mukamel.  
Phys. Rev. Lett. 38 (1977) 1131.
6. Hai-Lung Dai, E. Specht, M. R. Berman and C. B. Moore.  
J. Chem. Phys. 77 (1982) 4494.
7. W. Fuss and J. Hartmann.  
J. Chem. Phys. 70 (1979) 5468.
8. W. M. Shaub and S. H. Bauer.  
Int. J. Chem. Kinetics. 7 (1975) 509.
9. R. N. Zitter, D. F. Koster, A. Cantoni and J. Pleil.  
Chem. Phys. 46 (1980) 107.
10. R. N. Zitter, D. F. Koster, A. Cantoni, and A. Ringwelski.  
High Temp. Science 12 (1980) 209.
11. P. Kubat and J. Pola.  
Collection Czechoslovak Chem. Commun. 49 (1984) 1354.
12. D. F. McMillen, K. E. Lewis, G. P. Smith, and D. M. Golden.  
J. Phys. Chem. 86 (1982) 709.

13. J. P. Holland and R. N. Rosenfeld.  
Chem. Phys. Lett. 145 (1988) 481.
14. Ko-inchi Sugawara, T. Nakanaga, H. Takeo and  
C. Matsumura.  
Chem. Phys. 135 (1989) 301.
15. T. R. Fletcher and R. N. Rosenfeld.  
High\_Energy Processes in Organometallic Chemistry.  
ACS Symposium Series 333 (1987) 99.
16. R. N. Zitter, D. F. Koster and K. Cheung.  
J. Phys. Chem. 89 (1985) 1401.
17. R. N. Zitter, D. F. Koster, A. Cantoni and J. Pleil.  
Springer Ser. Chem. Phys. 6 (1976) 277.
18. R. N. Zitter, D. F. Koster.  
ASC Symp. Ser. 56 (1977) 130.
19. N. Selamoglu and C. Steel.  
J. Phys. Chem. 92 (1983) 1133.
20. J. Zhu and E. S. Yeung.  
J. phys. Chem. 92 (1988) 2184.

## CHAPTER 5

## LASER POWERED HOMOGENEOUS PYROLYSIS OF METHYL IODIDE

5.1 INTRODUCTION

$\text{CH}_3\text{I}$  and  $\text{CD}_3\text{I}$  were studied as examples of simple reactions during the course of the initial period of this study to gain experience with the technique. This was undertaken in order to study the mechanism of the reactions and the energy transfer from the photosensitizer to the reactants, and as a guide to understanding more complicated reactions, employing the technique of LPHP. Methyl iodide and deuterated methyl iodide were studied using a range of laser power. A mixture of the two was pyrolysed to study differences under the same conditions. A review of previous works carried out on the decomposition of  $\text{CH}_3\text{I}$  was also undertaken.

5.2 REVIEW

The pyrolysis of methyl iodide has been widely used by chemists and physicists as a simple example for many purposes: unimolecular reactions<sup>1-3</sup>, photochemical reactions,<sup>4-12</sup> and as a source of I atoms in the iodine laser<sup>14-17</sup>; this arises because of the weakness of the C-I bond.

In 1934 Ogg et al<sup>18</sup> were the first group to study the decomposition of  $\text{CH}_3\text{I}$ . From that time to the present many studies have been carried out to clarify the mechanism of the reaction and a great deal of kinetic data has been gathered. Table 5.1 lists some of the  $\text{CH}_3\text{-I}$  dissociation

**Table 5.1**

The bond dissociation energy of C-I in CH<sub>3</sub>I and the techniques used in its determination.

---

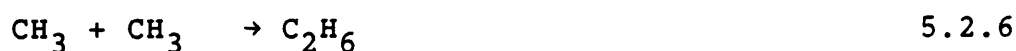
| D(CH <sub>3</sub> I)/kJ mol <sup>-1</sup> | Technique             | Ref |
|---|-----------------------|-----|
| 221                                       | thermochemical        | 26  |
| 228                                       | thermochemical        | 27  |
| 226                                       | thermochemical        | 28  |
| 224                                       | thermochemical        | 29  |
| 230                                       | thermal decomposition | 25  |
| 230                                       | thermal decomposition | 19  |
| 234                                       | LPHP                  | 20  |
| 224                                       | thermal decomposition | 21  |
| 178                                       | thermal decomposition | 22  |
| 220                                       | electron impact study | 24  |
| 192                                       | thermal decomposition | 23  |

---

energies determined, and the techniques employed.

The probable mechanism in a reaction of this sort involves the rupture of the weakest bond in the compound, which is the carbon iodine bond (C-I) in  $\text{CH}_3\text{I}$  rather than the C-H bond in this case.

The thermal decomposition of  $\text{CH}_3\text{I}$  has been studied by a number of workers<sup>18-22, 24, 30, 31</sup> both with and without radical scavengers such as HI. The mechanism of the thermal decomposition of  $\text{CH}_3\text{I}$  can be combined with the information obtained from photolysis studies, as below:

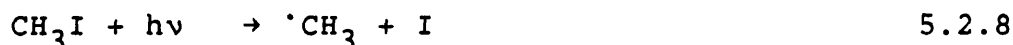


←

The thermal decomposition of  $\text{CH}_3\text{I}$  produces hot radicals, which are very reactive; these react readily with the starting material even in presence of radical scavengers, as in reaction (5.2.4), abstracting a hydrogen atom from

the starting material ( $\text{CH}_3\text{I}$ ) or from HI if present.

Frank et al<sup>6</sup> studied the moderation effects of added inert gases on the hot radicals produced by photolysis. They found the production of  $\text{CH}_4$  to be inversely dependent on the added moderator (Ar, Ne,  $\text{CO}_2$ ). Also, Chou et al<sup>8</sup> reported that the C-I bond ruptured using the photolysis method, as in reaction (5.2.8)



results in a hot ( $\text{CH}_3$ ) radical. Such radicals show enhanced chemical reactivity forming  $\text{CH}_4$  despite the presence of radical scavengers.

Souffie et al<sup>7</sup> studied hot radical reactions in the photolysis of methyl iodide vapor. They attributed the formation of  $\text{CH}_4$  to the  $\text{CH}_3$  radical which has excess energy (hot radicals), and which is capable of undergoing reactions in the early stage of its production, such as the reactions below:



The reaction of  $\text{CH}_3\text{I}$  is unaffected by the presence of iodine atoms initially added or produced during the reaction. Also, the formation of ethane ( $\text{C}_2\text{H}_6$ ) was the result of a hot radical reaction. Souffie et al also noticed that the production of  $\text{CH}_4$  was decreased on

addition of unreactive gases such as  $N_2$  and Ne.

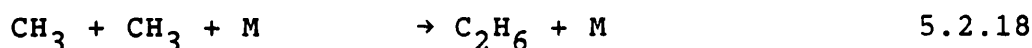
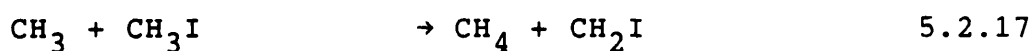
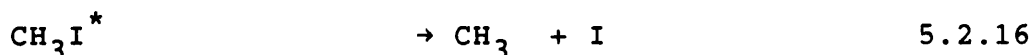
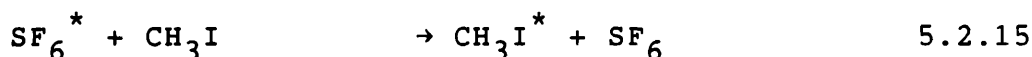
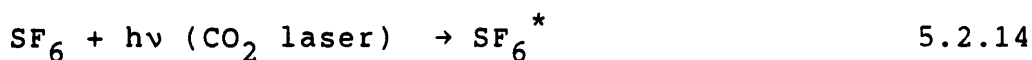
Benson et al <sup>20</sup> studied the thermal decomposition of  $CF_3I$  in a flow system and HI was used as a radical acceptor. When the latter was substituted for toluene, they observed that the formation of  $C_2F_6$  ceased, and the reaction was catalyzed by iodine atoms as in the mechanism below:



Saito et al <sup>22</sup> studied the thermal decomposition of  $CH_3I$  diluted by argon, Ar. The initiation of the reaction was the fission of the bond C-I. No elimination of HI was observed because the heat of the reaction of the HI elimination is about  $159 \text{ kJ mol}^{-1}$  higher than the C-I fission in the  $CH_3I$ .

Turning to LPHP studies, Dathe et al <sup>32</sup> reported that in the decomposition of  $CH_3I$  using a  $CO_2$  laser in the presence of  $SF_6$  as a photosensitizer  $I_2$ , ethane, ethene and ethyne were the products of the reaction. The decomposition rate and the nature of the products are found to be dependent on the irradiation power, the ratio of  $CH_3I/SF_6$ , and the energy of the exciting photon. IR spectroscopy and gas chromatography were used to assess and analyse the reaction products. In the  $CO_2$  laser region, methyl iodide

shows a bunch of Q-branches of the  $\nu_6$  rotational-vibrational band, some components of which almost coincide with the  $\text{CO}_2$  laser lines ( $R_{Q_8}$  949.20  $\text{cm}^{-1}$  with the P(14) line at 949.48  $\text{cm}^{-1}$ ,  $R_{Q_6}$  932.87  $\text{cm}^{-1}$  with the P(32) line at 932.96  $\text{cm}^{-1}$ , and  $R_{Q_5}$  924.83  $\text{cm}^{-1}$  with the P(40) line at 924.98  $\text{cm}^{-1}$ ). They found no reaction occurred during a long exposure to the  $\text{CO}_2$  laser without the presence of  $\text{SF}_6$  in the reaction cell. In presence of  $\text{SF}_6$  in the mixture, however, a bright red fluorescence appeared during the irradiation. No chemical participation of  $\text{SF}_6$  in the decomposition of  $\text{CH}_3\text{I}$  was observed. The mechanism of the reaction was proposed as below:



where  $\text{SF}_6^*$  is the excited molecule of the photosensitizer ( $\text{SF}_6$ ) and (M) a moderator (third body). The above mechanism proposed that energy is transferred by the excited molecules of the photosensitizer,  $\text{SF}_6$ , (Reactions 5.2.14 and 5.2.15) to the reactant, which then decomposes to give a iodine atom and  $\text{CH}_3$  radicals, (Reaction 5.2.16); then the

latter could react with the starting materials (Reaction 5.2.6), abstracting a hydrogen atom forming methane  $\text{CH}_4$ . On the other hand, methyl radicals having insufficient kinetic energy can undergo recombination forming ethane  $\text{C}_2\text{H}_6$  (Reaction 5.2.18). The formation of ethene ( $\text{C}_2\text{H}_4$ ) is due to the decomposition of 1,2 di-iodoethane as follows:



where the iodoethane is formed due to the recombination of  $\text{CH}_2\text{I}$  species:



The formation of acetylene is suggested to be due to the recombination of species  $\text{CH}$  as follows:



The decomposition of  $\text{CD}_3\text{I}$  was observed to be similar to that of  $\text{CH}_3\text{I}$ .

Rejnek et al <sup>33</sup> found in the decomposition of deuterated methyl iodide ( $\text{CD}_3\text{I}$ ) using the LPHP technique that the major products were  $\text{CD}_4$ ,  $\text{C}_2\text{D}_6$ ,  $\text{C}_2\text{D}_4$ , and  $\text{C}_2\text{D}_2$ . The formation of  $\text{CD}_4$  was found to be dependent on the total pressure in the reaction cell and to the line of excitation of the laser; maximum yields were found between the lines (P30-P42). Also, the formation of  $\text{C}_2\text{D}_6$  was found to be strongly dependent on the line of excitation of the  $\text{CO}_2$

laser (maximum yields found in between P10-P24) and decreasing the amount of SF<sub>6</sub> in the reaction mixture. The mechanism of the reaction was that suggested above by Dathe; however, the formation of an unusually high quantity of C<sub>2</sub>D<sub>4</sub> when the mixture was at a low total pressure was observed. The formation of carbene radicals (:CD<sub>2</sub>) was proposed as below to interpret that:

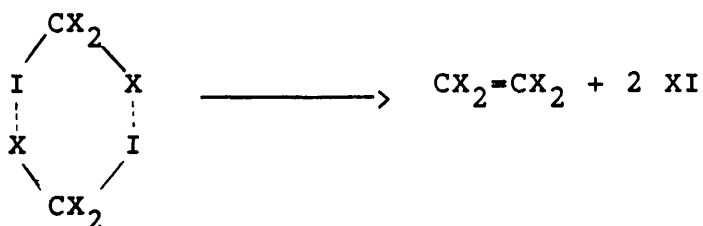


A comparative study of the decomposition of CH<sub>3</sub>I and CD<sub>3</sub>I and the products, under comparable conditions, has been carried out by Rejnek et al <sup>16</sup> using the LPHP technique. The rate of decomposition of CD<sub>3</sub>I was found to be faster than that of CH<sub>3</sub>I, particularly in the shorter wavelength region of the CO<sub>2</sub> laser spectrum. The decomposition of CH<sub>3</sub>I yielded methane, CH<sub>4</sub>, ethane, C<sub>2</sub>H<sub>6</sub>, and ethyne, C<sub>2</sub>H<sub>2</sub>, while in the decomposition of CD<sub>3</sub>I, methane-d<sub>4</sub>, CD<sub>4</sub>, ethane-d<sub>6</sub>, C<sub>2</sub>D<sub>6</sub>, ethene-d<sub>4</sub>, C<sub>2</sub>D<sub>4</sub> and ethyne-d<sub>2</sub>, C<sub>2</sub>D<sub>2</sub> were formed. Elementary iodine was liberated in both cases. The decomposition was initiated by irradiation of the mixture of CH<sub>3</sub>I/SF<sub>6</sub> by the P32 line of the CO<sub>2</sub> laser in a focused beam, with an output power of 8 W. The amount of CH<sub>4</sub> was found to be slightly dependent on the mixture composition before irradiation at a pressure of

12.4 Torr. The amount of ethane,  $C_2H_6$ , found was increased on decreasing the amount of  $SF_6$  in the mixture and prolonged irradiation decreased the amount of ethane,  $C_2H_6$ .

These workers proposed an explanation for the  $CD_3I$  decomposing faster than  $CH_3I$ , that the former ( $CD_3I$ ) has its  $\nu_3$  vibration closer than the latter ( $CH_3I$ ) to the energy of the excited  $SF_6$  (the photosensitizer), and that the energy could be transferred to the  $CD_3I$  rather than to the  $CH_3I$  efficiently. They also explained the formation of  $C_2X_4$  ( $X = H$  or  $D$ ) by two mechanisms: the first as in the reactions (5.2.21 and 5.2.22) above, and the second by bimolecular reaction as in the scheme below, in which two vibrationally excited molecules  $CX_3I$  of excitation energy insufficient for radical dissociation, produce  $C_2H_4$  and  $XI$ .

Scheme (I):



Saito et al<sup>17</sup> studied the thermal decomposition of  $CH_3I$  in He and Kr over a range of temperature 1000-1500 K at densities ranging from  $0.96-2.3 \times 10^{-5}$  mol  $cm^{-3}$  (about 5 torr). The  $CH_3I$  reacted according to a second order reaction. The reaction was found to be controlled by the efficiency of transferring the energy by the diluent gases in the order (He > Ar > Kr) respectively.

### 5.3 EXPERIMENTAL

The equipment and the chemicals which were used within this chapter were described in Chapter 3. The experiments which were carried out in this chapter were intended to study the LPHP technique using  $\text{CH}_3\text{I}$ ,  $\text{CD}_3\text{I}$  and a mixture of  $\text{CH}_3\text{I}$  and  $\text{CD}_3\text{I}$ . The measurements for the products and the starting material concentrations were initially carried out using a conventional IR spectrometer, and later a Fourier Transform IR spectrometer. Figure 5.1 illustrates typical measurements using the conventional IR spectrometer.

#### 5.3.1 Irradiation of Methyl Iodide ( $\text{CH}_3\text{I}$ ) in the absence of photosensitizer

Five torr of  $\text{CH}_3\text{I}$  was irradiated with about 8 Watts of  $\text{CO}_2$  laser for more than 10 minutes. No absorption of the  $\text{CO}_2$  laser was observed, and no reaction occurred. The IR spectra for the pre and post irradiated sample show no differences at all.

#### 5.3.2 Reaction of Methyl Iodide ( $\text{CH}_3\text{I}$ )

Five torr of  $\text{CH}_3\text{I}$  were mixed with 10 torr of  $\text{SF}_6$ , then irradiated with  $\text{CO}_2$  laser. The reaction was followed using the conventional IR spectrometer (CIRS). The degradation of the C-H stretching peak at  $2969\text{ cm}^{-1}$  of  $\text{CH}_3\text{I}$  and the appearance of methane (the band Q branch at  $3017\text{ cm}^{-1}$ ) were followed. The reaction was repeated with the same mixture using a range of laser power.

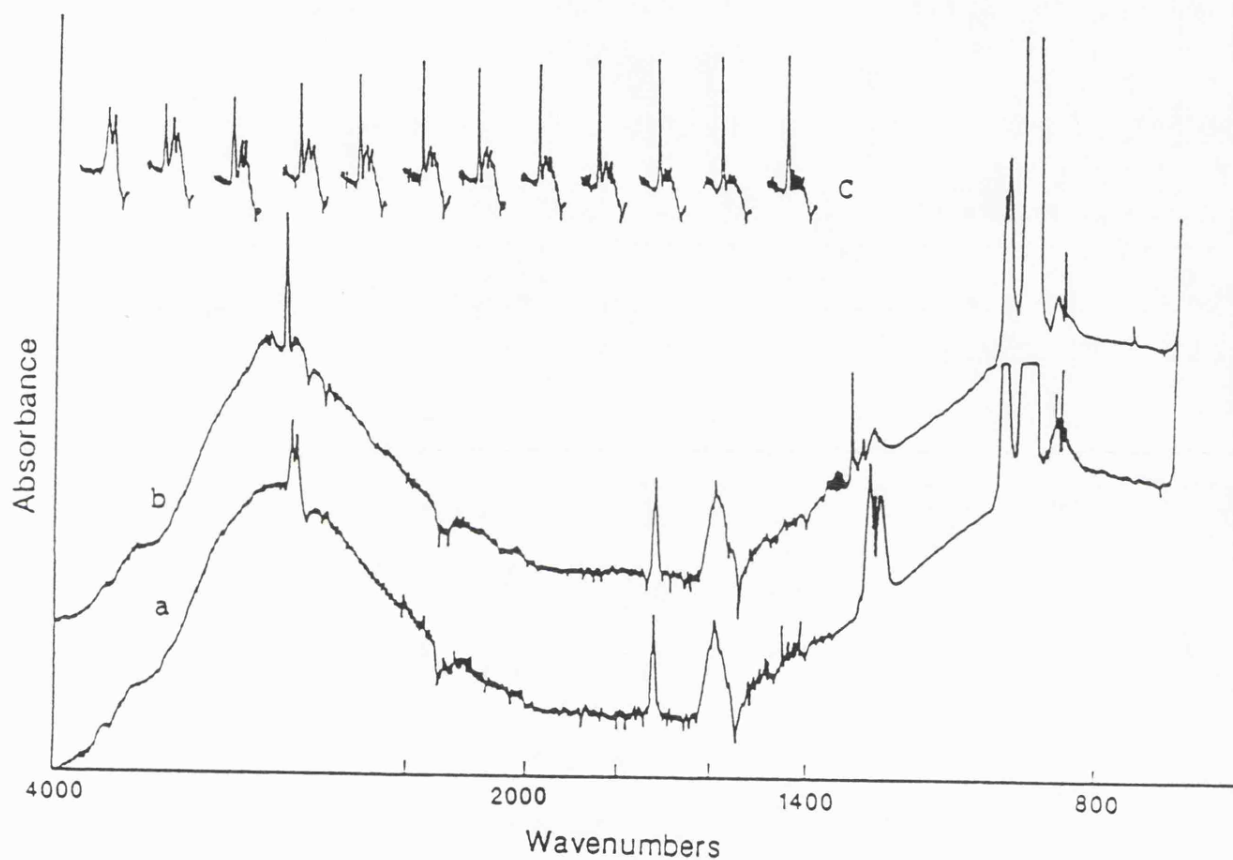


Figure 5.1:

Typical IR spectra for 5 torr of  $\text{CH}_3\text{I}$  and 10 torr of  $\text{SF}_6$  using a conventional spectrometer: a) before and b) after 21 minutes irradiation with 7.5 Watts of laser power. The region from 2990-3100 was followed in (c), which contains the strongest  $\text{CH}_4$  and  $\text{CH}_3\text{I}$  bands.

### 5.3.3 Reaction of Methyl Iodide-D3 ( $\text{CD}_3\text{I}$ )

Five torr of  $\text{CD}_3\text{I}$  were mixed with 10 torr of  $\text{SF}_6$  and the mixture was irradiated using the  $\text{CO}_2$  laser. The progress of the reaction was monitored using IR spectroscopy, following the formation of  $\text{CD}_4$  (Q branch at  $2258\text{ cm}^{-1}$ ) and the degradation of the  $\text{CD}_3\text{I}$  (the peak (C-D st) at  $2250\text{ cm}^{-1}$ ). The same mixture above was used with a range  $\text{CO}_2$  laser power.

### 5.3.4 Reaction of mixtures of Methyl Iodide ( $\text{CH}_3\text{I}$ ) and Methyl Iodide-D3 ( $\text{CD}_3\text{I}$ )

The purpose of this experiment was to study the decomposition of these compounds in comparison with each other. 5 torr of  $\text{CD}_3\text{I}$  was mixed with 5 torr of  $\text{CH}_3\text{I}$  and 10 torr of  $\text{SF}_6$ . The mixture was irradiated with 8.75 Watts of  $\text{CO}_2$  laser power. The reaction was followed using the FTIR spectrometer. The appearance of both the  $\text{CD}_4$  and  $\text{CH}_4$  (Q branches at  $2258\text{ cm}^{-1}$  and  $3017\text{ cm}^{-1}$  respectively) was followed.

## 5.4 RESULTS

The results of the irradiation of  $\text{CH}_3\text{I}$ ,  $\text{CD}_3\text{I}$ , and mixtures of  $\text{CD}_3\text{I}$  and  $\text{CH}_3\text{I}$  in Section 3, are described in the subsections below.

### 5.4.1 Irradiation of $\text{CH}_3\text{I}$ alone

Methyl iodide was irradiated using the  $\text{CO}_2$  laser to prove that no reaction occurs under the experimental conditions without using the photosensitizer ( $\text{SF}_6$ ). The  $\text{CO}_2$

laser spectrum line P20 at  $944.19 \text{ cm}^{-1}$  which was used in this work lies very close to the  $\nu_3$   $\text{CH}_3\text{I}$  vibrational-rotational bands, see Figures 5.2 and 5.3; and Table 5.2. This experiment resulted in no reaction for irradiation periods of over 10 minutes and laser power more than 10 Watts.

#### 5.4.2 The reaction of $\text{CH}_3\text{I}$ in the presence of $\text{SF}_6$

The IR spectra of the reaction of  $\text{CH}_3\text{I}$  shown in Figure 5.4, show that the major products were methane,  $\text{CH}_4$ , and a very small amount of  $\text{C}_2\text{H}_2$ , as characterized by their IR absorption spectra, Table 5.3; elementary iodine,  $\text{I}_2$ , was deposited on the front window and the cell wall. Also, a red fluorescence was emitted during the reaction, especially during the initial reaction; after a short time, the brightness of the emission decreased. This is due to the recombination of iodine atoms,  $\text{I} + \text{I} \rightarrow \text{I}_2$ .

#### 5.4.3 The reaction of $\text{CD}_3\text{I}$ in the presence of $\text{SF}_6$

IR spectra of the reaction of  $\text{CD}_3\text{I}$  reveal that new compounds were produced, which were characterized by their IR absorption (Table 5.4 and Figure 5.5). The major products were  $\text{CD}_4$  and also a very small amount of  $\text{C}_2\text{D}_2$ . The reaction was observed to be faster than the reaction of  $\text{CH}_3\text{I}$ .

#### 5.4.4 The reaction of the mixture of $\text{CH}_3\text{I}$ and $\text{CD}_3\text{I}$

The aim of this reaction was to observe the difference in the rate of their decomposition (by measuring the

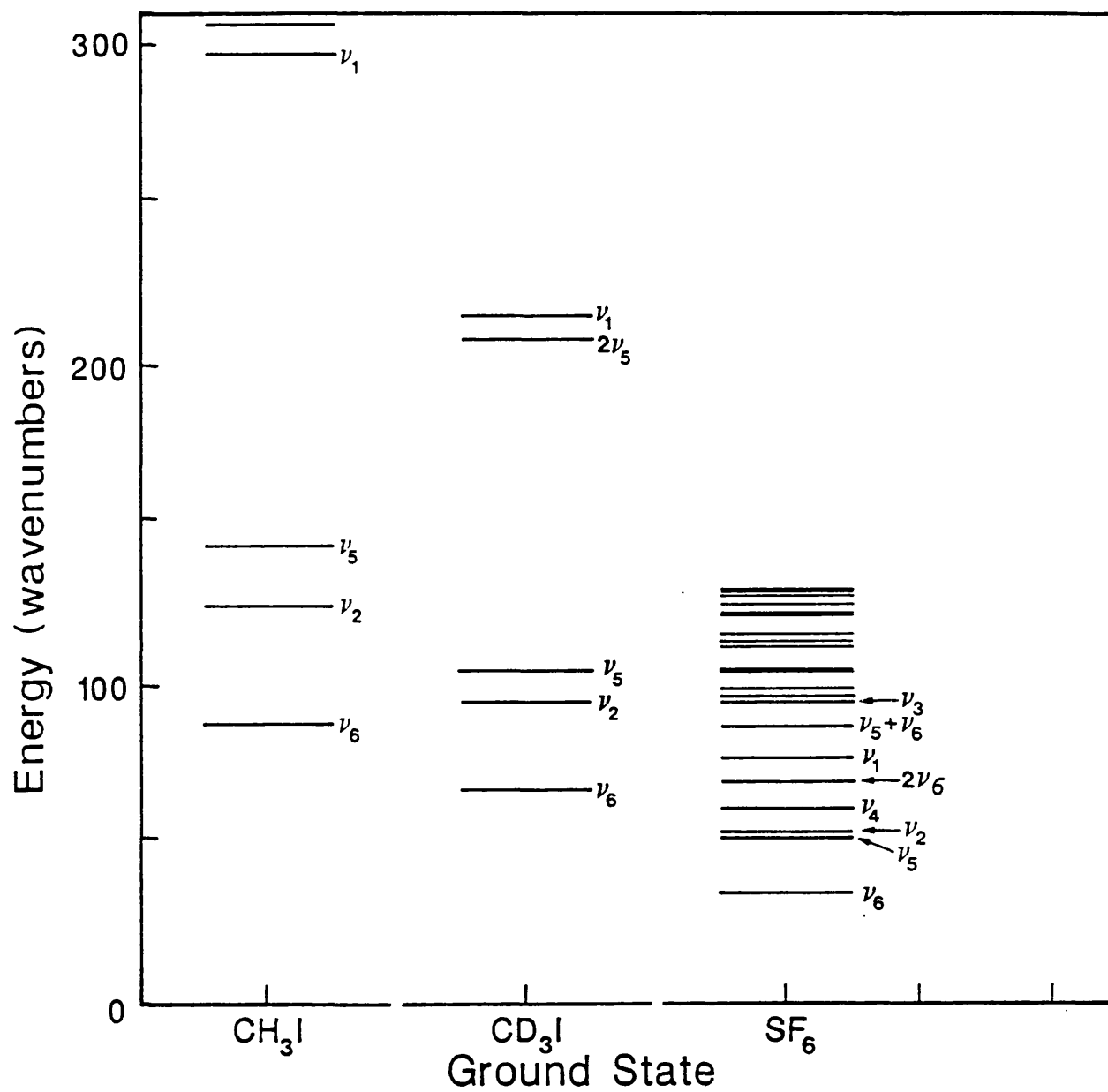


Figure 5.2:

Vibrational energy levels of SF<sub>6</sub>, CH<sub>3</sub>I and CD<sub>3</sub>I.

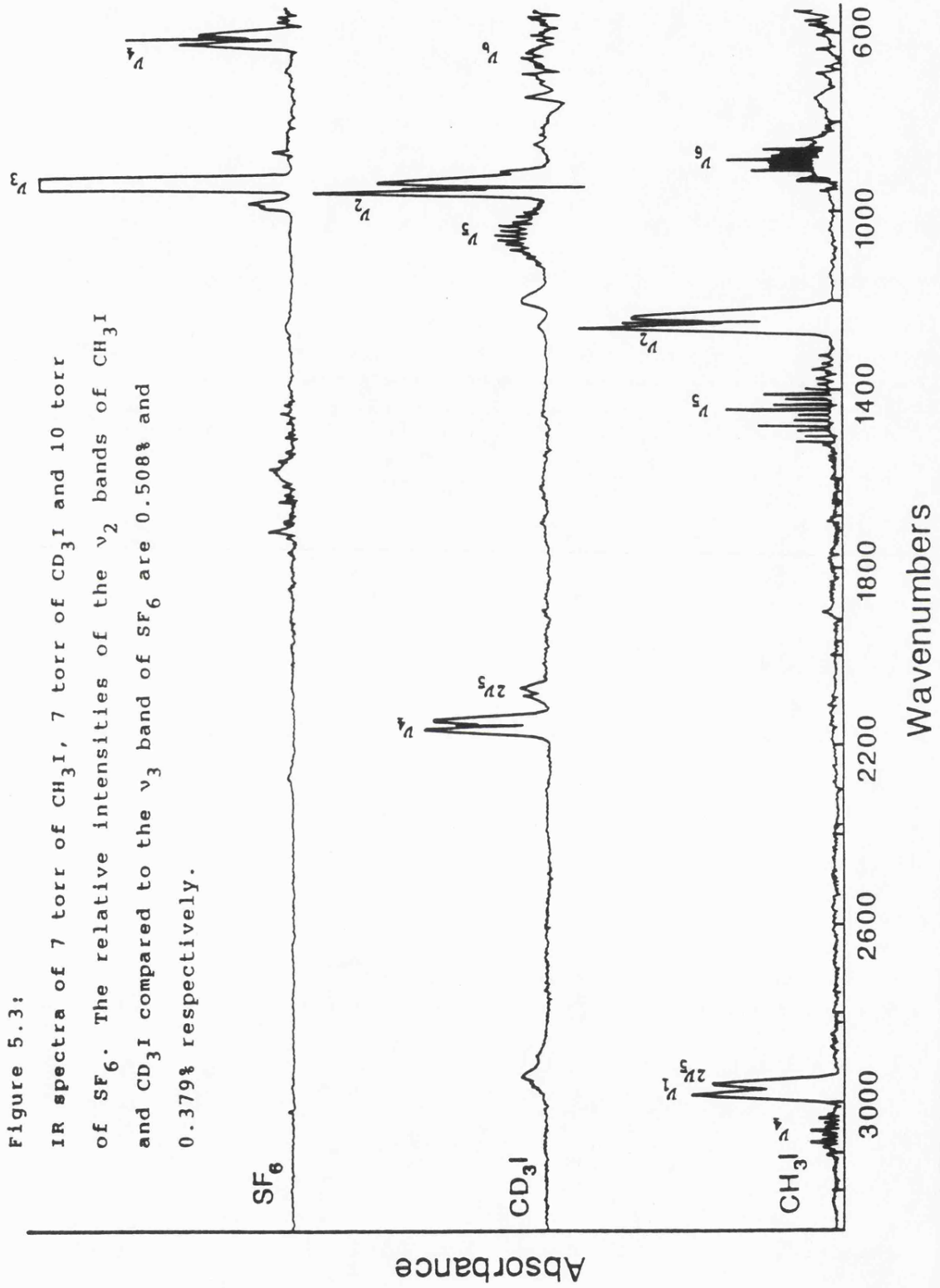


Table 5.2:

IR vibrations of  $\text{CH}_3\text{I}$  and  $\text{CD}_3\text{I}$  and their assignments

| $\text{CH}_3\text{I}$ bands ( $\text{cm}^{-1}$ ) | $\text{CD}_3\text{I}$ bands ( $\text{cm}^{-1}$ ) | Mode, assign. <sup>35</sup> |
|--|--|-----------------------------|
| 880  | 675  | $\nu_6$                     |
| 1251   | 950  | $\nu_2$                     |
| 1440   | 1048   | $\nu_5$                     |
| --   | 2081   | $2\nu_5$                    |
| 2969.8   | 2155   | $\nu_1$                     |
| 3060   | --   | $\nu_4^*$                   |

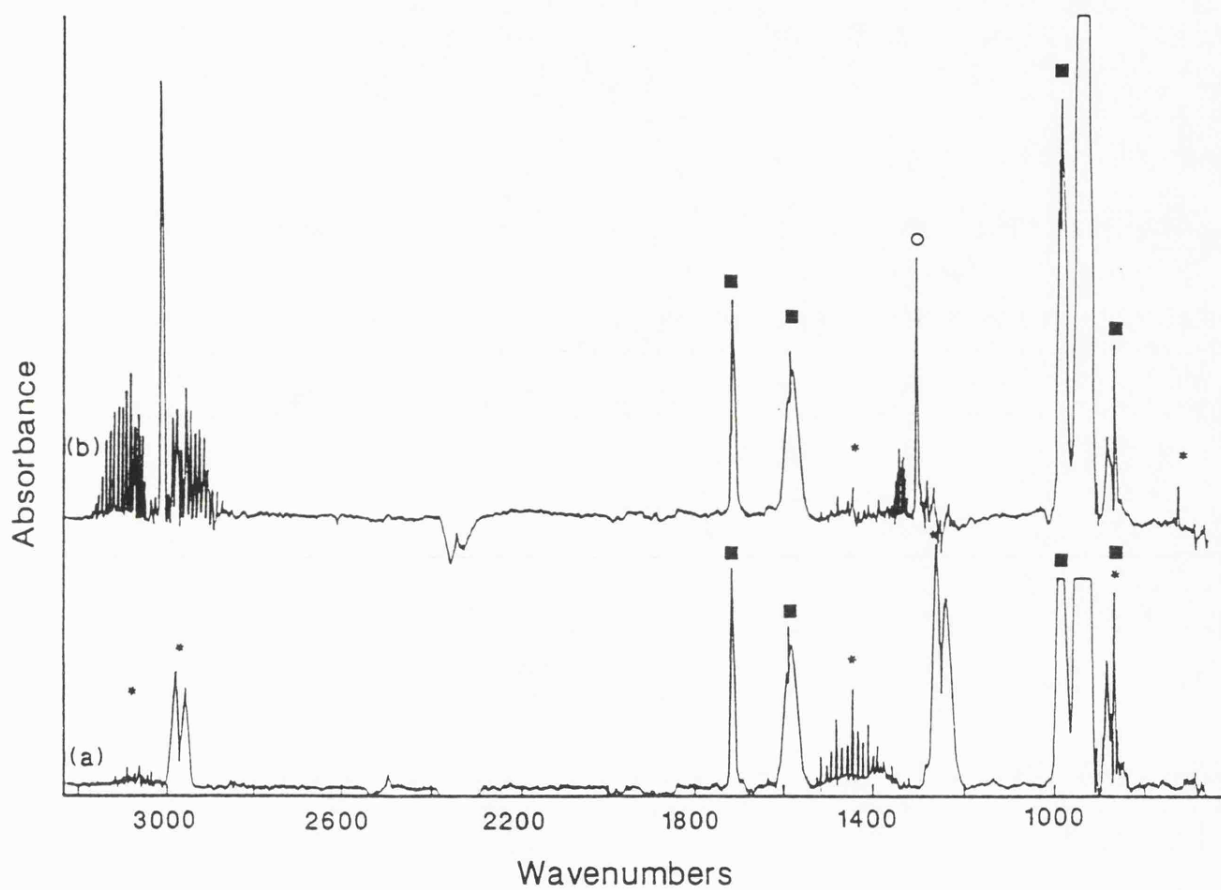


Figure 5.4:

IR spectra of 5 torr of  $\text{CH}_3\text{I}$  and 10 torr of  $\text{SF}_6$  irradiated with 8.0 watts of laser power for 10 minutes: a) before irradiation, and b) after irradiation. \* represents the starting material bands, o, represents the new bands, and ■ represents the photosensitizer ( $\text{SF}_6$ ) bands.

**Table 5.3:**

Wavenumbers of the characteristic product bands from the decomposition of  $\text{CH}_3\text{I}$ .

---

| New bands<br>( $\text{cm}^{-1}$ ) | Identified compounds   | Assignments |
|-----------------------------------|------------------------|-------------|
| 3017                              | $\text{CH}_4$          | C-H stretch |
| 1313                              | $\text{CH}_4$          | C-H bend    |
| 737                               | $\text{C}_2\text{H}_2$ | Bend        |

---

**Table 5.4:**

Wavenumbers of the characteristic product bands from the decomposition of  $\text{CD}_3\text{I}$ .

---

| New bands<br>( $\text{cm}^{-1}$ ) | Identified compounds   | Assignments |
|-----------------------------------|------------------------|-------------|
| 2278                              | $\text{CD}_4$          | C-D stretch |
| 1038                              | $\text{C}_2\text{D}_2$ | C-D bend    |
| 720                               | $\text{C}_2\text{D}_2$ | Bend        |

---

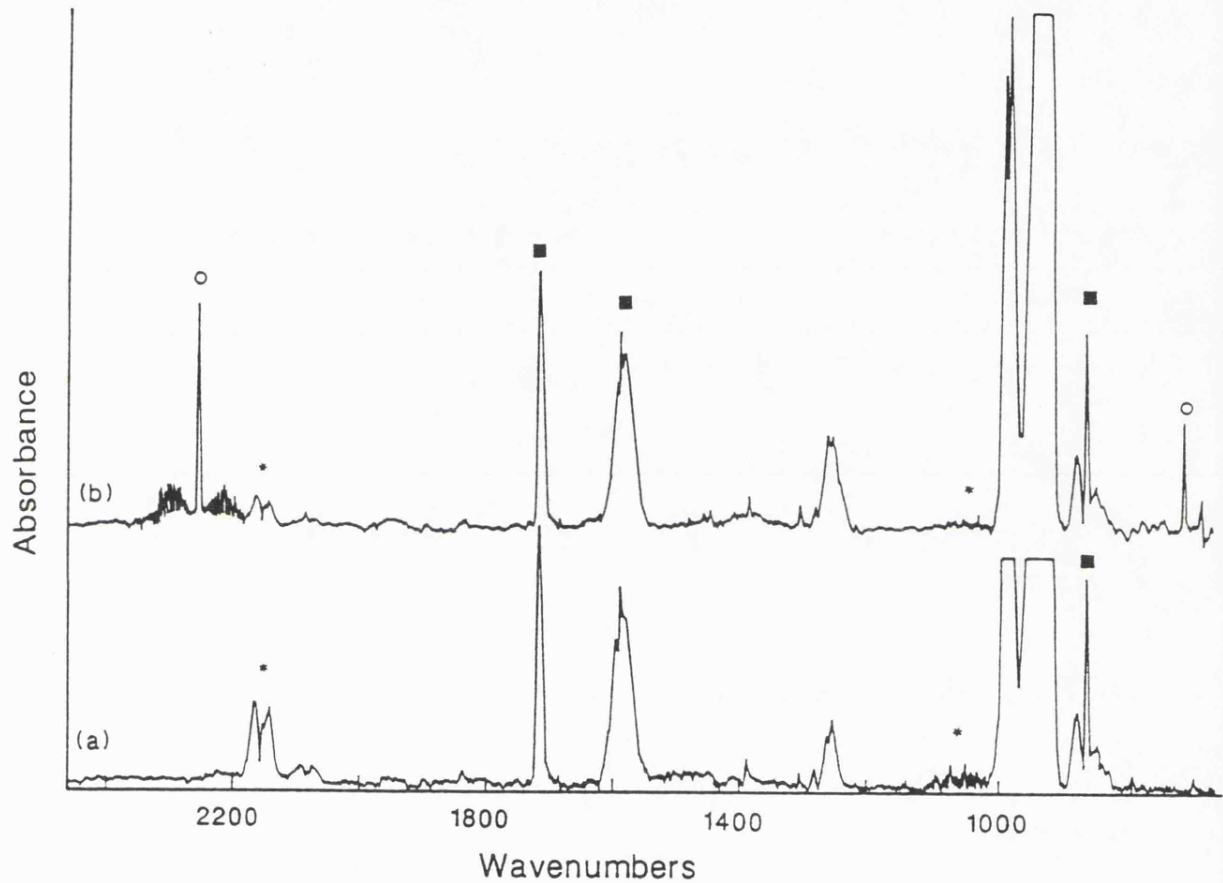


**Figure 5.5:**

IR spectra of 5 torr of  $\text{CD}_3\text{I}$  and 10 torr of  $\text{SF}_6$  irradiated with 10.0 Watts of laser power for 10 minutes: a) before irradiation and b) after irradiation. \* represents the starting material bands, o represents the new bands and ■ represents the photosensitizer bands.

difference in the decay of the starting material and the appearance of either  $\text{CH}_4$  and  $\text{CD}_4$ ), and thus the isotopic effects on the reaction. The rate of the decomposition of  $\text{CD}_3\text{I}$  was faster than  $\text{CH}_3\text{I}$ , Figure 5.6. The products of the reaction were mixture of  $\text{CH}_4$  and  $\text{CD}_4$ . Nothing was observed in any significant amount of the species  $\text{CH}_3\text{D}$ ,  $\text{CD}_3\text{H}$  or  $\text{CH}_2\text{D}_2$ .

### 5.5 DISCUSSION

The results observed from Experiment 3.1 revealed that no reaction occurs in the absence of the photosensitizer ( $\text{SF}_6$ ) in the reaction mixture. This was in spite of the fact that there is a band of vibration-rotation lines arising from the  $\nu_2$  band very close to the P20 line at  $944.19 \text{ cm}^{-1}$  of the  $\text{CO}_2$  laser. The results observed from the reaction of  $\text{CH}_3\text{I}$  showed the only products were  $\text{CH}_4$ , with a very small amount of  $\text{C}_2\text{H}_2$  and elementary iodine deposited on the windows and the cell wall. This probably means that the  $\text{CH}_3\text{I}$  decomposed to give  $\text{CH}_3$  radicals and iodine atoms; then  $\text{CH}_3$  radicals abstracted a hydrogen atom from the starting material ( $\text{CH}_3\text{I}$ ) to form methane,  $\text{CH}_4$ . From the results, no significant amount of ethane ( $\text{C}_2\text{H}_6$ ) and ethene ( $\text{C}_2\text{H}_4$ ) were observed, ie the same as conventional pyrolysis, the only way to explain the formation of ethyne ( $\text{C}_2\text{H}_2$ ) is that, probably, the  $\text{CH}_3$  radicals abstract more than one hydrogen atom from the  $\text{CH}_3\text{I}$ . The reaction steps can be arranged as follows:

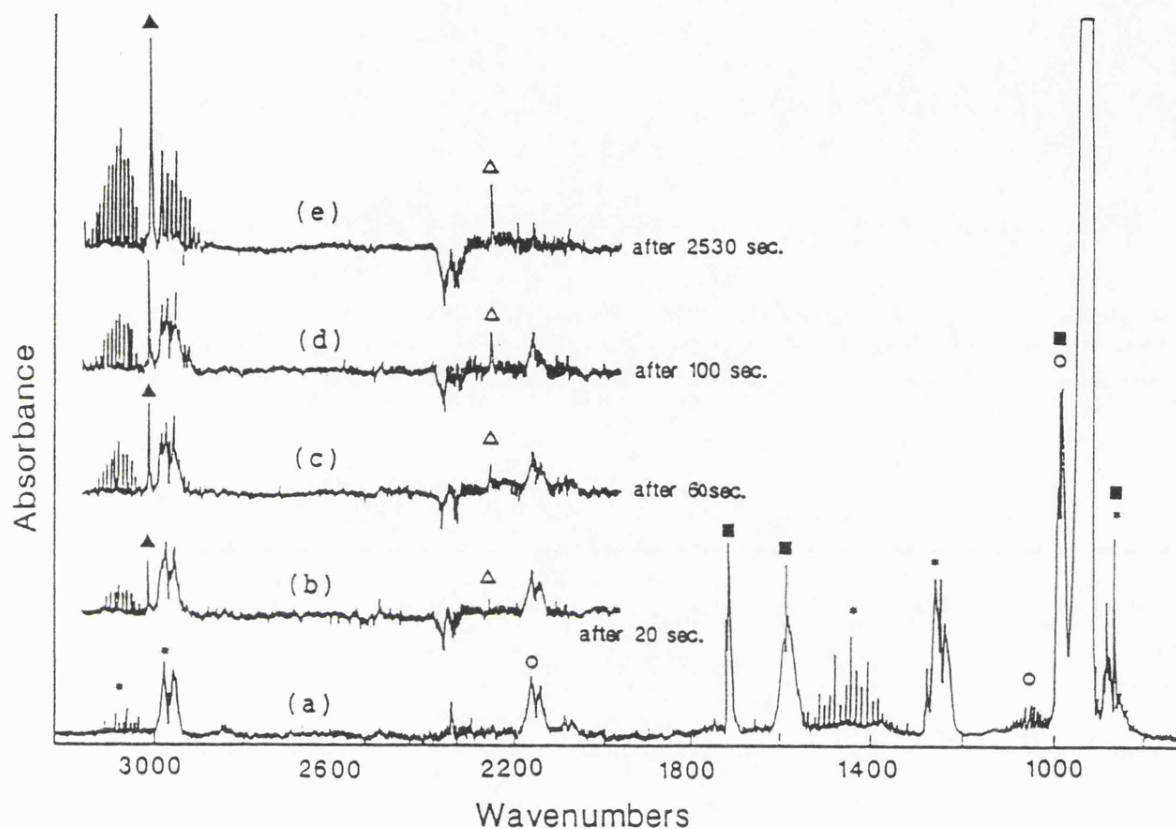
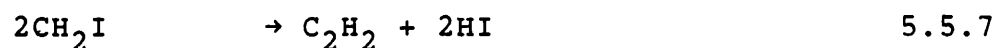
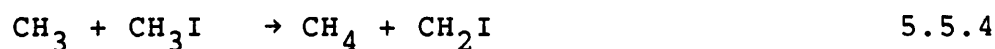
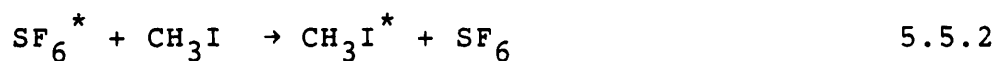


Figure 5.6:

IR spectra of mixture of 5 torr of  $\text{CD}_3\text{I}$ , 5 torr of  $\text{CH}_3\text{I}$  and 10 torr of  $\text{SF}_6$  irradiated with 8.75 Watts laser power: a) before irradiation, b, c, d, and e after irradiation. \*, o, and ■ represent the starting materials bands, new bands and the photosensitizer bands; and ▲ and Δ represent the  $\text{CH}_4$  and  $\text{CD}_4$  bands respectively.



The results of the experiment (3.3) show analogous information of the products in Experiment 3.2. The mechanism of the reaction is probably similar to the above mechanism in this section. That the only difference is in the rate of the reaction, which shows that the deuterated methyl iodide decomposes faster than the protonated form, Figures 5.7 and 5.8. The results from Experiment 3.4 support the results from Experiment 3.3, which shows that the deuterated methyl iodide reacts faster than methyl iodide. This is because the  $\nu_2$  mode of  $A_1$  symmetry ( $\text{CD}_3$  deformation vibration)<sup>35</sup> of the  $\text{CD}_3\text{I}$  interacts directly with the  $\text{CO}_2$  laser radiation at the line P20 (Figure 5.9) as well as obtaining energy from the photosensitizer,

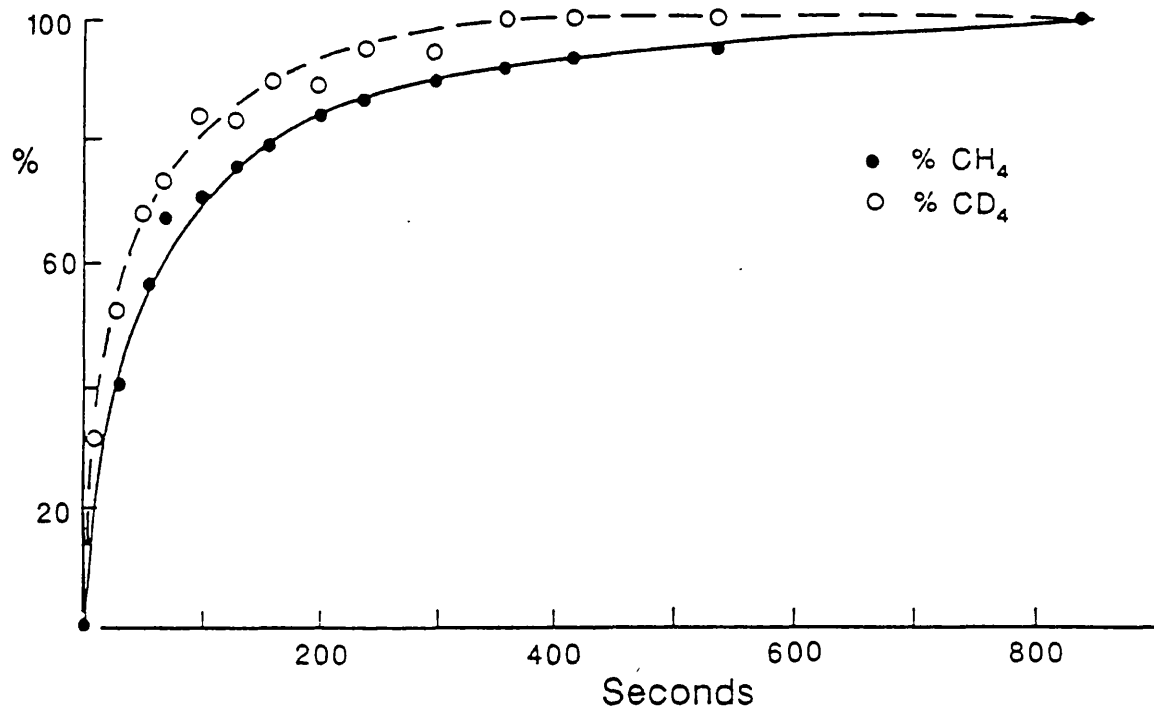


Figure 5.7:

Normalized plot of the appearance of CH<sub>4</sub> and CD<sub>4</sub> measured from their peak intensities from the reaction of a mixture of 5 torr of CH<sub>3</sub>I and CD<sub>3</sub>I, and 10 torr of SF<sub>6</sub> irradiated with 8.75 watts of laser power. The dashed and the solid lines are for the production of CD<sub>4</sub> and CH<sub>4</sub> respectively.

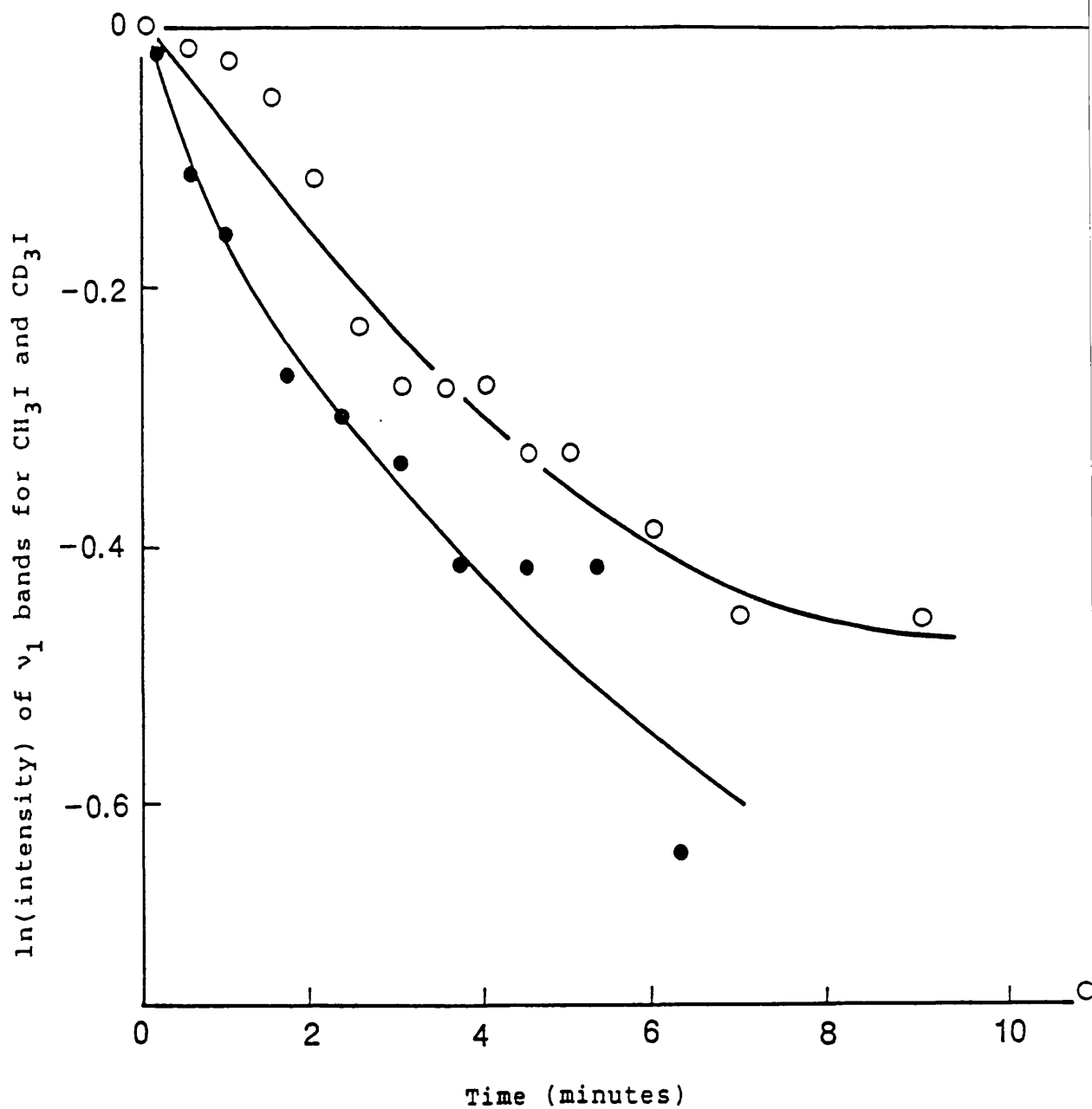


Figure 5.8:

"First order" plot for the reaction of 5 torr of  $\text{CH}_3\text{I}$  and 10 torr of  $\text{SF}_6$ ; and 5 torr of  $\text{CD}_3\text{I}$  and 10 torr of  $\text{SF}_6$  at laser power 8.75 Watts; the o and • represent the  $\text{CH}_3\text{I}$  and  $\text{CD}_3\text{I}$  reactions respectively.

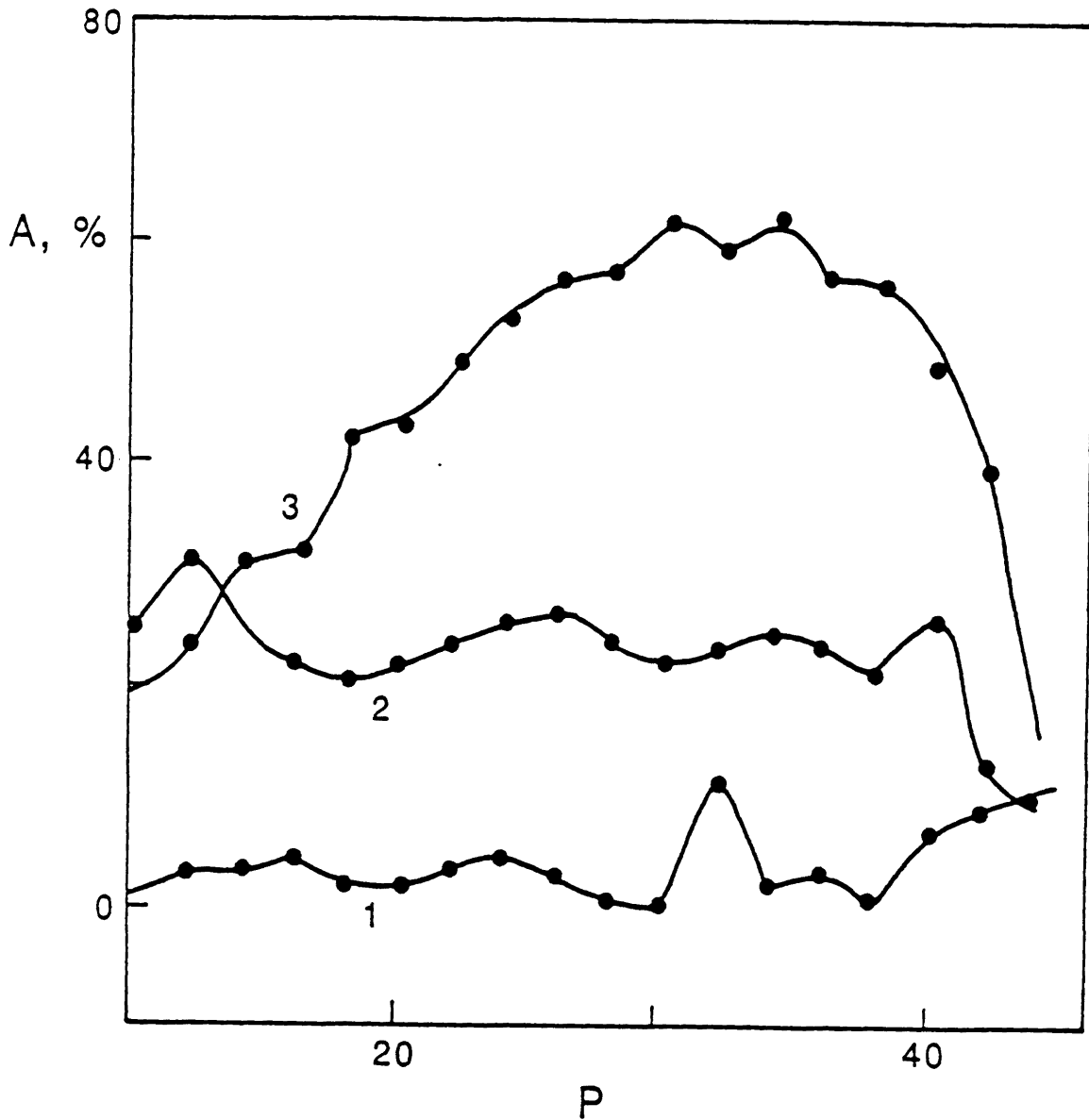


Figure 5.9:

IR radiation absorption (A) in  $\text{CH}_3\text{I}$ ,  $\text{CD}_3\text{I}$  and  $\text{SF}_6$  as a function of the excitation line of the 001-100 transition of  $\text{CO}_2$  laser. Output 8.0 Watts, focused by a lens 0.25 m; 6.64 kPa for  $\text{CH}_3\text{I}$  and  $\text{CD}_3\text{I}$ ; and 0.2 kPa of  $\text{SF}_6$ ; 1, 2 and 3 for  $\text{CH}_3\text{I}$ ,  $\text{CD}_3\text{I}$  and  $\text{SF}_6$  respectively. (taken from reference 34) (1 torr = 133.3 Pa).

whereas the nearest mode of  $\text{CH}_3\text{I}$  to the line P20 is about  $8 \text{ cm}^{-1}$  away, Figure 5.1.

## 5.6 CONCLUSION

The decomposition of  $\text{CH}_3\text{I}$  and  $\text{CD}_3\text{I}$  is a very good example of a simple molecular reaction under some circumstances. Utilizing the technique of LPHP allows us to eliminate the catalytic effect of iodine on the rate, because the  $\text{I}_2$  is deposited on the cell walls, which remain at room temperature. This point emphasises one of the major advantages of the LPHP technique, as compared with conventional (hot-wall) pyrolysis - some products are removed from the reaction zone, and the overall mechanism is less complex.

**5.7 REFERENCES**

1. W. Forst and P. St. Laurent.  
Can. J. Chem. 45 (1967) 3169.
2. W. Forst and P. St. Laurent.  
Can. J. Chem. 43 (1965) 3052.
3. A. Costela, J. M. Figuera, M. Martin, J. M. Pe'rez and  
L. Valle.  
J. C. S. Faraday I, 76 (1980) 30.
4. Y. Jiang, M. R. Giogi-Arnazzi and R. B. Bernstein.  
Chem. Phys. 106 (1986) 171.
5. G. N. A. Van Veen, T. Baller and A. E. DE. Vries.  
Chem. Phys. 97 (1985) 179.
6. F. P. Hudson, R. R. Williams, Jr., and W. H. Hamill.  
J. Phys. Chem. 21 (1954) 1894.
7. R. D. Souffie, R. R. Williams, Jr. and W. H. Hamill.  
J. Am. Chem. Soc. 78 (1956) 917.
8. C. C. Chou, P. Angelberger and F. S. Rowland.  
J. Phys. Chem. 75 (1971) 2536.
9. T. Donohue and J. R. Wiesenfeld.  
J. Phys. Chem. 80 (1976) 437.
10. C. Reiser, F. M. Lussier, C. C. Jensen, and J. I.  
Steinfeld.  
J. Amer. Chem. Soc. 101 (1979) 350.
11. W. Braun and W. Tsang.  
Chem. Phys. Lett. 44 (1976) 354.
12. T. Donohue and J. R. Wiesenfeld.  
Chem. Phys. Lett. 33 (1975) 176.
13. R. J. Butcher, R. J. Donovan, C. Fotakis, D. Fernie and  
A. G. A. Rae.

- Chem. Phys. Lett. 30 (1975) 398.
14. J. V. V. Kasper and G. C. Pimentel.  
Appl. Phys. Lett. 5 (1964) 231.
  15. D. M. Haaland and R. T. Meyer.  
Int. J. Chem. Kinet. 6 (1974) 297.
  16. Z-N. Gu, A. T. Young and P. L. Houston.  
Int. J. Chem. Kinet. 16 (1984) 669.
  17. J. V. V. Kasper, J. H. Parker and G. C. Pimentel.  
J. Chem. Phys. 43 (1965) 1827.
  18. R. A. Ogg, Jr..  
J. Amer. Chem. Soc. 56 (1934) 526.
  19. J. H. Sullivan.  
J. Phys. Chem. 56 (1961) 722.
  20. S. W. Benson and G. N. Spokes.  
J. Amer. Chem. Soc. 24 (1967) 2525.
  21. R. K. Boyd, G. W. Downs, J. S. Gow, and C. Horrex.  
Chem. Rev. 67 (1963) 719.
  22. K. Saito, H. Tahara, O. Kondo, T. Yokubo, T. Higashinara and I. Murakami.  
Bull. Chem. Soc. Jpn. 53 (1980) 1335.
  23. K. S. H. Tahara and I. Murakami.  
Bull. Chem. Soc. Jpn. 57 (1984) 3023.
  24. C. A. McDowell and B. G. Cox.  
J. Chem. Phys. 20 (1952) 1496.
  25. S. W. Benson and O'Neal.  
J. Phys Chem. 39 (1961) 514.
  26. H. Mackle and A. R. Ubbelohde.  
J. Chem. Soc. (1948) 1161.
  27. R. J. Nichol and A. R. Ubbelohde.

- J. Chem. Soc. (1952) 415.
28. A. S. Carson, K. Hartley and H. A. Skinner.  
Proc. Roy Soc. (London) A 195, 500.
29. M. Prichard and H. A. Skinner.  
Trans. Faraday Soc. 48 (1952) 220.
30. R. D. Schultz and H. A. Taylor.  
J. Chem. Phys. 18 (1950) 194.
31. D. M. Golden and S. W. Benson.  
Chem. Rev. 69 (1969) 125.
32. K. Dathe, P. Engst, J. Pola and M. Horak.  
Collec. Czechoslov. Chem. Commun. 45 (1980) 1910.
33. J. Rejnek, M. Jakoubkova, P. Engst and M. Horak.  
Collec. Czechoslov. Chem. Commun. 48 (1983) 3261.
34. J. Rejnek, P. Engst, M. Jakoubova and M. Horak.  
Collec. Czechoslav. Chem. Commun. 50 (1985) 215.
35. W. T. King, I. M. Mills and B. Crawford Jr..  
J. Chem. Phys. 27 (1957) 455.

## CHAPTER 6

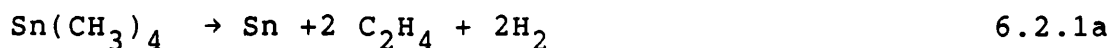
## PYROLYSIS OF TETRAMETHYLTIN AND HEXAMETHYLDITIN

6.1 INTRODUCTION

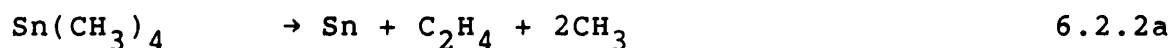
The thermal decompositions of tetramethyltin, TMT, and hexamethylditin, HMDT, were studied in this chapter, utilizing the LPHP technique. The reactions were also carried out in the presence of  $H_2$  or  $O_2$ , which were used as radical scavengers. A mechanism for the reaction is proposed, based on isotopic labelling of the products, using  $D_2$ . Preliminary kinetic measurements were carried out to estimate the activation energy for the TMT and HMDT reactions. The reactions were followed using the FTIR spectrometer. This chapter begins with a review of the work done on the thermal decomposition of TMT and HMDT followed by the experimental results, the kinetic measurements, discussion and the advantages and the disadvantages of using this technique.

6.2 REVIEW

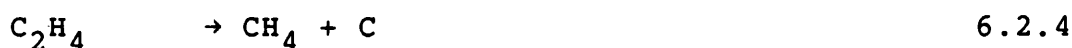
The thermal decomposition of TMT has been investigated volumetrically by Waring et al<sup>1</sup>. The reaction was found to be almost homogeneous and first order. The addition of nitric oxide NO was found to have no effect on the rate of the reaction, but had a slight catalytic effect on the initial stage of the reaction. The rate of the reaction in a packed vessel reactor, in which the ratio of surface to volume was increased by 9%, was increased by 30% in comparison to the normal unpacked vessel. Waring et al suggested that the overall reaction can be represented as one of the following:



They rationalised this by proposing that the major route was a rearrangement, and that a small percentage of free radicals was also produced during the processes:



They also identified secondary processes as follows:



The activation energy of the reaction was found to be 356 kJ mol<sup>-1</sup>.

Sathyamurthy et al<sup>2</sup> recalculated the results of Waring et al on the basis of a three halves order reaction supposing the reaction to involve free radicals and not a molecular rearrangement mechanism. The new activation energy was 318 kJ mol<sup>-1</sup>.

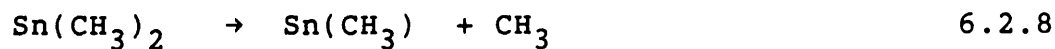
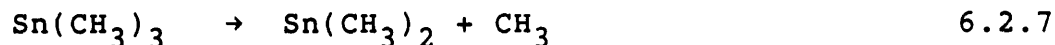
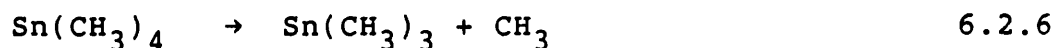
In 1965 Yergey et al<sup>3</sup> investigated the bond dissociation energy of TMT and HMDT using an electron impact study combined with thermochemical data. The dissociation energies

were found to be 218 and 146 kJ mol<sup>-1</sup> for (CH<sub>3</sub>)<sub>3</sub>Sn-CH<sub>3</sub> and (CH<sub>3</sub>)<sub>3</sub>Sn-Sn(CH<sub>3</sub>)<sub>3</sub>, respectively. In 1966, Tel'oni et al<sup>4</sup> found the Sn-C bond energy of TMT to be 210 ±20 kJ mol<sup>-1</sup> as measured calorimetrically.

Lappert et al<sup>5</sup> in 1969 investigated the dissociation energy of group IVA mass spectroscopically. They determined the dissociation energy by measuring the appearance ionization potential of the radicals. The dissociation energy of the (CH<sub>3</sub>)<sub>3</sub>Sn-CH<sub>3</sub> bond was found to be 255 kJ mol<sup>-1</sup>.

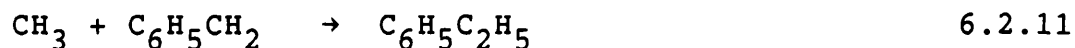
In 1970, they reinvestigated the dissociation energy of the C-Sn and Sn-Sn bonds utilizing the mass spectrometric technique, combined with thermodynamic data. These were measured to be 273.63 and 256 kJ mol<sup>-1</sup> for the bonds C-Sn of TMT and Sn-Sn of HMDT, respectively<sup>6</sup>.

Johnson et al<sup>7</sup> studied the pyrolysis of TMT in a toluene carrier flow system at temperatures from 803-941 K. The kinetics of the reaction were found to be first order. The mechanism of the reaction was based on successive loss of methyl radicals, Reactions 6.2.6-6.2.9,



The CH<sub>3</sub> radicals are either scavenged by toluene to form CH<sub>4</sub> and C<sub>6</sub>H<sub>5</sub>CH<sub>2</sub>, or recombined to form C<sub>2</sub>H<sub>6</sub> as in Reaction 6.2.10

and 6.2.12:



Their measurement of the activation energy of the reaction was  $270 \text{ kJ mol}^{-1}$ , consistent with that derived from mass spectrometric and the thermochemical data<sup>6</sup>.

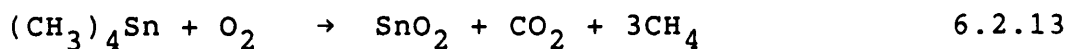
The pyrolysis of TMT was studied by Taylor et al using a wall-less reactor<sup>8</sup>. The major products of the decomposition were  $\text{C}_2\text{H}_6$  and  $\text{CH}_4$  at the higher temperature of 884 K. The ratio of  $\text{CH}_4/\text{C}_2\text{H}_6$  was 0.24. At lower temperature 794 K the ratio of  $\text{CH}_4/\text{C}_2\text{H}_6$  was 1.02. The temperature was thus found to have an effect on the products, which they assumed to be a function of the concentration of methyl radicals,  $[\cdot\text{CH}_3]$ . The methyl radicals are recombined to form  $\text{C}_2\text{H}_6$  at higher temperature, and reaction with starting material becomes more likely by abstraction of hydrogen atoms from the TMT, at lower temperature. The activation energy of the reaction was found to be  $230 \text{ kJ mol}^{-1}$ .

Baldwin et al<sup>9</sup> studied the thermal pyrolysis of TMT<sup>8</sup>, utilizing the very low pressure pyrolysis technique (VLPP) at temperatures from 1000 to 1260 K. The reaction was followed mass spectrometrically. The mechanism of the reaction at this temperature was proposed to be as in Reactions 6.2.3 to 6.2.6, in which TMT loses  $\text{CH}_3$  radicals very fast at this temperature. On addition of excess of deuterium iodide, DI, to

the reaction vessel it was noticed that  $\text{CH}_3\text{D}$  was formed and no evidence of any  $(\text{CH}_3)_3\text{SnD}$  was found. Using the VLPP method is very useful in eliminating chain reactions which could be initiated by  $\text{CH}_3$  radicals or the hydrogen atoms attacking the original reactants. The activation energy was found to be  $289 \pm 8 \text{ kJ mol}^{-1}$ .

Griller et al<sup>10</sup> studied the bond dissociation energy, (BDE) for TMT. It was calculated using the thermodynamic data available. The BDE of  $(\text{CH}_3)_3\text{Sn-CH}_3$  was found to be  $268 \text{ kJ mol}^{-1}$ .

Ashworth et al<sup>11</sup> in 1987 investigated the thermal decomposition of TMT in the presence of  $\text{O}_2$ . The reaction cell was heated by using an electric heater wound around the cell. The reaction of TMT in presence of  $\text{O}_2$ , Reaction 6.2.11, was found to be independent to the  $\text{O}_2$ , ie was zero order:



The activation energy of the reaction was found to be  $114 \text{ kJ mol}^{-1}$ , which indicates that heterogeneous reaction takes place on the wall of the cell. The observed activation energy of the reaction is rather lower than expected on the bases of the observed BDE, which revealed the reaction is catalyzed on the surface, especially when the  $\text{SnO}_2$  was deposited on the wall of the reaction cell

### 6.3 EXPERIMENTAL

The equipment and the chemicals which were used in this chapter were described in Chapter 3.

The experiments which were carried out to study the

thermal decomposition and the mechanism of the reaction of TMT and HMDT are described below.

### 6.3.1 Pyrolysis of TMT

Two torr of TMT were mixed with 10 torr of SF<sub>6</sub>. The mixture was irradiated with the IR CO<sub>2</sub> laser. The progress of the reaction was followed using the FTIR spectrometer, following the decay of TMT by the Sn-C stretching band at 771 cm<sup>-1</sup>, see Figure 6.1 and Table 6.1. The experiment was repeated varying the CO<sub>2</sub> laser power in the range from 5 up to 10 watts, at intervals of 1.25 watts.

### 6.3.2 The pyrolysis of TMT in presence of O<sub>2</sub>

Two torr of TMT, 3.5 torr of O<sub>2</sub> and 10 torr of SF<sub>6</sub> were mixed and irradiated with 6.25 watts laser power. The progress of the reaction was followed by using FTIR spectrometer and the decay of the Sn-C bond (771 cm<sup>-1</sup>).

### 6.3.3 The pyrolysis of TMT in presence of Deuterium D<sub>2</sub>

Two torr of TMT, 10 torr of SF<sub>6</sub> and 10 torr of D<sub>2</sub> were mixed and irradiated with CO<sub>2</sub> laser of 7.5 watts power. The progress of the reaction was followed using FTIR spectrometer. The same above mixture was irradiated with about 10 watts.

### 6.3.4 The pyrolysis of HMDT

Two torr of HMDT was mixed with 10 torr of SF<sub>6</sub>. The reaction was followed using FTIR spectrometer. The Sn-C bond was followed. The Sn-Sn bond absorption lies in the far IR region, so the IR spectrum for HMDT in the near IR region was identical to, and very hard to distinguish from, that of

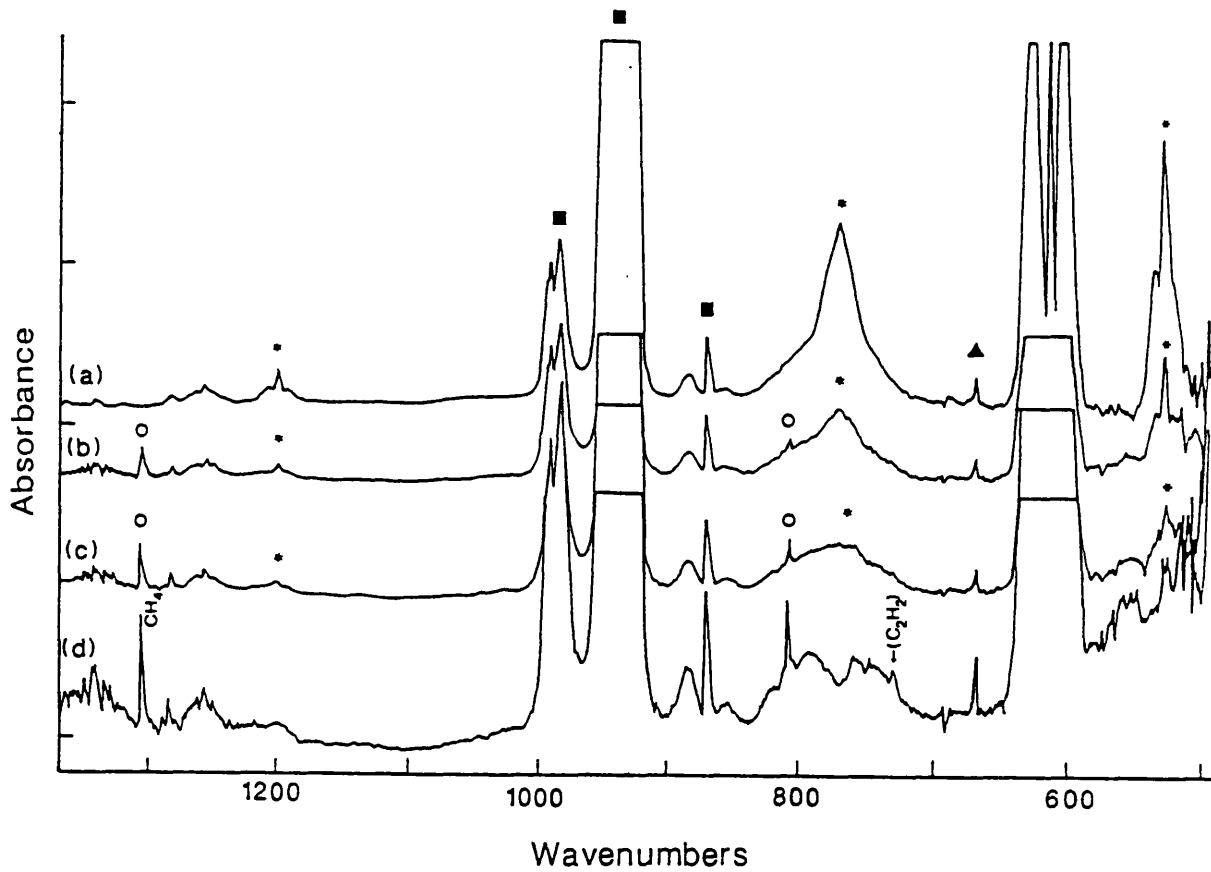


Figure 6.1:

IR spectra of 2 Torr of TMT and 10 Torr of  $\text{SF}_6$  irradiated with a laser power of 8.25 Watts: a) before, b) after 25 Sec., c) after 60 Sec. of irradiation. Here, \* represents the TMT bands, o the new bands, ■ the photosensitizer bands and ▲ is due to a solid material on the windows.

Table 6.1:

The IR bands of TMT and their assignments.<sup>12</sup>

---

| Bands ( $\text{cm}^{-1}$ ) | Assignments          |
|----------------------------|----------------------|
| 529 s                      | C-Sn stretch         |
| 535 s                      | CH <sub>3</sub> rock |
| 771 vs                     | CH <sub>3</sub> rock |
| 1192                       | C-H bend             |
| 1200                       | C-H bend             |
| 1208                       | C-H bend             |
| 2921                       | C-H stretch          |
| 2986                       | C-H stretch          |
| 2995                       | C-H stretch          |
| 3048                       | C-H stretch          |

---

TMT. The same above mixture was repeated varying the range of laser power from 5 to 12 watts, 1.25 watts interval.

## 6.4 KINETIC MEASUREMENTS

### 6.4.1 The kinetic measurements of TMT

The kinetic measurements of TMT were carried out by following the decay of the concentration of the reactants (integrating the area under the peak), which is proportional to the concentration. The plot of  $\ln(\text{concentration})$  of the peak vs time was a straight line up to 30% reaction (see Figure 6.2 and Table 6.2). Since the temperature of the cell is dependent on the conductivity of the contents of the cell, and the latter changes while the reaction goes on, the initial rate was taken supposing the change is negligible.

The reaction appeared to be first order; a plot of the rate of the reaction vs laser power showed that the rate of the reaction increased rapidly with laser power above 8.0 Watts, Figure 6.3.

### 6.4.2 The kinetic measurements of HMDT

HMDT was decomposed over a range of laser power which corresponds to a range of temperature (see Chapter 3). The intensity of the peak ( $771 \text{ cm}^{-1}$ )  $(\text{Sn-C})_{\text{st}}$  was followed as proportional to the concentration. The plot of the  $\ln(\text{intensity})$  of  $(\text{Sn-C})_{\text{st}}$  vs time gives the rate of the reaction, Figure 6.4. The reaction was indicated as first order, for the decomposition of up to about 30% of the sample; here, the plot started to curve from a straight line

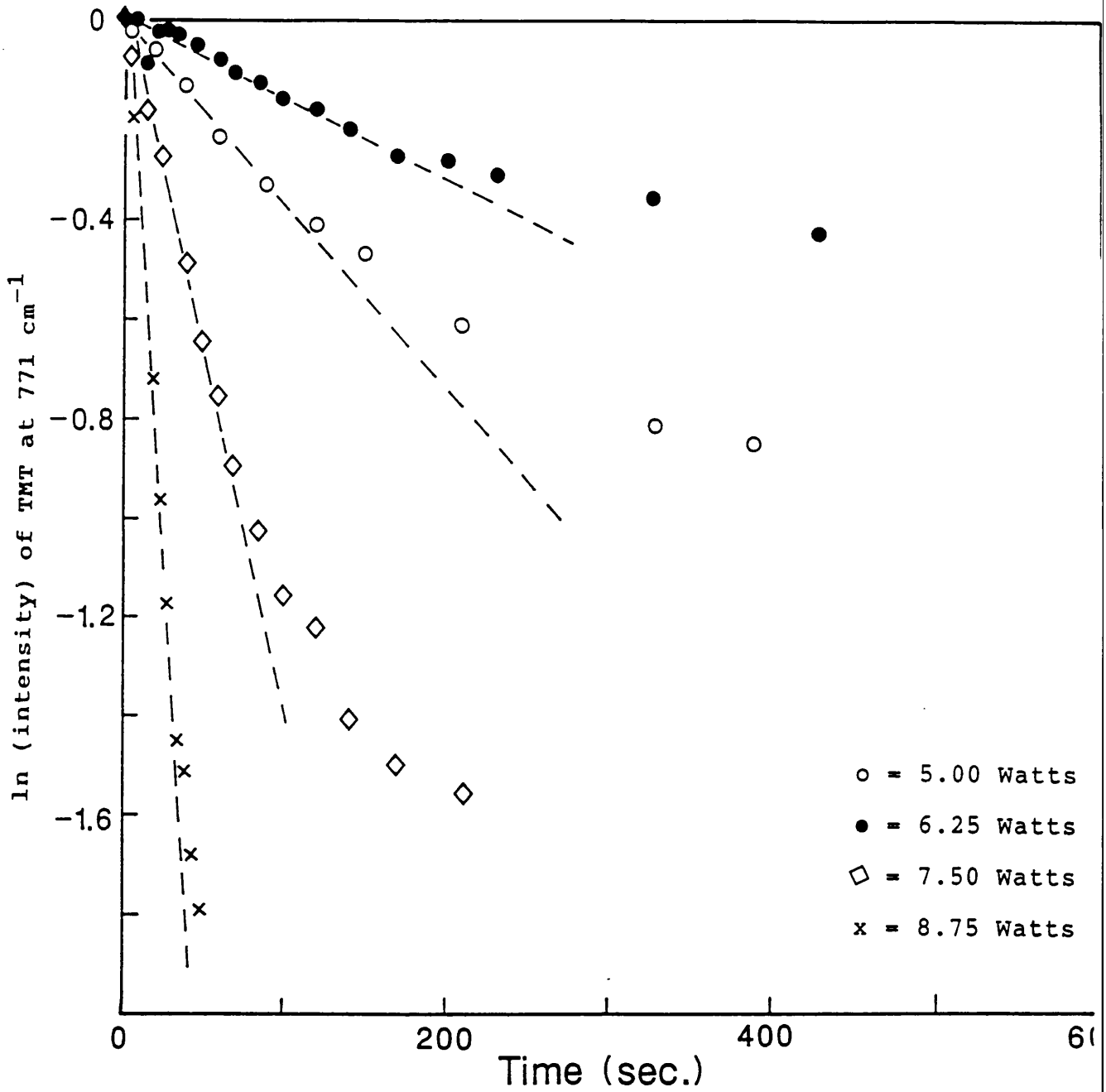


Figure 6.2:

ln (intensity) of TMT vs time at various laser powers.

Table 6.2:

Relative rates (signal intensity  $\text{sec}^{-1}$ ) of the reaction of TMT and HMDT at various laser powers. The pressure of the reactants was 2 torr, and of the photosensitizer 10 torr.

| Laser power<br>(Watts) | Rate of loss of<br>TMT | Rate of loss of<br>HMDT |
|------------------------|------------------------|-------------------------|
| 5.00                   | $1.07 \times 10^{-2}$  | $3.10 \times 10^{-4}$   |
| 6.25                   | $3.50 \times 10^{-3}$  | $2.66 \times 10^{-3}$   |
| 6.75                   | $1.81 \times 10^{-2}$  | -----                   |
| 7.00                   | -----                  | $4.25 \times 10^{-3}$   |
| 7.50                   | $1.29 \times 10^{-2}$  | $1.29 \times 10^{-2}$   |
| 8.00                   | -----                  | $1.25 \times 10^{-2}$   |
| 8.75                   | $3.66 \times 10^{-2}$  | $5.00 \times 10^{-2}$   |
| 10.00                  | $1.00 \times 10^{-1}$  | -----                   |

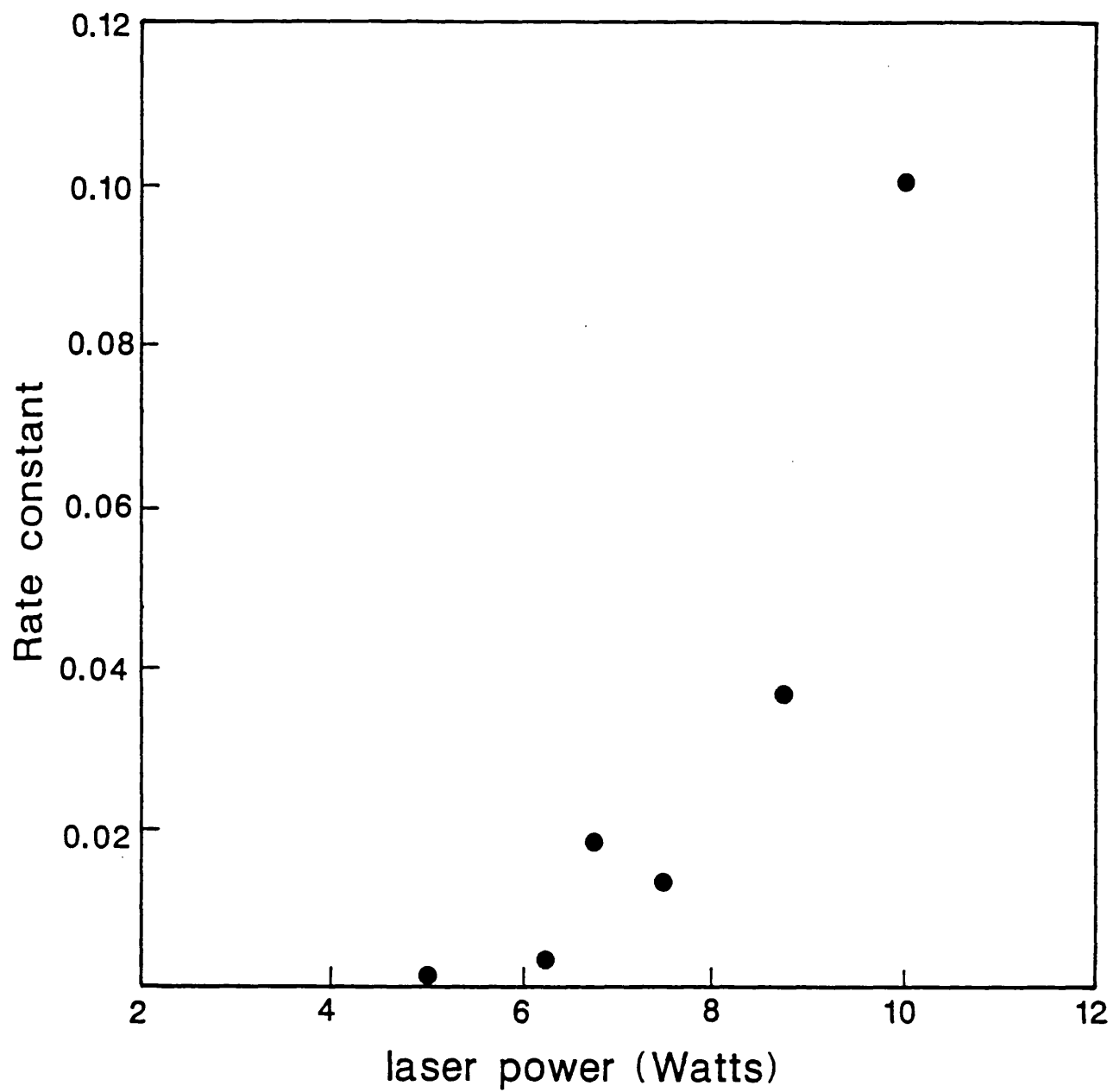


Figure 6.3:

Relative rate of the reaction of TMT vs laser power (Watts).

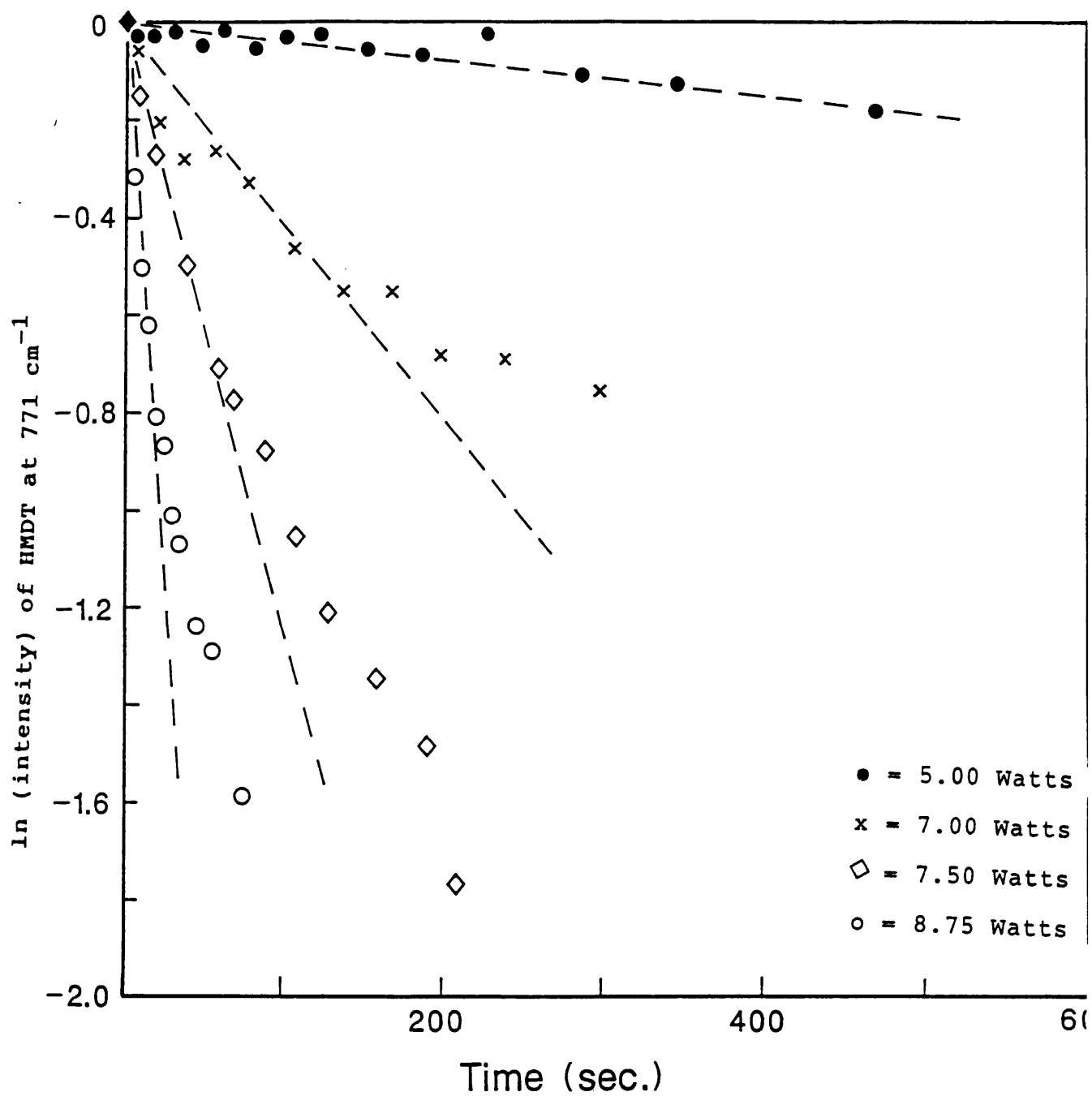


Figure 6.4:

ln (intensity) of HMDT vs time at various laser powers.

indicating that the reaction was slowing down because of the appearance of  $\text{CH}_4$ ; the latter increases the cell conductivity, cooling down the hot reaction zone.

The rate of the reaction increased rapidly with laser power, Figure 6.5. Measurements of the activation energy require precise calibration of the laser power to temperature (see Chapter 4).

## 6.5 RESULTS AND DISCUSSION

The results of the decomposition of TMT and HMDT in the conditions of our arrangements are discussed below.

### 6.5.1 The decomposition of TMT

This experiment showed that the TMT was decomposed above 5 Watts of laser power. The decomposition at this range of power was measurable. Above 25 Watts of laser power the decomposition appeared to be a very fast chain reaction. The pre and post IR spectra revealed extensive changes (Figure 6.1); the major product was methane,  $\text{CH}_4$ , and a brownish material was deposited on the reaction cell wall and the front window. Ethyne was indicated in very small amounts, during irradiation by laser power above 20 Watts only.

### 6.5.2 The decomposition of TMT in presence of $\text{O}_2$

The decomposition of TMT in presence of  $\text{O}_2$  showed that the major products were also methane  $\text{CH}_4$ ,  $\text{CO}_2$ , and a very small amount of carbon monoxide,  $\text{CO}$ , (Figure 6.6). The rate of the reaction was not affected by the addition of  $\text{O}_2$ . At a laser power of 15 watts, the reaction was very fast; the mixture was

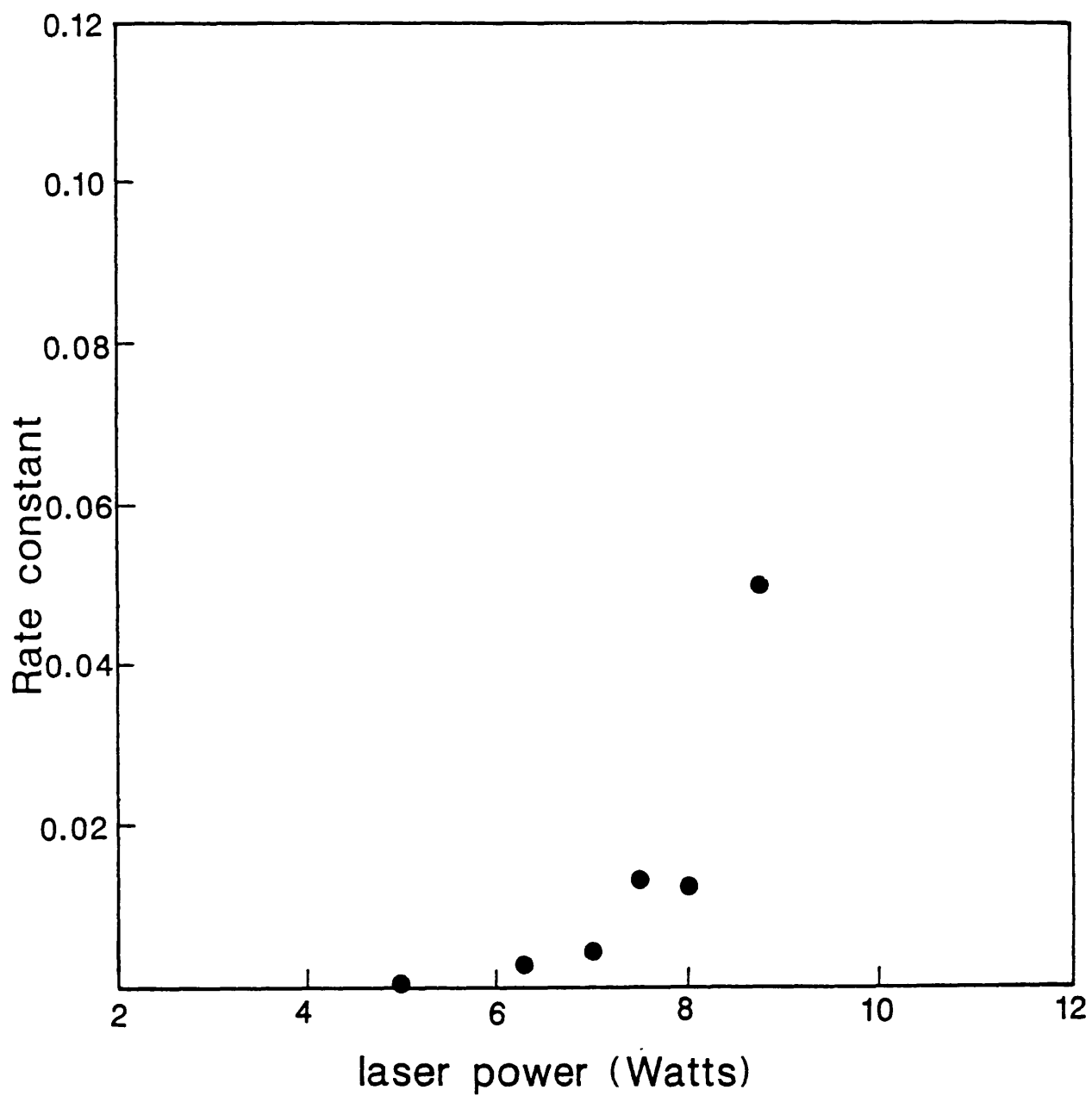
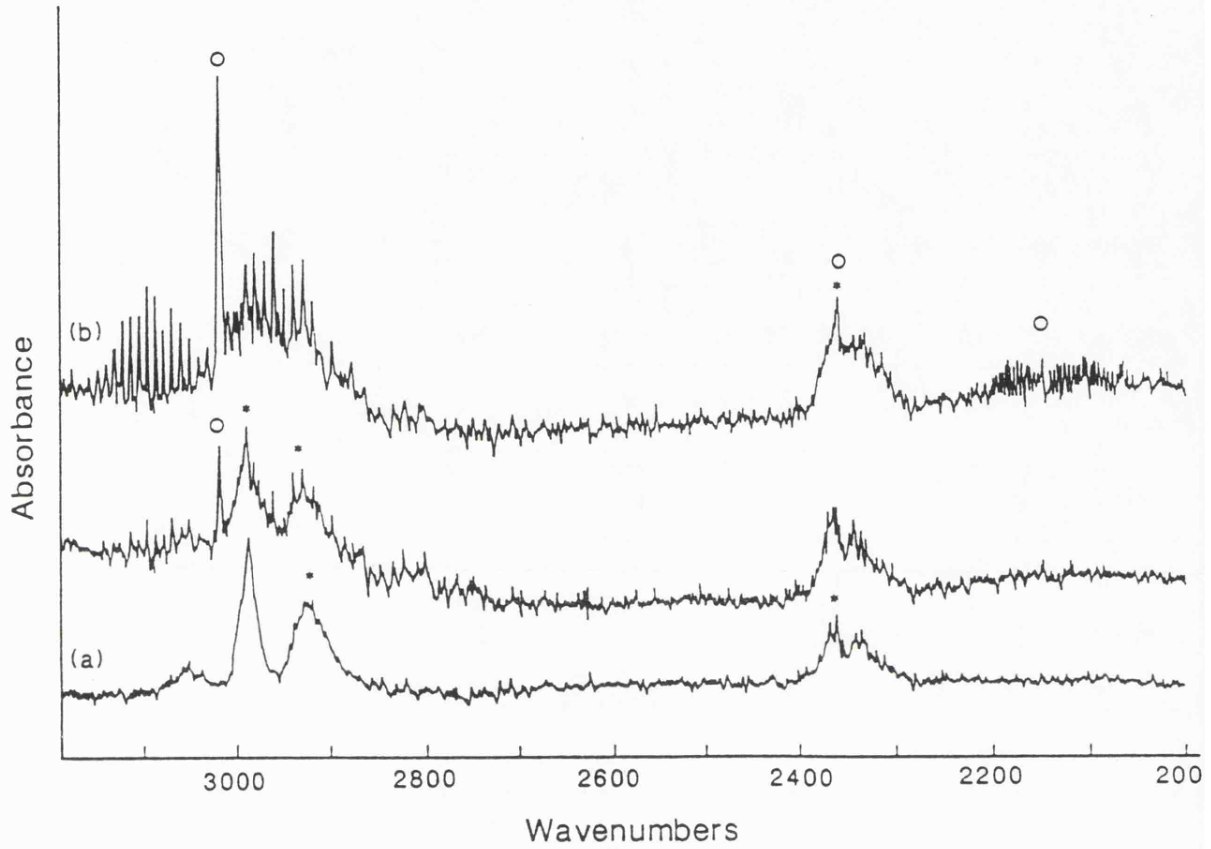


Figure 6.5:

Relative rates of the reaction of HMDT vs laser power.



**Figure 6.6:**

The IR spectra of 2 torr TMT, 3.5 torr O<sub>2</sub> and 10 torr SF<sub>6</sub> irradiated with a laser power of 6.25 Watts: a) before and b) after irradiation; \* and o are represent the starting material and the new bands respectively.

exploded and emitted green light.

### 6.5.3 The decomposition of TMT in presence of D<sub>2</sub>

The IR spectra of pre and post irradiated mixtures by CO<sub>2</sub> laser revealed that the major products were methane, CH<sub>4</sub>, and a significant amount of CH<sub>3</sub>D, which was identified by its characteristic absorption, Table 6.3 and Figure 6.7.

**Table 6.3:**

List of new bands after irradiating a mixture of 2 torr of TMT + 10 torr of D<sub>2</sub> and 10 torr SF<sub>6</sub>, with laser power 7.50 Watts.

| Identified compounds | Bands (cm <sup>-1</sup> ) | Assignments |
|----------------------|---------------------------|-------------|
| CH <sub>4</sub>      | 3017                      | C-H stretch |
| CH <sub>4</sub>      | 1306                      | C-H bend    |
| CH <sub>3</sub> D    | 2200                      | C-D stretch |
| CH <sub>3</sub> D    | 1156                      | C-D bend    |

### 6.5.4 Decomposition of HMDT

The decomposition of this compound under the experimental conditions showed that the major products were methane, CH<sub>4</sub>, and a thin layer of brownish unidentified material deposited on the front window and the reaction cell wall. The peak at 771 cm<sup>-1</sup> was followed to monitor the reaction. Unfortunately the (Sn-Sn)<sub>st</sub> bond absorptions lie in the far IR region, which cannot be

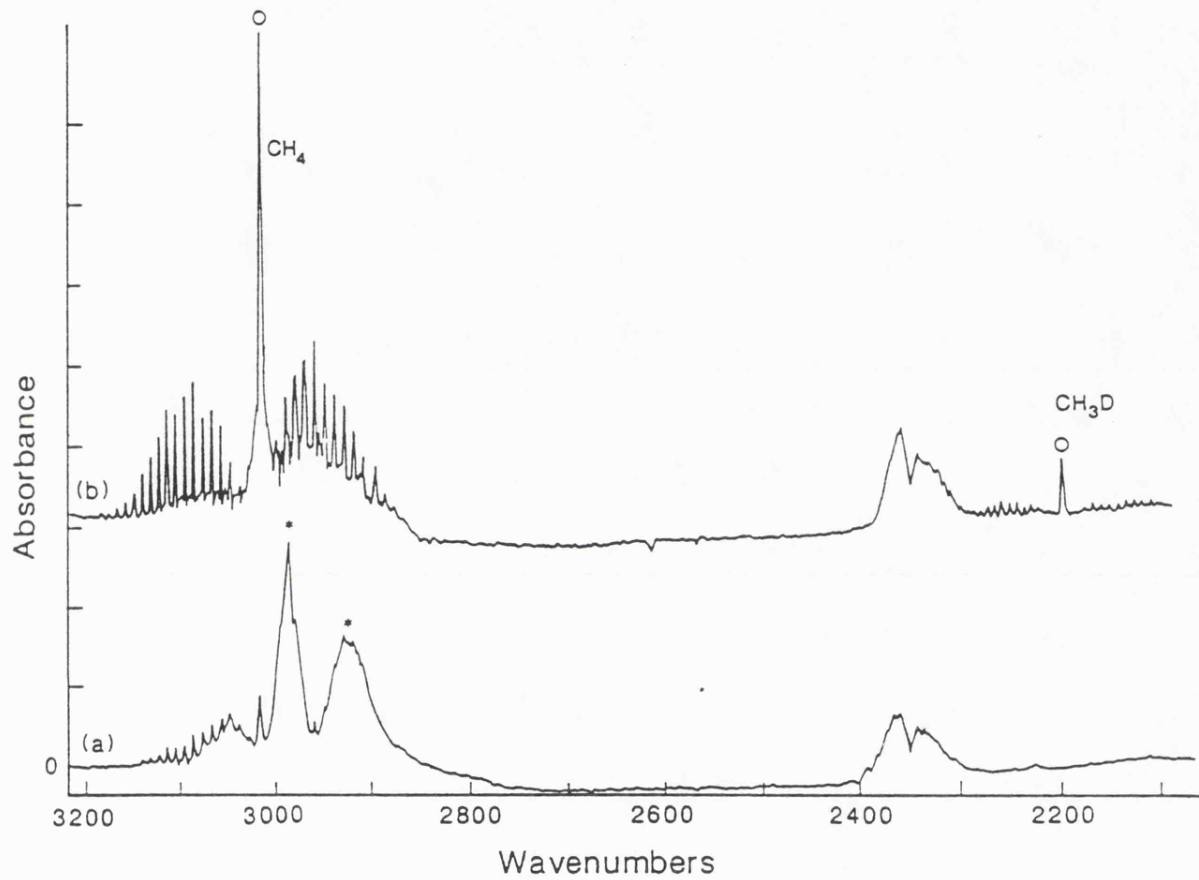


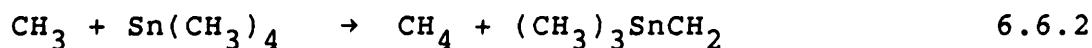
Figure 6.7:

IR spectra of 2 torr of TMT, 10 torr of D<sub>2</sub> and 10 torr SF<sub>6</sub> irradiated with 7.50 Watts laser power: a) before and b) after irradiation; \* and o are represent the starting material and the new bands respectively.

observed in our spectrometer.

## 6.6 DISCUSSION

The results of the experiments described in Section 5.1 suggested that the formation of  $\text{CH}_4$  can be ascribed to  $\text{Sn-CH}_3$  bond dissociation, producing  $\text{CH}_3$  radicals. A negligible amount of  $\text{C}_2\text{H}_2$  appeared at laser power above 20 Watts, at which a chain reaction was produced. The methyl radicals involved in secondary reactions are as follows:



No other mechanism is likely under the experimental conditions, except when the laser power is above 20 watts.

The results of the experiments described in Section 5.2 show the decomposition of TMT in the presence of  $\text{O}_2$  did not involve any chain reactions. It was very difficult to deduce mechanisms for this reaction, thus needs further investigation. An overall balanced reaction can be written, according to the major products:



The rate of the reaction in the presence of  $\text{O}_2$  was nearly the same as without  $\text{O}_2$ ; thus the presence of  $\text{O}_2$  in the reaction mixture did not affect the reaction. A very small amount of CO was observed.

In the presence of  $\text{D}_2$ , the decomposition of TMT indicates

clearly that the  $\text{CH}_3$  radicals formed attacked the original reactants, because the formation of  $\text{CH}_3\text{D}$  at the range of laser power up to 10 Watts was negligible. Above that, the amount of  $\text{CH}_3\text{D}$  increased, indicating that the  $\text{CH}_3$  radicals started to react with  $\text{D}_2$ :



## 6.7 CONCLUSION

This preliminary study of the thermal decomposition of TMT using the LPHP technique indicated its advantages over the previous methods. The surface catalysis effects were completely eliminated. The deposited tin materials, which have catalyzing effects, were deposited on the cell wall, far away from the reaction zone. The presence of the  $\text{D}_2$  in the reaction proved that the metal carbon bond was ruptured first, and the formation of  $\text{CH}_4$  occurred as a result of abstracting a hydrogen atom from the TMT at the experimental conditions. The formation of  $\text{CH}_3\text{D}$  was as a result of trapping  $\text{CH}_3$  radicals by the  $\text{D}_2$ . More investigation should be made to study the mechanism of the reaction and the  $\text{CH}_3$  radicals should be trapped by a convenient scavenger.

**6.8 REFERENCES**

1. C. E. Waring and Wm. S. Horton.  
J. Amer. Chem. Soc. 67, 1945, 540.
2. T. V. Sathyamurthy, S. Swaminathan and Lourdu M.  
Yaddanappalli.  
J. India. Chem. Soc. 27, 1950, 509.
3. A. L. Yergey and F. W. Lampe.  
J. Amer. Chem. Soc. 20, 1965, 4204.
4. V. I. Tel'noi and I. B. Robinovich.  
Russ. J. Phys. Chem. 40, 1966, 842.
5. M. F. Lappert, T. Simpson and T. R. Spalding.  
J. Organometal. Chem. 17, 1969, P1.
6. M. F. Lappert, J. B. Pedley, J. Simpson and T. R. Spalding .  
J. Organometal. Chem 29, 1971, 195.
7. R. P. Johnson and S. T. W. Price.  
Canad. J. Chem. 50, 1972, 50.
8. J. E. Taylor and Thomas S. Milazzo.  
Phys. Chem. 82, 1978, 847.
9. A. C. Baldwin, K. E. Lewis and D. M. Golden.  
Int. J. Chem. Kinetics, 11 (1979) 529.
10. D. Griller and J. M. Kanabus-Kaminska, A. Maccoll.  
J. Molecular. Structure. (Theochem) 163 (1988) 125.
11. A. P. Ashworth, E. N. Clark, and P. G. Harrison.  
J. Chem. Soc. Chem. Commun. 10 (1987) 782.
12. W. F. Edgell and C. H. Ward.  
J. Amer. Chem. Soc. 77 (1955) 6486.

## CHAPTER 7

## THE DECOMPOSITION OF TRIMETHYLALUMINIUM

7.1 INTRODUCTION

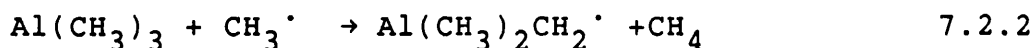
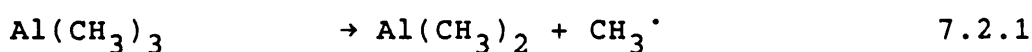
The laser powered pyrolysis of trimethylaluminium was studied under homogeneous conditions. This reaction was studied both with and without added radical scavengers. A mechanism for the reaction is proposed. The species formed by trapping radicals are characterized using FTIR Spectroscopy, NMR and cryoscopic measurements. Previous work is first reviewed in this chapter. An experimental description is given, and the results obtained are discussed; this is followed by a conclusion including a discussion of the advantages and disadvantages of the technique described in this chapter.

7.2 REVIEW

Most of the work which has been done previously on trimethylaluminium (TMAL) and reported in the literature is concerned with the applications involved; electronics, optics, and others, especially those concerned with growing semiconductor crystals<sup>1-9</sup>. The TMAL in the most of these studies was either pure vapour or carried by a carrier gas such as hydrogen (H<sub>2</sub>), helium (He), or nitrogen (N<sub>2</sub>). A very common technique utilised in the growth of crystals is the Organometallic Chemical Vapour Deposition, OMCVD, which is based on heating the substrate on which the aluminium is required to be deposited. As it is the decomposition of TMAL on a hot surface that is taking place, the mechanism of the

reaction is clearly of great importance; procedures for handling it are also reported, since it is very reactive and difficult to deal with<sup>10</sup>.

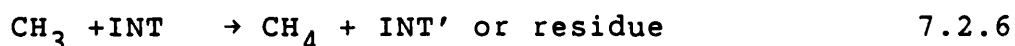
Yadanapalli et al<sup>11</sup>. were the first group to study the thermal decomposition reaction of TMAL in glass vessels in 1946. The reaction in absence of hydrogen, H<sub>2</sub>, was affected by the surface, and led to the conclusion that heterogeneous reactions contribute to the overall process. In the presence of hydrogen, it was observed that the overall rate of the decomposition decreased, and the ratio of methane, CH<sub>4</sub>, to the other products [ethane, C<sub>2</sub>H<sub>6</sub>, ethene, C<sub>2</sub>H<sub>4</sub>, H<sub>2</sub>, Al], was increased. The mechanism of the reaction proposed was as follows:



Al(CH<sub>3</sub>)CH<sub>2</sub><sup>·</sup> is relatively stable and so takes no further part in the overall reaction. The activation energy was reported to be 189 kJ mol<sup>-1</sup>.

Suzuki et al<sup>12</sup> studied the thermal decomposition of TMAL in a heated wall IR cell; H<sub>2</sub> and N<sub>2</sub> were used as carrier gases. The decomposition of TMAL showed a first order behaviour and the results were independent of the type

of carrier gas. The suggested mechanism of the reaction was that the TMAL decomposed to  $\text{CH}_3$  radicals and unknown intermediate species:



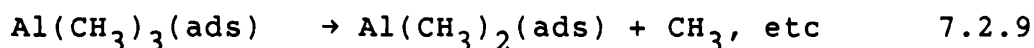
Alternatively, the intermediate could react further to give  $\cdot\text{CH}_3$  radicals and residue:



The generation of  $\text{CH}_4$  was found to be dependent on the nature of the carrier gas, and increased when  $\text{H}_2$  was used as a carrier. The activation energy for the reaction was found to be 0.4 eV ( $40 \text{ kJ mol}^{-1}$ ), which is considerably lower than the Al-C bond energy (about  $200 \text{ kJ mol}^{-1}$ ).

Squire et al<sup>13</sup> reported that the decomposition of TMAL under low pressure and on a hot surface gave  $\text{CH}_3$  radicals only. The production of  $\text{CH}_3$  radicals showed a surface temperature dependence above 550 K, and increased steeply. The reaction was independent of the type of substrate. The activation energy observed for the production of the  $\text{CH}_3$  radicals was  $46 \pm 9 \text{ kJ mol}^{-1}$ . No methane,  $\text{CH}_4$ , or other species such as ethane,  $\text{C}_2\text{H}_6$ , over a wide range of temperature were observed during the reaction. The low activation energy observed for the production of  $\text{CH}_3$  radicals led them to propose the formation of a

$(\text{CH}_3)_3\text{Al}-\text{Al}(\text{ads})$  surface bond, and that this could have weakened the first Al-C bond in the TMAL molecule:



Further investigations of TMAL were carried out by Squire et al<sup>14</sup> to study the decomposition of TMAL on a hot substrate and with different carrier gases. The decomposition of TMAL was found to be independent of the type of the carrier gas. The formation of  $\text{CH}_4$  and  $\text{C}_2\text{H}_6$  were the result of secondary reactions of  $\text{CH}_3\cdot$  radicals. The activation energy was measured to be  $55 \pm 9 \text{ kJ mol}^{-1}$ , which is also lower than any Al-C bond. They reasoned that this was due to formation of  $\text{Al}-\text{Al}_{(\text{Surf})}$  bonds which weakened the other Al-C bonds. This may be due to the electron deficiency of the Al atom, which can accept electrons readily from any electron donors.

Butler et al<sup>15</sup> proposed that the decomposition of TMAL on a hot surface would give  $\text{CH}_3\cdot$  radicals at  $590 \text{ }^\circ\text{C}$ ; IR Diode Laser spectroscopy was employed in their measurements to detect the  $\cdot\text{CH}_3$  radicals, but with no success. They reasoned that the experimental set-up was not sensitive enough, or that TMAL decomposed by a different mechanism, or that not enough  $\cdot\text{CH}_3$  radicals to detect were formed.

Suzuki and Sato<sup>16</sup> reported that the thermal cracking reaction of TMAL in  $\text{H}_2$  carrier was a first order reaction. The activation energy measured for TMAL was  $158.6 \text{ kJ mol}^{-1}$ .

The previous work done on TMAL shows that it is pyrolysed very readily, and has an activation energy smaller than Al-CH<sub>3</sub> dissociation energy.

### 7.3 PREPARATION OF THE SAMPLES

The cells used to study the TMAL reactions, and the rest of the equipment, were described in Chapter 3.

TMAL was supplied in a cylinder by Aldrich Chemical Company Ltd, and was transferred under nitrogen to a glass vessel by a syringe. Because of the reactivity of TMAL towards O<sub>2</sub> and H<sub>2</sub>O, the vacuum line and the cell were kept dry and always conditioned by TMAL to react with all water and oxygen for about 10 minutes, then pumped out for 10 minutes or so. After conditioning the line the TMAL was introduced to the cell and its pressure measured by oil manometer. The photosensitiser, SF<sub>6</sub>, and any other gases, were then added to the required pressure.

### 7.4 PYROLYSIS OF TRIMETHYLALUMINIUM, TMAL

The equipment used in the study of the pyrolysis of TMAL, and the preparation of the samples were described in Chapter 3 and the section above.

#### 7.4.1 TMAL during the pyrolysis

TMAL at room temperature is a dimer, but at the temperature of the pyrolysis is largely in the form of monomer. This form in the gaseous state, therefore, is the one involved in the reaction. This was confirmed by direct observation of the IR spectrum of the monomer. A special

cell was designed, with side windows perpendicular to the front window axis, allowing the probe IR radiation to pass through, as described in Chapter 3 (Figure 3.9), to study the contents of the cell during the reaction. About 3 Torr of TMAL and 5 torr of SF<sub>6</sub> were introduced into the cell, which was then placed in the sample compartment of the FTIR spectrometer; the cell was then irradiated with 12.5 Watts laser power along its axis, and the IR spectra were taken of the sample before, during and after the irradiation. The IR spectra revealed extensive changes in which new bands had appeared and others decayed or disappeared during the irradiation (see Figure 7.1). An analysis of this monomer spectrum, and that of (CD<sub>3</sub>)<sub>3</sub>Al will be undertaken.

#### 7.4.2 Pyrolysis of TMAL

A series of experiments was carried out on mixtures of 2 torr of TMAL with 10 Torr of the photosensitiser, SF<sub>6</sub>, irradiated by the CO<sub>2</sub> laser over a range of laser power from 5 to 15 Watts in steps of 1.25 Watts. The reaction was followed using the FTIR spectrometer. The decay of TMAL was followed using peaks in the region of 777 cm<sup>-1</sup> and 702 cm<sup>-1</sup> (these arise from rocking motion of the bridging and terminal groups respectively<sup>17</sup>). Tables 7.1a and 7.1b list all vibrations of TMAL in the IR and Raman spectra, together with their assignments and comparison with other references<sup>17-19</sup>. During the reaction new peaks appeared in the region of 740 cm<sup>-1</sup> and 617 cm<sup>-1</sup> (the last being overlapped with SF<sub>6</sub>). Simultaneously, C-H absorptions due to the bridging



**Table 7.1.a:**  
**IR absorption spectrum of TMAL.**

| present work<br>$\nu$ ( $\text{cm}^{-1}$ ) | ref 17<br>$\nu$ ( $\text{cm}^{-1}$ ) | assignments                         |
|--|--------------------------------------|-------------------------------------|
| 2942.7 s                                   | 2944                                 | $\text{CH}_3$ a sym. stretch        |
| 2902.6 s                                   | 2904                                 | $\text{CH}_3$ sym. stretch          |
| 2841.6 m                                   | 2845                                 | 2x $\text{CH}_3$ a.sym.def ?        |
| 1254 m                                     | 1255                                 | $\text{CH}_{3t}$ sym.def (bridge)   |
| 1208 s                                     | 1208                                 | $\text{CH}_{3t}$ sym.def (terminal) |
| 777 vs                                     | 774                                  | $\text{CH}_{3t}$ rock               |
| 702 vs                                     | 700                                  | Al- $\text{C}_t$ stretch            |
| 652.6 m                                    | 650                                  | $\text{CH}_{3t}$ rock               |
| 609.6 s                                    | 609                                  | $\text{CH}_{3b}$ rock               |
| 567.2 s                                    |                                      | Al- $\text{C}_b$ stretch            |

**Table 7.1.b:**  
**Raman absorption spectrum of TMAL**

| present work<br>$\nu$ ( $\text{cm}^{-1}$ ) | ref 19<br>$\nu$ ( $\text{cm}^{-1}$ ) | assignments                       |
|--|--------------------------------------|-----------------------------------|
| 2940 s                                     | 2932                                 |                                   |
| 2890 vs                                    | 2892                                 | } $\text{CH}_3$ stretch           |
| 2835 s                                     | 2824                                 |                                   |
| 1435 m                                     | 1436                                 | $\text{CH}_3$ b&t as.bend         |
| 1258 w                                     | 1255                                 | $\text{CH}_{3t}$ sym. bend        |
| 1007 m sharp                               |                                      |                                   |
| 790 vw                                     |                                      |                                   |
| 727 w sh.                                  | 725                                  | $\text{CH}_{3b}$ rock             |
| 688 s                                      | 683                                  | $\text{CH}_{3t}$ rock             |
| 596 vs                                     | 592                                  | $\nu_1$ Al- $\text{C}_t$ stretch  |
| 505 s                                      |                                      |                                   |
| 449 vs                                     | 453                                  | $\nu_2$ Al- $\text{C}_b$ stretch  |
| 318.5 vs                                   | 313                                  | $\nu_3$ Al- $\text{C}_2$ scissors |
| 150 vs                                     | 153                                  | $\nu_4$ ring deformation          |

CH<sub>3</sub> groups (in the region of 1254 cm<sup>-1</sup> and 777 cm<sup>-1</sup>) decayed, and other vibrations were shifted, as shown in Figure 7.2. The decay of the bridging peak at 777 cm<sup>-1</sup> was faster than that of the terminal at 702 cm<sup>-1</sup>, and it had completely disappeared by the time the terminal peak had fallen to half its initial value. The growing peaks reached a maximum when the bridging peaks had completely disappeared and then decayed slowly, as shown in Figure 7.3. A thin film of white material was deposited on the front window and the cell walls.

#### 7.4.3 Pyrolysis of TMAL in presence of Hydrogen, H<sub>2</sub>

A series of experiments was done using mixtures of 2 torr of TMAL, 10 torr of H<sub>2</sub> and 10 torr of SF<sub>6</sub> with different laser powers. The reaction was followed using the FTIR spectrometer. The decay of TMAL was followed using the peaks at 777 cm<sup>-1</sup> and 702 cm<sup>-1</sup> as above. The decay was considerably slower than in the absence of hydrogen. Both the bridging and the terminal peaks were observed to decay at the same rate in this case. The only new peaks observed were due to methane, CH<sub>4</sub>, in the regions of 3016 and 1306 cm<sup>-1</sup>. A thin metallic layer was deposited on the front window and the walls of the reaction cell.

#### 7.4.4 Pyrolysis of TMAL in presence of D<sub>2</sub>

The reaction of TMAL was also carried out in the presence of D<sub>2</sub>; 1 torr of TMAL was mixed with 5 torr of D<sub>2</sub> and 10 torr SF<sub>6</sub> and irradiated with 7.5 Watts laser power. The reaction was slow in comparison with that without D<sub>2</sub> but

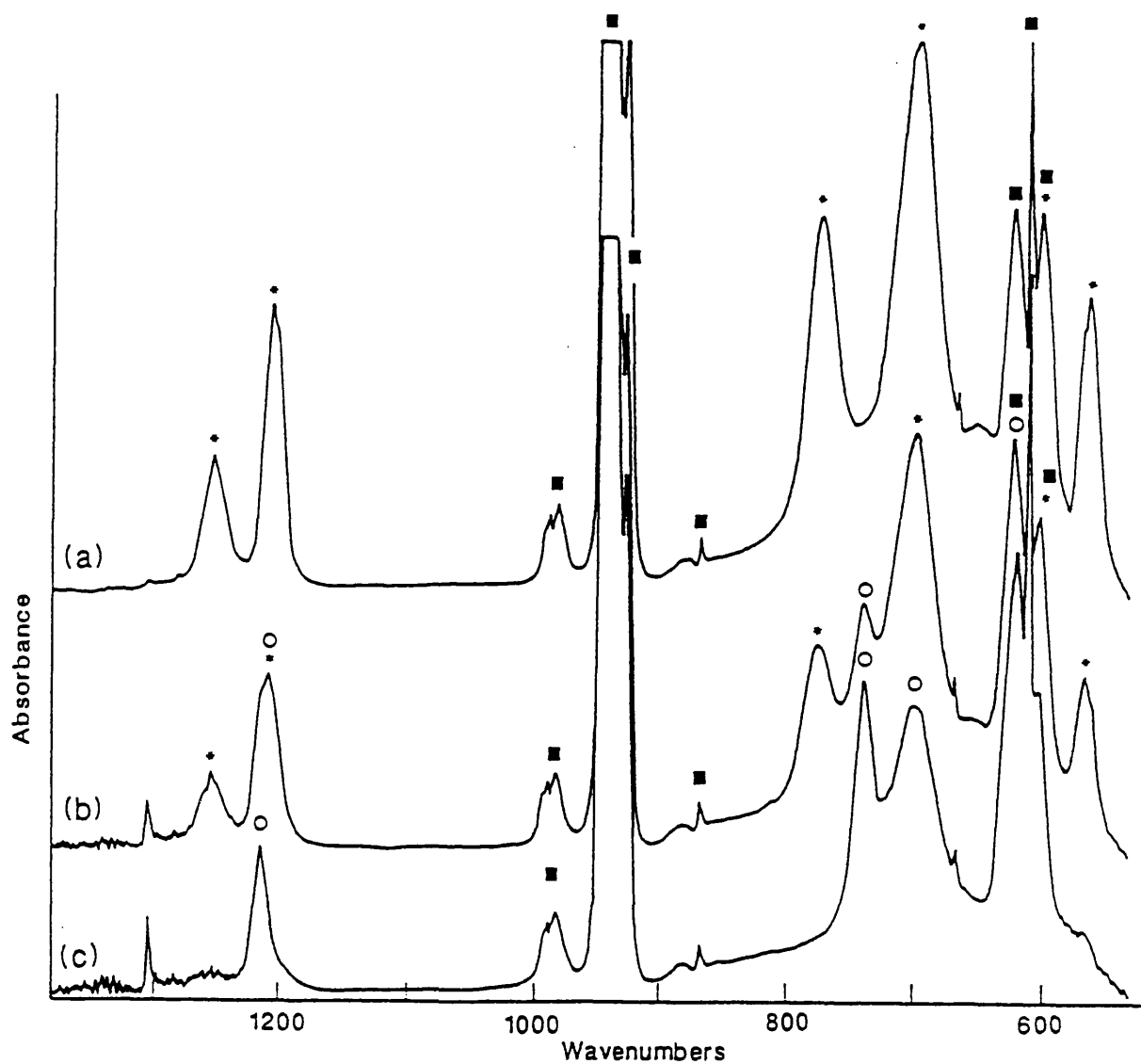


Figure 7.2:

2 torr of TMAL + 10 torr of SF<sub>6</sub> irradiated with 7.5 W laser power: (a) before, (b) after 2 minutes and (c) after 5 minutes irradiation. \*, o, and ■ represent the starting, new and SF<sub>6</sub> bands.

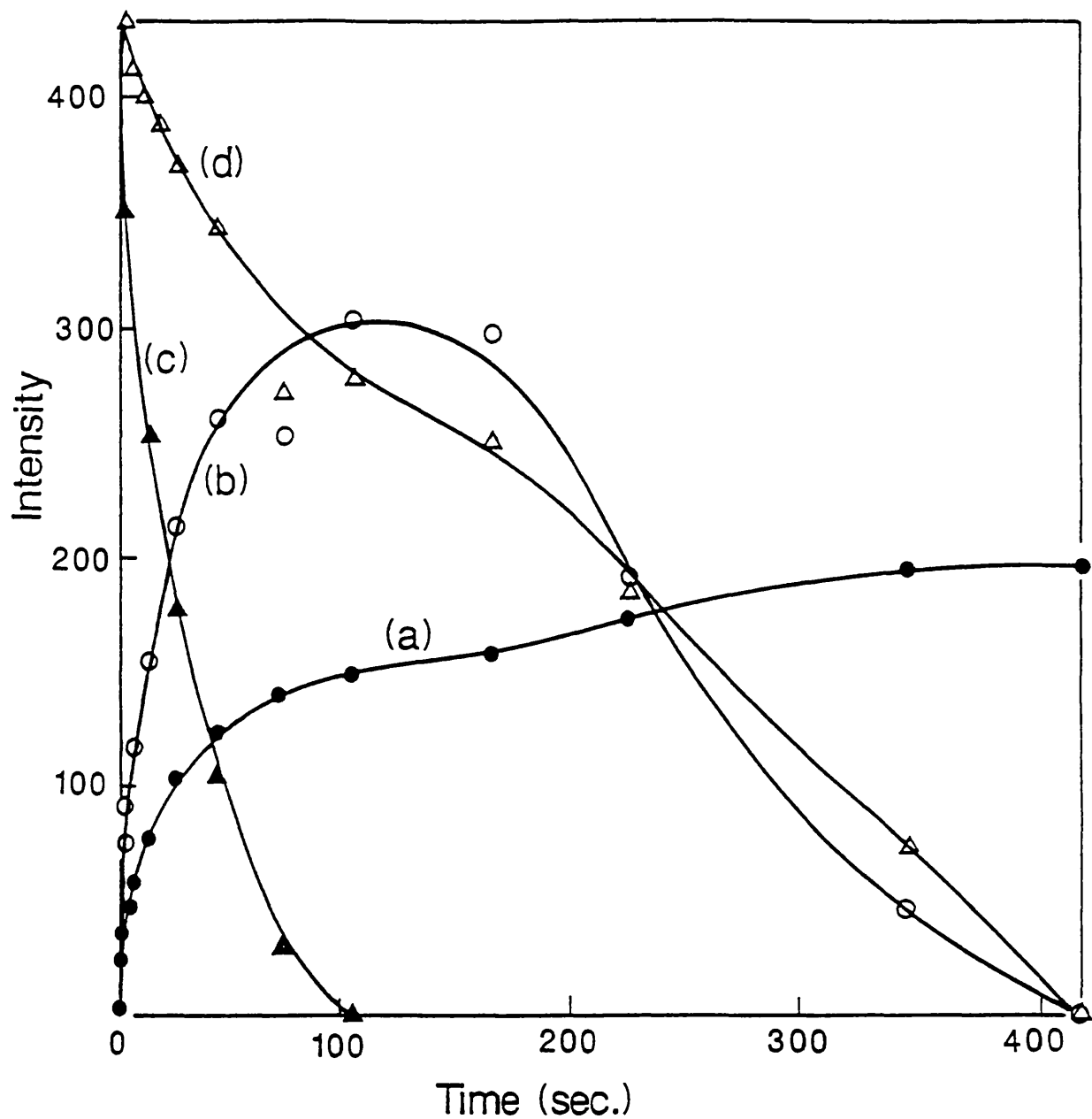


Figure 7.3:

Plot of the intensity of bands of TMAL and products in a mixture of 2 torr TMAL + 10 torr SF<sub>6</sub> irradiated with 7.5 W laser power: (a) CH<sub>4</sub> (3016 cm<sup>-1</sup>) (b) product (740 cm<sup>-1</sup>) (c) C-Al<sub>b</sub> peak (777 cm<sup>-1</sup>) and (d) C-Al<sub>t</sub> peak (702 cm<sup>-1</sup>).

faster than with  $H_2$ , as shown in Figure 7.4. Very little  $CH_3D$  was formed (from the absence of the peak at  $2200\text{ cm}^{-1}$ ), but the new peaks described in Section 7.4.2 were observed.

#### 7.4.5 Pyrolysis of TMAL in presence of Tetrachloromethane

##### $CCl_4$

Tetrachloromethane (carbon tetrachloride, CTC) was used in an attempt to trap radicals which may have been formed during the decomposition of TMAL as a stable compound. The thermal stability of CTC first was checked with  $SF_6$  to determine the range of laser power below the threshold of CTC decomposition.

##### 1. The Stability of Tetrachloromethane

The stability of CTC was checked by mixing about 2 torr of CTC with about 10 torr of  $SF_6$  and irradiating with the  $CO_2$  laser. The laser power was increased gradually, each step taking about 10 minutes. CTC was found to be stable at 5.0 Watts laser power. Above 5 Watts it was not stable, and it decomposed rapidly above 8 Watts of laser power. New peaks appeared in the spectrum; these are listed in Table 7.2 and shown in Figure 7.5.

##### 2. The Reaction of TMAL in Presence of CTC

Three torr of TMAL mixed with 2 torr of CTC and 10 torr of  $SF_6$  were irradiated with 1.5 and 4.5 W of laser power. A very strong new band appeared in the region of  $720\text{ cm}^{-1}$  (see Figure 7.6). The reaction was very slow and no deposit on the windows or the cell walls was observed.

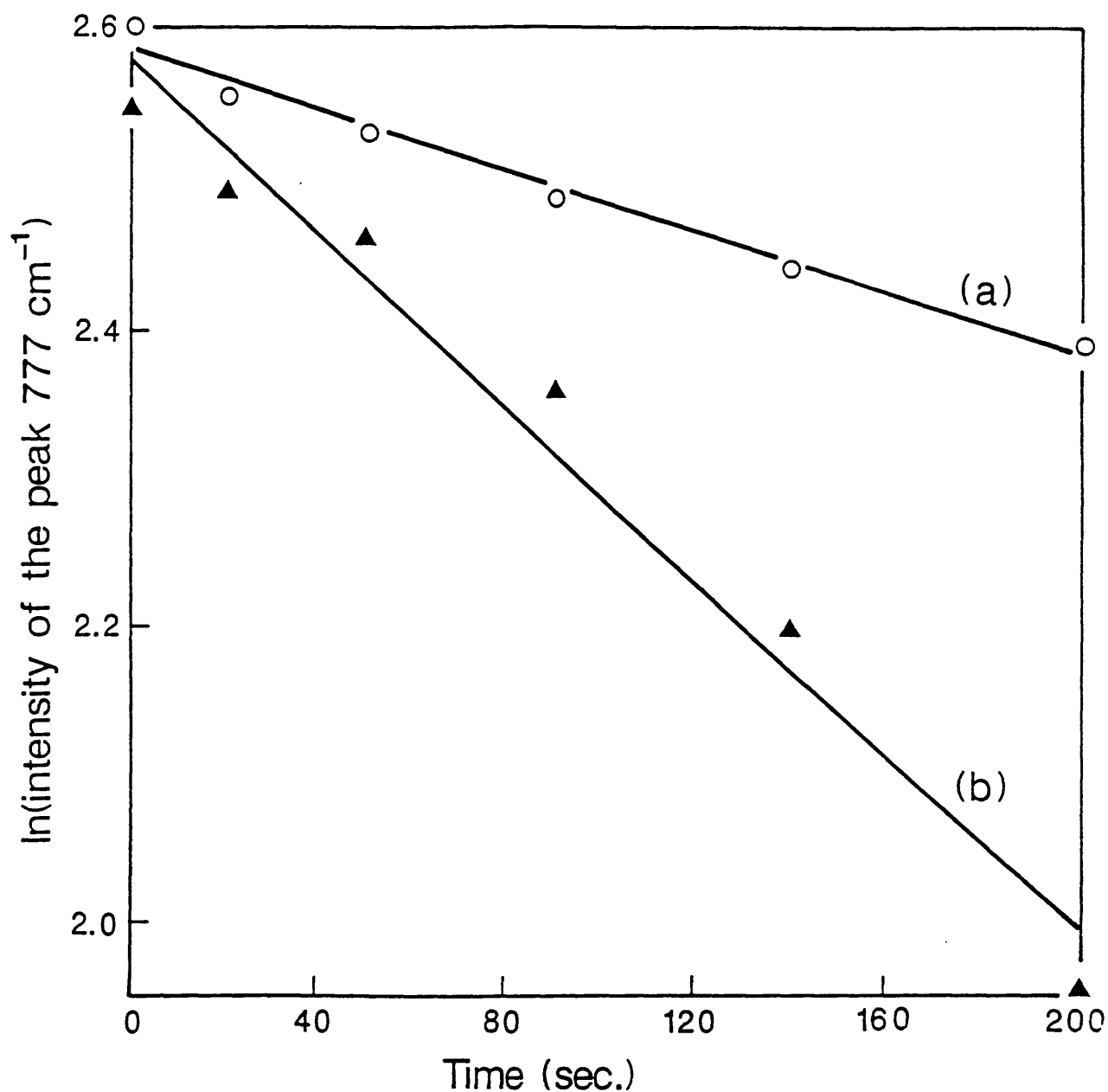


Figure 7.4:

Plot of  $\ln(\text{intensity})$  of the peak at  $777 \text{ cm}^{-1}$  vs time; (a) 1 torr of TMAL + 10 torr  $\text{SF}_6$  + 5 torr  $\text{H}_2$  irradiated with 7.5 W laser power (b) 1 torr TMAL + 10 torr  $\text{SF}_6$  + 5 torr  $\text{D}_2$  irradiated with 7.5 W laser power.

**Table 7.2:**

$\text{CCl}_4$  peaks before reaction and the new peaks appearing after 10 minutes irradiation with 7.5 W of laser power.

---

| $\text{CCl}_4$ before<br>irradiation ( $\text{cm}^{-1}$ ) | the new bands<br>after irradiation ( $\text{cm}^{-1}$ ) |
|---|---|
| 795   | 1836  |
| 779.7   | 1819  |
| 773   | 856   |
| 770   | 850   |
|   | 843   |

---

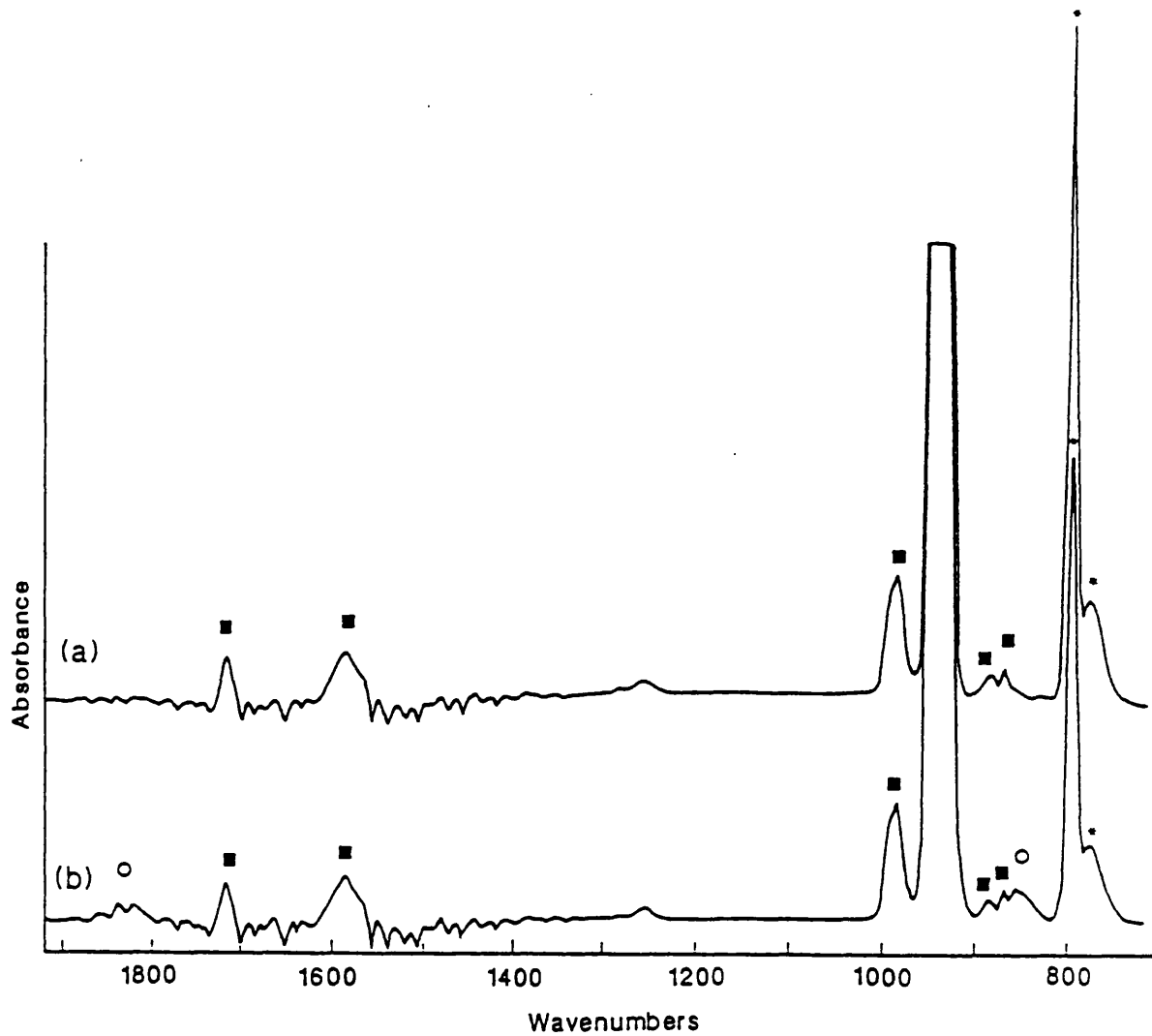


Figure 7.5:

IR spectra of 2 torr of  $\text{CCl}_4$  + 10 torr  $\text{SF}_6$  irradiated with 7.5 W laser power: (a) before irradiation and (b) after 10 minutes irradiation. \*, o and ■ are the starting material, new, and  $\text{SF}_6$  bands.

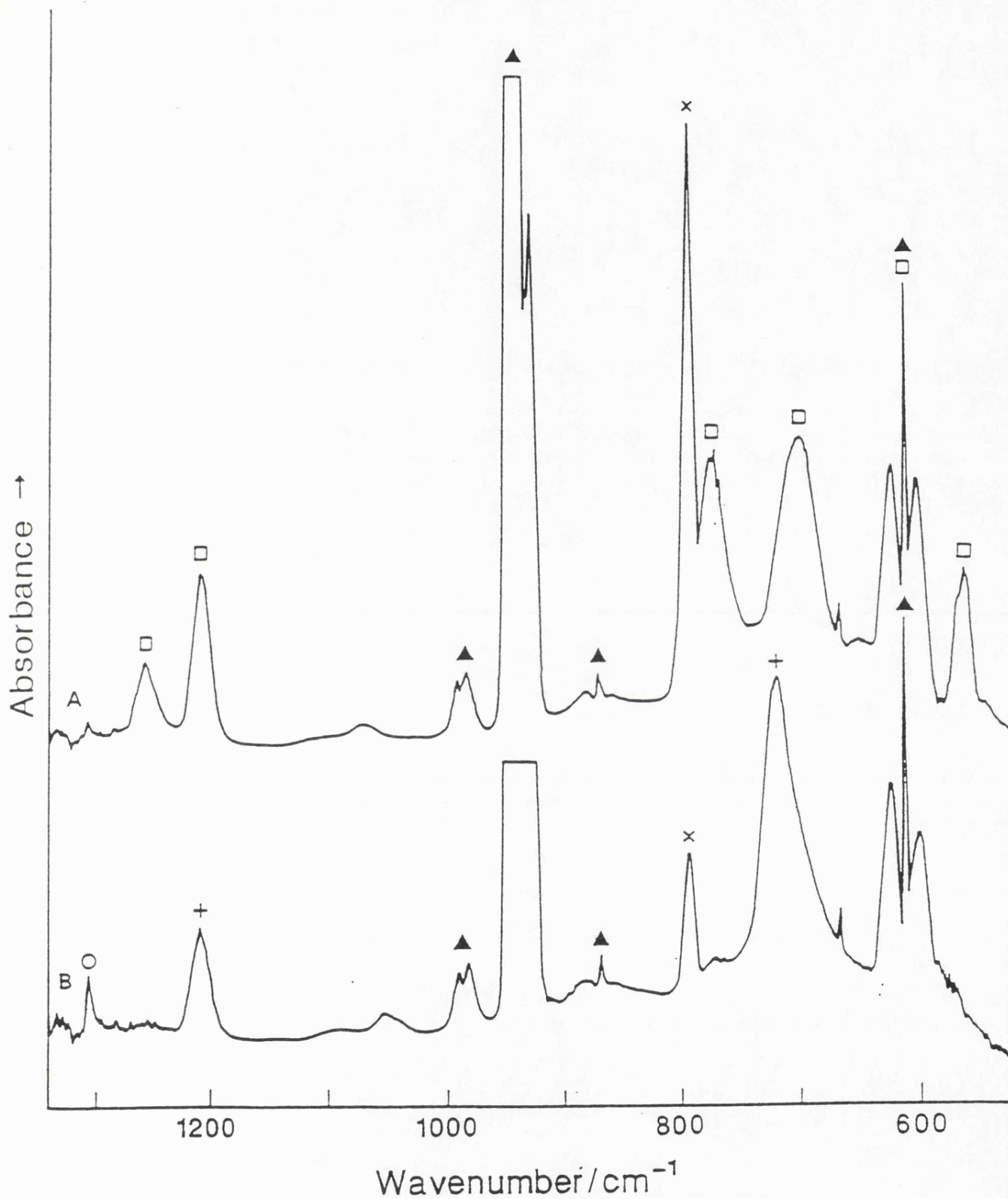


Figure 7.6:

IR spectra of 2 torr  $\text{CCl}_4$  + 3 torr TMAL + 10 torr  $\text{SF}_6$  irradiated with 3.75 Watts laser power: (a) before, (b) after 10 minutes. □ TMAL, x  $\text{CCl}_4$ , + new, o  $\text{CH}_4$  and ▲  $\text{SF}_6$  bands.

#### 7.4.6 The reaction of TMAL in presence of Chloroform, $\text{CHCl}_3$

##### 1. The Stability of the Chloroform in the Reaction Cell

The thermal stability of the chloroform was checked. The same procedure was used as with  $\text{CCl}_4$ ; this showed that at powers above 4.0 Watts  $\text{CHCl}_3$  was not stable. It decomposed to form  $\text{CCl}_4$  and other species as shown in the IR spectra of Figure 7.7 and listed in Table 7.3.

##### 2. The Pyrolysis of TMAL in Presence of Chloroform

A mixture of 2 torr of  $\text{CHCl}_3$ , 3 torr of TMAL and 10 torr of  $\text{SF}_6$  as photosensitizer, was irradiated together at a laser power of about 2.5 Watts. No new peaks appeared in the IR spectrum; the TMAL decomposed to give a very thin layer of aluminium as a metal deposited on the front window. At higher power (about 3.75 Watts) new peaks appeared; see Table 7.4 and Figure 7.8.

#### 7.4.7 The reaction of TMAL in presence of Deuterated Chloroform, $\text{CDCl}_3$

##### 1. The Stability of $\text{CDCl}_3$

The thermal stability of the deuterated chloroform was checked; it was found to be unstable at laser powers above 3.75 W. About 3 torr of  $\text{CDCl}_3$  was mixed with 10 torr of  $\text{SF}_6$  and irradiated with 3.75 W laser power; new peaks were observed as listed in Table 7.5 and shown in Figure 7.9.

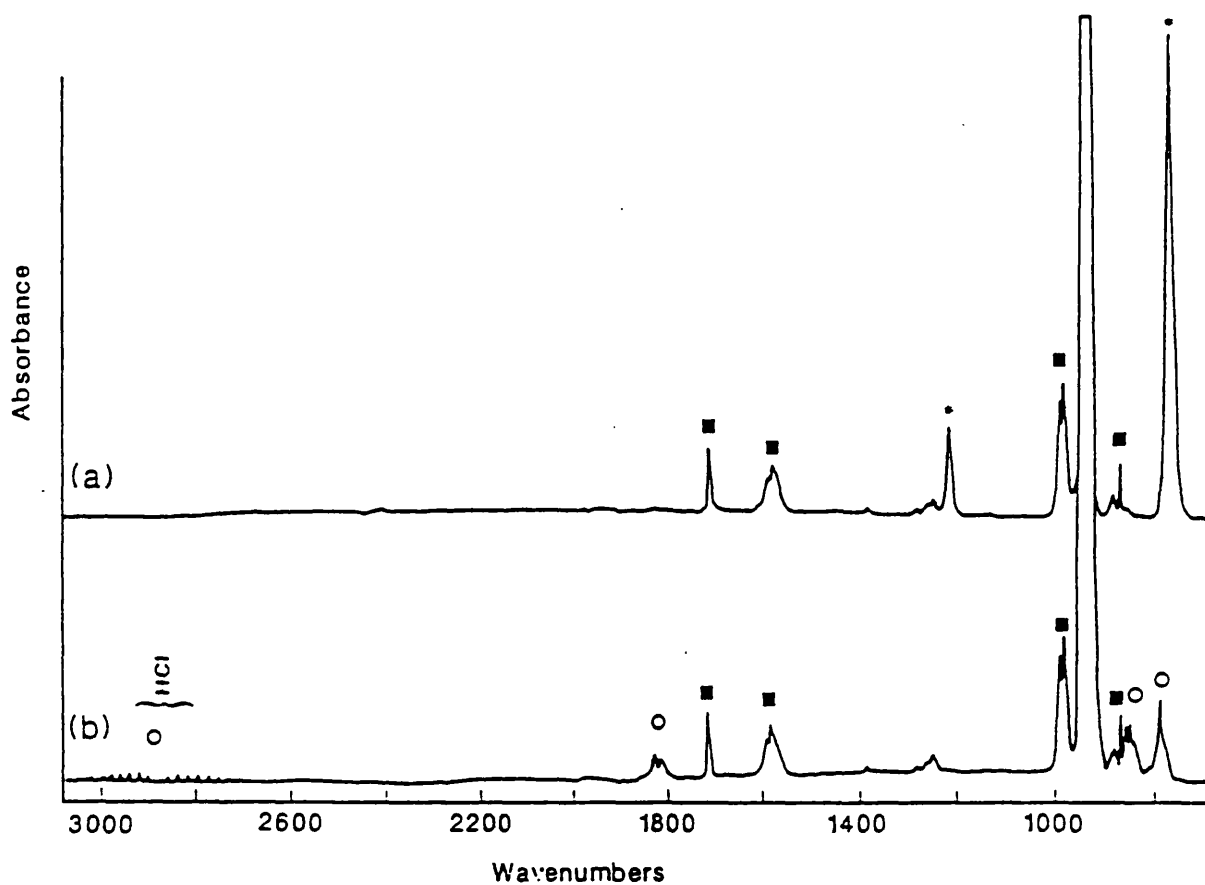


Figure 7.7:

IR spectra of 2 torr  $\text{CHCl}_3$  + 10 torr  $\text{SF}_6$ : (a) before (b) after 10 minutes irradiation with 5.0 W laser power. \* starting material, o the new and ■  $\text{SF}_6$  bands.

**Table 7.3:**

IR bands of  $\text{CHCl}_3$  before and after 10 minutes irradiation with 5.0 W laser power.

---

| $\text{CHCl}_3$ before<br>irradiation ( $\text{cm}^{-1}$ ) | New bands after<br>irradiation ( $\text{cm}^{-1}$ ) |
|--|---|
| 1219   | 1836  |
| 772  | 1819  |
|  | 856   |
|  | 850   |
|  | 846   |

---

Table 7.4:

IR bands of the new identified compounds and their assignments, appearing after irradiation of a mixture of 3 torr of TMAL, 2 torr of  $\text{CHCl}_3$  and 10 torr of  $\text{SF}_6$ .

| new bands<br>( $\text{cm}^{-1}$ ) | compounds  | assignments                       |
|-----------------------------------|--|-----------------------------------|
| 2956 (m)                          | DMACl  | $\nu$ ( $\text{CH}_3$ ) stretch   |
| 2908 (w)                          | DMACl  | $\nu$ ( $\text{CH}_3$ ) "         |
| 2115 (w)                          |  |                                   |
| 2128 (m) sharp                    | P,Q,R branch of unidentified compound(s),                          |                                   |
| 2143 (w)                          | due to the decomposition of $\text{CHCl}_3$ .                      |                                   |
| 1209 (m)                          | DMACl  | $\delta_s$ ( $\text{CH}_3$ ) bend |
| 856 (m)                           | unidentified compound, due to the decomposition of $\text{CHCl}_3$ |                                   |
| 720 (s)                           | DMACl  | $\nu$ (Al-C) stretch              |

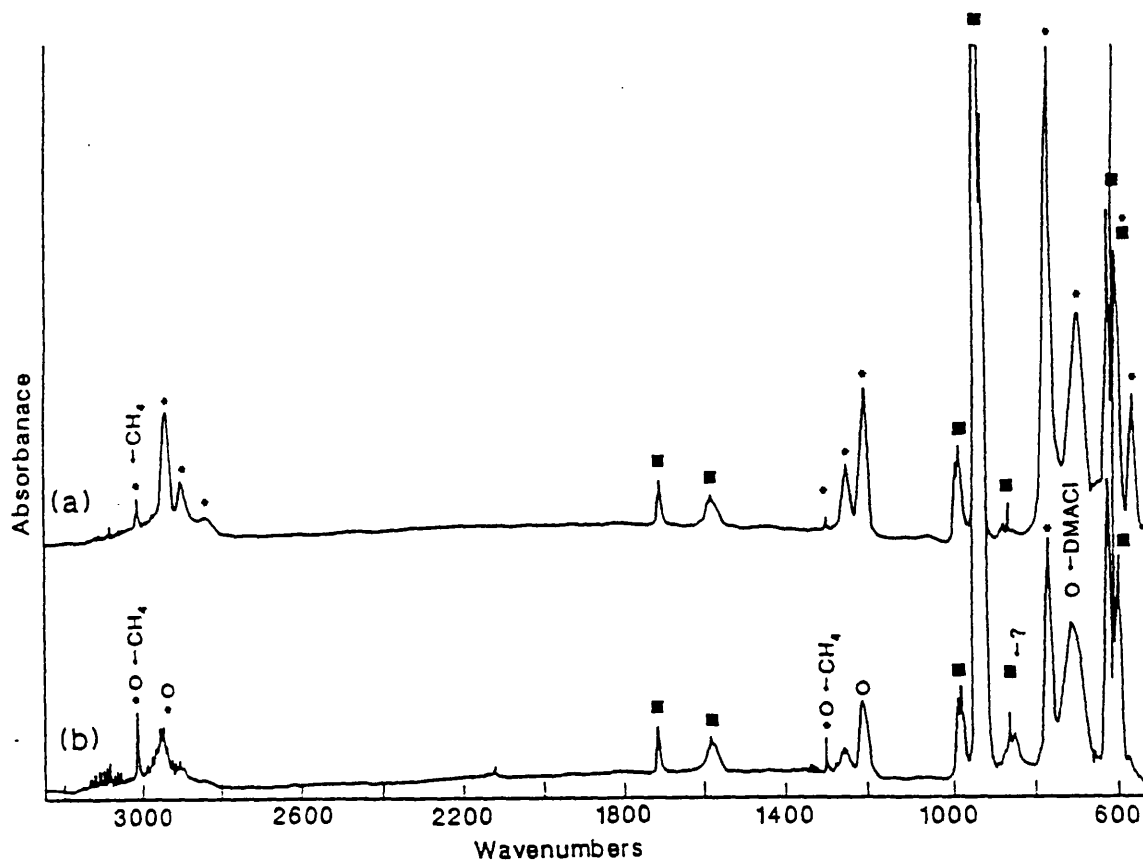


Figure 7.8:

IR spectra of a mixture of 2 torr  $\text{CHCl}_3$  + 3 torr TMAL + 10 torr  $\text{SF}_6$ : (a) before and (b) after irradiation with 2.5 W laser power. \* starting material bands, o new bands and ■  $\text{SF}_6$  bands.

**Table 7.5:**

IR bands of 3 torr  $\text{CDCl}_3$  + 10 torr  $\text{SF}_6$  before and after 10 minutes irradiation with 5.0 W laser power.

---

| $\text{CDCl}_3$ bands before irradiation ( $\text{cm}^{-1}$ ) | New bands after irradiation ( $\text{cm}^{-1}$ ) |
|---|--|
| 913   | 1836   |
| 748   | 1819   |
| 745   | 857  |
|   | 849  |
|   | 844  |
|   | 789  |
|   | 773  |

---

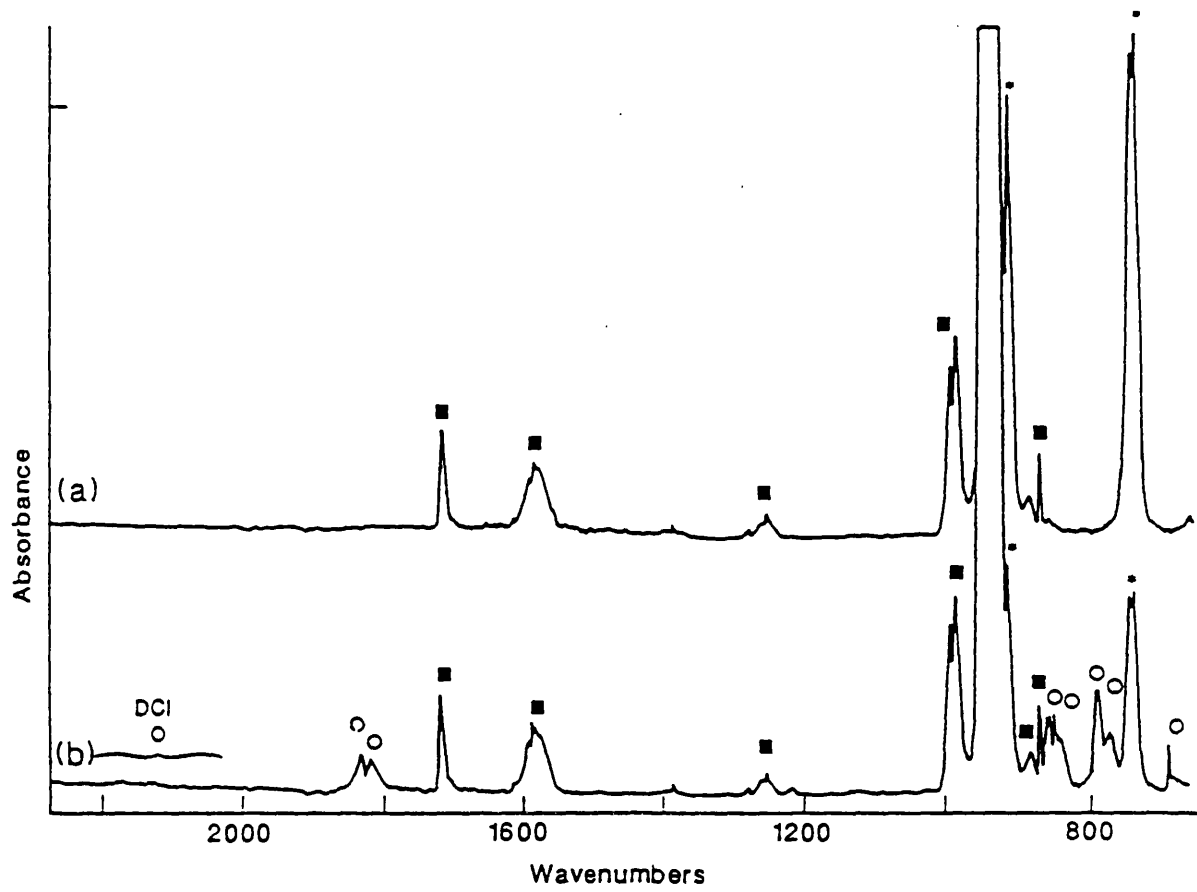


Figure 7.9:

IR spectra of a mixture of 3 torr  $\text{CDCl}_3$  + 10 torr  $\text{SF}_6$ : (a) before and (b) after 10 minutes irradiation with 5.0 W laser power. \* starting material bands, o, new bands and ■  $\text{SF}_6$  bands.

## 2. The Pyrolysis of TMAL in Presence of $\text{CDCl}_3$

A mixture of 2 torr of  $\text{CDCl}_3$ , 3 torr of TMAL and 10 torr of  $\text{SF}_6$  was irradiated with a laser power of about 3.75 Watts for about 5 minutes. A thin layer of Al as a metal was observed on the front window. The bridging peak of TMAL at  $776\text{ cm}^{-1}$  disappeared and the  $\text{CDCl}_3$  peaks at  $743\text{ cm}^{-1}$  and  $913\text{ cm}^{-1}$  decreased by a quarter of the starting intensity. The same mixture of TMAL,  $\text{CDCl}_3$  and  $\text{SF}_6$  was exposed to a higher power of about 7.5 Watts, for further investigation. New peaks appeared (Figure 7.10), a sharp medium strength peaks at  $730\text{ cm}^{-1}$  and two weak peaks at  $1156\text{ cm}^{-1}$  and  $2200\text{ cm}^{-1}$ ; the latter was identified as  $\text{CH}_3\text{D}$  formed during the irradiation with a higher laser power.

### 7.5 TRAPPING INTERMEDIATES AS STABLE COMPOUNDS

The reaction of TMAL in the presence of other molecules such as  $\text{CCl}_4$ ,  $\text{CHCl}_3$ ,  $\text{CDCl}_3$ ,  $\text{H}_2$ , and  $\text{D}_2$  as well as the  $\text{SF}_6$  photosensitizer led to the formation of new stable compounds. These products were trapped and characterized by a variety of techniques as described below.

#### 7.5.1 Products of the reaction of TMAL with $\text{SF}_6$

A mixture of about 2 torr of TMAL and 10 torr of  $\text{SF}_6$  was prepared in the reaction cell. A NMR tube fitted with a tap was attached to the body of the cell (see Chapter 3, Figure 3.7) for condensation of the products of the reaction. The mixture was irradiated with 7.50 Watts laser power. The experiment was carried out until all TMAL had reacted (ie,

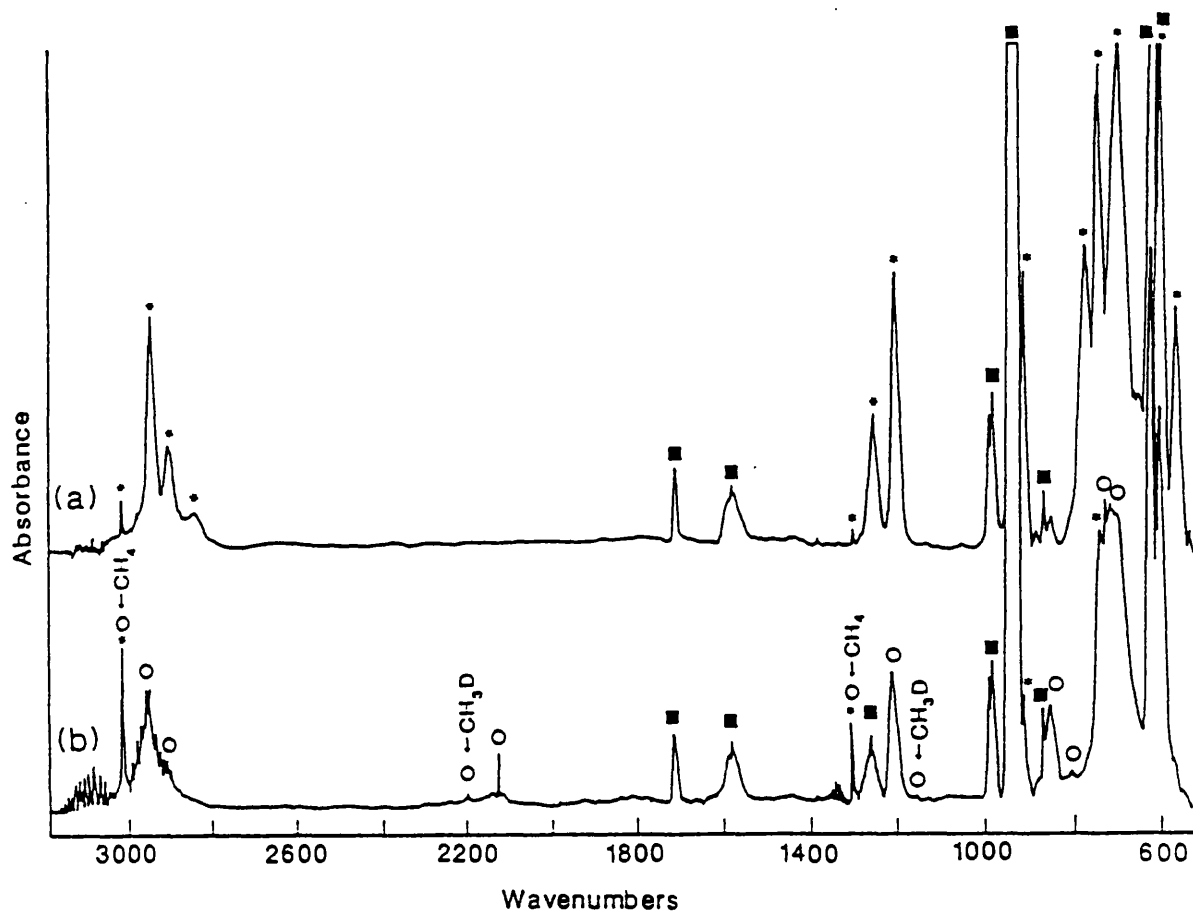


Figure 7.10:

IR spectra for 3 torr TMAL + 2 torr  $\text{CDCl}_3$  + 10 torr  $\text{SF}_6$ : (a) before and (b) after 10 minutes irradiation with 3.75 W laser power. \* starting material bands, o, new bands and ■  $\text{SF}_6$  bands.

until the bridging peak at  $777\text{ cm}^{-1}$  had disappeared completely), and the new peak at  $740\text{ cm}^{-1}$  reached a maximum. This process ensured maximum yield of the product and minimum contamination with TMAL to simplify the purification process with such a small amount of sample. The contents of the cell were then condensed in to the NMR tube at liquid nitrogen temperature. After each two such runs, the condensed product was degassed at dry ice temperature to remove  $\text{CH}_4$  and  $\text{SF}_6$ . The experiment was repeated about 30 times. A highly viscous colourless liquid was seen in the bottom of the tube. Deuterated chloroform  $\text{CDCl}_3$  (with a small amount of  $\text{CHCl}_3$ ) was dried over calcium hydride overnight, degassed, then transferred to the NMR tube as a solvent using a liquid nitrogen  $\text{N}_2$  bath. The NMR tube was sealed by flame and detached from the cell. Figure 7.11 shows the  $^1\text{H}$ ,  $^{19}\text{F}$  and  $^{13}\text{C}$  NMR spectra for the product.

A wider OD tube was attached to the reaction cell to collect the larger amount of sample needed for liquid and gas phase IR spectroscopy, Raman spectroscopy, elemental analysis and for molecular weight measurement by cryoscopic measurement or freezing point depression.

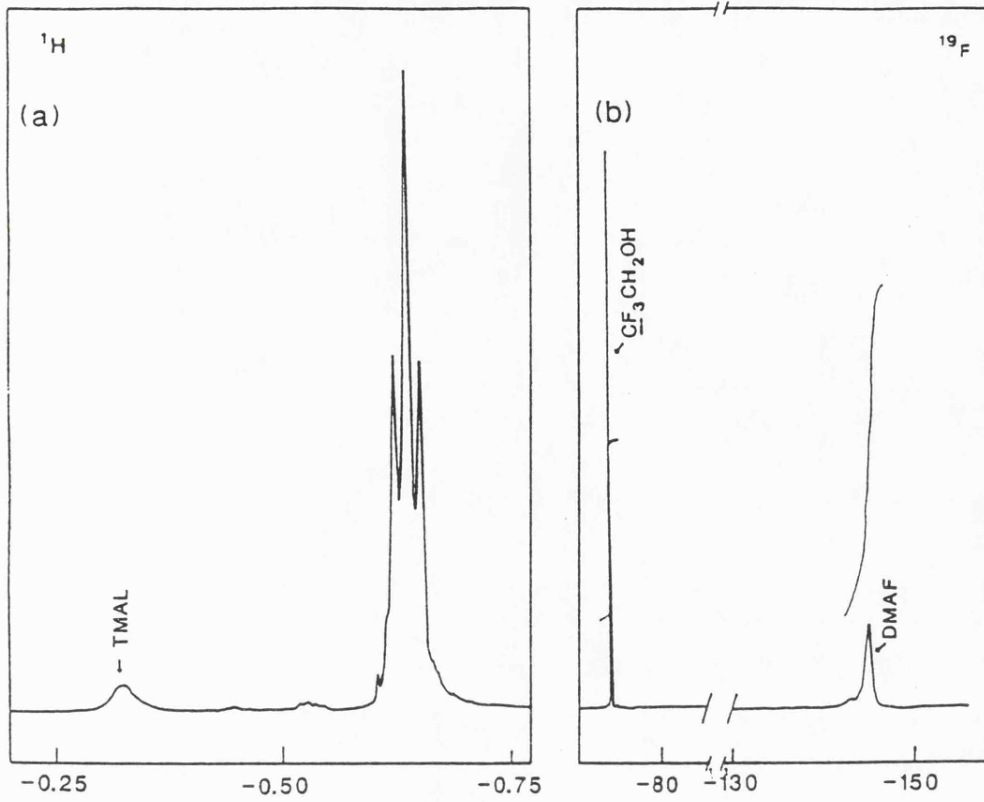
### 1. The NMR Experiment

The NMR sample was prepared as described in section 7.5.1. The proton  $^1\text{H}$  NMR gave a broad singlet centred at  $-0.636\text{ ppm}$ ; in the presence of a small amount of TMAL it appeared as a 1:2:1 triplet. The  $^{19}\text{F}$  NMR gave one broad peak at  $-144.92\text{ ppm}$ , and  $^{13}\text{C}$  NMR also gave one broad peak at  $-12.47\text{ ppm}$ ; see Figure 7.11 and

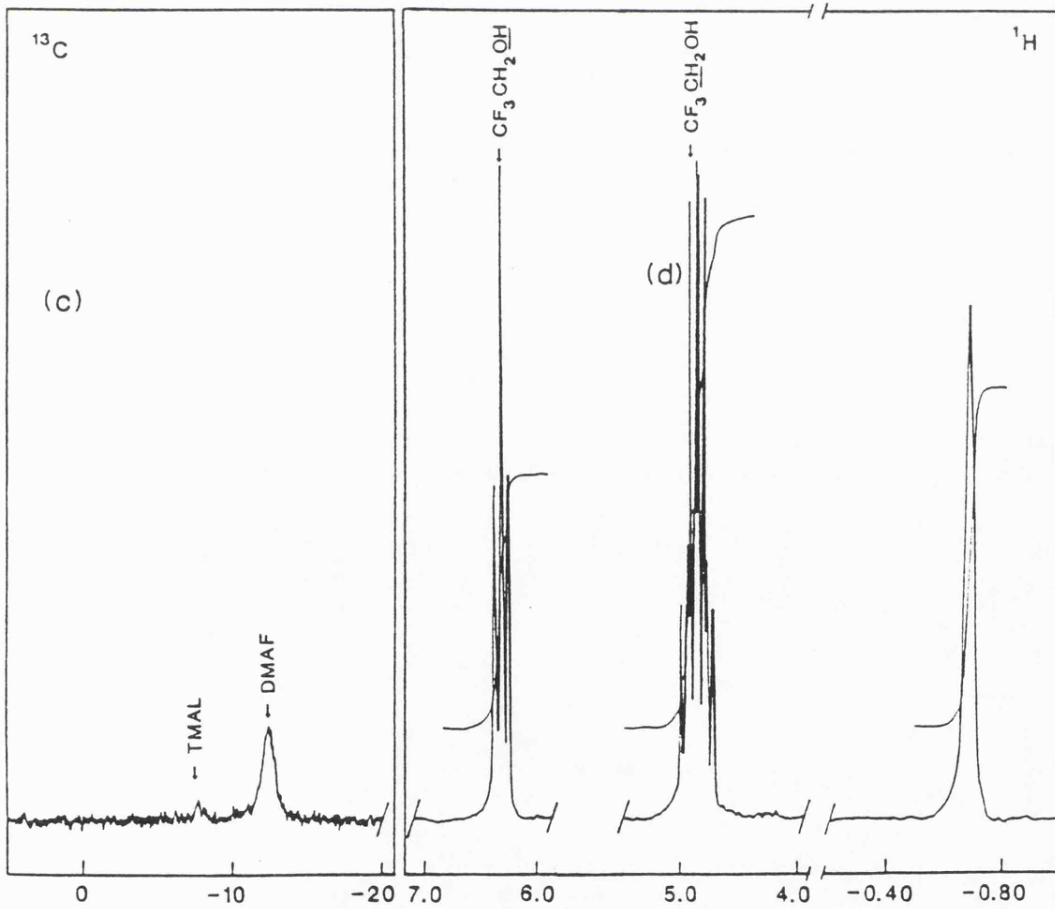
**Figure 7.11:**

$^1\text{H}$ ,  $^{19}\text{F}$  and  $^{13}\text{C}$  NMR spectra of DMAF:

(a)  $^1\text{H}$  in presence of TMAL, (b)  $^{19}\text{F}$  for DMAF in presence of  $\text{CF}_3\text{CH}_2\text{OH}$  as  $^{19}\text{F}$  reference, (c)  $^{13}\text{C}$  and (d)  $^1\text{H}$ ; spectra for DMAF and  $\text{CF}_3\text{CH}_2\text{OH}$ , the latter as  $^1\text{H}$  reference.



Chemical Shift



Chemical Shift

**Table 7.6.** A reference compound was used to estimate the ratio of the proton to the fluorine in the compound, namely 1,1,1-trifluoroethanol,  $\text{CF}_3\text{CH}_2\text{OH}$ . The NMR tube was placed in a 5 mm. OD standard NMR tube which contained the reference compound. The integrated area of the NMR spectra of both the reference and the product for the proton  $^1\text{H}$  and the fluorine  $^{19}\text{F}$  signals are listed in **Table 7.7.**

## **2. The Liquid and Gas Phase IR and Raman Spectra**

The sample which was collected for the IR experiment was degassed by using a slush bath of dry ice and acetone at  $-77\text{ }^\circ\text{C}$  (196 K) to separate it from  $\text{SF}_6$  and  $\text{CH}_4$ , the sample then being warmed up to room temperature to take Raman spectra for the liquied phase. The vapour pressure of the sample was introduced into the IR cell and IR spectra were taken, shown in **Figure 7.12.a.** For the liquid phase IR spectrum, special care was required because of the sensitivity of the product towards the air and moisture. The sample was transferred on to a KBr window in a dry box and squeezed between two such windows tightly enough to reduce air contact with the sample. The IR spectrum was taken and all peaks of **Figure 7.12.b** are listed in **Table 7.8.**

## **3. Estimation of Molecular Weight by Using Cryscopic Techniques (Freezing Point Depression)**

This technique was tested first by using TMAL, which is

Table 7.6:

$^1\text{H}$ ,  $^{19}\text{F}$  and  $^{13}\text{C}$  NMR chemical shift (ppm) for TMAL and DMAF, each in  $\text{CDCl}_3$  and  $\text{CHCl}_3$  solution.

| compound | $^1\text{H}$ | $^{19}\text{F}$ | $^{13}\text{C}$ |
|----------|--------------|-----------------|-----------------|
| TMAL     | -0.323       | -               | -7.616          |
|          | -0.650       |                 |                 |
| DMAF     | -0.636       | -144.8          | -12.473         |
|          | -0.621       |                 |                 |

Table 7.7:

The integrated area of  $^1\text{H}$  and  $^{19}\text{F}$  and ratios for DMAF and  $\text{CF}_3\text{CH}_2\text{OH}$ .

---

| compund   | $^1\text{H}$ Area | $^{19}\text{F}$ Area |
|---|-------------------|----------------------|
| DMAF  | 100.00            | 100.00               |
| $\text{CF}_3\text{CH}_2\text{OH}$                   | 12.15             | 52.73                |
| ratio of<br>DMAF/ $\text{CF}_3\text{CH}_2\text{OH}$ | 8.23              | 1.89                 |

---

These figures lead to a ratio of 6.4:1 for  $^1\text{H}:^{19}\text{F}$  in the sample.

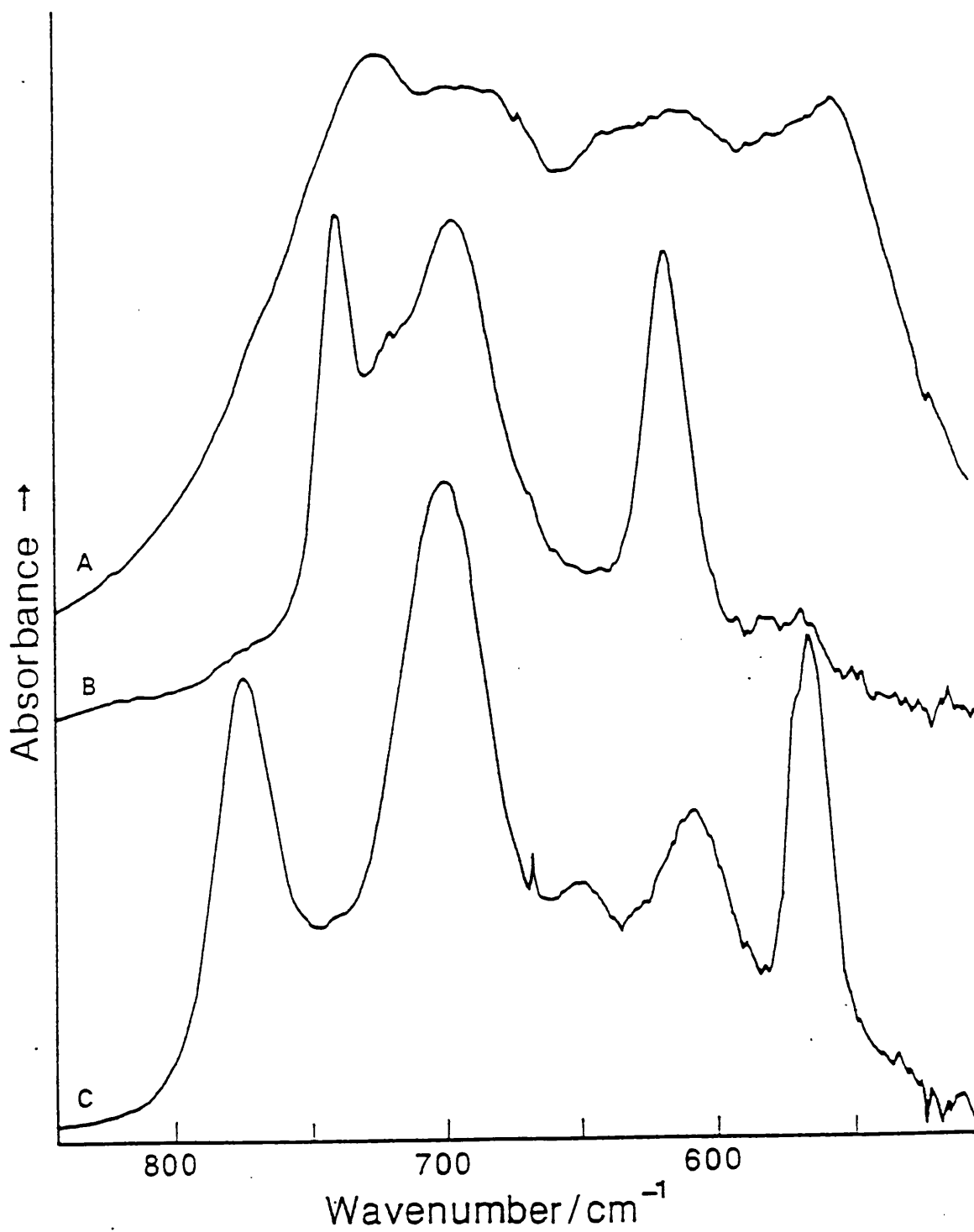


Figure 7.12a:  
IR spectra of DMAF: (a) IR (liquid) and (b) IR (gas), and (c)  
IR (gas) of TMAL.

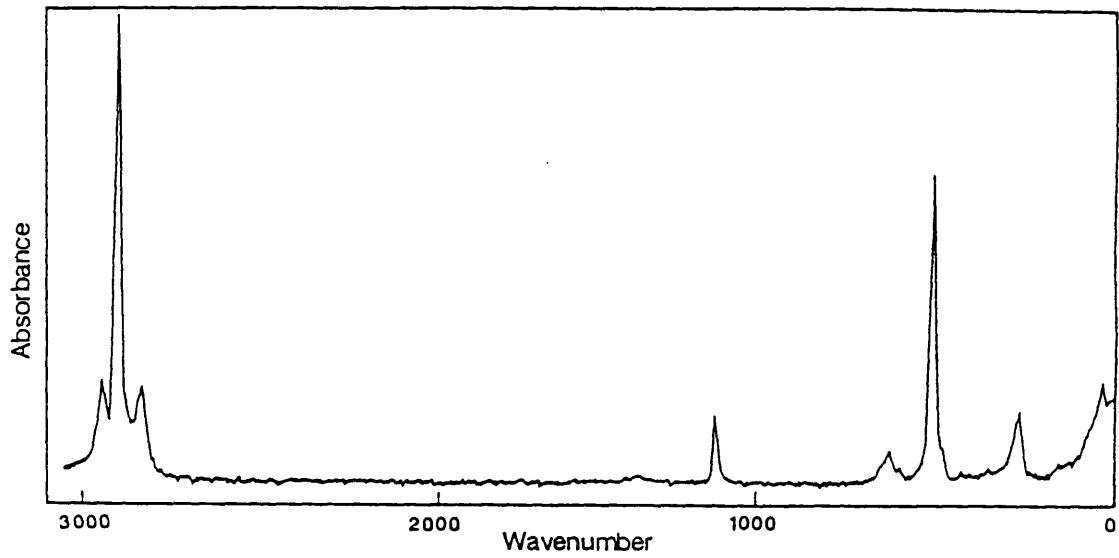


Figure 7.12b:  
Liquid phase Raman spectra of DMAF.

Table 7.8:

Liquid and gas phase IR bands ( $\text{cm}^{-1}$ ) for DMAF and their assignments with those of reference 20.

| IR<br>liquid | Raman<br>liquid | IR<br>ref 20 | Raman<br>ref 20 | IR<br>Gas | Assignment                              |
|--------------|-----------------|--------------|-----------------|-----------|---|
| 2943 (s)     | 2950 (w)        | 2946 (s)     | 2948 (w)        | 2949 (s)  | $\nu_{\text{as}}$ ( $\text{CH}_3$ )     |
| 2901 (m)     | 2908 (s)        | 2905 (m)     | 2904 (s)        | 2906 (w)  | $\nu_{\text{sym}}$ ( $\text{CH}_3$ )    |
| 2861 (w)     | 2840 (w)        | 2855 (w)     | 2845 (w)        | --        |   |
| 1435 (w)     | 1434 (w)        | 1430 (w)     | 1433 (w)        | --        | $\delta_{\text{as}}$ ( $\text{CH}_3$ )  |
| 1210 (s)     | 1220 (m)        | 1214 (s)     | 1213 (s)        | 1216 (s)  | $\delta_{\text{sym}}$ ( $\text{CH}_3$ ) |
| 988 (m)      | --              | 988 (w)      | 980 (w)         | --        |   |
| 718 (vs)     | 720 (w)         | 726 (vs)     | 717 (w)         | 740 (s)   | $\nu_{\text{as}}$ ( $\text{AlC}_2$ )    |
| 685 (s)      | --              | 689 (s)      | --              | 698 (s)   |   |
| 636 (m)      | --              | 638 (m)      | --              | 617 (s)   | $\nu_{\text{as}}$ ( $\text{AlF}_2$ )    |
| 608 (m)      | --              | 614 (m)      | --              | --        | $\nu_{\text{sym}}$ ( $\text{AlF}_2$ )   |
| 551 (s)      | 603 (vs)        | 560 (s)      | 599 (vs)        | --        | $\nu_{\text{sym}}$ ( $\text{AlC}_2$ )   |
| --           | 370 (m)         | --           | 370 (m)         | --        |   |

quite reactive, and therefore similar in behaviour to the product. 0.2254 g of TMAL was dissolved in 11.1687 g of dry  $\text{CCl}_4$  as a solvent in a dry box, and the solution introduced into a dry freezing point cell by a syringe through a rubber septum under  $\text{N}_2$ . The temperature was measured by a thermocouple which was calibrated to measure the temperature in Kelvin with an accuracy of about 0.001 K. The solution was cooled down slowly and a microcomputer was used to plot and read the temperature every 3 seconds; (see Chapter 3, Figure 3.17). The solution was stirred by a vertical stirrer connected to a motor to stir it continuously to avoid the supercooling condition.<sup>24</sup> The solution was warmed up, and this procedure was repeated many times. This gave a depression of 4.205 K and the molecular weight was calculated to be 144; this corresponds exactly to the TMAL dimer molecular weight of 144.

The same procedure was repeated for the products; 0.0377 g of the compound was dissolved in 8.6961 g of  $\text{CCl}_4$  in a dry box and transferred into the apparatus cell. A depression of 0.402 K was observed; this is rather smaller due to the small amount of sample. The relative molecular mass was as calculated a  $324 \pm 5$ .

#### 4. Elemental Analysis

A small amount of the product was sent to Butterworth Laboratories Ltd to be analyzed for the elements carbon, hydrogen, aluminium, and fluorine. The sample was found to be insufficient for fluorine and

aluminium. The results and the expected data are listed in Table 7.9.

### 7.5.2 Characterization of the products from TMAL pyrolysis in the presence of CCl<sub>4</sub>

The reaction of TMAL in the presence of CCl<sub>4</sub> yielded a new compound as described in Section 4.5.2. The characterization of this compound was carried out using gas phase IR, liquid phase Raman and <sup>1</sup>H NMR spectroscopy. This section is divided in to subsections according to the method used for characterization.

#### 1. IR and Raman Spectroscopy

Four torr of TMAL was mixed with 2 torr of CCl<sub>4</sub> and 10 torr SF<sub>6</sub> and irradiated with about 5.00 Watts laser power. The experiment was carried out in a cell similar to that described in Section 5. The products of 10 repeated experiments were condensed into a 4 mm. OD glass tube. A yellowish liquid was observed in the tube; this was degassed in a -77 °C bath of dry ice and acetone. The sample was warmed up to room temperature, in order to take the Raman spectrum of the liquid sample in the tube. The vapour of the sample was introduced back into the cell to take its IR spectrum, as shown in Figure 7.13 and Table 7.10.

#### 2. NMR Spectroscopy

The condensed sample in the NMR tube was dissolved in deuterated chloroform, CDCl<sub>3</sub>, with a small amount of

**Table 7.9:**  
Elemental analysis of DMAF.

---

| Elements | Expected % | Found % | % (found:expected) |
|----------|------------|---------|--------------------|
| H        | 7.9        | 7       | 85                 |
| C        | 31.6       | 27      | 88                 |
| F        | 25.0       | -       | -                  |
| Al       | 35.0       | -       | -                  |

---

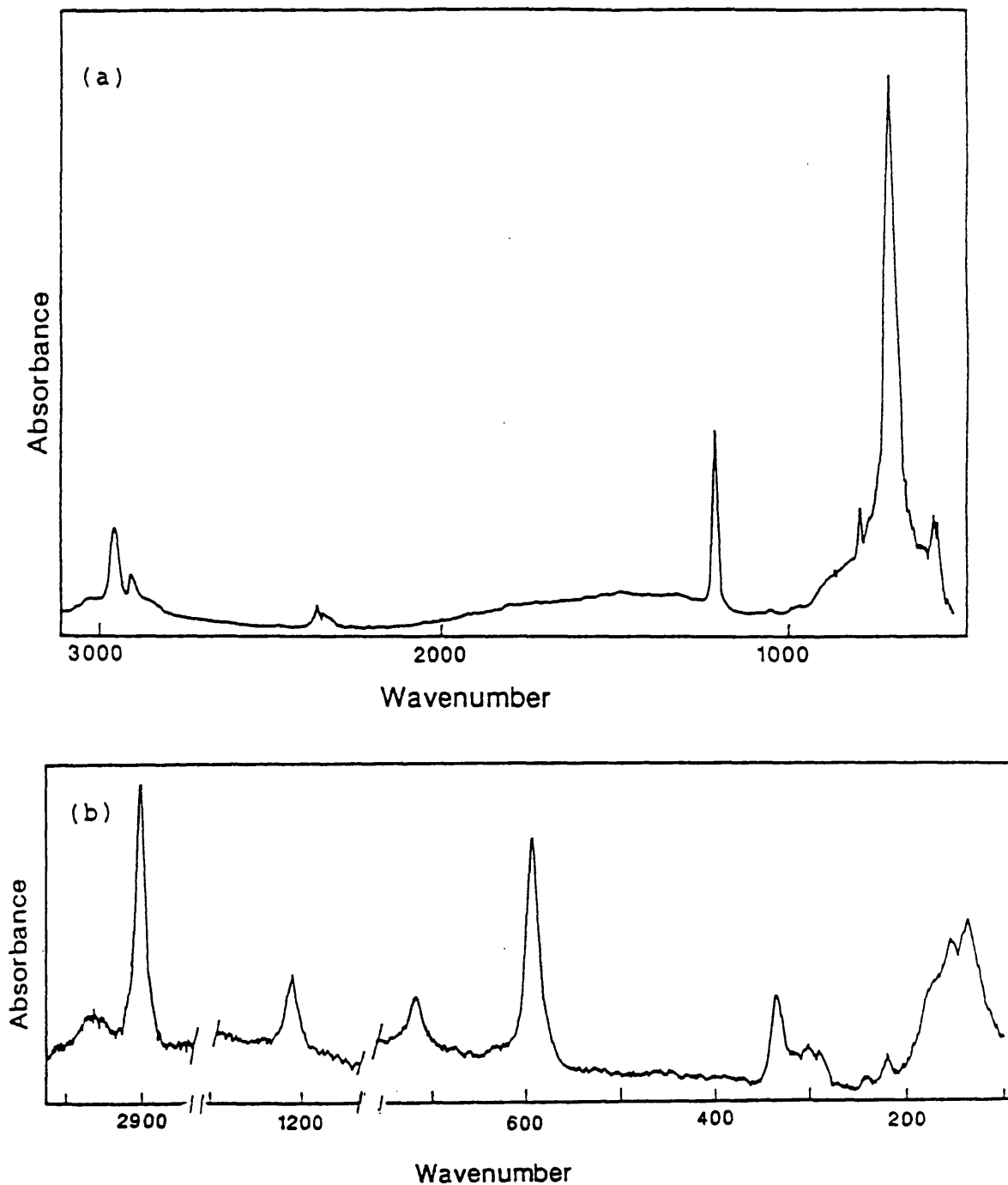


Figure 7.13:  
IR and Raman spectra of DMACl: (a) gas phase IR and (b) liquid phase Raman spectrum.

Table 7.10:

IR and Raman bands of DMACl ( $\text{cm}^{-1}$ ) compared with those of reference 24

| IR<br>(gas) | Raman<br>(liquid) | IR<br>ref 24 | Raman<br>ref 24 | assignments                      |
|-------------|-------------------|--------------|-----------------|----------------------------------|
| 3032 (m)    |                   |              |                 | CH <sub>3</sub> stretch          |
| 2956 (s)    | 2950 (w)          | --           | --              | " "                              |
| 2908 (s)    | 2904 (s)          | --           | --              | " "                              |
| 2848 (w)    | 2845 (w)          |              |                 |                                  |
| --          | --                | 1455         | --              | $\delta_{as}$ (CH <sub>3</sub> ) |
| --          | --                | 1440 }       | --              |                                  |
| --          | --                | 1300         |                 |                                  |
| --          | 1230              | --           | --              |                                  |
| 1209 (s)    | --                | 1205         | --              | $\delta_s$ (CH <sub>3</sub> )    |
| --          | --                | 980          | --              |                                  |
| 720 (vs)    | 718 (m)           | 720          | --              | $\nu_s$ (AlC) stretch            |
| 696 (sho)   | --                | --           | --              |                                  |
| 591 (m)     | 592 (vs)          | --           | --              | $\nu_{16}$ (AlCl) stretch        |
| 580 (w)     | --                | --           | 588             | (CH <sub>3</sub> ) rock          |
| --          | 335 (s)           | --           | --              |                                  |

chloroform used as a reference; tetramethylsilane (TMS) cannot be used as a reference as it has a large signal at the same region as TMAL and the new compound. The tube was sealed by flame and detached from the reaction cell. The  $^1\text{H}$  NMR showed one intense singlet; the chemical shift was  $\delta -0.2755$  ppm. Trace amounts of the compound observed with  $\text{SF}_6$  alone and another impurities were also observed, (see Figure 7.14).

### 7.5.3 Characterization of the products from TMAL pyrolysis in the presence of Chloroform, $\text{CHCl}_3$

In the reaction of TMAL in the presence of  $\text{CHCl}_3$  using a laser power of 3.75 Watts, the same compound was formed as with  $\text{CCl}_4$ . The new product was identified by its characteristic IR absorption in the region  $720\text{ cm}^{-1}$  (Figure 7.8).

### 7.5.4 Characterization of the products from TMAL pyrolysis in the presence of Deuterated Chloroform, $\text{CDCl}_3$

The reaction of TMAL in the presence of  $\text{CDCl}_3$  using a laser power of 3.75 Watts also gave a peak at  $720\text{ cm}^{-1}$  as with  $\text{CHCl}_3$  as in Figure 7.10. When a higher laser power was used (about 7.50 Watts), a small amount of  $\text{CH}_3\text{D}$  was formed, which was characterized by its IR absorption in the region of  $2200$  and  $1156\text{ cm}^{-1}$ .

## 7.6 KINETIC MEASUREMENTS OF TMAL PYROLYSIS

The pyrolysis of TMAL was carried out over a range of laser powers; an increase in laser power corresponds

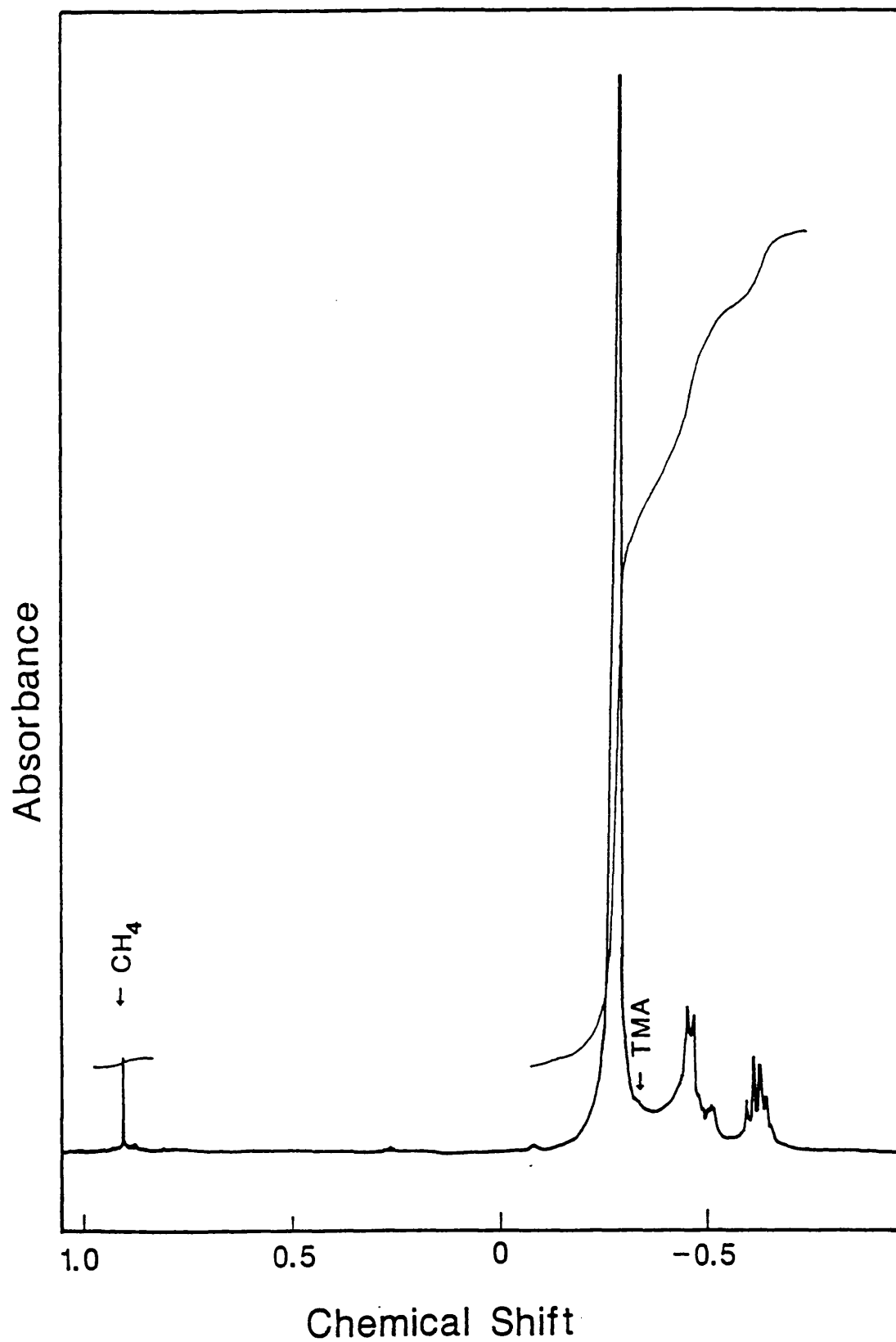


Figure 7.14:

$^1\text{H}$  NMR spectrum for DMACl, dissolved in  $\text{CDCl}_3$  with a trace amount of  $\text{CHCl}_3$  as lock reference.

approximately to an increase in temperature (see Chapter 4).

As described in Chapter 2 the intensity of the peak at  $777\text{ cm}^{-1}$ , corresponding to the bridging  $\text{CH}_3$  group, may be taken as proportional to the concentration of TMAL. Thus, the decay of the intensity of this peak was followed to measure the rate of the reaction, using the FTIR spectrophotometer. It was assumed that, in the presence of trapping agents, the decay of TMAL (7.6.1) follows first order kinetics (7.6.2),



$$d[\text{TMAL}]/dt = -k[\text{TMAL}] \quad 7.6.2$$

where  $[\text{TMAL}]$  is the concentration of TMAL and  $k$  is the effective rate constant. A plot of  $\ln(\text{intensity})$  of this peak vs time, under fixed experimental conditions, was linear, indicating a first order reaction; see (Figure 7.15). Values of rate constants determined in this way are listed in Table 7.11. An accurate measurement of the activation energy in this system requires a measurement of the temperature variation over the cell (see Figure 4.2, Chapter 4). The use of reference compounds in the cell, as described in the review Section 4.2, is not possible in this system because of its highly reactive nature. Figure 7.16 shows the plot of the rate constant vs laser power.

## 7.7 RESULTS AND DISCUSSION

The results obtained from Sections 7.5 and 7.6 for the TMAL pyrolysis in the presence of various compounds can be

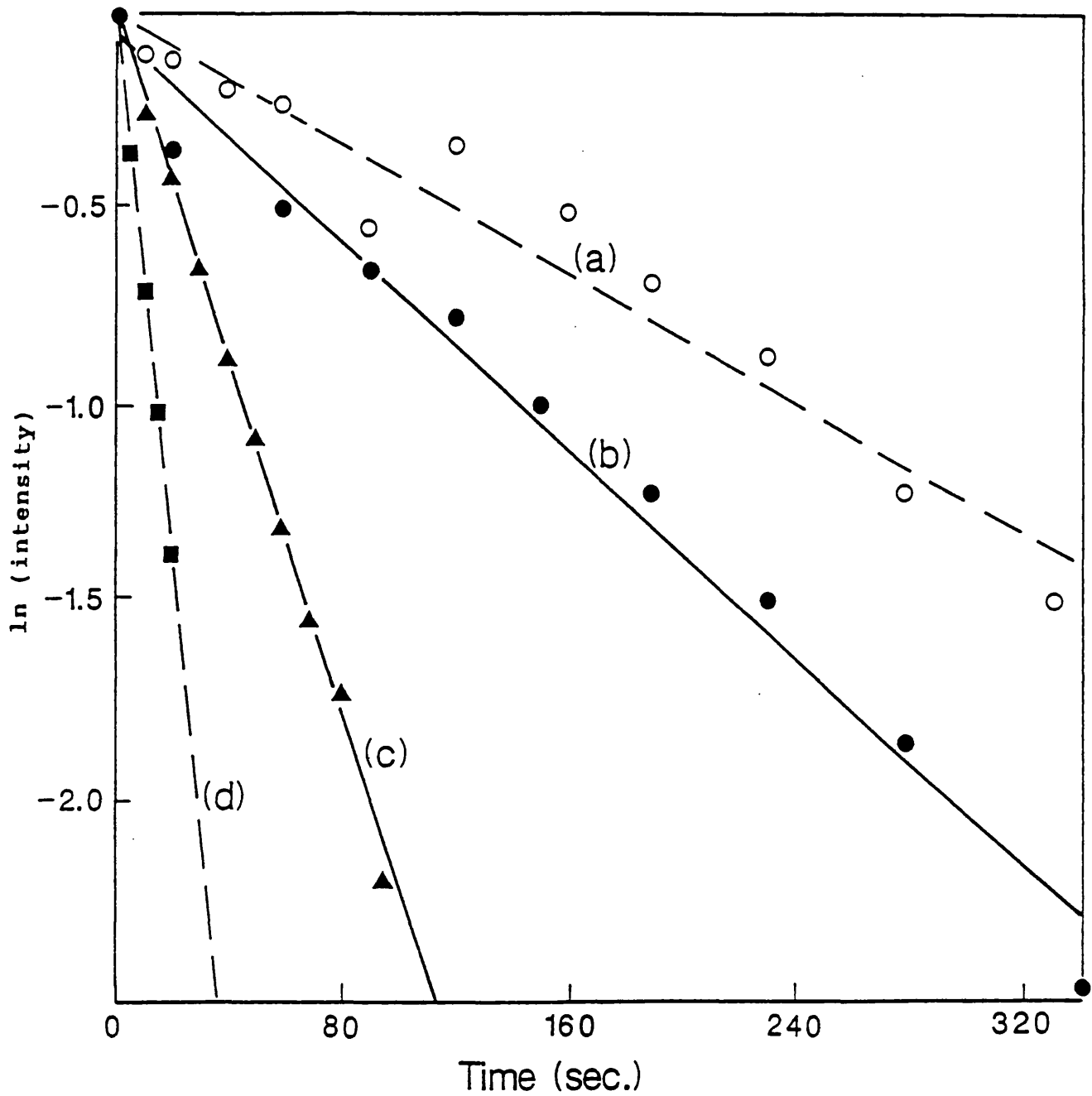


Figure 7.15:

The plot of  $\ln(\text{intensity})$  of the bridging peak at  $777\text{cm}^{-1}$  vs time for various laser powers: (a) 5.0, (b) 6.25, (c) 8.75 and (d) 12.50 Watts.

**Table 7.11:**

First order rate constants of the decomposition of 2 torr of TMA and 10 torr of SF<sub>6</sub> and the laser power.

---

| Laser power<br>(Watts) | Rate constant<br>(s <sup>-1</sup> ) |
|------------------------|-------------------------------------|
| 5.00                   | 0.68 x 10 <sup>-2</sup>             |
| 6.25                   | 0.77 x 10 <sup>-2</sup>             |
| 7.50                   | 0.90 x 10 <sup>-2</sup>             |
| 8.75                   | 2.20 x 10 <sup>-2</sup>             |
| 10.00                  | 3.78 x 10 <sup>-2</sup>             |
| 11.25                  | 4.25 x 10 <sup>-2</sup>             |
| 12.50                  | 6.80 x 10 <sup>-2</sup>             |

---

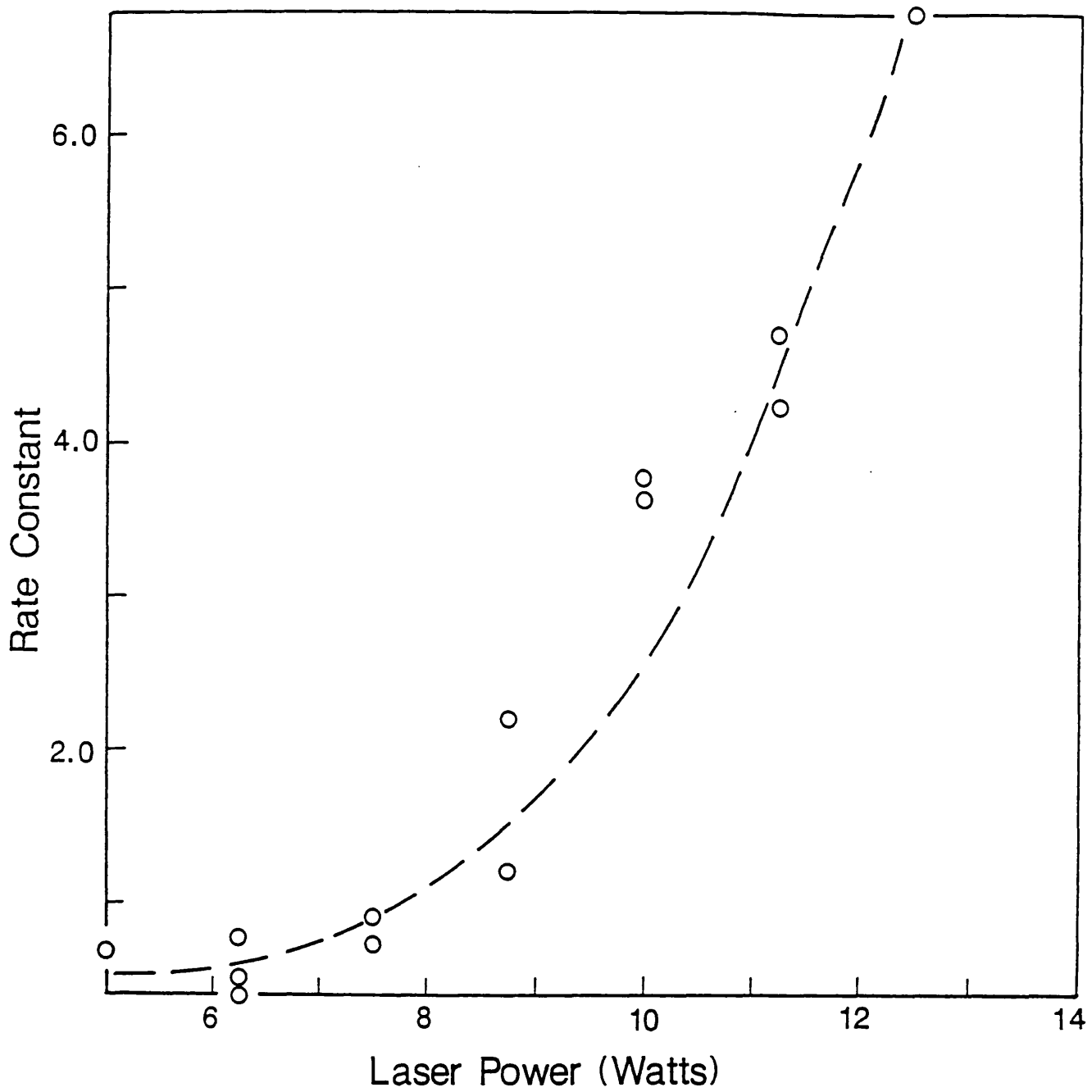


Figure 7.16:

Plot of the 1st order rate constant  $k$  vs laser power.

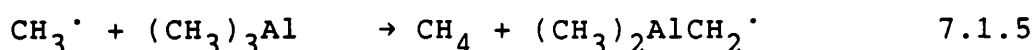
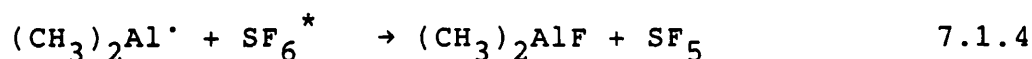
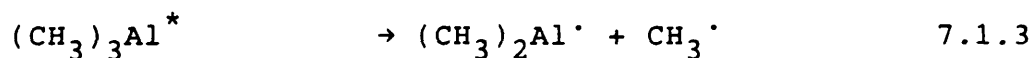
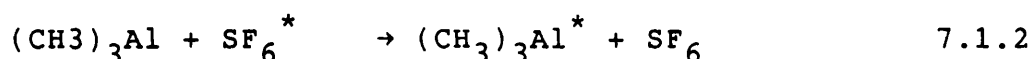
divided into the following subsections.

### 7.7.1 The decomposition of TMAL in the presence of SF<sub>6</sub>

The IR spectra in Figure 7.2 show that during the pyrolysis of TMAL the peaks at 777 and 1254 (CH<sub>3</sub> bridging) and 570 cm<sup>-1</sup> disappear faster than that at 702 cm<sup>-1</sup> (CH<sub>3</sub> terminal); at the same time, new peaks appear at 3016, 1312 and 740 cm<sup>-1</sup>. The first two of these are readily identified as methane, CH<sub>4</sub>. The IR and Raman liquid phase spectra of the product isolated as described in Section 7.5.1 (Figures 7.12.a and b) are in agreement with that of dimethyl aluminium fluoride (DMAF), (CH<sub>3</sub>)<sub>2</sub>AlF, of reference (20). In the gas phase IR spectrum, however, the strong peak at 551 cm<sup>-1</sup> is absent, and there are small changes elsewhere. Table 7.8 lists the IR and Raman spectra for the product and that published in reference 20. The <sup>1</sup>H NMR spectrum is consistent with that of DMAF<sup>26</sup>; the triplet of the proton resonance in the presence of TMAL arises from the two equivalent fluorine atoms bridged to the Al as noted by Schmidbauer et al.<sup>26</sup>. The <sup>13</sup>C NMR spectrum shows one broad peak at a chemical shift of -12.47 ppm, confirming the presence of one type of carbon atom. The <sup>19</sup>F NMR spectrum also shows a single type of fluorine atom. The ratio of fluorine atoms to protons was found to be 1:6.4 (±10%) using the external standard. From the cryoscopic measurements, the relative molecular mass of the liquid was found to be 324 (the expected value for tetrameric DMAF is 304). From these results the structure of the new product in the liquid state could be deduced as dimethyl aluminium fluoride, DMAF, {(CH<sub>3</sub>)<sub>2</sub>AlF}<sub>4</sub> in a

tetrameric form. The elemental analysis of the small amount of sample was of low accuracy, but was consistent with this identification. The difference in the IR spectra of the DMAF in the gas phase and liquid phase is probably due to the presence of a different form of DMAF in the vapour, perhaps a dimer or trimer. This behaviour is similar to that of  $(\text{CH}_3)_2\text{GaF}$ , for which the tetrameric  $[\text{Ga}(\text{CH}_3)_2\text{F}]_4$  is formed spontaneously when the liquid trimer is stored at 5 to 15 °C for 2 to 3 weeks<sup>22</sup>.

A probable mechanism for the formation of the observed products is as follows:



In Reactions 7.1.1 and 7.1.2 laser energy is absorbed by  $\text{SF}_6$  molecules and then passed on to TMAL. The excited TMAL undergoes Al-Me bond homolysis to give  $\text{CH}_3^\cdot$  and  $(\text{CH}_3)_2\text{Al}^\cdot$  (DMA $^\cdot$ ) radicals, both of which then react further. The DMA $^\cdot$  radicals abstract fluorine atoms from the  $\text{SF}_6$  molecules to

form DMAF, (Reaction 7.1.4). The formation of DMAF was observed only at laser powers above 5 Watts whereas at lower laser powers TMAL decomposes without formation of any fluorine compound; only CH<sub>4</sub> and a thin metallic layer of aluminium deposited on the front window were observed. This means that the reaction with SF<sub>6</sub> occurs above a certain temperature, implying a large activation energy for the abstraction reaction (7.1.4). It is assumed that the deposits observed are the C-containing Al observed in other studies. This probably arises from further reaction of the Al-containing free radicals in the reactions above.

### 7.7.2 The pyrolysis of TMAL in presence of H<sub>2</sub>

The reaction of TMAL in presence of H<sub>2</sub> led to increased CH<sub>4</sub> production (compared with the absence of H<sub>2</sub>) and a thin layer of Al (apparently as a metal) deposited on the front window. The rate of the reaction was slower than the reaction without H<sub>2</sub>; the reason for this is that the higher conductivity of H<sub>2</sub> flattens the temperature profile in the zone of the reaction, (see Figure 7.17). A small amount of the fluorine compound was formed during the reaction (compared with the absence of H<sub>2</sub>); IR spectroscopy shows that both the bridging and terminal CH<sub>3</sub> peaks decayed nearly at the same rate. These observations suggest that in addition to the reactions (7.1.1-7.1.6), the H<sub>2</sub> is involved as below:



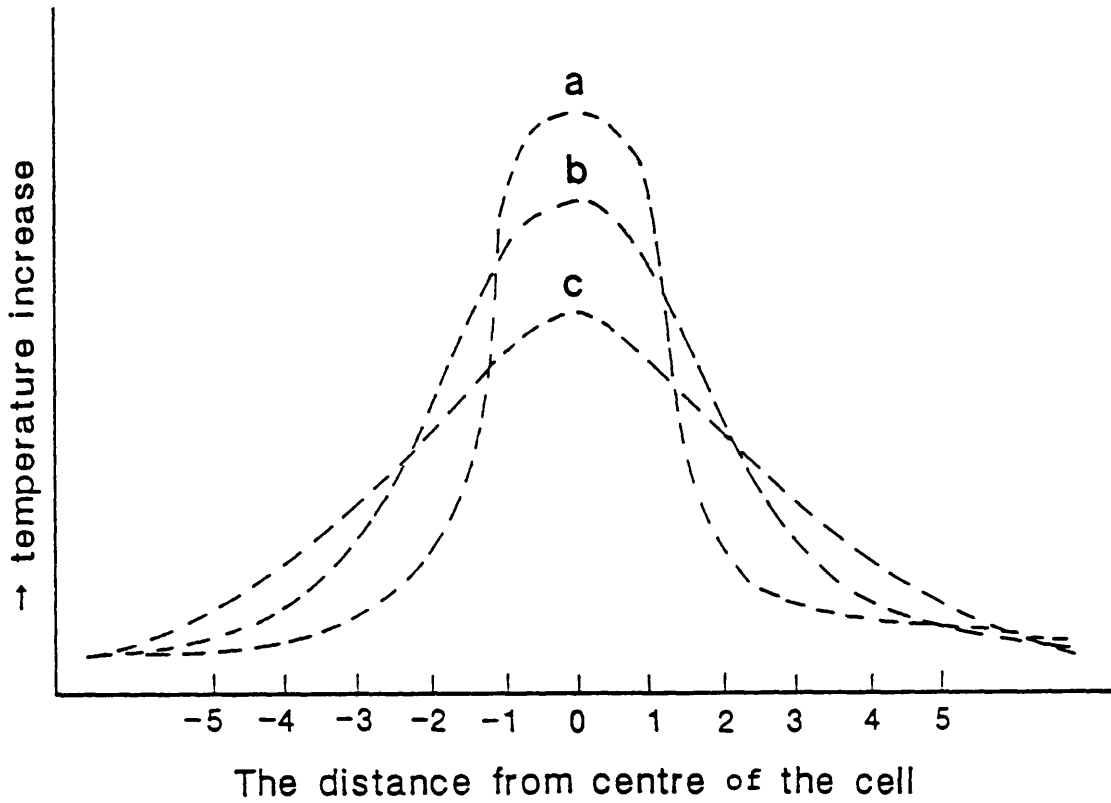
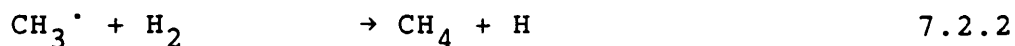


Figure 7.17:

Estimated temperature profiles in the reaction cell: (a)  $\text{SF}_6$  only, (b) with  $\text{D}_2$  and (c) with  $\text{H}_2$ .



The reason for increased production of methane,  $\text{CH}_4$ , is that the  $\text{CH}_3^\cdot$  radicals are trapped directly by abstracting H atoms from hydrogen molecules, (Reaction 7.2.2). The decrease of DMAF production results from the trapping of  $\text{DMA}^\cdot$  radicals to form dimethyl aluminium hydride, DMAH, as in Reaction 7.2.1. The latter is not stable in the range of the laser power used, and so reacts further to give elementary aluminium and methane (A. S. Grady, personal communication). The dissociation energy of the H-H bond ( $436 \text{ kJ mol}^{-1}$ ) is higher than that of the S-F bond in  $\text{SF}_6$  ( $343 \text{ kJmol}^{-1}$ )<sup>23</sup>, which suggests that kinetic factors determine the relative importance of Reactions 7.1.2 and 7.2.1. The smaller mass and increased collision rate of the  $\text{H}_2$  may also be important. Trapping of the methyl radicals (Reaction 7.2.2), and hence the reduction of Reaction 7.1.5, is probably the reason for the improved quality of the deposited Al.

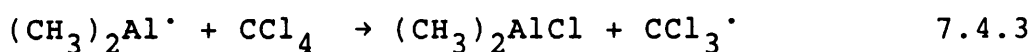
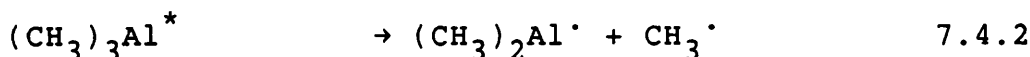
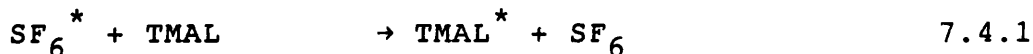
### 7.7.3 Pyrolysis of TMAL in presence of $\text{D}_2$

The aim of this experiment was to obtain further information about the mechanism of TMAL pyrolysis and the formation of  $\text{CH}_4$  during the reaction in presence of  $\text{H}_2$  as a carrier gas. This is important, as  $\text{H}_2$  is normally used as a carrier gas for many reagents such as  $\text{TMGa}$ <sup>26</sup> and other organometallics compounds in the semiconductor industry. This experiment revealed clearly that the formation of  $\text{CH}_4$  arises largely from the reaction of  $\text{CH}_3^\cdot$  radicals with TMAL or with other  $\text{CH}_3^\cdot$  radicals, since the IR spectra revealed only trace

amounts of  $\text{CDH}_3$  in comparison with  $\text{CH}_4$ . A significant amount of DMAF was formed during the reaction and the rate of the reaction was faster than in presence of  $\text{H}_2$ . The reason for this is that the conductivity of  $\text{H}_2$  ( $0.187 \text{ W m}^{-1} \text{ K}^{-1}$ ) is higher than  $\text{D}_2$  ( $0.140 \text{ W m}^{-1} \text{ K}^{-1}$ )<sup>23</sup>, and this affects the temperature distribution of the cell; the temperature in the centre of the cell is greater with  $\text{D}_2$  and subsequently the rate of the reaction is increased.

#### 7.7.4 The pyrolysis of TMAL in presence of $\text{CCl}_4$

The decomposition of TMAL in presence of  $\text{CCl}_4$  shows that  $\text{DMAL}^\cdot$  radicals abstracted chlorine atoms from  $\text{CCl}_4$ . From the experiment with TMAL:  $\text{CCl}_4$  in the ratio 4:1, it appeared that most of the chlorine atoms of  $\text{CCl}_4$  were abstracted; this is indicated by the IR spectra which showed that the  $\text{CCl}_4$  has completely disappeared when all TMAL was converted to  $\text{DMACl}$ . No fluorine compounds were observed. Methane and dimethyl aluminium chloride,  $\text{DMACl}$ , were formed; the latter is identified by NMR and IR spectroscopy. The proton NMR  $^1\text{H}$  gave one singlet centred at chemical shift  $-0.0755 \text{ ppm}$  which can be assigned to  $\text{DMACl}$ <sup>28</sup>. The Raman and IR spectra were in agreement with that published by Gray<sup>25</sup>. The probable reactions are presented in the Scheme below:

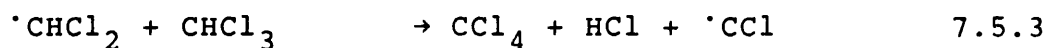
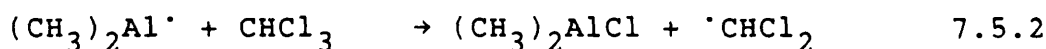
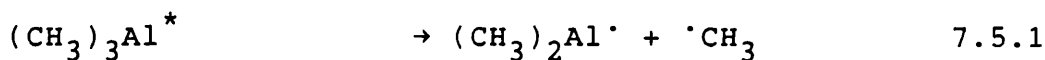


etc...

the majority of the products were DMAcI and CH<sub>4</sub>; there was no sign of any CH<sub>3</sub>Cl detected by IR spectroscopy.

#### 7.7.5 The pyrolysis of TMAL in presence of CHCl<sub>3</sub>

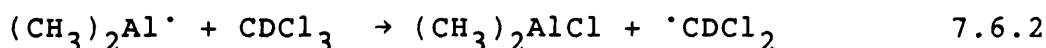
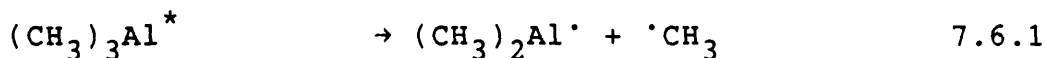
Chloroform, CHCl<sub>3</sub> was less stable than CCl<sub>4</sub>, and was pyrolyzed at laser powers of 3.75 Watts to form CCl<sub>4</sub> and HCl as indicated by IR spectroscopy. The reaction with TMAL was therefore carried at a laser power of 3.25 Watts. The reaction gave DMAcI as identified from its IR absorption at 720 cm<sup>-1</sup> and the reaction can be written as follows:



No DMAF was detected during the reaction.

#### 7.7.6 The pyrolysis of TMAL in presence of CDCl<sub>3</sub>

The reaction of TMAL in presence of CDCl<sub>3</sub> at a laser power of 3.25 Watts gave DMAcI and CH<sub>4</sub>. The mechanism is probably as illustrated in the scheme below:



The reaction was repeated at a higher laser power, and  $\text{CH}_3\text{D}$  was detected along with other products as listed in Table 7.6 and shown in Figure 7.9.

### 7.8 CONCLUSION

The thermal decomposition of TMAL has been studied using the technique of LPHP as described in Section 7.6. The results showed that the reaction proceeded far from the walls, and that surface reactions had a negligible effect. The highly reactive DMAL $\cdot$  radicals, which were formed during the reaction, can be trapped by the photosensitiser,  $\text{SF}_6$ , and fluorine atoms abstracted to form DMAF. Abstraction of fluorine atoms from  $\text{SF}_6$  can be a useful method of synthesis of such compounds. Trapping DMAL radicals with other scavengers,  $\text{CHCl}_3$ ,  $\text{CDCl}_3$ ,  $\text{CCl}_4$ , confirmed the mechanism, and also provided an easy method of synthesis of DMACl. The presence of  $\text{H}_2$  in the reaction mixture increased the production of  $\text{CH}_4$ , and subsequently the aluminium metal produced was less contaminated with aluminium carbide,  $\text{Al}_4\text{C}_3$ . The disadvantage of this technique for this particular system was that the photosensitiser was not inert toward the TMAL, unless protected by adding radicals scavengers such  $\text{H}_2$ ,  $\text{CCl}_4$ ,  $\text{CDCl}_3$ ,  $\text{D}_2$  and  $\text{CHCl}_3$ . The thin layer of aluminium which was deposited on the front window affected the transparency of the ZnSe window and subsequently slowed the reaction.

### 7.9 REFERENCES

1. T. F. Kuch, E. Venhoff, T. S. Kuan, V. Deline and R. Potemski.  
J. Crys Growth 77 (1986) 257.
2. R. W. Glew, B. Garrett, J. E. A. Whiteaway and E. J. Thrush.  
J. Crys Growth 77 (1986) 613.
3. T. Ohata, K. Honda, S. Hirata, K. Tamamura, H. Ishikawa, K. Miyahara, Y. Mori and C. Kojima.  
J. Crys Growth 77 (1986) 637.
4. H. Kukimoto, Y. Ban, H. Konatau, M. Takechi and M. Ishizaki.  
J. Crys Growth 77 (1986) 223.
5. N. Hayafujl, K. Mizuguchi, S. Ochi and T. Murotani.  
J. Crys. Growth 77 (1986) 281.
6. K. Kamon, M. Shimazu, K. Kimura, M. Minara and M. Ishii.  
J. Crys. Growth 77 (1986) 297.
7. J. P. Andre, E. Dupont\_Nivet, D. Moroni, J. N. Putillon, M. Erman and T. Ngo.  
J. Crys. Growth 77 (1986) 357.
8. D J. Ehrlich, R. M. Osgood, Jr., and T. F. Deutsch.  
Appl. Phys. Lett. 38 (1981) 946.
9. I. Hino and T. Suzuki.  
J. Crys. Growth 68 (1984) 483.
10. P. J. Baugh and A. Casson, M. W. Jones and A.C. Jones.  
J. Chromatography 411 (1987) 445.
11. L. M. Yeddanapalli and C. C. Schubert.  
J. Chem. Phys. 14 (1946) 1.

12. N. Suzuki, C. Anayama, K. Masu, K. Tsubouchi and N. Mikoshiba.  
Jap. J. Appl. Phys. 25 (1986) 1236.
13. D. W. Squire, C. S. Dulcy and M. C. Lin.  
Chem. Phys. Lett. 116 (1985) 525.
14. D. W. Squire, C. S. Dulcey and M. C. Lin.  
J Vac. Sci. Technol. B. 3 (1985) 1513.
15. J. E. Butler, N. Bottka, R. S. Sillmon and D. K. Gaskill.  
J. Crys. Growth 77 (1986) 163.
16. M. Suzuki and M. Sato.  
J. Electrochem. Soc. 132 (1988) 1684.
17. S. Kvisle and E. Rytter.  
Spectrochimica Acta. 10 (1984) 939.
18. T. Ogawa.  
Spectrochimica. Acta. 24 A (1968) 15.
19. T. Onishi and T. Shimanouchi.  
Spectrochimica. Acta 20 (1964) 325.
20. V. Krieg and J. Weidlein.  
J. Organometal. Chem. 21 (1970) 281.
21. J. Weidlein and V. Krieg.  
J. Organometal. Chem. 11 (1968) 9.
22. Gmelin Handbook of Inorganic Chemistry Part 1; Ga (1987)  
125.
23. Handbook of Chemistry and Physics  
62nd Edition (1981) F181
24. A. M. Cooney.  
Thermodynamic properties of binary liquid mixtures  
containing fluoroalcohols, Ph.D. Unieversity of  
Leicester (1988).

25. A. P. Gray.  
Can. J. Chem. 41 (1963) 1511.
26. H. Schmidbauer and H. F. Klein.  
Chem. Ber. 101 (1968) 2278.
27. C. A. Smith and M. G. H. Wallbridge  
3rd Symposium on Organometallic Chemistry, Abstract  
(1967) 346.
28. C. A. Larsen, N. I. Buchan and G. B. Stringfellow  
Appl. Phys. Lett. 52 (1988) 480.
29. E. G. Hoffmann.  
Z. Electrochem. 64 (1960) 616.

## CHAPTER 8

## PHOTOACOUSTIC MEASUREMENTS

8.1 INTRODUCTION

A study of the photoacoustic effect is described in this chapter. The validity of the use of this technique, applied to reactive chemical mixtures, has been studied. The effect of changing the volume of the reaction cell was also investigated. The usefulness of this technique was tested in comparison with IR spectroscopy measurements. This chapter begins with a review of previous studies using the photoacoustic effect for reactive and unreactive chemical systems.

8.2 REVIEW

As described in Chapter 2, the photoacoustic effect arises as a result of the modulated absorption of radiation and release of energy by an absorber gas in a closed cell. Thus an acoustic wave is produced. The latter can be detected by a microphone. The photoacoustic technique is widely used in reactive and unreactive chemical systems as a powerful tool in the study of microscopic energy transfer processes. Interests in photoacoustic measurements increased after the experimental tools applied to the investigation of molecular energy transfer in gases shifted from purely thermodynamic to optical methods. Early studies on measurements of vibrational relaxation showed that this technique can be very useful for this purpose. The basis of these studies, of course, is the measurement of the time required to transfer energy from an excited internal energy state to translational degrees of freedom. These measurements can be achieved by using either the frequency

dependent phase shift of the photoacoustic signal, or the signal amplitude. In recent measurements, very intense light sources (ie, lasers) have been used to excite the species of interest. The light used to induce the excitation was either modulated or pulsed light.

Measurements using an amplitude modulated laser beam and phase sensitive detection have been very common. This technique has provided a great deal of information about energy transfer pathways<sup>1-3</sup>. The pulsed technique<sup>4-8</sup> (measuring the amplitude of the photoacoustic signal) offers certain advantages over the continuously modulated configuration. One major advantage is the ability to delay interference from cell resonances by varying the cell length; an additional advantage is that the amplitude and time evolution are measured as separate quantities at the same time (during a single shot) rather than measuring the phase shift between modulated excitation and pressure response as a function of frequency.

The application of using photoacoustic techniques in some reactive chemical systems<sup>9-16</sup> has been in measuring the rate of the reaction or the evaluation of kinetic data, or spectroscopic applications.<sup>3,17-20</sup>

The rates of the reaction of the radicals  $\text{CH}_3$ ,  $\text{CD}_3$  and  $\text{CH}_2\text{I}$  with  $\text{I}$  and  $\text{I}_2$  have been studied by Hunter et al<sup>12</sup> using phase sensitive detection technique of the photoacoustic signal. They have also applied the photoacoustic technique to study the photophysical processes of biacetyl vapour<sup>10</sup>, benzene and deuterated benzene<sup>11</sup>. The rate of the reaction was measured using both the pressure rise from the heat deposited during the reaction and phase sensitive detection. Dibold<sup>15</sup> studied the kinetics of the reaction of  $\text{Cl}_2$  and  $\text{H}_2$ , using an Ar ion laser

to dissociate the Cl-Cl bond; the reaction was monitored using the photoacoustic technique. He measured the heat produced from the reaction of Cl radicals with  $H_2$ , which produced the acoustic wave. Barker et al<sup>14</sup> investigated the photolysis of  $N_2O_5$  using fluorescence and photoacoustic measurements, which gave comparable results. Rothberg et al<sup>13</sup> studied the heat of formation of meta stable photchemical intermediate species, by direct measurement of the amplitude of the photoacoustic signal (which is proportional to the fraction of the energy converted to heat).

The other important application of photoacoustic measurements is the measurement of the rate of relaxation and energy transfer of the excited molecules. Aoki et al<sup>7</sup> measured the rate of relaxation of  $CO_2$ ,  $SF_6$  and  $NH_3$  molecules using the photoacoustic technique. The time constant  $\tau$  for the V-T (vibration-translation) energy transfer is related to the phase difference between the modulation and the emitted sound wave. Schuurman et al<sup>2</sup> studied the vibrational energy relaxation of methyl halides,  $CH_3X$ , using the photoacoustic method. They were, first, measuring the phase angle as a function of modulation frequency and density. Secondly they used the signal resulting from a short laser pulse as directly monitored by the microphone and stored; the rise time of the microphone signal yielded the rate of energy dissipation as translation.

That is a brief review of previous work on the application of the photoacoustic technique. All of these applications, especially the studies of energy transfer and the reactive chemical systems, were based on measuring the phase lag of the modulation frequency and the amplitude of the acoustic signal. In this study, however, the measurements were carried out in a

very different manner, as discussed in Chapter 2.

### **8.3 EXPERIMENTAL**

The equipment and block diagrams of the experimental arrangements were described in Chapter 2. Experiments were carried out using three different types of reaction cell. These are described in the following subsections.

#### **8.3.1 Long pyrex photoacoustic cell**

Experiments were carried out using a pyrex photoacoustic cell, about 27 cm long, to study (1) the effect of laser power on the amplitude of the acoustic wave, (2) the resonance frequency (r.f.) of the cell, (3) the calibration curve of the cell by varying the composition of unreactive mixtures, (4) effects of the pressure of the photosensitiser, (5) the effects of the laser power on the r.f. of the cell, and the r.f. of the cell in unreactive (6) and reactive (7) chemical mixtures.

##### **1. Laser Power Effects on the Amplitude of the Acoustic Wave.**

Ten torr of the SF<sub>6</sub> photosensitiser were introduced into the cell. The cell was exposed to a CO<sub>2</sub> laser beam chopped at the resonant frequency of the cell (using a mechanical chopper). The photoacoustic signal was fed to an amplifier to be measured and displayed on an oscilloscope. The laser power was varied by controlling the laser gas and the current. The change in the amplitude of the acoustic wave on varying the laser power is plotted in Figure 8.1.

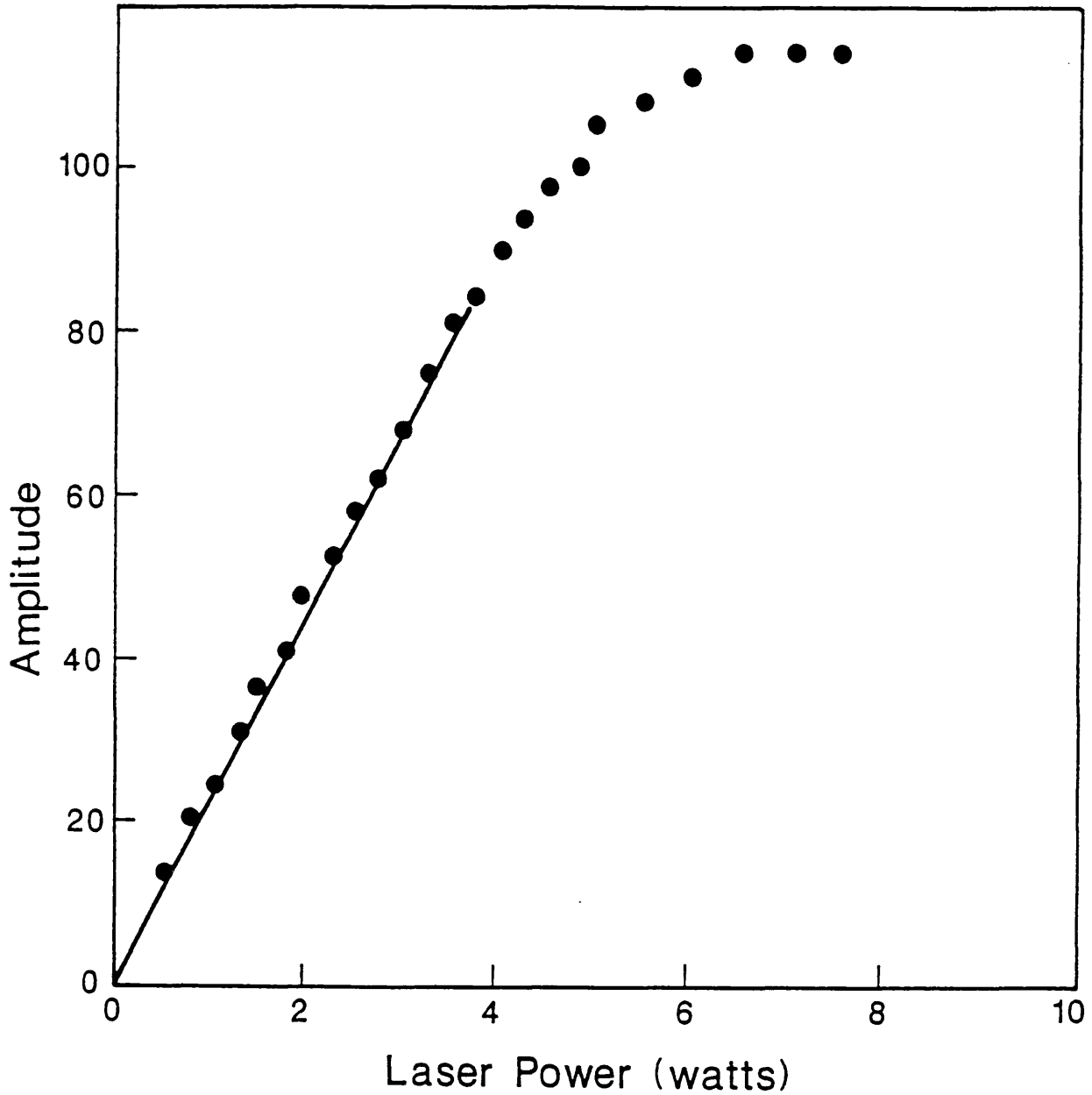


Figure 8.1:

Plot of amplitude of the photoacoustic signal vs laser power  
Cell length was 27 cm, and pressure of  $\text{SF}_6$  was 10 torr; th  
laser beam was chopped with the mechanical chopper.

## 2. The Resonance Frequency Spectrum of the Cell

Ten torr of  $\text{SF}_6$  was introduced into the cell and exposed to about 5.0 Watts laser power. The frequency of the chopper was varied from 1 up to 1000 Hz (the maximum speed of the chopper), in order to determine the r.f. spectrum of the cell. The amplitude of the acoustic wave was measured on tuning the frequency of the chopper, and is illustrated in Figure 8.2.

## 3. The Calibration Curve of the r.f. of the Cell

In order to demonstrate the feasibility of measurements of gas composition by r.f. of the cell, a calibration was undertaken using mixtures of  $\text{SF}_6$  and  $\text{H}_2$ . A total pressure of 20 torr of  $\text{SF}_6$  and  $\text{H}_2$  in varying ratios was used. The partial pressure of each of the components was varied from 2 to 18 torr. The mixture was irradiated with a fixed laser power (5.0 Watts). The r.f. of the cell was measured for each mixture after exposure for about 15 minutes; see Figure 8.3.

## 4. The Effects of the Pressure of the Photosensitiser ( $\text{SF}_6$ ) on the r.f. of the Cell

The aim of this experiment was to determine the effects of the pressure of the photosensitiser,  $\text{SF}_6$  on the r.f. of the cell using a fixed power of  $\text{CO}_2$  laser. The r.f. of the cell was measured using different pressures; see Table 8.1.

## 5. The Effects of Laser Power on the r.f. of the Cell

The aim of this experiment was to determine whether the

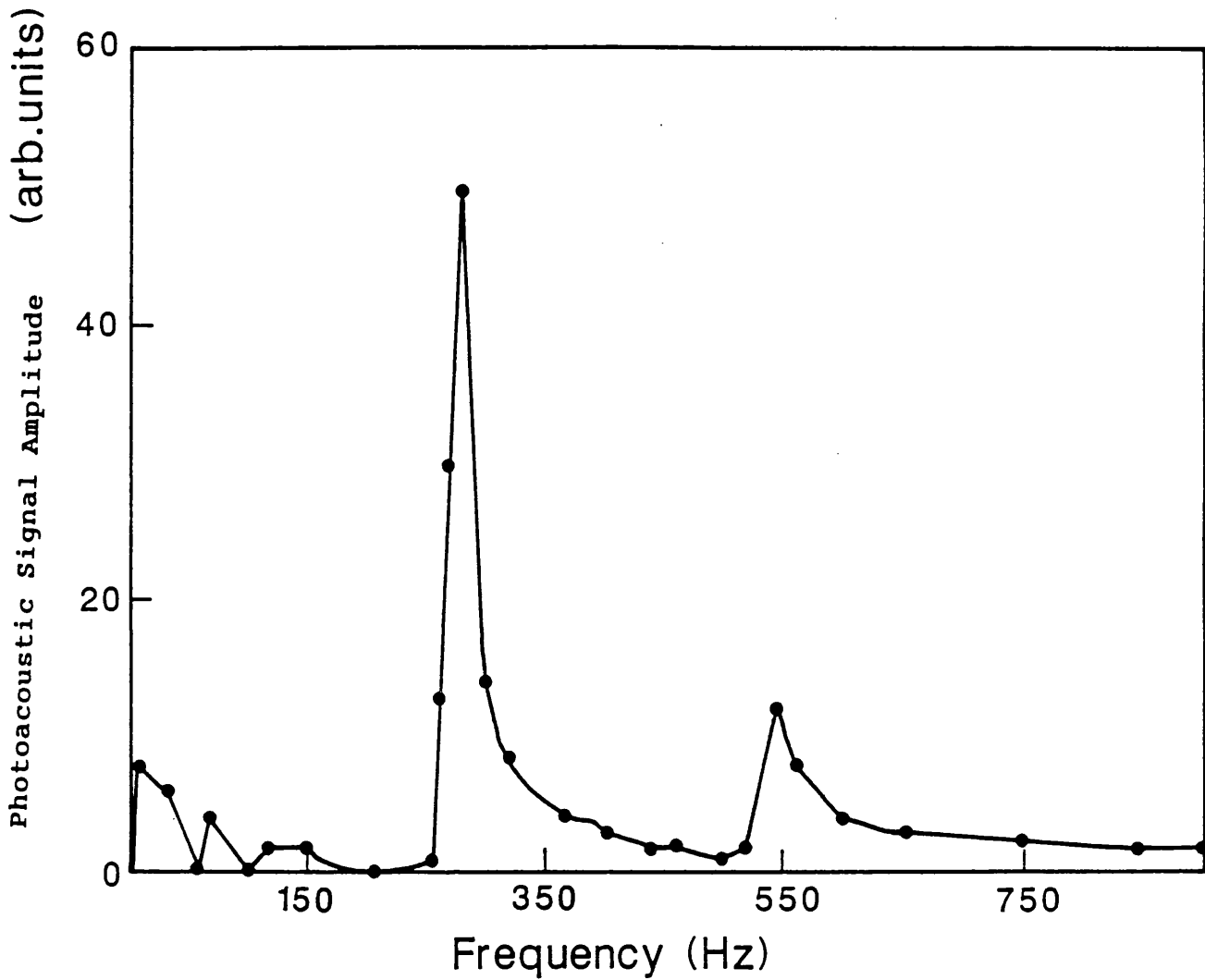


Figure 8.2:

Resonance frequency spectrum for the 27 cm long photoacoustic cell.  $\text{SF}_6$  pressure was 10 torr, irradiated with mechanically chopped laser beam at a power of 5.0 Watts.

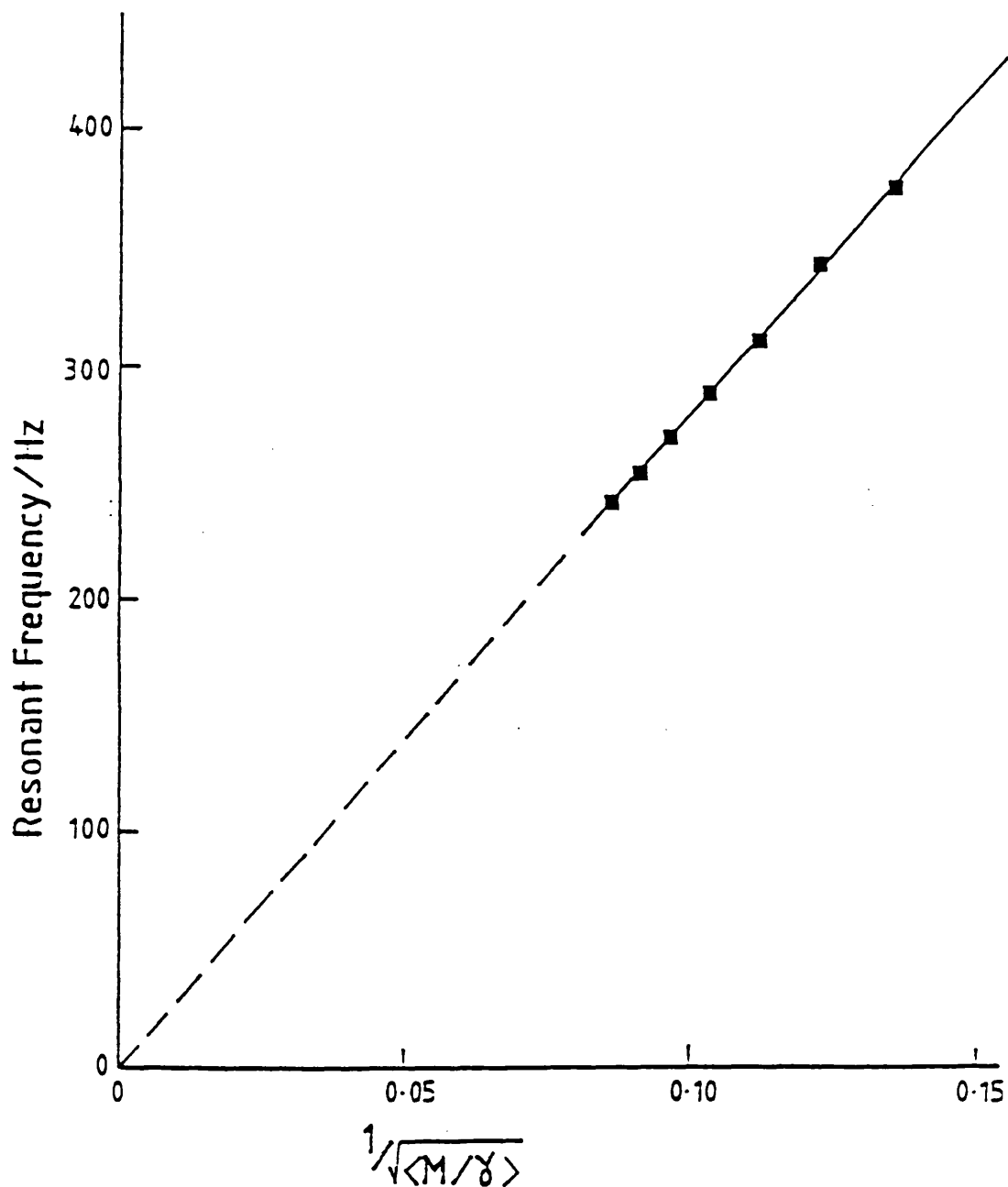


Figure 8.3: Plot of reaction cell resonant frequency vs.  $1/\sqrt{\langle M/\gamma \rangle}$ , averaged over gas composition, for  $\text{SF}_6 + \text{H}_2$  mixtures. The correlation coefficient of the calibration line is 0.999.

Table 8.1:

Effect of the pressure of the photosensitizer on the  
r.f.  
of the cell.

---

| SF <sub>6</sub> Pressure<br>(torr) | r.f.<br>(Hz) |
|------------------------------------|--------------|
| 10                                 | 243          |
| 15                                 | 245          |
| 20                                 | 247          |

---

laser power level had any effect on the r.f. of the cell. 10 torr of SF<sub>6</sub> was introduced into the cell and exposed to various laser powers; the variation interval was about 0.4 Watts. The amplitude and the r.f. of the cell were measured; see Figure 8.4.

## 6. The r.f. in Unreactive Chemical Mixtures

The aim of these experiments was to determine the effects of chemically unreactive mixtures on the r.f. of the cell. The r.f. of the cell was studied using hydrogen, water vapour and air mixtures with SF<sub>6</sub>.

### 6.a. Hydrogen and SF<sub>6</sub> Mixtures.

Ten torr of H<sub>2</sub> were mixed with 10 torr of SF<sub>6</sub> and irradiated with laser power about 5 Watts. No change in the r.f. of the cell was observed even after a long time of exposure.

### 6.b. Air and SF<sub>6</sub> Mixtures.

Ten torr of air were mixed with 10 torr of SF<sub>6</sub>. The mixture was exposed to about 6.0 Watt laser power. Again, no change was observed in the r.f. of the cell after about 40 minutes exposure.

### 6.c. Water H<sub>2</sub>O and SF<sub>6</sub> Mixtures.

About 8 torr of purified water were mixed with 10 torr of SF<sub>6</sub>. The mixture was exposed to up to 15.0 Watts of laser power. Once again, no change was observed in the r.f. of the cell after about 50 minutes exposure.

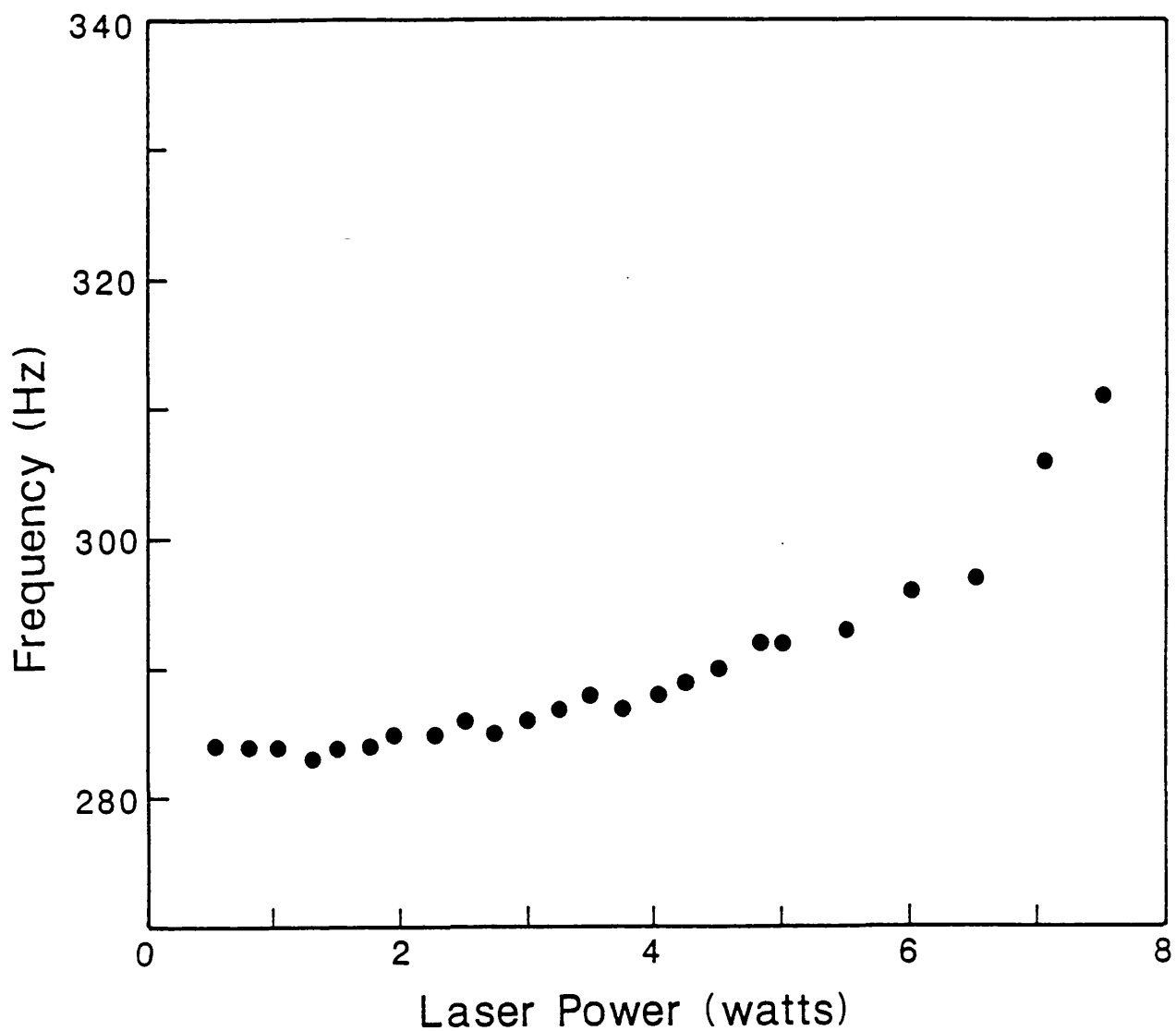


Figure 8.4:

Plot of the laser power vs r.f; 10 torr of  $\text{SF}_6$  was used and cell length was 25 cm.

## 7. Chemically Reactive Mixtures.

The goal of these experiments was to determine the effects of chemically reactive systems on the r.f. of the cell. The r.f. of the cell was studied using the following reactive mixtures (a) acetaldehyde,  $\text{CH}_3\text{CHO}$ , (b) methyl iodide,  $\text{CH}_3\text{I}$  and (c) a mixture of oxygen,  $\text{O}_2$ , and carbon monoxide,  $\text{CO}$ , with  $\text{SF}_6$ .

### 7.a. Acetaldehyde, $\text{CH}_3\text{CHO}$ and $\text{SF}_6$ Mixtures.

A mixture of 10 torr of  $\text{CH}_3\text{CHO}$  and 10 torr of  $\text{SF}_6$  was irradiated with the  $\text{CO}_2$  laser. The experiment was repeated at different laser powers. The r.f. of the cell was observed to change with time as shown in Figure 8.5.a. At the end of each experiment the products were checked using the IR spectrometer which showed the major products were  $\text{CH}_4$  and  $\text{CO}$  as shown in Figure 8.6.

### 7.b. Methyl Iodide, $\text{CH}_3\text{I}$ and $\text{SF}_6$ Mixtures.

A mixture of 5 torr of  $\text{CH}_3\text{I}$  and 10 torr of  $\text{SF}_6$  was introduced into the reaction cell. The mixture was irradiated with about 12.0 Watts laser power; a regular increase in the r.f. of the cell with time was observed, Figure 8.5.b. Crystals of iodine were deposited on the walls of the cell.

### 7.c. Mixtures of Oxygen, Carbon monoxide, and $\text{SF}_6$

A mixture of 10 torr of  $\text{O}_2$ , 20 torr of carbon monoxide,  $\text{CO}$  and 10 torr of  $\text{SF}_6$  was irradiated with about 24.0 Watts of laser power. After 10 seconds of

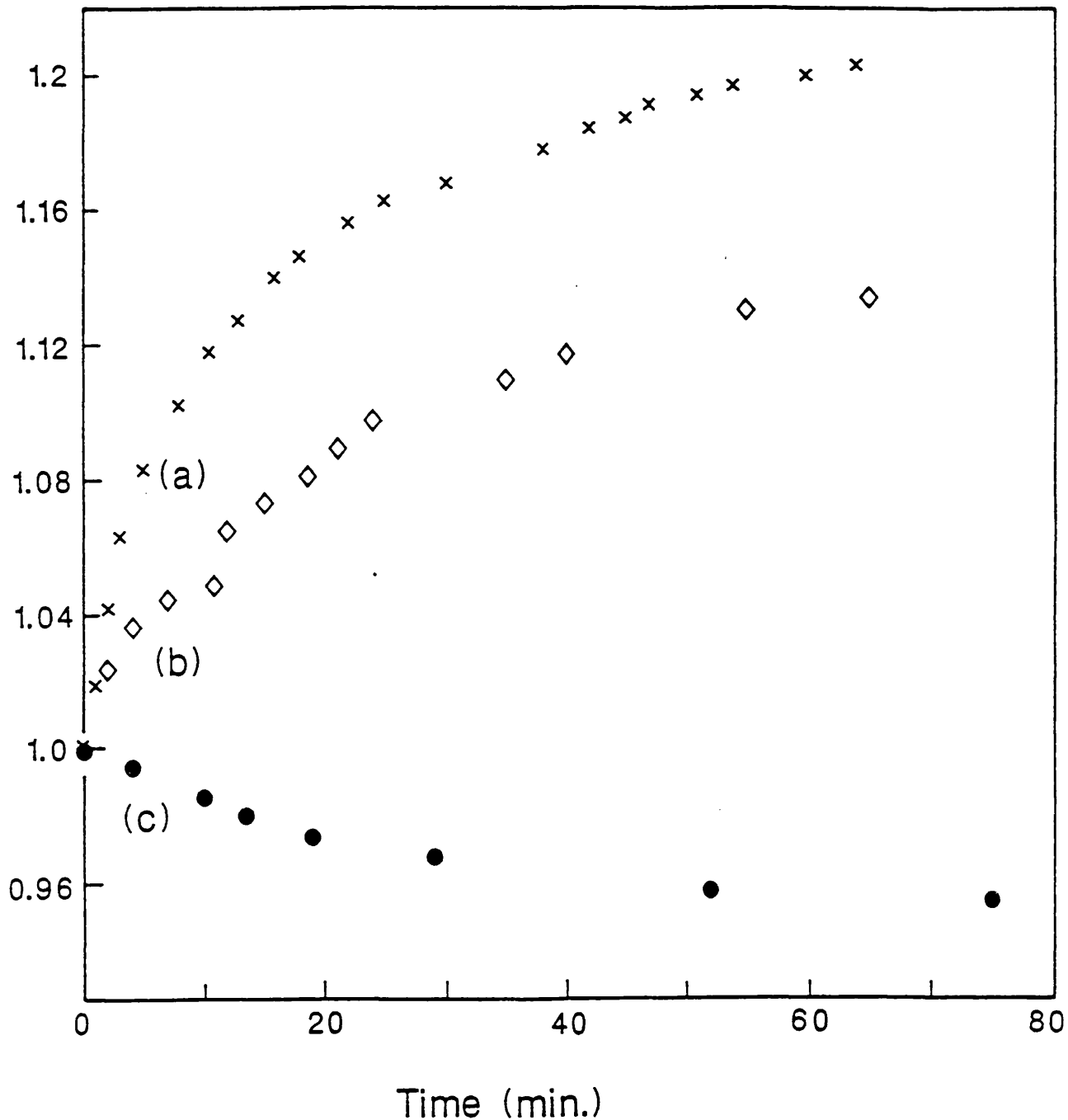


Figure 8.5:

Plot of the change in the r.f. of the photoacoustic cell vs time for different compounds. The changes in the r.f. of the cell are normalized to 1: (a) mixture of 10 torr of  $\text{CH}_3\text{CHO}$  and 10 torr of  $\text{SF}_6$ , (b) mixture of 5 torr of  $\text{CH}_3\text{I}$  and 10 torr of  $\text{SF}_6$ , (Laser power was 12.0 Watts) and (c) mixture of 10 torr  $\text{O}_2$ , 20 torr of  $\text{CO}$  and 10 torr of  $\text{SF}_6$  (laser power was 24.0 Watts).

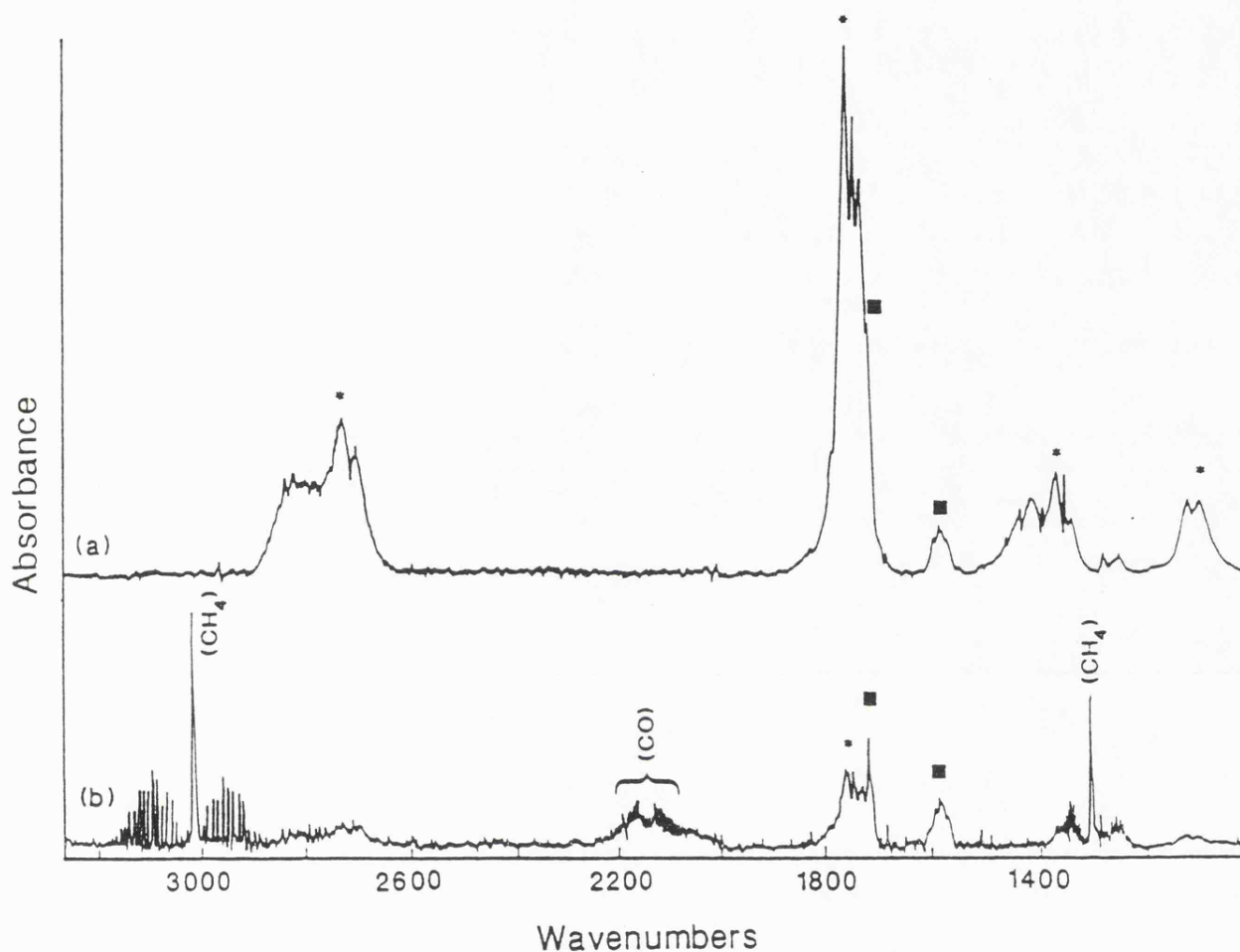


Figure 8.6:

IR spectra of a mixture of 10 torr of  $\text{CH}_3\text{CHO}$  and 10 torr of  $\text{SF}_6$  irradiated with 10 Watts of laser power: (a) before and (b) after the reaction. \* the starting material bands and ■ the  $\text{SF}_6$  bands.

exposure a chain reaction occurred and blue emission was observed (the burning of CO to CO<sub>2</sub>). The r.f. of the cell was dropped suddenly after the reaction from 447 to 418 Hz. The experiment was repeated using 5 torr of O<sub>2</sub> and 10 torr of CO with 10 torr of SF<sub>6</sub>. The laser power was also reduced to about 18.0 Watts. A regular decrease in the r.f. of the cell was observed, **Figure 8.5.c.**

### 8.3.2 Adjustable length cell

The aim of the design of this cell was to study the effects of the volume of the cell on the rate of the reaction. This section is divided into subsections: (a) study of the effect of the cell length on the r.f. of the cell, (b) the decomposition of CH<sub>3</sub>CHO using various volumes of the cell, and (c) different vapour pressures.

#### **1. The Calibration Curve of the r.f. of the Cell with the Cell Length**

The purpose of this experiment was to determine the relation of the r.f. of the cell to the change of the volume of the cell. The cell was adjusted to the appropriate volume and filled with 10 torr of SF<sub>6</sub>. The contents were then exposed to about 3.0 Watts of laser power. The r.f. of the cell was measured at each volume; **Figure 8.7.**

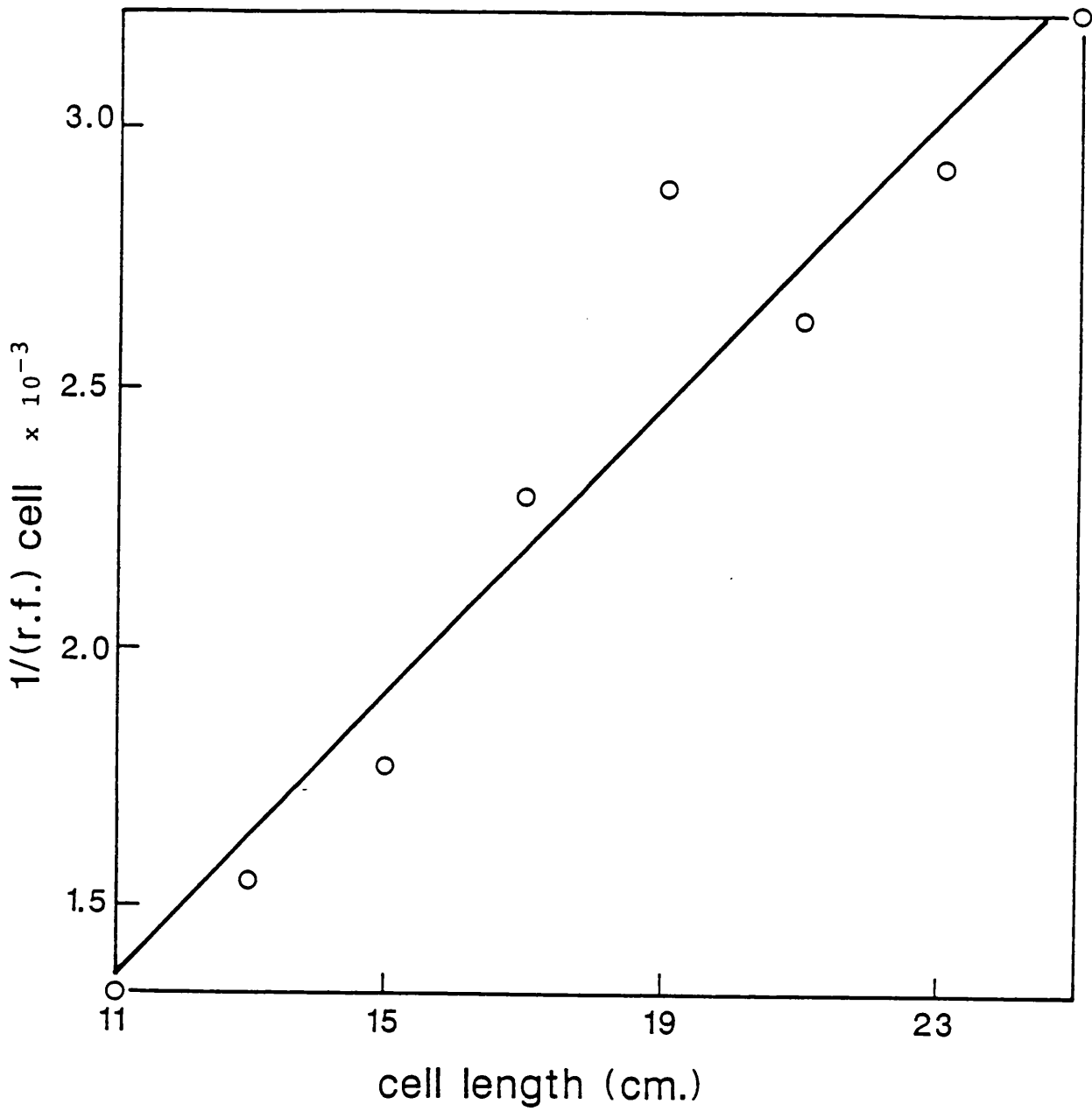


Figure 8.7:  
Plot of the 1/r.f. of the cell vs cell length.

## 2. The Decomposition of $\text{CH}_3\text{CHO}$

### 2.a. Varying the Volume.

In this experiment the decomposition of 10 torr of  $\text{CH}_3\text{CHO}$  was studied using different cell volumes. The laser power used to induced the reaction was about 10.0 Watts. The rate of the reaction was calculated by converting the r.f. to pressure (as described in Chapter 2); see Table 8.2.

### 2.b. Varying the Vapour Pressure.

A further experiment was carried out using different vapour pressures of  $\text{CH}_3\text{CHO}$  with about 11.0 Watts laser power. The pressure of  $\text{SF}_6$  was always kept at 10 torr always. The acetaldehyde vapour pressure was set at 2,4,6,8 and 10 torr. The experiment was repeated in different volumes. The rate of the reaction was calculated as in Section 1. The results are listed in Table 8.2.

### 8.3.3 The short length photoacoustic cell

In these experiments, IR and photoacoustic measurements were carried out on the same sample in order to compare the two methods for measuring the rate of the reaction. Thus, a short IR-photoacoustic reaction cell was required in order to fit into the IR spectrometer. The laser power was modulated using the signal generator as discussed in Chapter 3. The r.f. pattern of the cell, the effects of the modulation on the laser power, the modulation signal power on the r.f. of the cell were also studied.

Table 8.2:

Effects of pressure, laser power, and cell length on the rate of pyrolysis of  $\text{CH}_3\text{CHO}$ .

| Cell length (cm) | Laser Power (Watts) | $\text{SF}_6$ Pressure (torr) | $\text{CH}_3\text{CHO}$ Pressure (torr) | Rate loss ( $\text{min}^{-1}$ ) |
|------------------|---------------------|-------------------------------|---|---------------------------------|
| 15               | 12.5                | 10.0                          | 2                                       | 0.1                             |
| 15               | 12.5                | 10.0                          | 4                                       | $6.8 \times 10^{-3}$            |
| 15               | 12.5                | 10.0                          | 6                                       | $2.3 \times 10^{-2}$            |
| 15               | 12.5                | 10.0                          | 8                                       | $2.3 \times 10^{-2}$            |
| 15               | 12.5                | 10.0                          | 10                                      | $2.7 \times 10^{-2}$            |
| 27               | 5.0                 | 10.0                          | 10                                      | $9.5 \times 10^{-3}$            |
| 27               | 7.5                 | 10.0                          | 10                                      | $2.7 \times 10^{-2}$            |
| 27               | 10.0                | 10.0                          | 10                                      | $2.6 \times 10^{-2}$            |
| 27               | 12.5                | 10.0                          | 10                                      | $3.3 \times 10^{-2}$            |
| 27               | 15.0                | 10.0                          | 10                                      | $4.7 \times 10^{-2}$            |
| 15               | 12.5                | 10.0                          | 10                                      | $3.1 \times 10^{-2}$            |
| 17               | 12.5                | 10.0                          | 10                                      | $2.7 \times 10^{-2}$            |
| 23               | 12.5                | 10.0                          | 10                                      | $3.1 \times 10^{-2}$            |
| 25               | 12.5                | 10.0                          | 10                                      | $2.9 \times 10^{-2}$            |
| 27               | 12.5                | 10.0                          | 10                                      | $3.1 \times 10^{-2}$            |

Table 8.3:

Measurements of IR Absorbance of  $\text{CH}_3\text{CHO}$  at  $1124 \text{ cm}^{-1}$ , and resonance frequency of the cell, as a function of time. Laser power = 12.5 Watts, pressure of  $\text{SF}_6 = 10 \text{ torr}$ .

| time<br>(Sec.) | IR intensity of<br>the peak $1124 \text{ cm}^{-1}$ | Photoacoustic<br>frequency (Hz) |
|----------------|--|---------------------------------|
| 0.0            | 0.544  | 3550                            |
| 30.0           | 0.444  | 3556                            |
| 45.0           | 0.428  | 3666                            |
| 65.0           | 0.400  | 3728                            |
| 100.0          | 0.365  | 3777                            |
| 120.0          | 0.360  | 3788                            |
| 165.0          | 0.346  | 3816                            |
| 200.0          | 0.332  | 3825                            |
| 300.0          | 0.306  | 3846                            |
| 340.0          | 0.308  | 3853                            |
| 400.0          | 0.309  | 3872                            |
| 460.0          | 0.295  | 3902                            |
| 520.0          | 0.284  | 3917                            |
| 589.0          | 0.276  | 3980                            |
| 700.0          | 0.271  | 4034                            |
| 820.0          | 0.247  | 4062                            |
| 1000.0         | 0.231  | 4075                            |
| 1120.0         | 0.226  | 4103                            |
| 1300.0         | 0.216  | 4124                            |
| 1560.0         | 0.195  | 4160                            |
| 4080.0         | 0.085  | 4377                            |

### 1. The r.f. Pattern of the Cell.

The aim of this experiment was to determine the resonance frequencies of the cell. 10 torr of SF<sub>6</sub> was introduced into the cell and exposed to about 7.0 Watts of laser power; the laser was modulated electrically to create an acoustic wave in the cell. The frequency of the modulator was varied manually, and read using a frequency meter. The amplitude of the acoustic wave was monitored using an amplifier and an oscilloscope (Figure 8.8).

### 2. The Effects of the Modulation on the Laser Power

The goal of this experiment was to determine the effects of the modulation on the laser power. The experiment was carried out by tuning the modulator frequency over its entire range and monitoring the laser power using a power meter. Very little change in the laser power (less than 5% of output laser power) was observed.

### 3. The Calibration Curve of the Cell

This experiment was carried out following the same procedure as in Section 3.1.3. The results are shown in Figure 8.9.

### 4. Effects of Modulation Amplitude on the r.f. of the Cell

The experiment was carried out to determine the effects of the amplitude of the modulating signal on the r.f. of the cell. 10 torr of SF<sub>6</sub> was introduced to the cell. The sample was irradiated using about 10.0 Watts of laser power. The modulator was tuned to each r.f. of the cell, and the amplitude of the modulating signal was varied from

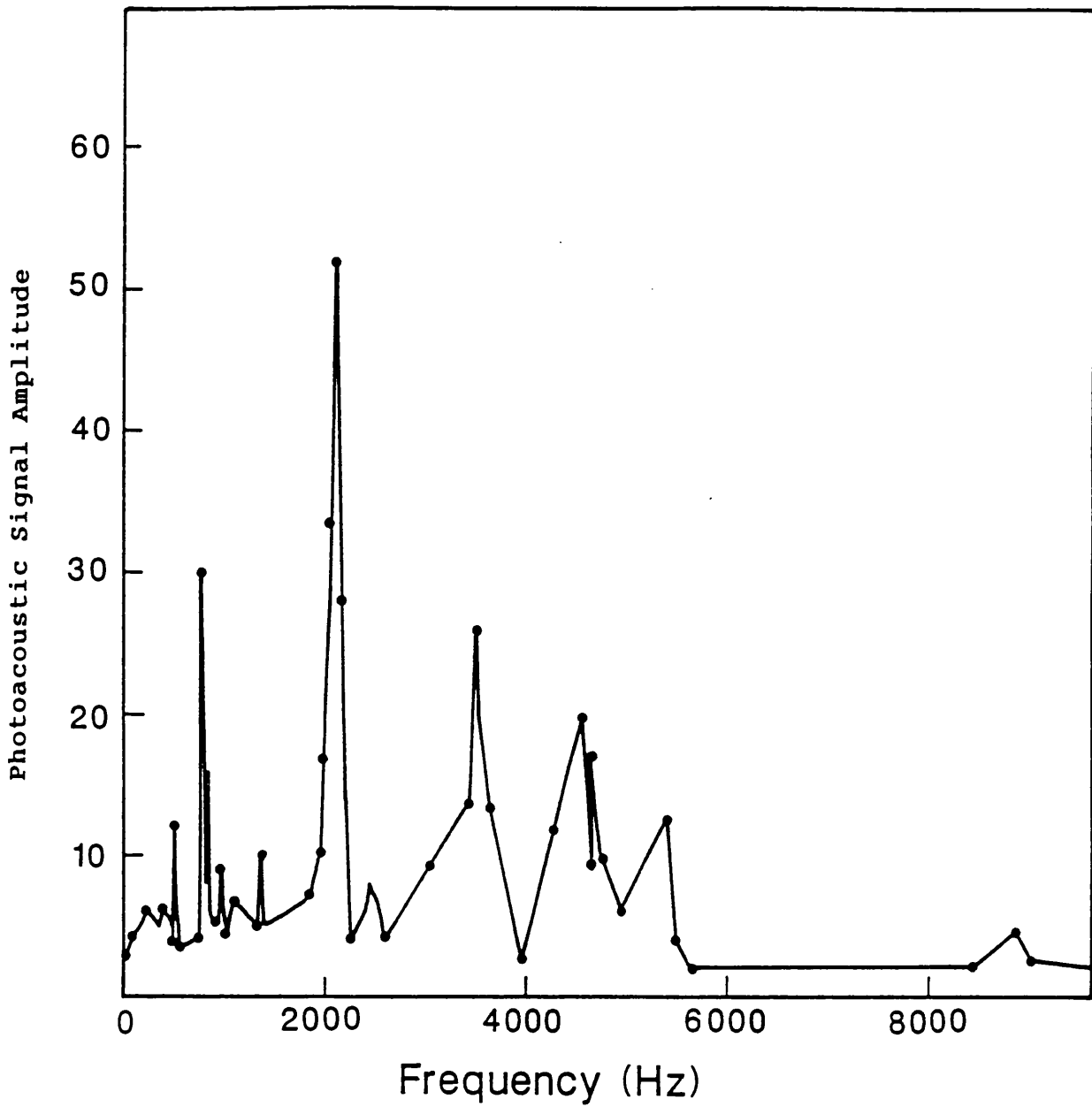


Figure 8.8:

Resonance frequency spectrum for the short length IR-Photoacoustic cell. 10 torr of  $\text{SF}_6$  was used and about 7.0 Watts of laser power; the power was modulated electrically.

x 10

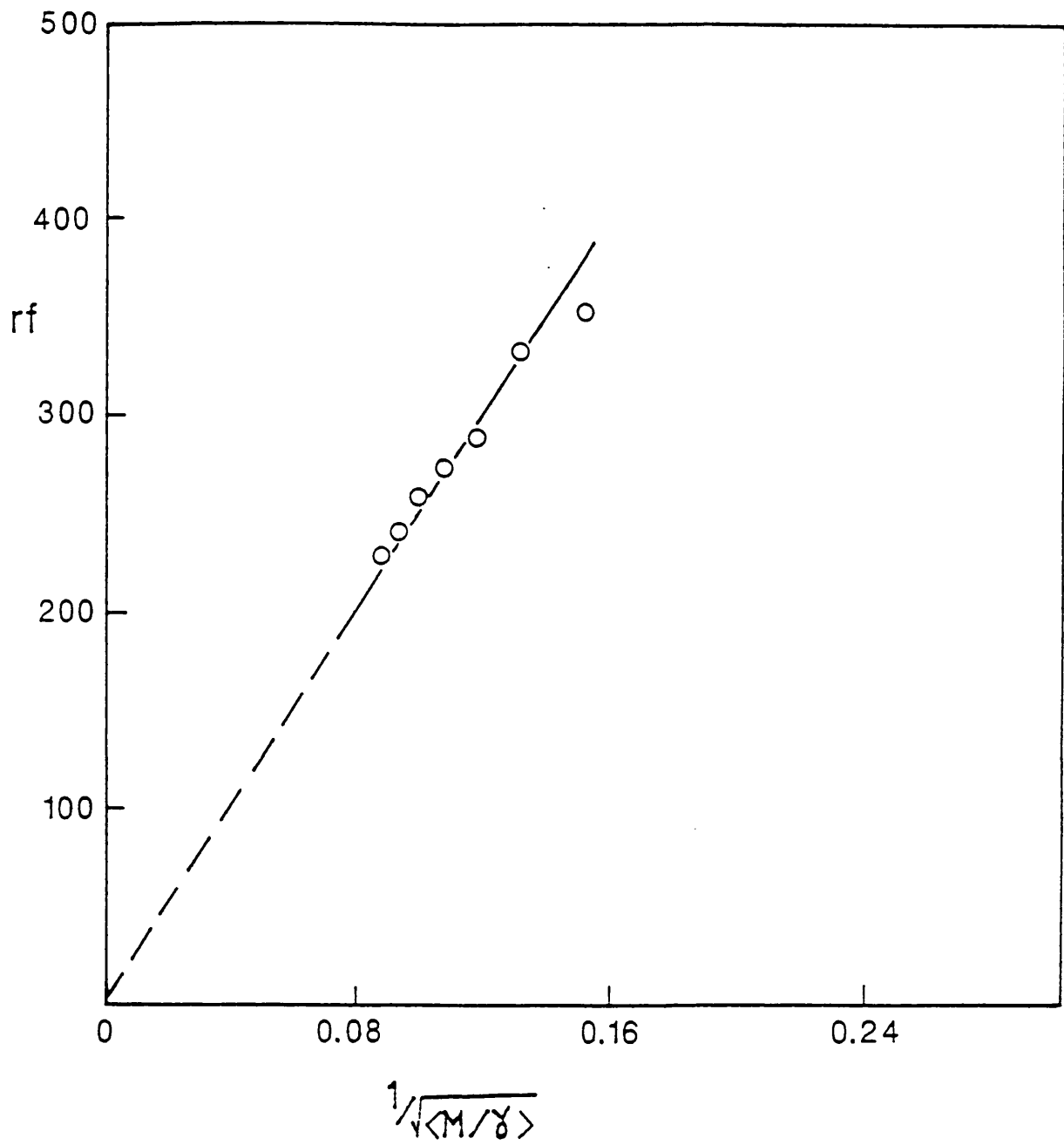


Figure 8.9:

Calibration curve for the IR-photoacoustic cell.

10.0 to a maximum of 30.0 volts at each r.f.. The results showed that the modulation amplitude had no effect on the r.f. of the cell. The minimum amplitude of this signal required to produce sufficient variation in the laser power to induce an acoustic wave was found to be 10.0 volts. Below that, it was very difficult to optimize the signal. Using amplitudes above 20.0 Volts in long experiments caused the efficiency of the laser to decrease.

#### **5.a. The IR and Photoacoustic Measurements of the Reaction of $\text{CH}_3\text{CHO}$**

The aim of this experiment was to compare results from the photoacoustic measurements and the IR measurements. 10 torr of  $\text{CH}_3\text{CHO}$  and 10 torr of  $\text{SF}_6$  were introduced into the reaction cell. The power of the laser used to induce the reaction was 10 Watts. The experiment was repeated using 12.5 Watts laser power. The reaction was followed using both the photoacoustic and IR spectroscopy; the observations are listed in Table 8.3 and plotted in Figure 8.10.

#### **5.b. IR and Photoacoustic Measurements of the Reaction of Ethylacetate.**

Ten torr of  $\text{CH}_3\text{COOCH}_2\text{CH}_3$  and 10 torr of  $\text{SF}_6$  were introduced into the reaction cell. The mixture was irradiated with laser power at about 5.3 Watts. The measurement was carried out using both the IR and photoacoustic spectroscopy on the same sample; see Figure 8.11.

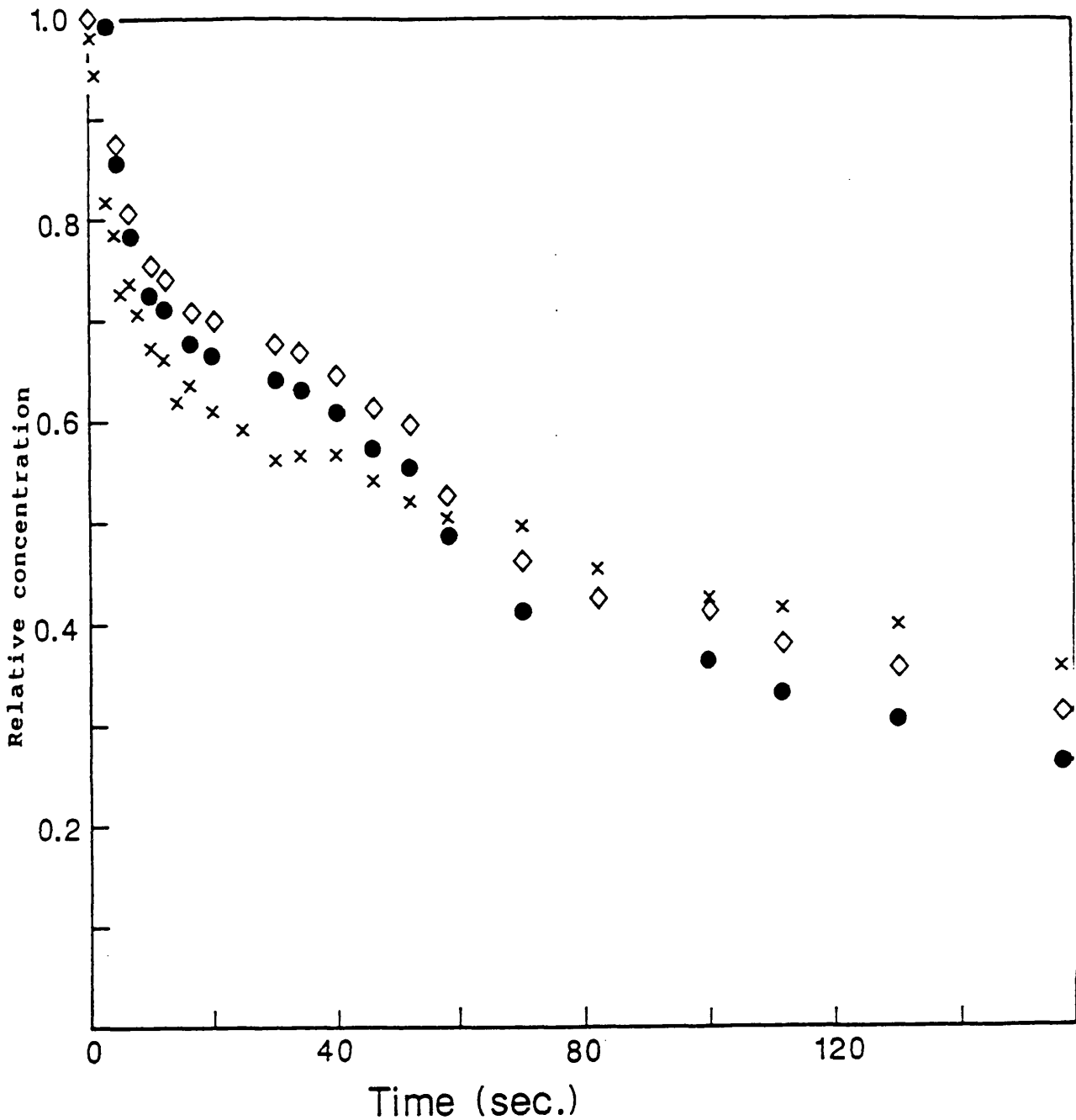


Figure 8.10:

Plots of normalized results of the reaction of  $\text{CH}_3\text{CHO}$  vs time using mixture of 10 torr of  $\text{CH}_3\text{CHO}$  and 10 torr of  $\text{SF}_6$  irradiated with 10 Watts of laser power. (x) IR measurement, the decay of the intensity of the peak  $1124\text{ cm}^{-1}$ ; (◇) photoacoustic measurement, the decay in the pressure of  $\text{CH}_3\text{CHO}$ ; (●) the change in the r.f. of the cell.

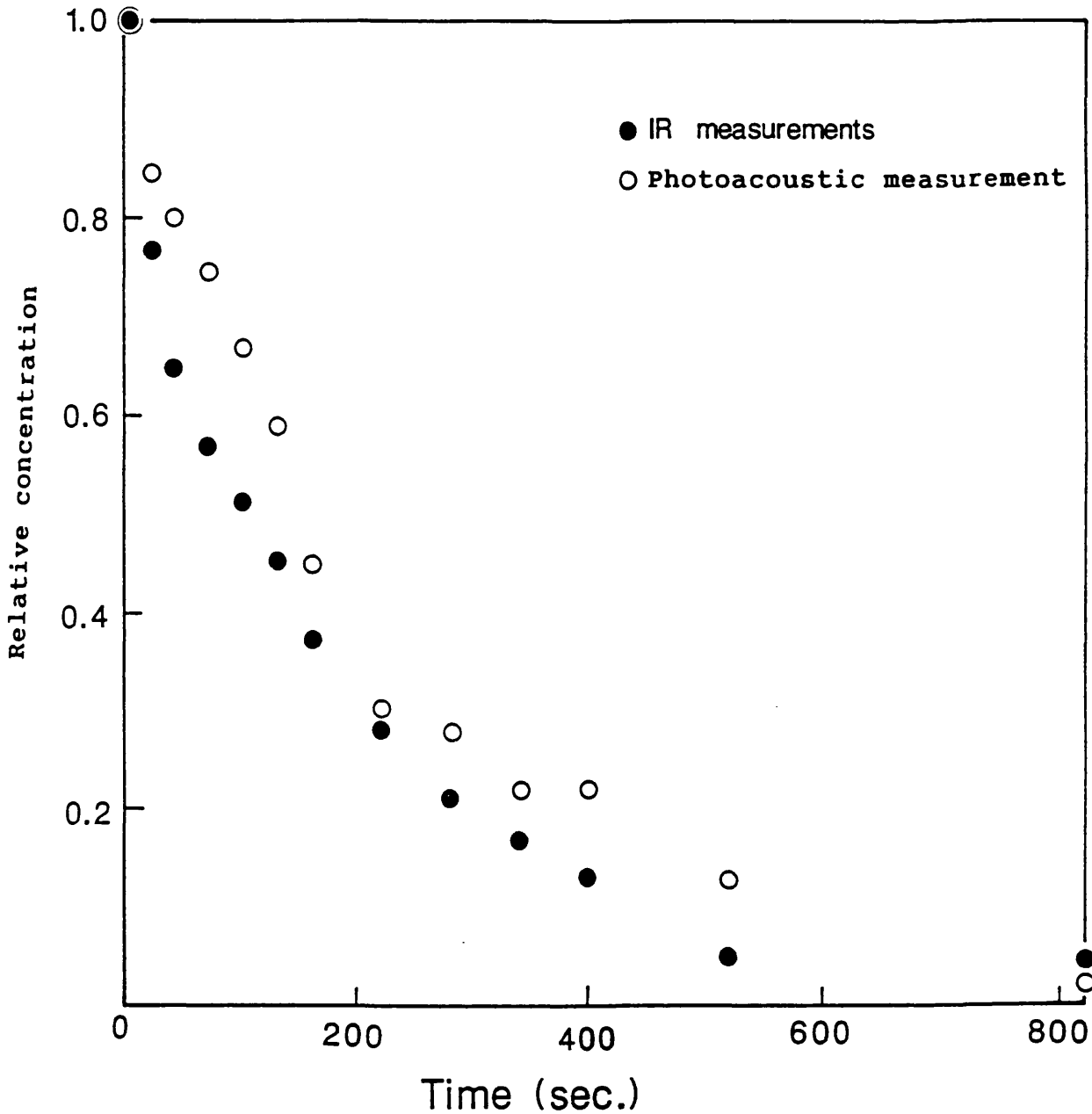


Figure 8.11:

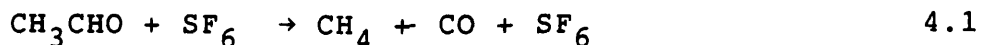
Plot of normalized results of the intensity of the peak at  $1123\text{ cm}^{-1}$  of ethyl acetate and the change in the difference of the r.f. of the cell vs time. The mixture was 10 torr of ethyl acetate and 10 torr of  $\text{SF}_6$ , irradiated with 5.3 Watts of laser power. (●) IR and (○) Photoacoustic results respectively.

## 8.4 RESULTS

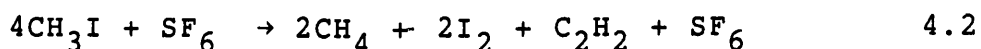
The experiments described in the previous section were carried out in order to understand and test the feasibility of applying this technique to reactive chemical systems; the conclusions drawn are noted below.

### 8.4.1 Results using the long pyrex cell

1. The r.f. of the cell was linearly related to the reciprocal of the square root of the average molecular weight of the contents of the cell (Figure 8.3).
2. Increasing the pressure of the photosensitizer, SF<sub>6</sub> in the cell as a single component had no effect on the r.f. of the cell (Table 8.1).
3. Increasing the laser power causes a considerable change in the r.f. of the cell. Thus stabilizing the laser power is very important in this type of measurement; (Figure 8.4).
4. Mixtures of chemically unreactive compounds showed no change in the r.f. of the cell over a period of time.
5. The decomposition of compounds, such as CH<sub>3</sub>CHO and CH<sub>3</sub>I, which lead to an increase in the number of components as in the reactions



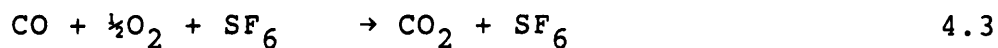
and



yielded an increase in the r.f. of the cell; as shown

in Figure 8.5.

6. Reactions which reduce the number of components in the reaction cell showed a decrease the r.f. of the cell (Figure 8.5c) as in the reaction below:



#### 8.4.2 Results using the adjustable length cell

1. Varying the volume (ie length) of the cell gave a linear relation with the reciprocal of the r.f. of the cell (Figure 8.7).
2. The rate of decomposition of  $\text{CH}_3\text{CHO}$  using different volumes showed very little dependence on the volume of the reaction cell (Table 8.2).
3. Varying the pressure of  $\text{CH}_3\text{CHO}$  led to an increase in the rate of the reaction with increasing pressure (Table 8.3).

#### 8.4.3 Results using the IR-Photoacoustic cell

1. Modulation of the  $\text{CO}_2$  laser had very little effect on the average laser power (less than 5% of the applied power).
2. The most important result obtained (Table 8.3) was that the rate of decomposition of  $\text{CH}_3\text{CHO}$ , measured using the photoacoustic method, was comparable with that using IR measurements. Figure 8.10 shows a plot (as a function of time) of (i) the intensity of the IR peak of  $\text{CH}_3\text{CHO}$  at  $1124 \text{ cm}^{-1}$ , normalised to its initial

value, (ii) the extent of decomposition of  $\text{CH}_3\text{CHO}$ , calculated using the relative change in r.f. of the cell, and (iii) the extent of decomposition, calculated using Equation 2.6.5.

3. The results of the decomposition of  $\text{CH}_3\text{COOCH}_2\text{CH}_3$ , unfortunately, cannot be calculated using the analysis as applied in the reaction of acetaldehyde. The reason for that is one of the products (i.e.  $\text{CH}_3\text{COOH}$ ) which exists during the measurement of the photoacoustic in two forms, as a monomer and a dimer (see Figure 8.12 and 8.13). The normalized IR and the normalized differences in the r.f. are plotted in Figure 8.11.

## 8.5 DISCUSSION

The results clearly show the feasibility of using the photoacoustic technique for monitoring chemical reactions in the gas phase. One of the important things which must be known is the products of the reaction, because the r.f. of the cell depends on the average molecular weight of the composition of the cell. Reactions giving no differences in the molecular weights will showed no change in the r.f. of the reaction cell. Reactions resulting in a reduction of the components of the reaction cell gave a change in the r.f. of the cell in the negative direction, Figure 8.5. Controlling

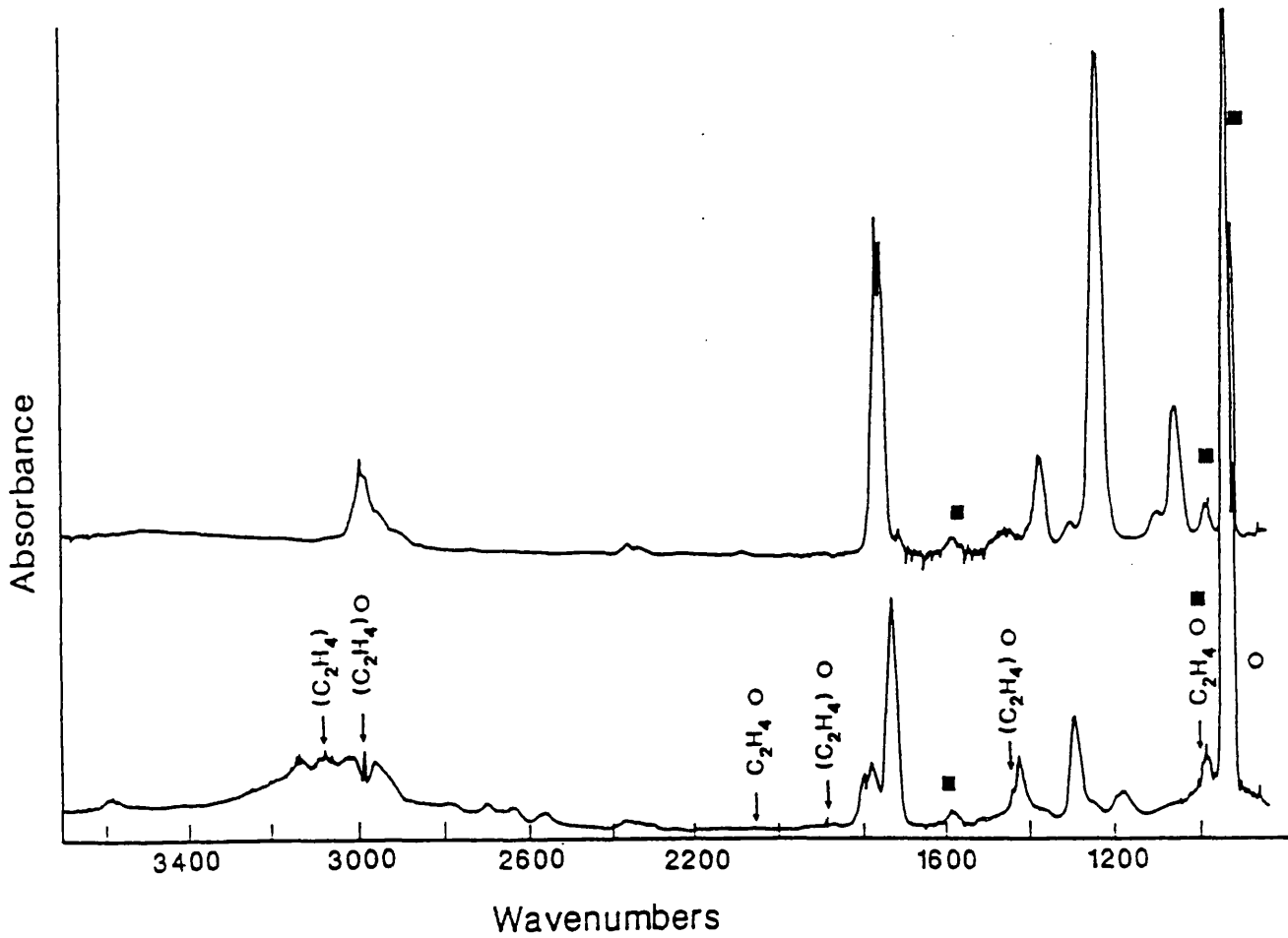


Figure 8.12:

IR spectra of the decomposition of mixture of 10 torr of  $\text{CH}_3\text{COOCH}_2\text{CH}_3$  and 10 torr of  $\text{SF}_6$  irradiated with 5.3 Watts of laser power: (a) before and (b) after 15 minutes irradiation; o the new products and ■ the  $\text{SF}_6$  bands.

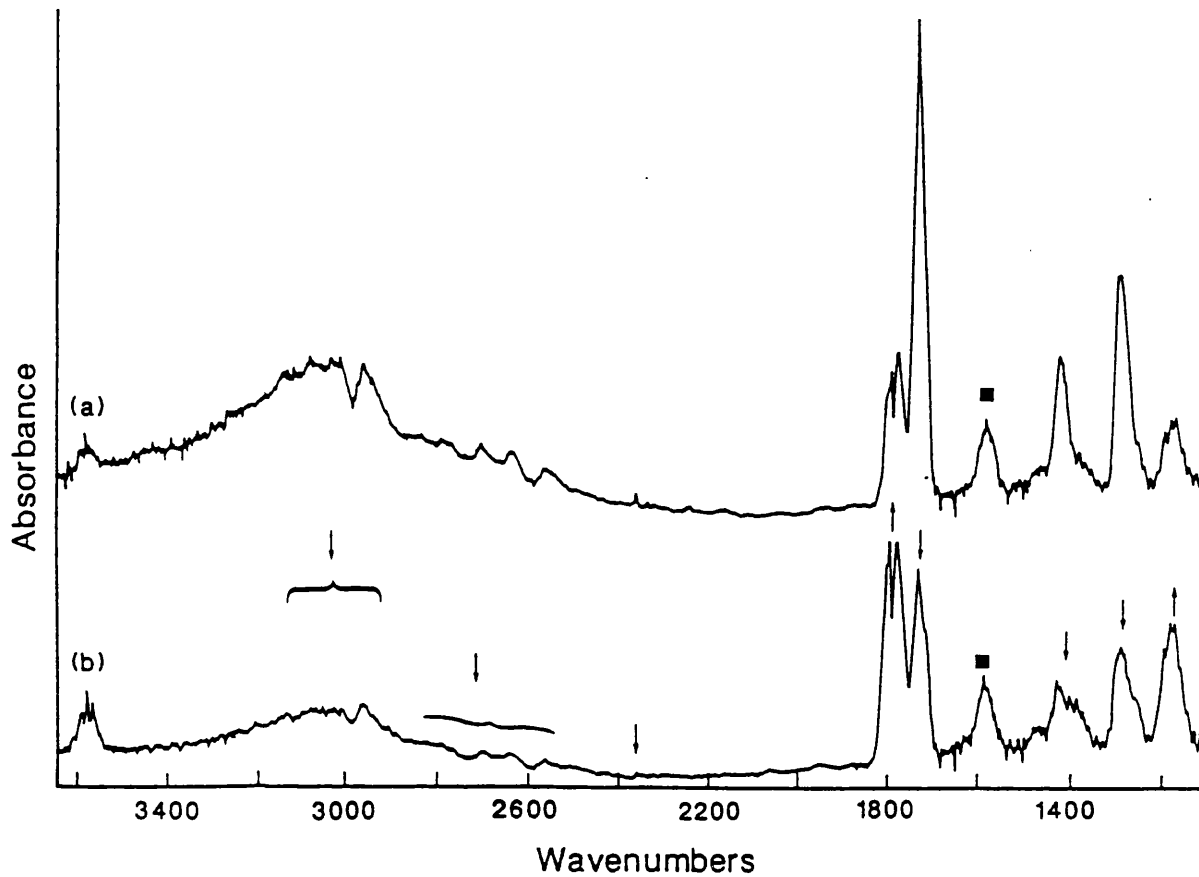


Figure 8.13:

IR spectra of mixture of 10 torr of  $\text{CH}_3\text{COOH}$  and 10 torr of  $\text{SF}_6$  irradiated with about 5.0 Watts: (a) before and (b) during the irradiation. The upward and the downward arrows indicate the increased and the decreased intensity of the monomer and the dimer peaks respectively.

the temperature inside the reaction cell is very important, because the r.f. of the cell depends strongly on the temperature as proved experimentally (Figure 8.7).

From the experiments, varying the pressure of  $\text{CH}_3\text{CHO}$  and varying the power of the laser, it was concluded that this technique can be useful in monitoring such chemical reactions. The rate of the reaction was shown to depend on the vapour pressure and the laser power.

The results from the experiment which was carried out using the adjustable length cell, showed that the rate of the reaction slightly depended on the volume of the cell, decreased with increasing the volume of the cell.

Using a modulation technique to vary the laser power offers a very good method to study the rate of decomposition of  $\text{CH}_3\text{CHO}$  in comparison with IR spectroscopy measurements. The technique is based on modulating the power of the laser instead of chopping the laser beam mechanically. This causes very little variation in the laser power, and is just enough to make acoustic wave in the cell for the photoacoustic measurements.

The initial rate, obtained from plotting  $\ln(\text{the difference between the final and the initial r.f. of the cell})$  vs time, shows close agreement with the results deduced from IR spectroscopic measurements.

Only the initial rate was important in our measurements because after 5 minutes of the reaction, significant amount of new products will appear and the conductivity of the cell contents will change, causing a drop in the absorption coefficient of the photosensitiser,  $\text{SF}_6$  and subsequently changing the temperature profile of the reaction cell<sup>20</sup>.

## 8.6 CONCLUSION

The above results demonstrate that the photoacoustic technique, using the r.f. of the cell, offers certain advantages over the previous photoacoustic measurements.

One of the most important advantage of using this technique is that the effects of the absorption gas, the lensing, and the distortion of the laser beam and the turbulence effects are ignored. These factors have significant effects on the previous methods.

The measurements based on this technique reflect the average changes in the entire reaction cell, not simply the hot reaction zone, while spectroscopic methods measure only the zone in the path of the radiation scanning the reaction.

This technique can also be useful as a monitor of a fixed composition of gas, as a controller of composition, as well as a method of measurement of kinetic parameters for gases.

The disadvantage of this technique is in its inapplicability to reactions yielding unknown products and to reactions which give no difference in the average molecular weight (eg, isomerisation).

**8.7 REFERENCES**

1. R. B. Stewart, S. M. Didascalou and G. J. Diebold.  
Optics Communication II 58 (1963) 103.
2. J. Schuurman and G. H. Wegdam.  
Chem. Phys. Letters 73 (1980) 429.
3. Hans-Jorg Bauer.  
J. Chem. Phys. 57 (1972) 3130.
4. G. J. Diebold.  
Proc. Int. Conf. lasers 1964 Pub 1985 620.
5. J. E. Rudzki, J. L. Goodman and K. S. Peters.  
J. Am. Chem. Soc. 107 (1985) 7849.
6. K. M. Beck, A. Ringwelski and R. J. Gordon.  
Chem. Phys. Letters 121 (1985) 529.
7. T. Aoki and M. Katayama.  
Japan. J. Appl. Phys. 10 (1971) 1303.
8. H. E. Bass and H. Yan.  
J. Acoust. Soc. Am. 74 (1983) 1817.
9. T. F. Hunter, D. Rumbles and M. G. Stock.  
J. Chem. Soc. Faraday Trans. II 70 (1974) 1010.
10. T. F. Hunter and M. G. Stock.  
J. Chem. Soc. Faraday Trans. II 70 (1974) 1022.
11. T. F. Hunter and M. G. Stock.  
J. Chem. Soc. Faraday Trans. II 70 (1974) 1028.
12. T. F. Hunter and K. S. Kristjansson.  
J. Chem. Soc. Faraday Trans. II 78 (1982) 2067.
13. L. J. Rothberg, J. D. Simon, M. Bernstein and  
K. S. Peters.  
J. Am. Chem. Soc. 105 (1983) 3464.
14. J. R. Barker, L. Brouwer, R. Patrick, M. S. Rossi, P. L.  
Trevor and D. M. Golden.

- Int. J. Chem. Kinetics 17 (1985) 991.
15. G. J. Dieboled.  
J. Phys. Chem. 84 (1980) 2213.
  16. J. Wrobel and M. Vala.  
Chem. Phys 33 (1978) 93.
  17. L. B. Kreuzer.  
J. Appl. Phys. 42 (1971) 2934.
  18. H. L. Fang and R. L. Swofford.  
Appl. Optics 21 (1982)' 55.
  19. P. Helander, I. Lundstrom and D. McQueen.  
J. Appl. Phys. 51 (1980) 3841.
  20. J. F. Steinfeld, I. Burak, D. G. Sutton and A. V.  
Nowack.  
J. Chem. Phys. 52 (1970) 5421.

## CHAPTER 9

### CONCLUSIONS

The results of this study demonstrate the importance of the LPHP technique in promoting the chemical reactions of many types of compound, and to conduct mechanistic studies of such reactions in gas phase. The use of very sensitive detection equipment has made such investigation possible.

The temperature, produced by IR  $\text{CO}_2$  laser radiation, was been characterized, indicating that the hot zone in which the reaction took place was far away from the cell walls, and that the hottest part of the cell was estimated to be about 0.5 cm from the entrance window. This was also demonstrated photographically. The spectroscopic technique showed that the temperature decreases along the laser beam down the reaction cell. The test of the diffusion effects on reaction indicated that there were no effects under the conditions of the experiments.

The decompositions of  $\text{CH}_3\text{I}$  and  $\text{CD}_3\text{I}$  and their mixture indicated similar results to those reported previously. The decomposition of  $\text{CD}_3\text{I}$  was faster than that of  $\text{CH}_3\text{I}$ . The decomposition of a 1:1 mixture of the two compounds revealed that the majority of the products were  $\text{CH}_4$  and  $\text{CD}_4$ , with no mixed isotopes of methane or other compounds being observed.

The preliminary investigations of the reactions of TMT and HMDT using LPHP techniques showed that their decompositions were approximately first order. The contribution of the surface to the reaction was negligible. The majority of the products of the decompositions were

methane, small amount of unidentified species in gas phase, and a brownish metal layer deposited on the front window and the cell walls. Methane, carbon dioxide, a small amount of carbon monoxide and a thin black layer on the front window were the products in presence of  $O_2$ . Observation of a significant amount of  $CH_3D$  in the presence of  $D_2$  indicated that  $D_2$  played a part in the reaction only when a high laser power was used.

The most interesting results in the decomposition of TMAL, are as below:

- i. TMAL existed as a monomer under the conditions of LPHP.
- ii. TMAL decomposed to give  $DMAL^{\cdot}$  and  $CH_3^{\cdot}$  radicals.
- iii. The  $DMAL^{\cdot}$  radical were trapped as DMAF and DMACl using  $SF_6$ ,  $CCl_4$ ,  $CHCl_3$  and  $CDCl_3$  as radical scavengers.
- iv. The DMAF formed in the gas phase was a dimer or trimer, but after a long time in the liquid phase changed to a tetrameric form,  $\{(CH_3)_2AlF\}_4$ .
- v. The addition of  $H_2$  to the reaction mixture slowed the reaction in comparison with the addition of  $D_2$ , indicating that the conductivity of the cell contents played a major part in the reaction in such systems.
- vi. The small amount of  $CH_3D$  formed in the presence of  $D_2$  in the mixture also indicated that the addition of  $D_2$  to the reaction mixture made no important chemical contribution to the reaction.

Examination of the photoacoustic work demonstrated that

reasonable results may be obtained. It showed its high applicability to the chemical reactions by using the change of the r.f. of the cell as a measure of the change in the composition of the contents of the cell. Its main limitation was that the products of the reaction and their thermodynamic data must be known. One possible application of such a technique is to monitor the composition in the chemical process in the gas phase.

The major disadvantages of this technique were the possible interference of the photosensitizer in the reaction of some compounds, and the inhomogeneity of the temperature produced by the incident laser beam, which made it rather complex for kinetic studies, unless special modifications or assumptions can be made.